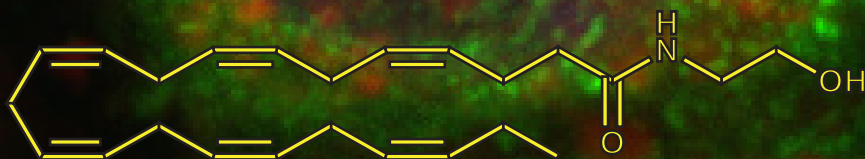


Unravelling the interaction targets and metabolic fate of docosahexaenoyl ethanolamide



Ian-Arris de Bus

Propositions

1. Re-formulation of the definition of the 'endocannabinoid system' is required.
(this thesis)
2. Adherence to the synonym 'synaptamide' for docosahexaenoyl ethanolamide (Kim, H. Y.; et al., A synaptogenic amide N-docosahexaenylethanolamide promotes hippocampal development. *Prostaglandins Other Lipid Mediat.* 2011, 96, 114-20) does not do justice to the variety of biological effects observed for this molecule.
(this thesis)
3. Multidisciplinary research can only exist by interdisciplinary research management.
4. A complete understanding of the full metabolic physiology of organisms is a utopia.
5. Personalized medicine leads to cost reduction of healthcare.
6. Team athletes are better equipped for top functions than others.
7. Introduction of quota is not a proper solution to create a balanced workplace.

Propositions belonging to the thesis, entitled

Unravelling the interaction targets and metabolic fate of docosahexaenoyl ethanolamide

Ian-Arris de Bus
Wageningen, 8 October 2021

Unravelling the interaction targets and metabolic fate of docosahexaenoyl ethanolamide

Ian-Arris de Bus

Thesis committee

Promotors

Prof. Dr H. Zuilhof

Professor of Organic Chemistry

Wageningen University & Research

Prof. Dr R. F. Witkamp

Professor of Nutritional Biology

Wageningen University & Research

Co-promotors

Dr B. Albada

Assistant professor, Laboratory of Organic Chemistry

Wageningen University & Research

Dr M.G.J. Balvers

Senior Scientist, Division of Human Nutrition and Health

Wageningen University & Research

Other members

Prof. Dr Ir. A. H. Kersten, Wageningen University & Research

Dr M. Al Houayek, Université catholique de Louvain, Belgium

Prof. Dr J. Garssen, Utrecht University

Prof. Dr M. van der Stelt, Leiden University

This research was conducted under the auspices of the Graduate School VLAG (Advanced studies in Food Technology, Agrobiotechnology, Nutrition and Health Sciences).

Unravelling the interaction targets and metabolic fate of docosahexaenoyl ethanolamide

Thesis

Submitted in the fulfilment of the requirements for the degree of doctor
at Wageningen University
by the authority of the Rector Magnificus,
Prof. Dr A.P.J. Mol,
in the presence of the
Thesis Committee appointed by the Academic Board
to be defended in public
on Friday October 08th, 2021
at 1.30 p.m. in the Aula

Ian-Arris de Bus

Ian-Arris de Bus

Unravelling the interaction targets and metabolic fate of docosahexaenoyl
ethanolamide

238 pages

Thesis Wageningen University, Wageningen, The Netherlands (2021)

With references, with summary in English

DOI <https://doi.org/10.18174/549701>

ISBN 978-94-6395-885-1

“Pressure makes Diamonds,
Not Silver or Gold”

Danny Vera

Table of Contents

Abbreviations		9
Preface		13
Chapter 1	Introduction	15
Chapter 2	The role of <i>n</i> -3 PUFA derivatives and their oxygenated metabolites in the modulation of inflammation	43
Chapter 3	Bi-functional probes of PUFA-derived <i>N</i> -acyl amines identify peroxiredoxins and small GTPase-signaling proteins as their molecular targets in LPS-stimulated RAW264.7 macrophages	73
Chapter 4	Novel COX-2 products of <i>n</i> -3 polyunsaturated fatty acid-ethanolamine conjugates identified in RAW264.7 macrophages	113
Chapter 5	Immunomodulating effects of 13- and 16-hydroxylated docosahexaenoyl ethanolamide in LPS stimulated RAW264.7 macrophages	143
Chapter 6	Effects of docosahexaenoyl ethanolamide on symptoms of colitis, liver inflammatory markers and hepatic PUFA metabolism in a model of DSS-induced colitis	171
Chapter 7	Discussion	199
Summary		221
Acknowledgements		227
About the author		233

Abbreviations

15-HEDPEA – 15-Hydroxy-16,(17)-epoxy-docosapentaenoyl ethanolamide

2-AG – 2-Arachidonoyl glycerol

36B4 – Acidic ribosomal phosphoprotein P0

Δ 9-THC – delta-9-tetrahydrocannabinol

AA – Arachidonic acid

aAA – Alkynyl arachidonic acid

AANATL2 – Arylalkylamine N-acyltransferase-like 2

ABHD – α , β -Hydrolase domain-containing protein

ABPP – Activity-based protein profiling

ACN – Acetonitrile

AEA –Arachidonoyl ethanolamide or Anandamide

ALA – α -Linolenic acid

AP-1 – Activator protein 1

BSA – Bovine serum albumin

BV-2 – Mouse brain microglia cell line

cAMP – Cyclic adenosine monophosphate

CB – Cannabinoid receptor

CCL-20 – C-C motif chemokine ligand 20

ConA – Concanavalin A

COX-2 – Cyclooxygenase-2

CD-14 – Cluster of differentiation 14

CuAAC – Copper (I) mediated azide alkyne click reaction

CYP450 – Cytochrome P450

CXB – Celecoxib

CXCL1 – C-X-C motif chemokine ligand 1

DAGL – Diacylglycerol lipase

DCM – Dichloromethane

DHA – Docosahexaenoic acid

DHEA – Docosahexaenoyl ethanolamide

DMEM – Dulbecco's modified Eagle medium

DMSO – Dimethylsulfoxide

DSS – Dextran sodium sulfate

EA – Ethanolamine/ethanolamide

ECS – Endocannabinoid system

EDP-EA – Epoxydocosapentaenoic acid ethanolamide

ELISA – Enzyme-linked immunosorbent assay

EEQ-EA – Epoxyeicosatetraenoic acid ethanolamide

Abbreviations

EP – Prostaglandin E receptor
EPA – Eicosapentanoic acid
EPEA – Eicosapentaenoyl ethanolamide
Et₃N – Triethylamine
EtOAc – Ethyl acetate
EtOH – Ethanol
eV – Electronvolt
FA – Formic acid
FAAH – Fatty acid amide hydrolase
FCS – Fetal calf serum
GP-NAE – Glycerophospho-N-acyl ethanolamine
GPR – G-coupled protein receptor
HCD – Higher-energy collisional dissociation
HDHEA – Hydroxydocosahexaenoyl ethanolamide
HEK293 – Human embryonic kidney 293
HEPE – Hydroxyeicosapentaenoic acid
HETE – Hydroxyeicosatetraenoic acid
HMVEC – Human microvascular endothelial cells
HNSCC – Head and neck squamous cell carcinomas
HPLC – High pressure liquid chromatography
HRMS – High resolution mass spectrometry
HUVEC – Human umbilical vein endothelial cell
IBD – Inflammatory Bowel Disease
ICAM-1 – Intercellular adhesion molecule 1
IFN – Interferon
IKK – Inhibitor of nuclear factor- κ kinase
IL – Interleukin
iNOS – Inducible nitric oxide synthase
IPA® – Ingenuity pathway analysis
IRF – Interferon-regulating factor
kV – Kilovolt
LBP – LPS binding protein
LC-PUFA – Long chain polyunsaturated fatty acid
LC-MS – Liquid chromatography coupled to mass spectrometry
LDH – Lactate dehydrogenase
LOX – Lipoxygenase
LPL – Lipoprotein lipase
LPS – Lipopolysaccharide
LT – Leukotriene

MAGL – Monoacylglycerol lipase
 MAPK – Mitogen-activated protein kinase
 MCP-1 – Monocyte chemoattractant protein-1
 MD-2 – Myeloid differentiation factor 2
 MeOH – Methanol
 MPO – Myeloperoxidase
 MRM – Multiple reaction monitoring
 MS – Mass spectrometry
 MS/MS – Mass fragmentation
 MUFA – Mono-unsaturated fatty acid
 MyD88 – Myeloid differentiation primary response 88
 NAAA – *N*-acylethanolamine-hydrolyzing acid amidase
 NAE – *N*-acyl ethanolamine
 MAGL – Monoacylglycerol lipase
 NAPE – *N*-acyl phosphatidylethanolamine
 NAPE-PLC – *N*-acyl phosphatidylethanolamine phospholipase C
 NAPE-PLD – *N*-acyl phosphatidylethanolamine phospholipase D
 NF- κ B – Nuclear factor kappa-light-chain-enhancer of activated B cells
 NMR – Nuclear magnetic resonance
 NO – Nitric oxide
 NSAID – Non-steroidal anti-inflammatory drug
 PA – Palmitic acid
 PAF – Platelet activator factor
 PBS – Phosphate buffered saline
 PEA – Palmitoyl ethanolamide
 PG – Prostaglandin
 PLA – Phospholipase A
 PMN leukocytes – Polymorphonuclear leukocytes
 PPAR – Peroxidase proliferator activator receptor
 P/S – Penicillin/Streptomycin
 PUFA – Poly-unsaturated fatty acid
 RAW264.7 – Murine macrophage cell line
 ROS – Radical oxygen species
 RT – Room temperature
 SD – Standard deviation
 SEM – Standard error of the mean
 SPAAC – Strain-promoted azide alkyne click reaction
 SPE – Solid phase extraction
 TFA – Trifluoroacetic acid

Abbreviations

TGF- β – Transforming growth factor β
Th17 – T-helper 17 cell
TLR – Toll-like receptor
TNF – Tumor necrosis factor
TRAF – TNF receptor associated factor
TRIF – TIR-domain-containing adapter-inducing interferon- β
TRPV – Transient receptor potential channel
TQ-S – Triple Quadrupole mass Spectrometer
TX – Thromboxane
UPLC – Ultra Performance Liquid Chromatography
UV – Ultraviolet
V – Volt

Preface

Samenvatting voor de niet-wetenschapper

Voeding en gezondheid zijn nauw met elkaar verbonden, en het is dan ook geen verrassing dat goede voeding helpt bij het voorkomen en verlichten van ziekten en/of ziekteverschijnselen. Samen met koolhydraten en eiwitten zijn vetten de belangrijkste voedingsstoffen in ons voedsel. Vetten zijn niet alleen belangrijk als energiebron en energieopslag, maar ook als bouwstenen van stoffen die belangrijke processen in het lichaam reguleren. Hiertoe behoren ook processen die ontsteking controleren. Vooral de invloed van zogenaamde omega-3 (*n*-3) vetzuren, die bijvoorbeeld veel voorkomen in vette vis, op ontstekingen is relevant. Dit zijn meervoudig onverzadigde vetzuren met ontstekingsremmende effecten. Ons lichaam zet dit soort vetzuren zelf ook weer om, in momenteel nog veel minder goed bekende producten. Tijdens mijn promotieonderzoek heb ik specifiek gekeken naar de omzetting van dergelijke omega-3 vetzuren in het lichaam, en de effecten die de ontstane producten hebben op ontsteking. In eerder onderzoek van de afdeling Humane Voeding en Gezondheid is aangetoond dat een specifiek omzettingsproduct van zo'n vetzuur, docosahexaenoyl ethanolamide (DHEA), zeer sterke ontstekingsremmende eigenschappen heeft. Aangezien DHEA door de mens zelf wordt geproduceerd na de inname van visvetzuren, was het interessant om onderzoek te doen naar de effecten van dit specifieke product en de rol ervan in de regulatie van ontstekingen. Vragen die ik heb onderzocht zijn hoe het ontstekingsremmende effect van DHEA precies werkt, en hoe dit product zelf weer wordt afgebroken op de plek van de ontsteking.

Uitkomsten van het onderzoek zijn dat DHEA een specifieke interactie heeft met verschillende eiwitten in de cel. Waarschijnlijk spelen deze interacties een belangrijke rol bij de beweging van cellen door het lichaam en de vorming of vermindering van schadelijke zuurstofmoleculen. Door middel van kleine chemische aanpassingen aan de vetzuren heb ik deze eiwitinteracties kunnen identificeren. Naast het aantonen van de eiwitinteracties, heb ik ook een fluorescerend label aan het vetzuur gezet waarmee ik ze kon lokaliseren in de cel (rode kleur op de omslag). Tijdens deze en eerdere onderzoeken vond ik een specifieke interactie tussen DHEA en het enzym cyclooxygenase-2 (COX-2). COX-2 speelt een belangrijke rol bij het ontstaan van de ontstekingsreactie (COX-2 is ook het enzym dat je remt als je een aspirine of ibuprofen inneemt). De interactie van DHEA met COX-2 verhindert de productie van ontstekingsregulators, en het resulteerde zelfs in twee nieuw ontdekte vetzuurmetabolieten, 13- en 16-hydroxydocosahexaenoyl ethanolamide (13-HDHEA en 16-HDHEA). Deze metabolieten bleken zelf ook licht ontstekingsremmende eigenschappen te bevatten. Helaas hebben we de vorming van 13-HDHEA en 16-HDHEA nog niet kunnen aantonen in diermodellen of in de mens,

en is meer onderzoek nodig om zowel het ontstaan als de bijdrage van deze stoffen tijdens ontstekingsprocessen beter in kaart te brengen. In een colitis (darmontsteking) muismodel hebben we laten zien dat DHEA weliswaar ontstekingsremmende eigenschappen heeft, maar ook dat verder onderzoek naar het metabolisme van de *n*-3 vetzuren en vetzuurmetabolieten nodig is om hun rol tijdens de preventie en vermindering van ontstekingen te begrijpen.

Chapter 1

Introduction

1.1 Nutrition and Health

1.1.1 Nutrition and health: A matter of lifestyle

Lifestyle factors constitute important determinants of an individual's health and life expectancy. For instance, participation in sports activities and regular exercise are known to improve mental health, limit the effects of stress,¹⁻² and help to prevent the occurrence of (non-communicable) diseases.³⁻⁴ Together with physical exercise, and other lifestyle factors, including sleep quality and limitation of stress, nutrition is one of the major determinants of health. In addition to providing energy, fluids, and macro- and micronutrients that are required for proper functioning of the body, a well-balanced diet and nutritional habits reduce risks for developing non-communicable diseases such as cancer and cardiovascular diseases.⁵⁻⁷ To this end, the Dutch Health Council (Gezondheidsraad) issues dietary guidelines that are translated into practical advice by the Dutch Nutrition Centre (Voedingscentrum) including well-known tools like the 'Wheel of Five' ('Schijf van Vijf').⁶

1.1.2 Health and nutrition: A short historical perspective

The importance of nutrition for health has been acknowledged for centuries, as evidenced by written proof from the time of the ancient Greeks. '*Let thy food be thy medicine, and medicine be thy food*' is a famous quote that is often attributed to the Greek Hippocrates. Although this quote has never literally been found in one of Hippocrates' original texts, the *Corpus Hippocraticum*, Hippocrates is assumed by some as one of the founders of the scientific fields that study the medical/biological effects of nutrition.⁸⁻⁹ At later times, awareness of the preventive and/or curative role of food started to decline, until renewed awareness in lifestyle arose in the past few decades. Ever since, nutritional perspectives on disease development, treatment strategies, and current understanding of health in general can hardly be omitted.⁵

1.2 Nutrition and lipids

Our diet consists of three main molecular components, also named macronutrients: proteins, carbohydrates, and lipids, next to fluids and micronutrients (vitamins and minerals). In an average Western diet lipid intake usually provides about 42% of daily ingested calories,¹⁰ showing the importance of lipid intake for our energy metabolism. To better understand the biochemical aspects of lipids and their importance in biology, first lipid nomenclature and biological functionality will be introduced.

1.2.1 Lipid nomenclature and biological functionality

According to the IUPAC, lipid is a loosely defined term for a class of biological macromolecules that are nonpolar and hydrophobic in nature.¹¹ Major types of lipids include fats, oils, waxes, steroids, phospholipids (**1** of **Figure 1-1A**), glycolipids (**2** of **Figure 1-1A**), and triacylglycerols (**3** of **Figure 1-1A**).¹² The main precursors and/or building blocks of these lipids are fatty acids, which generally provide their hydrophobic properties.^{10, 12} Fatty acids are divided in classes depending on their level of saturation: saturated fatty acids, mono-unsaturated fatty acids (MUFAs), and poly-unsaturated fatty acids (PUFAs). All fatty acids are abbreviated according to their structure using the specific notation ' $n_{\text{carbons}}:n_{\text{unsaturated bonds}}$ ' (**Figure 1-1B**), next to their systematic naming convention. In addition, some fatty acids also bear a more common name. Compound **5** and **6**, for example, are better known as oleic acid and arachidonic acid, derived from their chemical characteristics (**Figure 1-1B**).¹³⁻¹⁵

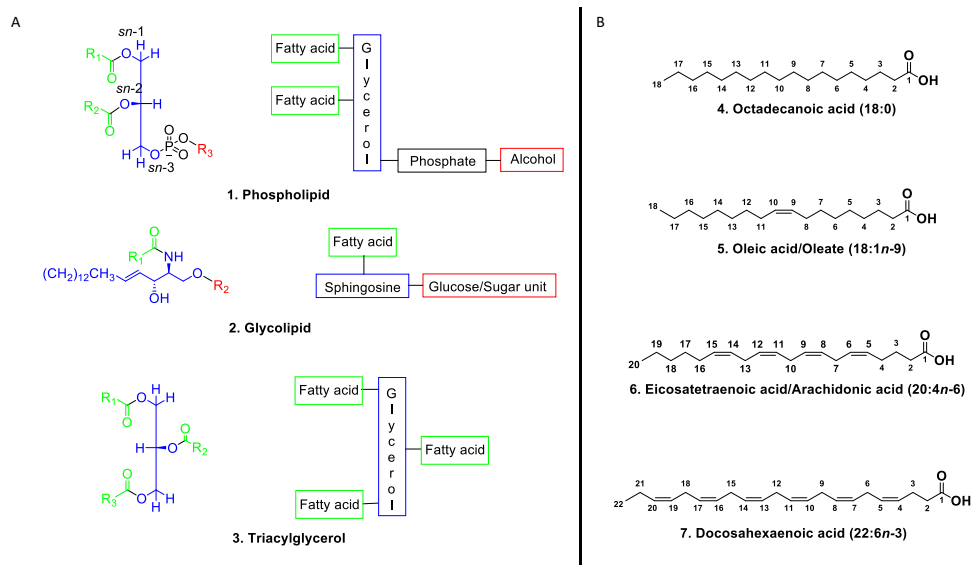


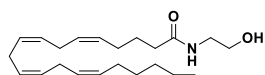
Figure 1-1 Chemical structure of several common lipids in biology (A). Chemical structure and nomenclature of four fatty acids (B).

In diets, the most predominant form of lipids are triacylglycerols, which approximately provides 95% of the total lipid content. The remainder is present in the form of phospholipids (approximately 4.5%) and cholesteryl esters (approximately 0.5%).¹⁰ When taken up by the body, lipids are involved in various physiological processes.¹² In quantitative terms, fatty acids are mainly used for direct energy supply or to provide energy storage in the form of triacylglycerols.¹² In addition, lipids also function as

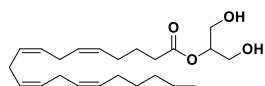
structural building blocks of membranes as phospholipids or glycolipids. Next, lipids can be used to label proteins with a localization 'label', allowing proper transport and localization of the proteins.¹² Lipidation often occurs with membrane proteins, which require the attachment of lipids to provide extra hydrophobicity to the proteins.¹² ¹⁶ In addition, lipids in the cytosol are bound to fatty acid-binding proteins (FABPs) and albumin to enable specific transportation within the cell.¹⁷ Last but not least, fatty acids and lipids can be converted to hormones, inflammatory regulators, and other signaling molecules that cause specific cellular effects through, *e.g.*, cell surface receptors or nuclear receptors.^{12, 18} This latter function of lipid-derived metabolites will be further outlined in this thesis, especially in the context of immune regulation and inflammation.

1.2.2 Fatty acid metabolites and endocannabinoids

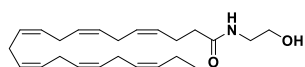
Next to being degraded via the β -oxidation pathway to generate energy, lipids and fatty acids can undergo extensive derivatization such oxidation, esterification, and amidation, yielding new bio-active signaling molecules.¹⁸⁻²⁰ Oxidation occurs either spontaneously via auto-oxidation or controlled via enzymatic conversion. Esterification and amidation, on the other hand, can only occur via enzymatic routes.^{18-19, 21} Esterification and amidation lead to the production of novel signaling lipids that are usually named after their fatty acid and conjugated group. For example, compound **8** in **Figure 1-2** is the conjugate of the fatty acid arachidonic acid and ethanolamine, and thus known as arachidonoyl ethanolamide (AEA, also known as anandamide). Similarly, compound **9** is named 2-arachidonoyl glycerol (2-AG), and compound **10** is known as docosahexaenoyl ethanolamide (DHEA).¹⁹ Interestingly, AEA and 2-AG are agonists of the cannabinoid receptor type 1 and 2 (CB₁ and CB₂), although with higher affinity for CB₁ than for CB₂.²² Because of their structural differences but biological similarities in receptor affinity with cannabis-related compounds like delta-9-tetrahydrocannabinol (Δ 9-THC), AEA and 2-AG were classified as 'endocannabinoids'.²²⁻²³



8. Arachidonoyl ethanolamide (AEA)



9. Arachidonoyl glycerol (2-AG)



10. Docosahexaenoyl ethanolamide (DHEA)

Figure 1-2 Chemical structure, name, and abbreviation in brackets, of three commonly known endocannabinoids.

1.3 The endocannabinoid system

1.3.1 The endocannabinoid system and endocannabinoidome

The endocannabinoid system (ECS) is defined as the collection of endocannabinoid compounds in combination with their metabolizing enzymes and biological receptors.²²⁻²³ The ECS regulates many physiological processes, including but not limited to metabolism, appetite, and immune response, and consists of only two cannabinoid receptors CB₁ and CB₂, nine endogenous PUFA derivatives interacting with CB₁ and CB₂, and a few enzymes involved in the synthesis and metabolism of the PUFA derivatives.²³⁻²⁴ During the years following its discovery, more PUFA-derived structures were identified resembling endocannabinoid structures, most of which showed interactions and/or regulation of members of the ECS. In addition to such intertwined interactions also new regulatory pathways and indirect immune regulatory effects of several ECS-members via PUFA metabolism were observed. For example, non-CB binding fatty acid-derivatives like oleyl-, linoleoyl-, and palmitoyl ethanolamide are able to induce CB stimulation by competing with AEA hydrolysis and increasing levels of the CB binding compound AEA.²⁴ This process is known as the entourage effect, and proves that the original classification of the endocannabinoid system based on CB agonism only may be too narrow. The term endocannabinoidome was introduced to classify these ECS interfering interactions.²³ A recent overview of the original endocannabinoid system and the still expanding endocannabinoidome is provided in **Figure 1-3**.

1.3.2 Synthesis, breakdown and metabolization of endocannabinoids

The biosynthesis of acyl fatty acid metabolites is regulated by various enzymes. For instance, 2-AG is synthesized by diacylglycerol lipase (DAGL), although alternative pathways were later identified as well.²⁵⁻²⁷ In *Drosophila* serotonin, dopamine, and glycine conjugated PUFA metabolites are produced by arylalkylamine *N*-acyltransferase-like 2 (AANATL2).^{23, 28-29} Currently, the formation of *N*-acyl ethanolamides (NAEs), such as for AEA, is the most commonly studied biosynthetic pathway. This route involves fatty acyl transfer from the *sn*-1 position of phosphatidyl choline (**Figure 1-1**, compound **1** with choline as phosphate-bound alcohol) to the ethanolamine moiety of phosphatidylethanolamine, forming an *N*-acyl phosphatidylethanolamine (NAPE) intermediate. The phosphatidyl moiety of NAPE is subsequently hydrolyzed by NAPE-phospholipase D (PLD), resulting in the formation of NAE derived lipids.^{23, 26-27, 30-31} This NAPE-PLD-dependent biosynthesis is well-characterized for AEA, and seems to be the most likely synthesis route for DHEA as supported by decreased DHEA levels in the brain of NAPE-PLD knock out mice.³² Besides the NAPE-PLD-dependent route, other synthetic mechanisms for NAEs do exist. For example, the glycerol moiety of NAPE can also be deacylated twice leading to formation of glycerophospho-*N*-acyl ethanolamines (GP-

NAEs), which are converted to NAEs by glycerophosphodiesterases.^{27, 31, 33} Additionally, an *in-situ* study in mice neurons containing NAPE-PLD and glycerophosphodiesterase knockouts indicated that NAPE hydrolysis still occurred, suggesting that other uncharacterized NAPE-catabolizing enzymes could exist.³⁴ Indeed, a NAPE-PLC-dependent catabolism has been proposed, although direct NAPE-PLC activity has never been experimentally proven.^{27, 31, 34-35}

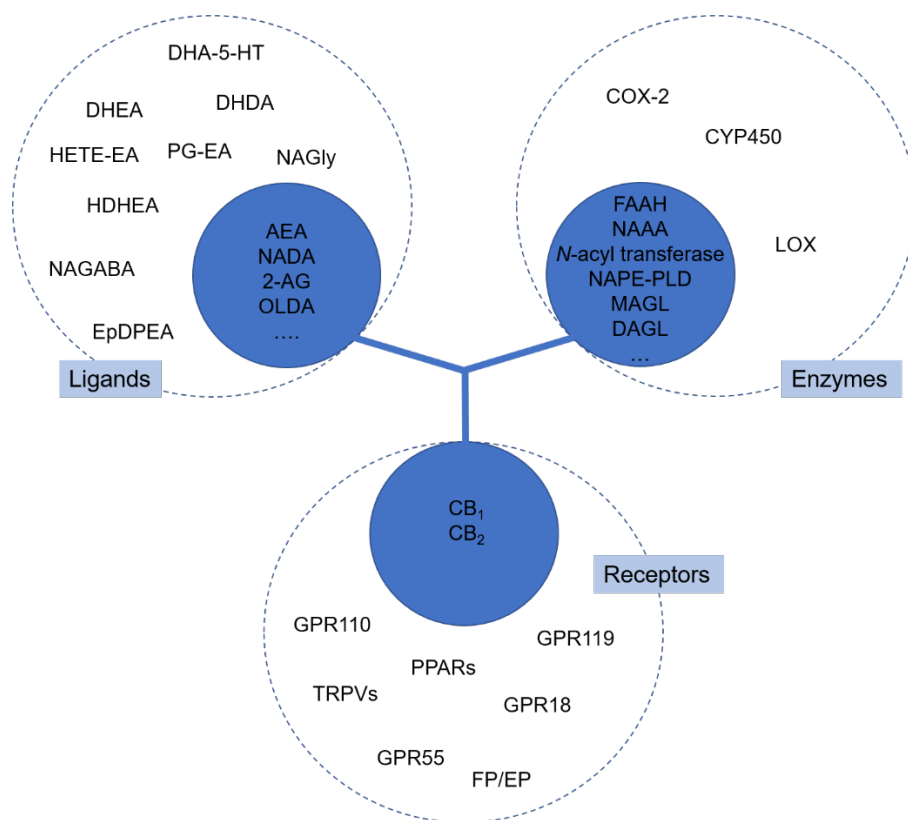


Figure 1-3 Recent illustration of the 'expanding' view on the endocannabinidiome (updated from Witkamp, 2016²³). Next to the classical ECS that comprises two cannabinoid receptors and a limited number of ligands and enzymes involved in their synthesis and breakdown (filled circles), new PUFA-derived compounds and its interactions that intertwine with the ECS were classified as the endocannabinoidome (dotted circles).

Breakdown of endocannabinoids often occurs via hydrolysis, resulting in the recovery of the parent (or precursor) fatty acid and alcohol or amine. Again, different enzymes are involved in the hydrolysis of the various endocannabinoids. The most commonly known hydrolysis route for amides is mediated by fatty acid amide hydrolase (FAAH),

but an *N*-acylethanolamine-hydrolyzing acid amidase (NAAA) also exists.^{23, 27} Although NAAA is mainly active with saturated and mono-unsaturated NAEs, such as palmitoyl ethanolamide,^{27, 30} various reports showed that NAAA is also capable of hydrolyzing AEA and DHEA next to the more commonly known AEA and DHEA hydrolysis by FAAH.³⁶⁻³⁷ The best-described hydrolysis routes for 2-AG are those via monoacylglycerol lipase (MAGL), α,β -hydrolase domain-containing 6 protein (ABHD6), and α,β -hydrolase domain-containing 12 protein (ABHD12).^{25, 27} Hydrolysis of 2-AG via FAAH is also possible, although to a limited extent.^{23, 38}

Besides hydrolysis, endocannabinoids can also be catabolized via oxidation, most notably by oxygenases like lipoxygenases (LOX), cyclooxygenase-2 (COX-2), and cytochrome P450 (CYP450) (**Figure 1-3**).^{26, 30, 39} Implications of their mechanisms are only limitedly described, and some of them will be discussed in this thesis in more detail.^{19,}

26, 39-41

1.3.3 Biological role of PUFA derivatives

New interactions between existing PUFA derivatives and regulators of the ECS are continuously being characterized to provide the growing scope of the endocannabinoidome. Interestingly, many of these interactions are involved in immune-regulation and inflammatory processes.²³⁻²⁴ Next, I will introduce several important aspects of the immune system and inflammation.

1.4 Immune system

1.4.1 General introduction to the immune system

Even though we spend our lives surrounded and inhabited by many potentially pathogenic microorganisms, we rarely become ill. This is because the immune system effectively defends our body against unwanted intrusion of pathogenic microorganisms. The immune system defends the body through a highly complex interplay between the bone marrow, lymphatic system, various immune cells, regulatory proteins and lipids that orchestrate the response to invading pathogens. The immune system has been functionally divided in an innate and an adaptive immunity to distinguish between the faster non-specific immune response and the slower specific immune response,⁴² although their borders are becoming more blurred. The continuous response of the innate immune system relies on many different cell types, of which macrophages and neutrophils are two important ones for the regeneration of homeostasis after pathogen infection.

1.4.2 Macrophages and neutrophils

Macrophages are the most common cell type of the innate immune system, and are widely distributed in all body tissues as well as in the circulation. They have important roles during the first phase of an immune response; recognition of pathogens via pathogen-associated molecular patterns (PAMPs). PAMP-induced activation of macrophages leads to the production of inflammation markers, which results in the recruitment of neutrophils in the damaged tissue (chemotaxis). Neutrophils are the most numerous and important cells during the innate immune response, because together with the macrophages they are involved in the ultimate destruction of the invading pathogen. Pathogen destruction is accomplished by forming neutrophil extracellular traps (a web of chromatin fibers with high concentrations of anti-microbial compounds and proteases), releasing anti-microbial peptides from their cytoplasmic granules, and producing toxic radical oxygens species (ROS). This may also cause damage to the host tissue. Moreover, neutrophils can engulf the pathogen (phagocytosis), and present pathogen peptides to cells of the adaptive immune system through the MHC system. Usually the anti-microbial and toxic responses also lead to apoptosis of the neutrophils, after which they are cleared by macrophages (efferocytosis) in the resolution phase. In the final stage of acute inflammation damaged tissue is repaired and homeostasis is regenerated.⁴²⁻⁴⁴

1.4.3 Macrophage activation by LPS

Macrophage activation via PAMPs is crucial for the initiation of the innate immune response. One commonly known PAMP is lipopolysaccharide (LPS), a cell wall component extracted from Gram-negative bacteria. LPS-induced macrophage activation is initiated by recognition of LPS by the LPS-binding protein (LBP), followed by association with the CD-14 protein. The resulting complex splits LPS aggregates into monomers, after which they are presented to the toll-like receptor 4 (TLR4)/ myeloid differentiation factor 2 (MD-2) complex. Aggregation of the TLR4/MD-2 complex ultimately leads to the activation of multiple downstream-signaling pathways that start the immune response.^{42, 45-46}

Downstream of the TLR4 receptor the signal transduction pathway is divided in a myeloid differentiation primary response 88 (MyD88)-dependent and a MyD88-independent pathway (the latter proceeds via the TIR-domain-containing adapter-inducing interferon- β (TRIF)). The MyD88-dependent pathway mediates expression of pro-inflammatory cytokines like interleukin 1 (IL-1) via regulation of TNF receptor-associated factor 6 (TRAF-6) mediated nuclear factor kappa-light-chain-enhancer of activated B cells (NF- κ B) stimulation, and mitogen-activated protein kinase (MAPK) induced activator protein 1 (AP-1). The MyD88-independent pathway mediates the

induction of type I interferons and interferon inducible genes via TRAF-3 mediated activation of interferon regulatory factor 3 (IRF3), but can also activate NF- κ B expression via TRAF-6.^{45, 47} Depending on both the PAMP and the accessory receptor displayed on the macrophages, MyD88-dependent and MyD88-independent routes can be activated simultaneously leading to the production of pro-inflammatory cytokines and interferons.^{45, 48} Activation of different immune-regulating pathways results in different macrophage phenotypes and finally specific immune orchestration. LPS activates both MyD88-dependent and MyD88-independent routes leading to the production of NF- κ B, AP-1, and IRFs that initiate the production of interleukins, interferons, and lipid-mediator producing enzymes like cyclooxygenase 2 (COX-2) (**Figure 1-4**).^{45, 48}

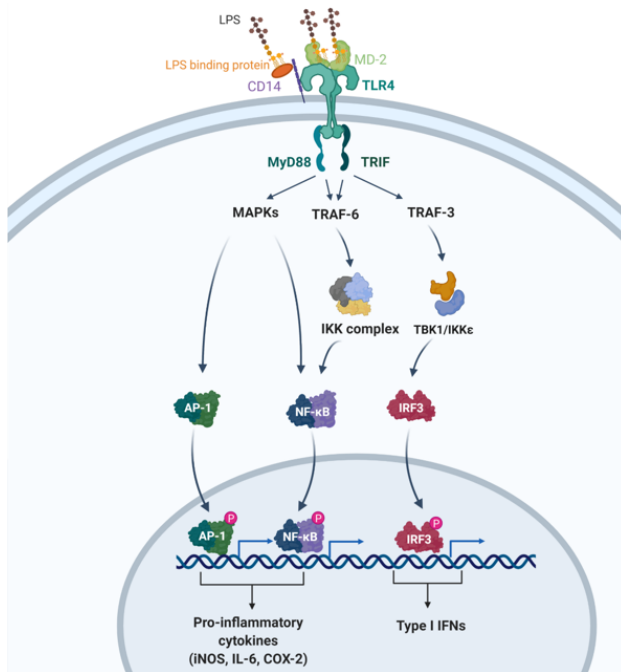


Figure 1-4 TLR-4 mediated inflammatory signaling cascade in macrophages, leading to the production of pro-inflammatory cytokines and type I interferons. The signaling cascade is activated by binding of LPS and mediated via MyD88-dependent or MyD88-independent routes. Figure was created using biorender.com.

1.4.4 RAW264.7 macrophage model

A commonly utilized *in vitro* model to study LPS-induced immune response is the RAW264.7 model. RAW264.7 is a murine monocyte/macrophage-like cell model that originates from Abelson leukemia virus transformed BALB/c mice.⁴⁹ RAW264.7 macrophages are cultured in a humidified atmosphere at 37 °C with 5% CO₂ in Dulbecco's Modified Eagle Medium (DMEM) containing 10% fetal calf serum (FCS), and produce IL-6, nitric oxide (NO), and COX-2 together with its pro-inflammatory lipid-derived mediators upon stimulation with LPS.⁵⁰⁻⁵¹

1.5 Inflammation

1.5.1 General introduction to inflammation and inflammatory diseases

Pathogenic infection or tissue damage often leads to inflammation, a functional and protective tissue response to injury or destruction of tissues, which serves to destroy, dilute, or wall off both the injurious agent and the injured tissues. Acute, clinical manifest inflammation is classically characterized by redness, heat, swelling, and sometimes pain. These characteristics are caused by vasodilation and increased vascular permeability, as a result of the innate immune response. This allows immune cells to migrate to the damaged tissue where they restore homeostasis as described in section 1.4.⁴² Although inflammation is often resolved by the innate immune system, continuous stimulation of the immune system or distorted signal transduction and/or regulation in the resolution phase of inflammation can lead to chronic inflammation.⁴⁴ Chronic inflammation leads to the overactivation of the innate immune system generating the overproduction of pro-inflammatory regulators. Many diseases like inflammatory bowel diseases (IBD), asthma, arthritis, but also increased risk for cancer development, cardiovascular diseases, and osteoporosis have been linked to chronic inflammation.^{44, 52-53} Consequently, medical intervention is sometimes required to prevent uncontrollable inflammation, severe tissue damage, and major pathogenicity.^{42, 44, 54} Usually, specific receptors and/or enzymes can be blocked by pharmaceuticals to prevent inflammatory propagation. A common example are non-steroidal anti-inflammatory drugs (NSAIDs) that inhibit the enzyme COX-2 thereby preventing the production pro-inflammatory regulators.⁵⁵⁻⁵⁶ Interestingly, nutrition was more recently reported as a useful new (or at least complementary) intervention strategy for the prevention and alleviation of chronic inflammation.⁵

1.5.2 Inflammatory regulation: a role for lipids

Several inflammatory mediators with crucial roles in inflammation are derived from lipids.^{18, 44} Generally, the more pro-inflammatory lipid-derived mediators are *n*-6 lipid based, whereas the less pro-inflammatory or anti-inflammatory mediators are *n*-3 lipid based. As such the dietary *n*-3/*n*-6 lipid ratio is believed to play an essential role in the development and progression of (chronic) inflammation.^{5, 57-59} Apart from lipid content the production of (anti-)inflammatory mediators also relies on the expression of the lipid-metabolizing enzymes such as LOXs, CYP450s, and COXs in the inflamed tissue. Next to PUFAs, these enzymes can also convert several PUFA-derived endocannabinoid compounds (**Figure 1-3**).^{23, 26, 39-40} LOXs are involved in peroxidation leading to mono-hydroxylated lipid compounds after reduction of the peroxide, CYP450s generate lipid peroxides, and cyclooxygenases produce cyclooxygenated lipid derivatives. Sequential oxygenation by multiple oxygenases ultimately leads to more complex di-, tri-, or

multi-hydroxylated and epoxidated lipid products.^{18, 26} All these oxidized lipid products have a specific role in inflammation, and tight regulation of lipid derived chemokine metabolism is thus essential for proper immune function.⁴⁴

1.6 Cyclooxygenases

1.6.1 Cyclooxygenases and inflammation

As their name already suggests, cyclooxygenases produce cyclooxygenated inflammatory regulating lipids like prostaglandins and thromboxanes (*vide infra*). Cyclooxygenases exist as two isoforms; the constitutive isoform COX-1, and the inducible isoform COX-2.⁶⁰ Due to differences in transcriptional regulation it is believed that COX-1 is involved in maintaining homeostasis, whereas COX-2 is involved in the regulation of inflammation and tumorigenesis.^{26, 61-62} Because of its well-described role in inflammation, COX-2 became an interesting target for anti-inflammatory drugs like aspirin and the NSAIDs, *e.g.* ibuprofen, diclofenac, celecoxib.^{55-56, 63-64} Due to unexpected cardiovascular and renal side effects of second-generation COX-2-selective NSAIDs (in particular rofecoxib, marketed as Vioxx) it was discovered that COX-2 expression in the brain, thymus, gut, and kidney could also be constitutive, where it is suggested to be involved in homeostatic regulation.⁶⁵⁻⁶⁶

Next to differences in expression profile, the substrate selectivity between COX-1 and COX-2 also differs. COX-1 activity is mainly limited to cyclooxygenation of negatively charged lipids such as AA, whereas COX-2 also oxygenates neutral lipid derivatives like the endocannabinoids AEA and 2-AG.^{26, 67-69} Structure-activity relationship studies showed that the broader substrate scope of COX-2 is caused by the flexibility of a Leu531 side chain that is positioned at the entry point of the substrate, allowing for an increased opening of the cyclooxygenase channel in mCOX-2.⁶⁹ Enzymatic conversion of endocannabinoids by COX-2 leads to novel products, some of which even have anti-inflammatory effects.⁴⁰ In summary, COX-2 is mainly associated with the onset of inflammation and overactivation of this enzyme leads to development and progression of (chronic) inflammatory diseases. Nonetheless, inflammatory regulation of COX-2 is tightly regulated and the enzyme also appeared to be involved constitutive functions. Consequently, understanding the activity of this enzyme in chronic inflammation might help in resolution or reduction of the symptoms.

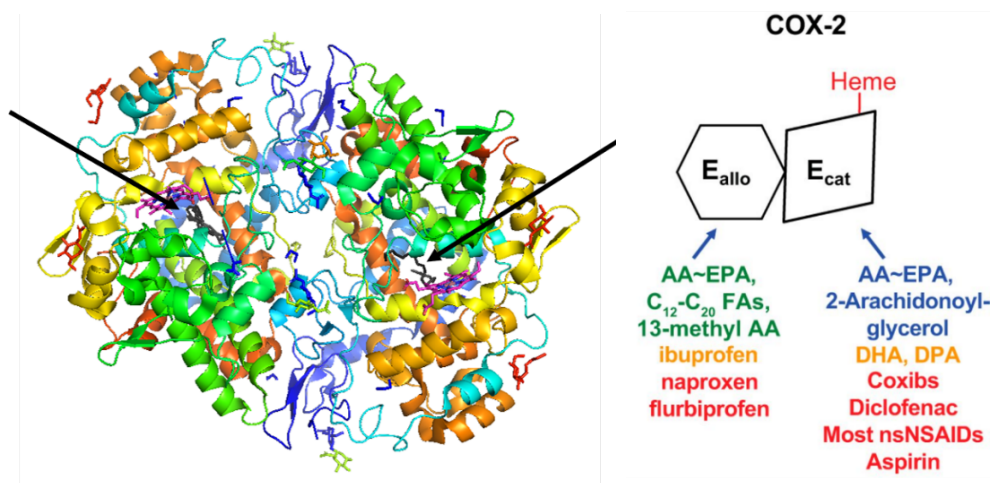


Figure 1-5 Single-crystal X-ray structure of mCOX-2 when bound to AA (in black, indicated with arrows) (*left*). Crystal structure was reported by Vecchio *et al.* 2010.⁶⁷ hCOX-2 isoform-specific interactions of substrates, non-substrate FAs, and inhibitors. hCOX-2 functions as a conformational heterodimer composed of an allosteric (E_{allo}) and a catalytic (E_{cat}) subunit (*right*). The individual subunits of hCOX-2 differ both in their affinities for and responses to different ligands. Efficient hCOX-2 substrates for the E_{cat} part of the dimer are shown in blue, in the approximate order of their catalytic efficiencies. Inefficient hCOX-2 fatty acid substrates that can interfere with prostaglandin formation, typically by competing with AA for the E_{cat}, are shown in orange (*e.g.*, DHA and DPA). Ligands shown in green allosterically stimulate hCOX-2 activity via the E_{allo} domain. Ligands shown in red interfere with hCOX-2 activity either allosterically by binding E_{allo} or competitively by binding E_{cat}. Ligands that bind E_{allo} can also affect responses of the E_{cat} domain to COX inhibitors. This figure taken from Smith, W.L., Malkowski, G.M., *J. Biol. Chem.*, **2019**, 1697-1705.⁵⁶ Reproduced with permission from Elsevier.

1.6.2 Kinetics of COX-2 catalysis

The inflammatory regulating prostaglandins, prostacyclins, and thromboxanes are produced from PUFAs by COX-2 via sequential bis-oxygenation and peroxidation. Both processes are catalyzed by separate but interconnected active sites in the same enzyme.⁵⁶ Apart from the unconventional presence of two active sites, COX-2 exists as a sequence homodimer that functions as a heterodimer with both an allosteric and a catalytic subunit (**Figure 1-5**). Fatty acid substrates, inhibitors, and non-substrate fatty acids can thus bind to both the allosteric and/or catalytic sites, resulting in differential enzyme kinetics.^{56, 70} One striking example of the heterodimer functionality of COX-2 is illustrated by the catalysis of AA and EPA. Both substrates have similar K_M values for COX-2, but when incubated together, COX-2 preferentially oxygenates AA. Only

recently it was discovered that EPA, when bound to the allosteric site, promotes AA oxygenation in the active site.^{56, 71} Similarly, binding events of COX-2 inhibitors and non-substrate fatty acids also influence the catalytic turnover of AA by interacting with the allosteric subunit. Examples include the inhibitors naproxen, flurbiprofen, but also the fatty acid palmitic acid (PA, C16:0) which increased AA oxygenation to about 128%.^{56, 72} A better understanding of the binding interactions between COX-2 and its substrates, regulators, and/or inhibitors may allow catalytic control over the activity of the enzyme.

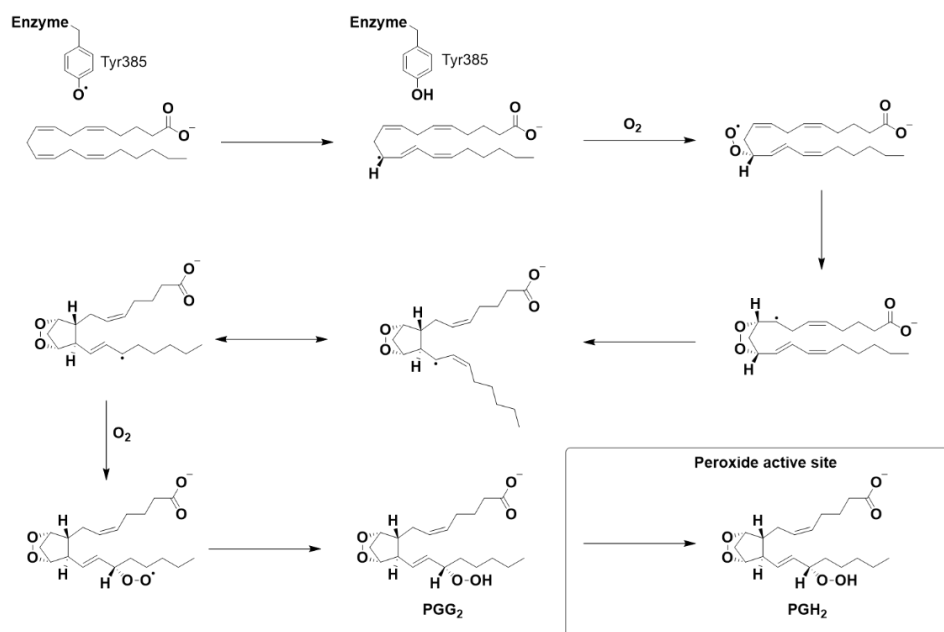


Figure 1-6 Bisdioxygenation of arachidonic acid to PGG₂ and finally PGH₂ by COX-2. Figure was modified from Rouzer *et al.* 2011.²⁶

1.6.3 Prostaglandin synthesis

The prototypical substrate for COX-2 is AA, which results in the production of the general prostaglandin precursor PGH₂. The enzymatic mechanism of AA conversion by COX-2 starts at the cell membrane where phospholipases like phospholipase A₂ (PLA₂) release the fatty acid AA. Subsequently, bisdioxygenation of AA is initiated by extraction of the 13-*pro*-(*S*) hydrogen atom by a catalytic tyrosyl radical at Tyr385. The radical rapidly migrates to position 11 followed by incorporation of molecular oxygen to form an 11-(*R*)-peroxyl radical. From this radical, a prostanoid five membered ring is produced after formation of an endoperoxide bond between carbon 9 and 11, and a

single bond between carbons 8 and 12. The radical then migrates to carbon 15, where a second oxygen molecule is incorporated to form a 15-(S)-peroxyl radical. This radical is reduced to PGG₂, and leaves the COX active site to be further reduced to PGH₂ in the peroxide active site (**Figure 1-6**).^{26, 56, 60, 67, 73}

After enzymatic production of the instable PGH₂ precursor, various synthases produce the final pro-inflammatory regulators. Prostaglandins PGE₂, PGF₂, and PGD₂ are produced by prostaglandin synthase E, prostaglandin synthase F, or prostaglandin synthase D, respectively. Prostacyclins, like PGI₂ are produced from PGH₂ by prostacyclin synthase; and thromboxanes are produced from PGH₂ by thromboxane synthases (**Figure 1-7**).^{26, 62, 67} Concentrations of the lipid regulators are therefore also dependent on tissue-specific concentrations of these synthases.⁶²

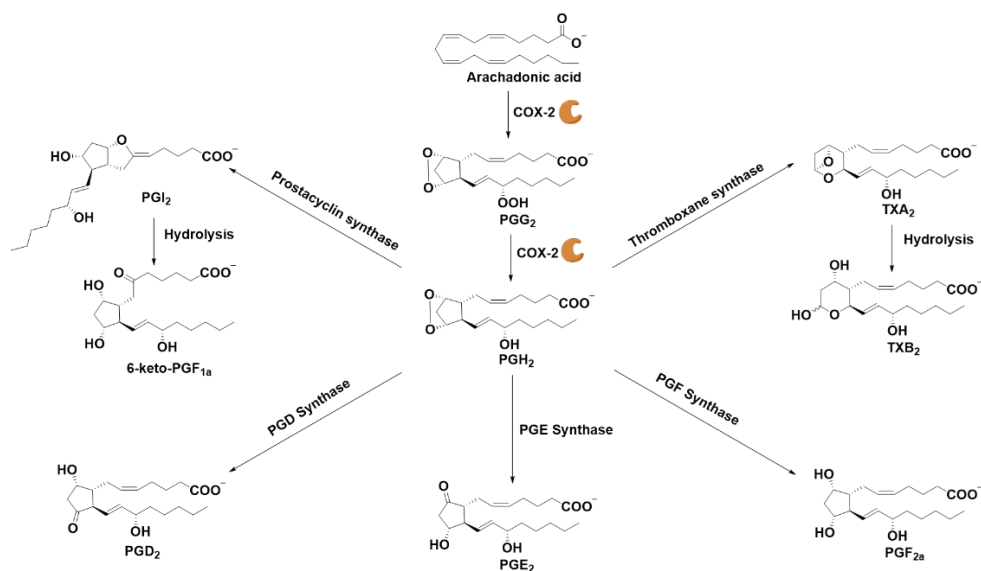


Figure 1-7 Synthesis of various pro-inflammatory chemokines from the general COX-2 derived precursor PGH₂. Figure was modified from Rouzer *et al.* 2011.²⁶

1.7 Chemical methods to study lipid biology

This thesis follows a multi-disciplinary approach to unravel the anti-inflammatory properties, a manifold of interactions, and the metabolic fate of DHEA by combining a variety of biological techniques with chemical methodologies and novel chemical probes. In this section, a brief introduction of bio-orthogonal chemistry, click reactions, and the use of chemical probes is given.

1.7.1 Bio-orthogonal chemistry

To further unravel chemical interactions between (bio)molecules in their complex biological environment, bio-orthogonal reactions have been developed. Such reactions do not interact with biological molecules, nor interfere with biological and cellular processes,⁷⁴⁻⁷⁵ thereby allowing accurate study of the molecular basis of biological processes. The concept of bio-orthogonal reactions was initiated by Bertozzi and coworkers, who first developed a methodology to selectively visualize azide-containing glycan moieties using a fluorescent tag.⁷⁶ For this, a Staudinger ligation was initially applied to link the fluorescent tag to the azide-enriched glycans (**Figure 1-8A**). The impact and potential of this first bio-orthogonal chemical methodology led to the rapid expansion of the chemical bio-orthogonal toolbox and the advancement of chemical biology. Nowadays, bio-orthogonal reactions are widely used in many -omics-based interaction studies, but also for the chemical engineering of therapeutic proteins.⁷⁷ Most currently used bio-orthogonal reactions avoid the slow rates of the Staudinger ligation, and rely on fast cycloaddition reactions between two bio-orthogonal moieties and strain release as driving force.^{75, 77-78}

1.7.2 Click chemistry

The term 'click chemistry' originates from early 2000 when Sharpless and coworkers defined a set of stringent criteria for the production of novel heteroatom-linked (C-X-C) products.⁷⁹ Most notable criteria require that click reactions are modular, wide in scope, high yielding, stereospecific, simple, and contain high thermodynamic driving forces. Following this definition of click chemistry, Sharpless and Meldal noted the potential semi-bio-orthogonal use of the Huisgens 1,3-dipolar cycloaddition of azides with linear alkynes. Both groups independently and simultaneously reported the dramatic rate enhancement of this reaction after the addition of a Cu(I) catalyst (**Figure 1-8B**).^{75, 80-81} Today, this so-called copper-mediated azide-alkyne click reaction (CuAAC) is one of the most widely applied click reactions in all fields of chemistry. The use of this classical CuAAC reaction in biological settings is, however, limited by the cytotoxic properties of the transition metal catalyst. In an endeavor to increase the bio-orthogonal scope of azide alkyne click chemistry, Bertozzi and coworkers used a strained cyclooctyne that readily reacted with azides without displaying any apparent cytotoxicity (**Figure 1-8C**).⁸² Inspired by the potential of this [3+2] cycloaddition, commonly referred to as the strain-promoted azide alkyne click (SPAAC) reaction, new strain-promoted alkynes were developed to improve the water solubility of the constructs and products, and to increase the reaction kinetics.⁷⁵

Although the CuAAC and SPAAC reaction are among the earliest identified click reactions, the scope of click reactions rapidly expanded in the last decade. Currently,

click reactions also include *e.g.*, inverse electron demand Diels-Alder (IEDDA) reactions, [4+1] cycloadditions with isonitriles, and SuFEX reactions, all of which are summarized in several recent reviews.⁷⁷⁻⁷⁸ Interestingly, apart from using unnatural functional groups for click chemistry, certain biologically relevant functional groups can also be used as or converted into one of the two reacting components in click chemistry.⁷⁸

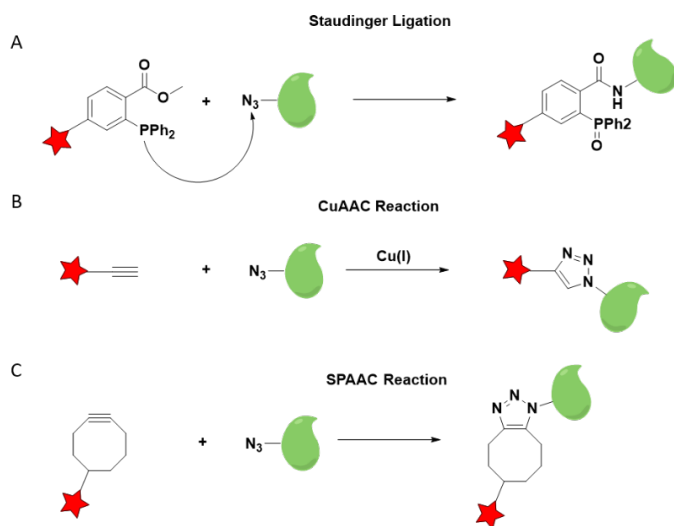


Figure 1-8 Overview of classical bio-orthogonal and click reactions. (A) Staudinger ligation, (B) CuAAC reaction, (C) SPAAC reaction.

1.7.3 Chemical probes

For a detailed study of biological molecular mechanisms, precisely tailored chemical probes have proven particularly useful. Such probes are synthetic congeners of biomolecules that contain all relevant functionalities found in the biologically active moiety, but now enriched with one or more functional group(s) that were designed to unravel the role of the (bio)molecule in its natural biological context. One of the main goals of these probes is that they are readily incorporated into the cellular systems of the natural lead structure, despite the presence of the unnatural functional groups. For example, the clickable handles that are often incorporated for enrichment or visualization purposes, only allow researchers to study their biological interaction(s) in a meaningful manner if the behavior of the probe resembles that of the native (bio)molecule closely. However, it is also crucial that, upon exposure to click conditions, the chemical probes efficiently react with molecules that contain additional functionalities, such as fluorescent labels or a biotin moiety. Of these, reaction of the chemical probe to a fluorescent label gives the researcher a ‘snapshot’ of the localization of the chemical probe, whereas reaction with a biotin-containing moiety allows the researcher to perform an affinity-based purification protocol to identify potential biological interactions of the chemical probe.

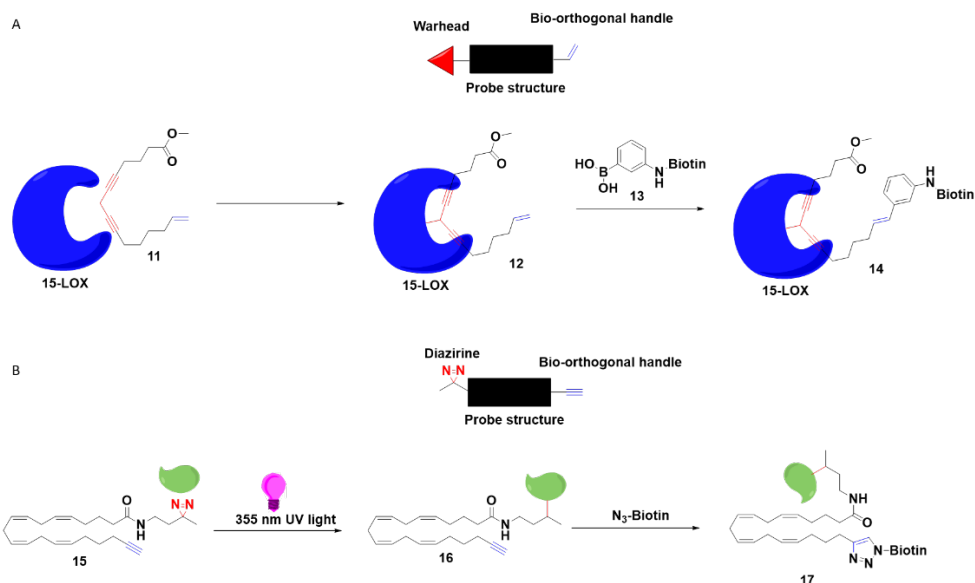


Figure 1-9 Overview of two commonly used designs for chemical probes, each illustrated with a recent literature example. (A) Activity-based protein profiling probe for 15-LOX, reported by the group of Dekker and coworkers.⁸⁴ (B) Diazirine-based chemical probe for the characterization of arachidonic acid binding proteins, reported by the group of Cravatt and coworkers.⁸⁸

As illustration for the general design, a chemical probe used for so-called activity-based protein profiling (ABPP) is shown (**Figure 1-9A**). In ABPP, the chemical probe consists of a reactive group, which is often called warhead, that is combined with a bio-orthogonal handle. These are used for the covalent attachment of the probe to its biological interaction partner and subsequent reaction with a functionality of interest, respectively.^{83–86} An example of a lipid-based ABPP is the bis(alkyne) 15-LOX probe **11**, which covalently attaches to the catalytic site of 15-LOX to generate compound **12**. Subsequent purification was facilitated by the terminal alkene using an oxidative Heck reaction to biotin-functionalized boronic acid **13**, to give biotinylated product **14** (**Figure 1-9A**).⁸⁴ Alternatively, bi-functional chemical probes can also be used to characterize unknown binding interactions with biomolecules. For this, probes are equipped with a photo-activatable group, *e.g.*, diazirine, to covalently attach the probe molecule to its intracellular interaction partner. Diazirines are small photo-activatable handles that form reactive carbenes when irradiated with light of around 355 nm wavelength. Major advantages for the use of diazirines are their relatively small size, sufficient stability towards biological nucleophiles and biological conditions when in the dark, and the short lifetime of the extremely reactive carbenes that are generated upon irradiation. Several diazirine-based chemical lipid probes, including compound **15** for arachidonic

acid, have successfully been used to characterize novel protein interactions (compound **16** and **17**, **Figure 1-9B**).⁸⁷⁻⁸⁸

Although, the use of chemical and bi-functional chemical probes has increased our current level of understanding of many chemical biological interactions, it is important to realize that these probes do contain small chemical deviations when compared to the natural (bio)molecule. Ideally, the chemical perturbations should be as small as possible and the entire probe should closely imitate the biological activity of its natural congener.⁷⁵ To exemplify that chemical alterations can lead to different biological regulation when compared to its natural congener, alkyne-derived arachidonic acid (aAA) showed different metabolic properties when compared to its natural AA counterpart. Especially, its reactivity towards the oxidative enzymes COX-2, 12-LOX, and 5-LOX was reduced, and the aAA-derived COX-2 products were different from oxidation profiles seen for AA, *i.e.*, a complex mixture of alkynyl prostaglandins, alkynyl 11-hydroxy-eicosatetraenoic acid, and alkynyl 11-hydroxy-8,9-epoxy-eicosatrienoic acid were identified.⁸⁹⁻⁹⁰ This example clearly illustrates the importance of the design of a chemical probe, proper evaluation of its biological behavior, and close comparison to that of the natural counterpart.

1.8 Aim of the thesis

Previously the endocannabinoid DHEA showed strong anti-inflammatory effects in LPS-stimulated RAW264.7 macrophages.^{50, 91} Interestingly, these anti-inflammatory effects were significantly more potent than those of its *n*-3 PUFA precursor DHA.⁹¹ These effects make DHEA an interesting metabolite from a nutritional perspective, since increased intake of DHA, through *e.g.*, fatty fish like tuna, mackerel, and salmon, or fish oil^{19, 92} leads to increased DHEA levels in the tissue and blood of animals.^{57, 92-93} The aim of the work described in this thesis was to further unravel the mechanisms of the anti-inflammatory effects of DHEA. To this end, synthetic bi-functional chemical probes of DHEA were used to study the interactions between DHEA and cellular proteins during inflammation. Affinity-based protein purification followed by proteomics was used to characterize the protein interaction partners of DHEA (and AEA). Apart from cell-wide interactions, the second main goal was to explore the specific interaction between COX-2 and DHEA. Based on the previous observation that prostaglandin concentrations are decreased by DHEA with barely affected COX-2 expression levels,⁵⁰ it was hypothesized that DHEA could act as a competitive substrate for AA in COX-2, resulting in the production of novel DHEA-derived immune-regulators. This hypothesis was verified in the work outlined in this thesis and the immune-regulating effect and metabolic

consequences of this new metabolic route were studied. Hopefully, the insights from this thesis could contribute to an increased understanding of the effects of *n*-3 PUFA metabolism on the resolution of inflammation. Ultimately, new insights from this field might be used to develop novel treatments and/or dietary regulations to treat and prevent the abundance of (chronic) inflammatory diseases in the future.

1.9 Outline of the thesis

In **Chapter 2** a state-of-the-art literature overview is given on the interplay between PUFAs, endocannabinoids, and inflammation. Additionally, it introduces some novel chemical tools (*e.g.*, chemical probes) that can be used to study molecular interaction partners of lipids.

In **Chapter 3** bi-functional chemical probes of DHEA were synthesized and used to characterize the molecular interaction targets of DHEA in LPS-stimulated RAW264.7 macrophages. ELISA assays showed that DHEA probes had similar anti-inflammatory effects as their DHEA parent, indicating that the chemical modifications on the probe did not alter their biological interactions. Confocal microscopy with fluorescently labelled probes showed that the probes were effectively taken up by RAW264.7 macrophages and resulted in a localization pattern that is consistent with ER and vesicle localization. Subsequent proteomics analysis revealed that 62 proteins significantly interacted with the DHEA probe. Peroxiredoxin-1 and peroxiredoxin-4, as well as Ras-related proteins 1 and 5, cyclooxygenase 2, and proteins involved in small GTPase signaling were identified as DHEA binding targets. Characterization of these proteins could be linked with previously described regulatory roles in ROS production, cell migration, cytoskeletal remodeling, and reduction in prostaglandin production.

In **Chapter 4** the interaction between *n*-3 PUFA ethanolamine derived metabolites and COX-2 is described. We showed for the first time that the EPEA and DHEA are converted by hCOX-2. EPEA is metabolized into PGE₃-EA, 11-, 14-, and 18-HEPE-EA, and DHEA is metabolized into 13-HDHEA, and 16-HDHEA. Additionally, *in vitro* studies were used to show that the metabolites of DHEA could also be produced in LPS-induced RAW264.7 macrophages in a COX-2 dependent mechanism, further underlining the biological relevance of this novel metabolic route.

In **Chapter 5** the hypothesized anti-inflammatory roles of 13-HDHEA and 16-HDHEA were studied. Cytokine analysis, LC-MS/MS based targeted lipidomic analyses, and transcriptional analysis were used to demonstrate that 13-HDHEA and 16-HDHEA have

interesting immune-modulatory roles in LPS-stimulated RAW264.7 macrophages. Nonetheless, compared to the parent compound DHEA, the metabolites 13-HDHEA and 16-HDHEA were less potent, suggesting that 13- and 16-HDHEA may be products of an DHEA inactivation route.

In **Chapter 6** the anti-inflammatory effects of intraperitoneally injected DHEA in a mouse model of colitis were studied. In the model C57Bl/6 mice with DSS-induced colitis were treated with intraperitoneally injected DHEA, which reduced several symptoms of colitis, like body weight loss, rectal bleeding and loose stool. Nonetheless, DHEA injection did not significantly reduce colon inflammation. Livers of the DHEA injected and DSS administered mice were further analyzed using LC-MS/MS to study DHEA uptake and metabolism *in vivo*. Identification of DHEA-derived metabolites, like the COX-2 derived 13-HDHEA and 16-HDHEA, and CYP450 derived 10,11-EDP-EA and 19,20-EDP-EA, as well as quantification of DHEA and AEA was performed. Although systemic availability of DHEA in the liver was increased with increasing dose of DHEA, DHEA- derived metabolites from, *e.g.*, COX-2 in the liver could not be detected. This may be explained by the limited expression of COX-2 in the livers of DSS colitis mice. In **Chapter 7** the main results of the current research are discussed and placed into context in the fields of nutrition, and inflammation. Next to this, the chapter will describe alternative research avenues and future perspectives.

1.9 References

1. Mikkelsen, K.; Stojanovska, L.; Polenakovic, M.; Bosevski, M.; Apostolopoulos, V., Exercise and mental health. *Maturitas* **2017**, *106*, 48-56.
2. Chekroud, S. R.; Gueorguieva, R.; Zheutlin, A. B.; Paulus, M.; Krumholz, H. M.; Krystal, J. H.; Chekroud, A. M., Association between physical exercise and mental health in 1.2 million individuals in the USA between 2011 and 2015: a cross-sectional study. *Lancet Psychiatry* **2018**, *5* (9), 739-746.
3. Lee, I. M.; Shiroma, E. J.; Lobelo, F.; Puska, P.; Blair, S. N.; Katzmarzyk, P. T., Effect of physical inactivity on major non-communicable diseases worldwide: an analysis of burden of disease and life expectancy. *Lancet* **2012**, *380* (9838), 219-229.
4. Anderson, E.; Durstine, J. L., Physical activity, exercise, and chronic diseases: A brief review. *Sports Med. Health Sci.* **2019**, *1* (1), 3-10.
5. Witkamp, R. F.; van Norren, K., Let thy food be thy medicine....when possible. *Eur. J. Pharmacol.* **2018**, 836, 102-114.
6. Brink, E.; van Rossum, C.; Postma-Smeets, A.; Stafleu, A.; Wolvers, D.; van Dooren, C.; Toxopeus, I.; Buurma-Rethans, E.; Geurts, M.; Ocké, M., Development of healthy and sustainable food-based dietary guidelines for the Netherlands. *Public Health Nutr.* **2019**, *22* (13), 2419-2435.
7. Cena, H.; Calder, P. C., Defining a Healthy Diet: Evidence for the Role of Contemporary Dietary Patterns in Health and Disease. *Nutrients* **2020**, *12* (2), 334.
8. Cardenas, D., Let not thy food be confused with thy medicine: The Hippocratic misquotation. *e-SPEN Journal* **2013**, *8* (6), e260-e262.
9. Tountas, Y., The historical origins of the basic concepts of health promotion and education: the role of ancient Greek philosophy and medicine. *Health Promot. Int.* **2009**, *24* (2), 185-192.
10. Wang, T. Y.; Liu, M.; Portincasa, P.; Wang, D. Q. H., New insights into the molecular mechanism of intestinal fatty acid absorption. *Eur J Clin Invest* **2013**, *43* (11), 1203-1223.
11. IUPAC. Compendium of Chemical Terminology, 2nd ed. (the "Gold Book"). Compiled by A. D. McNaught and A. Wilkinson. Blackwell Scientific Publications, Oxford (1997). Online version (2019-) created by S. J. Chalk. ISBN 0-9678550-9-8. <https://doi.org/10.1351/goldbook..>
12. Berg, J. M.; Tymoczko, J. L.; Stryer L. *Biochemistry*, 7th edition. W.H. Freeman & Company, **2010**.
13. E., V, An Etymological Dictionary of Chemistry and Mineralogy. *Nature* **1929**, *124* (3134), 789-790.
14. Lewkowitsch, J., Chemical Technology and Analysis of Oils, Fats, and Waxes. *Nature* **1913**, *92* (2303), 449-449.
15. Martin, S. A.; Brash, A. R.; Murphy, R. C., The discovery and early structural studies of

- arachidonic acid. *J. Lipid Res.* **2016**, *57*(7), 1126-1132.
16. Brunsvel, L.; Waldmann, H.; Huster, D., Membrane binding of lipidated Ras peptides and proteins – The structural point of view. *Biochim.Biophys. Acta Biomembr.* **2009**, *1788* (1), 273-288.
 17. Glatz, J. F. C., Lipids and lipid binding proteins: A perfect match. *Prostaglandins Leukot. Essent. FattyAcids* **2015**, *93*, 45-49.
 18. Serhan, C. N.; Levy, B. D., Resolvins in inflammation: emergence of the pro-resolving superfamily of mediators. *J. Clin. Investig.* **2018**, *128*(7), 2657-2669.
 19. Meijerink, J.; Balvers, M. G. J.; Witkamp, R. F., N-acyl amines of docosahexaenoic acid and other n-3 polyunsaturated fatty acids – from fishy endocannabinoids to potential leads. *Br. J. Pharmacol.* **2013**, *169*(4), 772-783.
 20. Prusakiewicz, J. J.; Turman, M. V.; Vila, A.; Ball, H. L.; Al-Mestarihi, A. H.; Marzo, V. D.; Marnett, L. J., Oxidative metabolism of lipoamino acids and vanilloids by lipoxygenases and cyclooxygenases. *Arch. Biochem. Biophys.* **2007**, *464*(2), 260-268.
 21. Porter, N. A., A Perspective on Free Radical Autoxidation: The Physical Organic Chemistry of Polyunsaturated Fatty Acid and Sterol Peroxidation. *J. Org. Chem.* **2013**, *78* (8), 3511-3524.
 22. Pertwee, R. G.; Howlett, A. C.; Abood, M. E.; Alexander, S. P. H.; Di Marzo, V.; Elphick, M. R.; Greasley, P. J.; Hansen, H. S.; Kunos, G.; Mackie, K.; et al., International Union of Basic and Clinical Pharmacology. LXXIX. Cannabinoid Receptors and Their Ligands: Beyond CB1 and CB2. *Pharmacol. Rev.* **2010**, *62*(4), 588-631.
 23. Witkamp, R., Fatty acids, endocannabinoids and inflammation. *Eur. J. Pharmacol.* **2016**, *785*, 96-107.
 24. Mechoulam, R.; Fride, E.; Di Marzo, V., Endocannabinoids. *Eur. J. Pharmacol.* **1998**, *359* (1), 1-18.
 25. Baggelaar, M. P.; Maccarrone, M.; van der Stelt, M., 2-Arachidonoylglycerol: A signaling lipid with manifold actions in the brain. *Prog. Lipid Res.* **2018**, *71*, 1-17.
 26. Rouzer, C. A.; Marnett, L. J., Endocannabinoid Oxygenation by Cyclooxygenases, Lipoxygenases, and Cytochromes P450: Cross-Talk between the Eicosanoid and Endocannabinoid Signaling Pathways. *Chem. Rev.* **2011**, *111* (10), 5899-5921.
 27. Ueda, N.; Tsuboi, K.; Uyama, T., Chapter 8 - Metabolic Enzymes for Endocannabinoids and Endocannabinoid-Like Mediators. In *The Endocannabinoidome*, Di Marzo, V.; Wang, J., Eds. Academic Press: Boston, **2015**; 111-135.
 28. Dempsey, D. R.; Jeffries, K. A.; Anderson, R. L.; Carpenter, A.-M.; Rodriguez Opsina, S.; Merkler, D. J., Identification of an arylalkylamine N-acyltransferase from *Drosophila melanogaster* that catalyzes the formation of long-chain N-acylserotonins. *FEBS Lett.* **2014**, *588*(4), 594-599.
 29. Jeffries, K. A.; Dempsey, D. R.; Behari, A. L.; Anderson, R. L.; Merkler, D. J., *Drosophila melanogaster* as a model system to study long-chain fatty acid amide metabolism. *FEBS*

- Lett.* **2014**, *588* (9), 1596-1602.
30. Kim, H.-Y.; Spector, A. A., N-Docosahexaenylethanolamine: A neurotrophic and neuroprotective metabolite of docosahexaenoic acid. *Mol. Aspects Med.* **2018**, *64*, 34-44.
 31. Ueda, N.; Tsuboi, K.; Uyama, T., Enzymological studies on the biosynthesis of N-acylethanolamines. *Biochim. Biophys. Acta Mol. Cell Biol. Lipids* **2010**, *1801* (12), 1274-1285.
 32. Leishman, E.; Mackie, K.; Luquet, S.; Bradshaw, H. B., Lipidomics profile of a NAPE-PLD KO mouse provides evidence of a broader role of this enzyme in lipid metabolism in the brain. *Biochim. Biophys. Acta Mol. Cell Biol. Lipids* **2016**, *1861* (6), 491-500.
 33. Simon, G. M.; Cravatt, B. F., Anandamide Biosynthesis Catalyzed by the Phosphodiesterase GDE1 and Detection of Glycerophospho-N-acyl Ethanolamine Precursors in Mouse Brain. *J. Biol. Chem.* **2008**, *283* (14), 9341-9349.
 34. Simon, G. M.; Cravatt, B. F., Characterization of mice lacking candidate N-acyl ethanolamine biosynthetic enzymes provides evidence for multiple pathways that contribute to endocannabinoid production in vivo. *Mol. Biosyst.* **2010**, *6* (8), 1411-1418.
 35. Liu, J.; Wang, L.; Harvey-White, J.; Osei-Hyiaman, D.; Razdan, R.; Gong, Q.; Chan, A. C.; Zhou, Z.; Huang, B. X.; Kim, H.-Y.; et al., A biosynthetic pathway for anandamide. *Proc. Natl. Acad. Sci. U.S.A.* **2006**, *103* (36), 13345.
 36. Alhouayek, M.; Botteman, P.; Makriyannis, A.; Muccioli, G. G., N-acylethanolamine-hydrolyzing acid amidase and fatty acid amide hydrolase inhibition differentially affect N-acylethanolamine levels and macrophage activation. *Biochim. Biophys. Acta Mol. Cell Biol. Lipids* **2017**, *1862* (5), 474-484.
 37. Sun, Y.-X.; Tsuboi, K.; Zhao, L.-Y.; Okamoto, Y.; Lambert, D. M.; Ueda, N., Involvement of N-acylethanolamine-hydrolyzing acid amidase in the degradation of anandamide and other N-acylethanolamines in macrophages. *Biochim. Biophys. Acta Mol. Cell Biol. Lipids* **2005**, *1736* (3), 211-220.
 38. Fonseca, B. M.; Costa, M. A.; Almada, M.; Correia-da-Silva, G.; Teixeira, N. A., Endogenous cannabinoids revisited: A biochemistry perspective. *Prostaglandins Other Lipid Mediat.* **2013**, *102-103*, 13-30.
 39. Urquhart, P.; Nicolaou, A.; Woodward, D. F., Endocannabinoids and their oxygenation by cyclo-oxygenases, lipoxygenases and other oxygenases. *Biochim. Biophys. Acta Mol. Cell Biol. Lipids* **2015**, *1851* (4), 366-376.
 40. Alhouayek, M.; Muccioli, G. G., COX-2-derived endocannabinoid metabolites as novel inflammatory mediators. *Trends Pharmacol.* **2014**, *35* (6), 284-292.
 41. Watson, J. E.; Kim, J. S.; Das, A., Emerging class of omega-3 fatty acid endocannabinoids & their derivatives. *Prostaglandins Other Lipid Mediat.* **2019**, *143*, 106337.
 42. Janeway, C. A; Travers, P.; Walport, M.; Shlomchik, M., *Immunobiology, 5th edition*. Garland Publishing: New York, **2001**.
 43. Kuhns, D. B.; Priel, D. A. L.; Chu, J.; Zarembek, K. A., Isolation and Functional Analysis of

- Human Neutrophils. *Curr. Protoc. Immunol.* **2015**, *111*, 7.23.1-7.23.16.
44. Schett, G.; Neurath, M. F., Resolution of chronic inflammatory disease: universal and tissue-specific concepts. *Nat. Commun.* **2018**, *9*(1), 3261.
 45. Lu, Y.-C.; Yeh, W.-C.; Ohashi, P. S., LPS/TLR4 signal transduction pathway. *Cytokine* **2008**, *42*(2), 145-151.
 46. Park, B. S.; Lee, J. O., Recognition of lipopolysaccharide pattern by TLR4 complexes. *Exp Mol Med* **2013**, *45*(12), e66.
 47. Kawai, T.; Akira, S., Signaling to NF- κ B by Toll-like receptors. *Trends. Mol. Med.* **2007**, *13*(11), 460-469.
 48. Takeda, K.; Akira, S., Toll-like receptors in innate immunity. *Int. Immunol.* **2005**, *17*(1), 1-14.
 49. Taciak, B.; Białasek, M.; Braniewska, A.; Sas, Z.; Sawicka, P.; Kiraga, Ł.; Rygiel, T.; Król, M., Evaluation of phenotypic and functional stability of RAW 264.7 cell line through serial passages. *PLoS ONE* **2018**, *13*(6), e0198943-e0198943.
 50. Meijerink, J.; Poland, M.; Balvers, M. G. J.; Plastina, P.; Lute, C.; Dwarkasing, J.; van Norren, K.; Witkamp, R. F., Inhibition of COX-2-mediated eicosanoid production plays a major role in the anti-inflammatory effects of the endocannabinoid N-docosahexaenoyl ethanolamine (DHEA) in macrophages. *Br. J. Pharmacol.* **2015**, *172*(1), 24-37.
 51. Hwang, D.; Jang, B. C.; Yu, G.; Boudreau, M., Expression of mitogen-inducible cyclooxygenase induced by lipopolysaccharide: Mediation through both mitogen-activated protein kinase and nf-kb signaling pathways in macrophages. *Biochem. Pharmacol.* **1997**, *54*(1), 87-96.
 52. Buckley, C. D.; Gilroy, D. W.; Serhan, C. N., Proresolving Lipid Mediators and Mechanisms in the Resolution of Acute Inflammation. *Immunity* **2014**, *40*(3), 315-327.
 53. Serhan, C. N.; Chiang, N.; Van Dyke, T. E., Resolving inflammation: dual anti-inflammatory and pro-resolution lipid mediators. *Nat. Rev. Immunol.* **2008**, *8*(5), 349-361.
 54. Xiao, T. S., Innate immunity and inflammation. *Cell. Mol. Immunol.* **2017**, *14*(1), 1-3.
 55. Zarghi, A.; Arfaei, S., Selective COX-2 Inhibitors: A Review of Their Structure-Activity Relationships. *Iran. J. Pharm. Res.* **2011**, *10*(4), 655-683.
 56. Smith, W. L.; Malkowski, M. G., Interactions of fatty acids, nonsteroidal anti-inflammatory drugs, and coxibs with the catalytic and allosteric subunits of cyclooxygenases-1 and -2. *J. Biol. Chem.* **2019**, *294*(5), 1697-1705.
 57. Balvers, M. G. J.; Verhoeckx, K. C. M.; Bijlsma, S.; Rubingh, C. M.; Meijerink, J.; Wortelboer, H. M.; Witkamp, R. F., Fish oil and inflammatory status alter the n-3 to n-6 balance of the endocannabinoid and oxylipin metabolomes in mouse plasma and tissues. *Metabolomics* **2012**, *8*(6), 1130-1147.
 58. Calder, P. C., Omega-3 polyunsaturated fatty acids and inflammatory processes: nutrition or pharmacology? *Br. J. Clin. Pharmacol.* **2013**, *75*(3), 645-662.
 59. Calder, P. C., Omega-3 fatty acids and inflammatory processes: from molecules to man. *Biochem. Soc. Trans.* **2017**, *45*(5), 1105-1115.
 60. Smith, W. L.; DeWitt, D. L.; Garavito, R. M., Cyclooxygenases: Structural, Cellular, and

- Molecular Biology. *Annu. Rev. Biochem.* **2000**, *69*(1), 145-182.
61. Hashemi Goradel, N.; Najafi, M.; Salehi, E.; Farhood, B.; Mortezaee, K., Cyclooxygenase-2 in cancer: A review. *J. Cell. Physiol.* **2019**, *234* (5), 5683-5699.
 62. Ricciotti, E.; FitzGerald, G. A., Prostaglandins and Inflammation. *Arterioscler. Thromb. Vasc. Biol.* **2011**, *31* (5), 986-1000.
 63. Sharma, N. P.; Dong, L.; Yuan, C.; Noon, K. R.; Smith, W. L., Asymmetric acetylation of the cyclooxygenase-2 homodimer by aspirin and its effects on the oxygenation of arachidonic, eicosapentaenoic, and docosahexaenoic acids. *Mol. Pharmacol.* **2010**, *77*(6), 979-986.
 64. Lucido, M. J.; Orlando, B. J.; Vecchio, A. J.; Malkowski, M. G., Crystal Structure of Aspirin-Acetylated Human Cyclooxygenase-2: Insight into the Formation of Products with Reversed Stereochemistry. *Biochemistry* **2016**, *55*(8), 1226-1238.
 65. Kirkby, N. S.; Chan, M. V.; Zaiss, A. K.; Garcia-Vaz, E.; Jiao, J.; Berglund, L. M.; Verdu, E. F.; Ahmetaj-Shala, B.; Wallace, J. L.; Herschman, H. R.; et al., Systematic study of constitutive cyclooxygenase-2 expression: Role of NF- κ B and NFAT transcriptional pathways. *Proc. Natl. Acad. Sci. U.S.A.* **2016**, *113*(2), 434-439.
 66. Kirkby, N. S.; Zaiss, A. K.; Urquhart, P.; Jiao, J.; Austin, P. J.; Al-Yamani, M.; Lundberg, M. H.; MacKenzie, L. S.; Warner, T. D.; Nicolaou, A.; et al., LC-MS/MS Confirms That COX-1 Drives Vascular Prostacyclin Whilst Gene Expression Pattern Reveals Non-Vascular Sites of COX-2 Expression. *PLoS ONE* **2013**, *8*(7), e69524.
 67. Rouzer, C. A.; Marnett, L. J., Structural and functional differences between cyclooxygenases: Fatty acid oxygenases with a critical role in cell signaling. *Biochem. Biophys. Res. Commun.* **2005**, *338*(1), 34-44.
 68. Rouzer, C. A.; Marnett, L. J., Non-redundant Functions of Cyclooxygenases: Oxygenation of Endocannabinoids. *J. Biol. Chem.* **2008**, *283*(13), 8065-8069.
 69. Vecchio, A. J.; Malkowski, M. G., The Structural Basis of Endocannabinoid Oxygenation by Cyclooxygenase-2. *J. Biol. Chem.* **2011**, *286*(23), 20736-20745.
 70. Dong, L.; Vecchio, A. J.; Sharma, N. P.; Jurban, B. J.; Malkowski, M. G.; Smith, W. L., Human Cyclooxygenase-2 Is a Sequence Homodimer That Functions as a Conformational Heterodimer. *J. Biol. Chem.* **2011**, *286*(21), 19035-19046.
 71. Wada, M.; DeLong, C. J.; Hong, Y. H.; Rieke, C. J.; Song, I.; Sidhu, R. S.; Yuan, C.; Warnock, M.; Schmaier, A. H.; Yokoyama, C.; et al., Enzymes and Receptors of Prostaglandin Pathways with Arachidonic Acid-derived Versus Eicosapentaenoic Acid-derived Substrates and Products. *J. Biol. Chem.* **2007**, *282*(31), 22254-22266.
 72. Yuan, C.; Sidhu, R. S.; Kuklev, D. V.; Kado, Y.; Wada, M.; Song, I.; Smith, W. L., Cyclooxygenase Allosterism, Fatty Acid-mediated Cross-talk between Monomers of Cyclooxygenase Homodimers. *J. Biol. Chem.* **2009**, *284*(15), 10046-10055.
 73. Hermanson, D. J.; Gamble-George, J. C.; Marnett, L. J.; Patel, S., Substrate-selective COX-2 inhibition as a novel strategy for therapeutic endocannabinoid augmentation. *Trends Pharmacol.* **2014**, *35*(7), 358-367.

74. Sletten, E. M.; Bertozzi, C. R., Bioorthogonal Chemistry: Fishing for Selectivity in a Sea of Functionality. *Angew. Chem. Int. Ed.* **2009**, *48* (38), 6974-6998.
75. Sletten, E. M.; Bertozzi, C. R., From Mechanism to Mouse: A Tale of Two Bioorthogonal Reactions. *Accounts of Chemical Research* **2011**, *44* (9), 666-676.
76. Saxon, E.; Bertozzi, C. R., Cell Surface Engineering by a Modified Staudinger Reaction. *Science* **2000**, *287* (5460), 2007.
77. Smeenk, M. L. W. J.; Agramunt, J.; Bongers, K. M., Recent developments in bioorthogonal chemistry and the orthogonality within. *Current Opinion in Chemical Biology* **2021**, *60*, 79-88.
78. Albada, B.; Keijzer, J. F.; Zuilhof, H.; van Delft, F., Oxidation-Induced "One-Pot" Click Chemistry. *Chem. Rev.* **2021**, *121* (12), 7032-7058.
79. Kolb, H. C.; Finn, M. G.; Sharpless, K. B., Click Chemistry: Diverse Chemical Function from a Few Good Reactions. *Angew. Chem. Int. Ed.* **2001**, *40* (11), 2004-2021.
80. Rostovtsev, V. V.; Green, L. G.; Fokin, V. V.; Sharpless, K. B., A Stepwise Huisgen Cycloaddition Process: Copper(I)-Catalyzed Regioselective "Ligation" of Azides and Terminal Alkynes. *Angew. Chem. Int. Ed.* **2002**, *41* (14), 2596-2599.
81. Tornøe, C. W.; Christensen, C.; Meldal, M., Peptidotriazoles on Solid Phase: [1,2,3]-Triazoles by Regiospecific Copper(I)-Catalyzed 1,3-Dipolar Cycloadditions of Terminal Alkynes to Azides. *J. Org. Chem.* **2002**, *67* (9), 3057-3064.
82. Agard, N. J.; Prescher, J. A.; Bertozzi, C. R., A Strain-Promoted [3+2] Azide-Alkyne Cycloaddition for Covalent Modification of Biomolecules in Living Systems. *J. Am. Chem. Soc.* **2004**, *126* (46), 15046-15047.
83. Blankman, J. L.; Cravatt, B. F., Chemical Probes of Endocannabinoid Metabolism. *Pharmacol. Rev.* **2013**, *65* (2), 849-871.
84. Eleftheriadis, N.; Thee, S. A.; Zwinderman, M. R. H.; Leus, N. G. J.; Dekker, F. J., Activity-Based Probes for 15-Lipoxygenase-1. *Angew. Chem. Int. Ed.* **2016**, *55* (40), 12300-5.
85. Baggelaar, M. P.; van Esbroeck, A. C. M.; van Rooden, E. J.; Florea, B. I.; Overkleeft, H. S.; Marsicano, G.; Chaouloff, F.; van der Stelt, M., Chemical Proteomics Maps Brain Region Specific Activity of Endocannabinoid Hydrolases. *ACS Chem. Biol.* **2017**, *12* (3), 852-861.
86. van Esbroeck, A. C. M.; Varga, Z. V.; Di, X.; van Rooden, E. J.; Tóth, V. E.; Onódi, Z.; Kuśmierczyk, M.; Leszek, P.; Ferdinandy, P.; Hankemeier, T., et al., Activity-based protein profiling of the human failing ischemic heart reveals alterations in hydrolase activities involving the endocannabinoid system. *Pharmacol. Res.* **2020**, *151*, 104578.
87. Feltes, M.; Moores, S.; Gale, S. E.; Krishnan, K.; Mydock-McGrane, L.; Covey, D. F.; Ory, D. S.; Schaffer, J. E., Synthesis and characterization of diazirine alkyne probes for the study of intracellular cholesterol trafficking. *J. Lipid Res.* **2019**, *60* (3), 707-716.
88. Niphakis, M. J.; Lum, K. M.; Cognetta III, A. B.; Correia, B. E.; Ichu, T.-A.; Olucha, J.; Brown, S. J.; Kundu, S.; Piscitelli, F.; Rosen, H., et al., A Global Map of Lipid-Binding Proteins and Their Ligandability in Cells. *Cell* **2015**, *161* (7), 1668-1680.

89. Beavers, W. N.; Serwa, R.; Shimozu, Y.; Tallman, K. A.; Vaught, M.; Dalvie, E. D.; Marnett, L. J.; Porter, N. A., ω -Alkynyl Lipid Surrogates for Polyunsaturated Fatty Acids: Free Radical and Enzymatic Oxidations. *J. Am. Chem. Soc.* **2014**, *136* (32), 11529-11539.
90. Robichaud, P. P.; Poirier, S. J.; Boudreau, L. H.; Doiron, J. A.; Barnett, D. A.; Boilard, E.; Surette, M. E., On the cellular metabolism of the click chemistry probe 19-alkyne arachidonic acid. *J. Lipid Res.* **2016**, *57* (10), 1821-1830.
91. Meijerink, J.; Plastina, P.; Vincken, J.-P.; Poland, M.; Attya, M.; Balvers, M.; Gruppen, H.; Gabriele, B.; Witkamp, R. F., The ethanolamide metabolite of DHA, docosahexaenoylethanolamine, shows immunomodulating effects in mouse peritoneal and RAW264.7 macrophages: evidence for a new link between fish oil and inflammation. *Br. J. Nutr.* **2011**, *105* (12), 1798-1807.
92. Balvers, M. G. J.; Wortelboer, H. M.; Witkamp, R. F.; Verhoeckx, K. C. M., Liquid chromatography-tandem mass spectrometry analysis of free and esterified fatty acid N-acyl ethanolamines in plasma and blood cells. *Anal. Biochem.* **2013**, *434* (2), 275-283.
93. Balvers, M. G. J.; Verhoeckx, K. C. M.; Meijerink, J.; Bijlsma, S.; Rubingh, C. M.; Wortelboer, H. M.; Witkamp, R. F., Time-dependent effect of in vivo inflammation on eicosanoid and endocannabinoid levels in plasma, liver, ileum and adipose tissue in C57BL/6 mice fed a fish-oil diet. *Int. Immunopharmacol.* **2012**, *13* (2), 204-214.

Chapter 2

The role of *n*-3 PUFA derivatives and their oxygenated metabolites in the modulation of inflammation

This chapter was adapted from:

Ian de Bus,
Renger F. Witkamp,
Han Zuillhof,
Bauke Albada,
and Michiel G.J. Balvers

Prostaglandins and Other Lipid Mediators, **2019**, 144, 106351;
doi: 10.1016/j.prostaglandins

2.1 Abstract

Notwithstanding the ongoing debate on their full potential in health and disease, there is general consensus that *n*-3 PUFAs play important physiological roles. Increasing dietary *n*-3 PUFA intake results in increased DHA and EPA content in cell membranes as well as in an increase in *n*-3 derived oxylipin and endocannabinoid concentrations, like fatty acid amides and glycerol-esters. These shifts are (partly) explained by the pharmacological and anti-inflammatory effects of *n*-3 PUFAs. Recent studies discovered that *n*-3 PUFA-derived endocannabinoids can be further metabolized by the oxidative enzymes CYP450, LOX, and COX, similar to that of *n*-6 derived endocannabinoids. Interestingly, these oxidized *n*-3 PUFA derived endocannabinoids of eicosapentaenoyl ethanolamide (EPEA) and docosahexaenoyl ethanolamide (DHEA) have higher anti-inflammatory and anti-proliferative potential than their non-oxidized precursors. In this chapter, an overview of *n*-3 PUFA derivatives and their metabolites is provided. In addition, the use of chemical probes will be presented as a promising approach to study *n*-3 PUFA and *n*-3 PUFA metabolism within the field of lipid biochemistry.

2.2 Introduction to *n*-3 PUFAs in health and disease

There is general scientific consensus that *n*-3 long-chain poly unsaturated fatty acid (LC-PUFAs) are essential for normal growth and development of multicellular organisms. Notwithstanding this, the debate on their full potential to prevent or cure disease continues. A major cause of these apparent knowledge gaps is their complex versatile metabolism that is directly linked to numerous molecular interconnections and pathways involved in the formation and breakdown of PUFA-derived mediators. Main dietary *n*-3 LC-PUFAs are α -linolenic acid (ALA; 18:3*n*-3), predominantly obtained from plant sources, and the longer eicosapentaenoic acid (EPA; 20:5*n*-3), docosahexaenoic acid (DHA; 22:6*n*-3) and, to a lesser extent, docosapentaenoic acid (DPA; 22:5*n*-3). Those latter three fatty acids are particularly found in “fatty” fish (*e.g.*, herring, salmon, mackerel) as well as in certain types of algae and krill (**Figure 2-1**). In general, ALA can be converted to EPA by desaturation and subsequent elongation of the acyl chain of stearidonic acid (18:4*n*-3). Insertion of an extra double bond then results in the formation of EPA (20:5*n*-3). EPA can be further metabolized to DPA, and finally to DHA. However, in human adults the endogenous conversion of ALA to EPA and DHA is limited, and therefore we have to rely on dietary intake or on their administration via food supplements or pharmaceutical preparations for adequate provision of *n*-3 LC-PUFAs.¹⁻³

Intake of *n*-3 LC-PUFAs in particular DHA and/or EPA, has been associated with a variety of positive health effects. Examples include improvement of endothelial function,⁴⁻⁵ lowered plasma triglyceride levels,⁶ a reduced risk for ischemic stroke,⁷ neuroprotective and antidepressant effects,⁸⁻⁹ prevention of cognitive decline,¹⁰ positive effects in rheumatoid arthritis,¹¹⁻¹³ fatty liver disease,¹⁴⁻¹⁷ cancer-associated cachexia,¹⁸ and a possibly reduced risk for developing certain tumors, in particular colorectal cancer.¹⁹⁻²⁰ However, these apparently pleiotropic effects are continuously challenged, in particular when it comes to cardiovascular health. For example, the originally assumed antiarrhythmic effects of EPA and DHA are disputed.²¹ A recent meta-analysis²² and Cochrane review²³ raised doubt concerning the overall clinical usefulness of *n*-3 PUFAs for prevention of cardiovascular diseases. Data from a number of recently reported randomized controlled trials (RCTs) fueled the debate even further. The Tromsø study found no protective effects of fatty fish consumption or fish oil supplements on atherosclerotic plaque formation or plaque area in a general population.²⁴ Similarly, the more recent ASCEND study –an RCT among more than 15,000 patients with diabetes and no evidence of cardiovascular disease taking 460 mg of EPA and 380 mg of DHA for a median of 7 years– showed no significant difference from placebo in the risk of serious vascular events.²⁵ Another recently completed study, VITAL,²⁶⁻²⁷ also indicated that the use of *n*-3 PUFAs was not effective in preventing the combined end point

of myocardial infarction, stroke, or death from cardiovascular causes in unselected patients. By contrast, in persons already taking a statin, positive effects of high doses (4 g daily) of EPA on cardiovascular events in the randomized, double-blind REDUCE-IT trial were reported after a median follow-up of 4.9 years.^{26, 28-29} Several explanations were offered for these apparent discrepancies. For example, it has been suggested that administered dose, intake and presence of other fatty acids in the diet, like *n*-6 PUFAs, chemical differences between EPA and DHA, and inter-individual differences –such as polymorphisms, sex, and age– are also playing a role.^{26, 30-32}

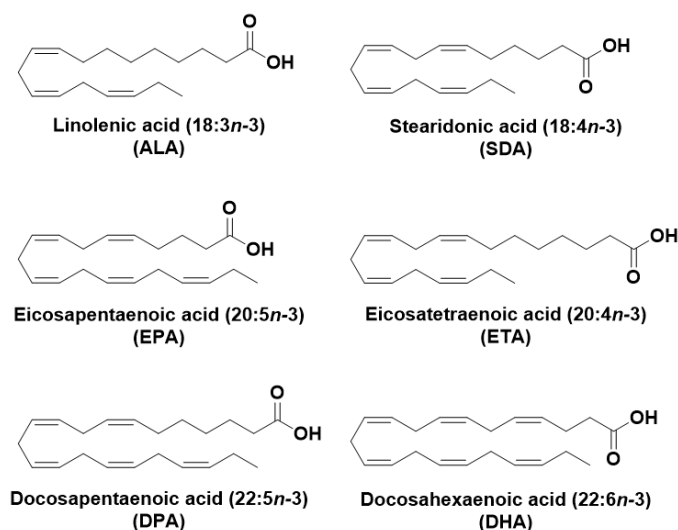


Figure 2-1 Chemical structures of main *n*-3 PUFAs.

Mechanistic studies *in vitro* and in rodent models indicate that many, though perhaps not all, activities of *n*-3 PUFAs found can be linked to their interaction with immunological mechanisms.^{2, 9} However, amounts used in those studies are often rather high, which complicates extrapolation to humans. Effects on inflammatory markers have been reported from human studies as well, although doses are sometimes high compared to those commonly obtained from the diet. The observed immune-modulating and/or anti-inflammatory effects have been explained from different mechanisms, *i.e.*, their effects on cell membranes and modulating eicosanoid production,^{2-3, 9} interactions with different receptors, including peroxidase proliferator activator receptors (PPARs), G-protein coupled receptor 40 (GPR40),³³ and GPR120.³⁴ Highly intriguing, and at the same time further complicating, are the roles of the different intermediates and metabolites of *n*-3 PUFAs. In recent years, many novel classes of endogenously produced *n*-3 LC-PUFA lipid metabolites with potent anti-inflammatory properties were identified. These exciting findings suggest the presence

of many more bio-active lipids than previously assumed, although for most of these metabolites an accurate identification of their specific role in inflammation is not yet fully established. More research is needed to shed light on both the formation as well as the bio-activity of those novel, including yet unknown, metabolites in the future.

2.3 Lipid metabolite profiles reflect dietary lipid intake: the relation between dietary *n*-3 fatty acid intake and *n*-3 fatty acid-derived endocannabinoids

Over the last decades, researchers tried to elucidate the molecular and cellular pathways through which dietary *n*-3 lipids affect health and physiology. A better understanding of the underlying mechanisms could not only help to explain the sometimes apparently contradictory findings, but potentially also provide new targets for intervention. Specifically, it has been demonstrated that *n*-3 fatty acids and their metabolites have various effects on different components of the immune system. For instance, DHA can be converted into resolvins and protectins, a class of lipid metabolites for which potent pro-resolving properties have been described.³⁵⁻³⁷ Additionally, work in animal and *in vitro* models demonstrated that dietary lipids directly affect circulating and tissue concentrations of various oxylipins. Typically, concentrations of *n*-6 fatty acid derived oxylipins, including prostaglandin D₂ (PGD₂), PGE₂, thromboxane B₂ (TXB₂) and 5-hydroxyeicosatetraenoic acid (5-HETE) decreased after a diet rich in *n*-3 fatty acids, whereas higher concentrations of *n*-3 derived oxylipins were detected after a diet rich in *n*-3 fatty acids.³⁸⁻⁴⁰ These *n*-3 derived metabolites were reported to have reduced pro-inflammatory activity compared to their *n*-6 derived counterparts, which could at least partly explain the anti-inflammatory effects observed for *n*-3 fatty acids (**Figure 2-2**).⁴¹ It thus seems clear that circulating profiles of lipid mediators are a reflection of dietary intake of fatty acids, and that high dietary intakes of *n*-3 fatty acids results in measurable changes in the lipidome, which may have physiological consequences.

In addition to oxylipins, many other classes of lipid-derived signaling molecules are known, such as ceramides, sphingolipids, and endocannabinoids. The latter compound class regulates various immune responses via the endocannabinoid system. This system consists of the cannabinoid type 1 and type 2 receptors, CB₁ and CB₂, their endogenous ligands ('endocannabinoids'), and the enzymes involved in the synthesis and metabolism of these molecules.⁴²⁻⁴³ It has become clear that the endocannabinoid system is involved in many physiological processes, including metabolism, appetite and the regulation of food intake, differentiation of adipose tissue, and immune regulation. The prototypical endocannabinoid, arachidonoyl ethanolamide (AEA,

also known as anandamide), is the conjugate of ethanolamine and arachidonic acid (AA; 20:4n-6),⁴⁴ but other AA conjugates such as 2-arachidonoylglycerol (2-AG) and *N*-arachidonoyl dopamine⁴⁵ (**Figure 2-3**), have also been described to possess affinity for the endocannabinoid receptors.^{18, 42, 45}

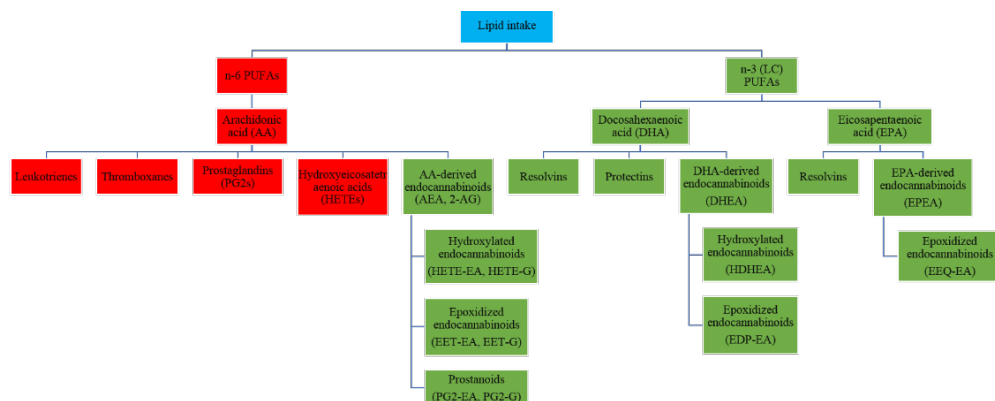


Figure 2-2 Overview of lipid profile and lipid metabolism. In red are the suggested pro-inflammatory regulators, in green the proposes less pro- or anti-inflammatory regulators. Changes in lipid intake can change the lipid profile in the body, which in turn may reduce pro-inflammatory responses and/or downregulate inflammatory processes.

In addition to variation in the conjugate group, also the fatty acid backbone is known to vary, and conjugates with various fatty acids have been detected in animals or humans, such as oleoyl ethanolamide (OEA), palmitoyl ethanolamide (PEA), oleoyl dopamine (OLDA) or *N*-arachidonoyl glycine (NAGly) (**Figure 2-3**).⁴⁶⁻⁴⁹ Interestingly, similar conjugates derived from DHA and EPA, including docosahexaenoyl ethanolamide (DHEA), eicosapentaoyl ethanolamide (EPEA), and eicosapentaoyl glycerol (2-EG) have also been detected in animals and humans (**Figure 2-3**).^{48, 50-53} Considering the number of different dietary fatty acids (*e.g.*, 16:0, C18:0, C18:1n-9), which can be multiplied by their conjugation to the available endogenous amines (*e.g.*, ethanolamine, dopamine, various amino acids), potentially >200 of these lipid metabolites may be formed. However, thus far only a few of these molecules have received detailed attention, such as AEA, 2-AG, OEA, PEA, DHEA and EPEA. This suggests that only the tip of the iceberg has been explored, and much more remains to be discovered. It is important to note that not all conjugates mentioned above have significant affinity for the CB receptors. Instead, these conjugates may activate other receptors such as (PPARs) or transient receptor potential channels (TRPs), which can sometimes also be activated by 'true' endocannabinoids, *i.e.*, ligands for the CB₁ or CB₂ receptors such as AEA.^{42, 54-}

⁵⁵ Taken together, endocannabinoids and their congeners behave as 'promiscuous' ligands, displaying patterns of receptor interactions which has been suggested to play a role in 'fine tuning' metabolic and inflammatory regulation.⁴¹ Indicative of this fine tuning is a comparative study on CB and TRPV receptor activation by various *N*-acyl ethanolamines, showing that all *n*-6 PUFA derivatives are agonists of the CB₁, CB₂, and TRPV1 receptor, whereas *n*-3 PUFA derivatives are much weaker CB₁ and TRPV1 agonists, and equally as effective CB₂ agonists.⁵⁶

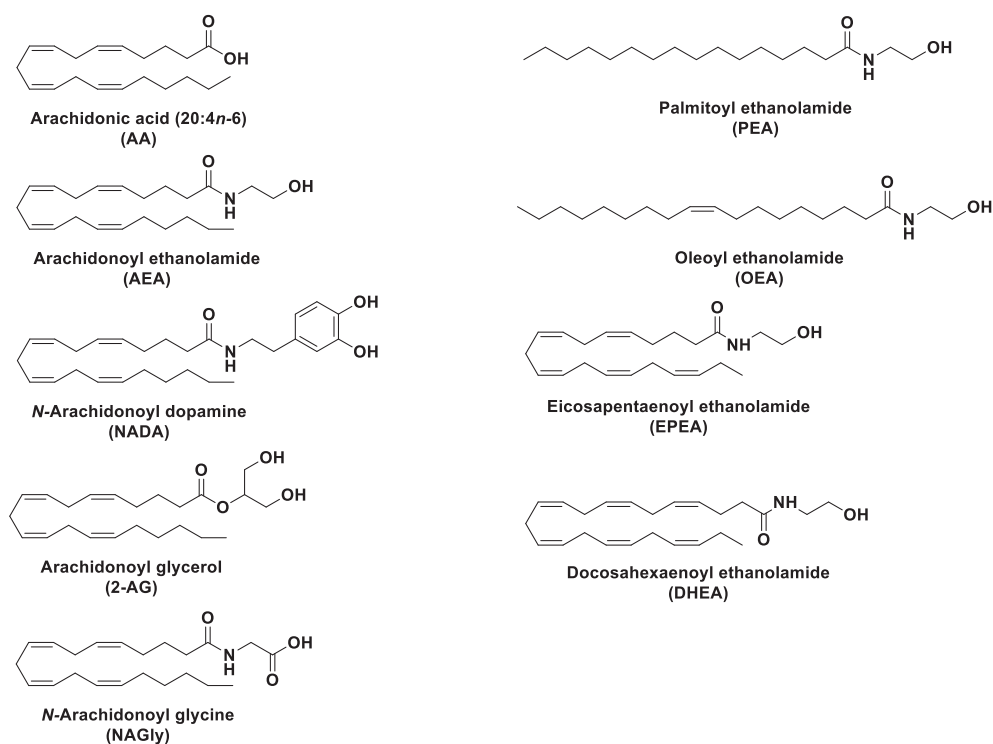


Figure 2-3 Chemical structures of well-known endocannabinoids and structurally related molecules. This family of lipids shows variation in both the lipid backbone as well as in the conjugate (e.g., glycerol, dopamine, ethanolamine, amino acid residues).

Several studies demonstrated that *n*-3 fatty acids affect endocannabinoid formation profiles and related compounds in a way similar as observed for oxylipins.⁵⁷ A large body of evidence, comprising of *in vitro*, animal and human data, underlines that increasing the supply of *n*-3 fatty acids results in decreased concentrations of, e.g., *n*-6 PUFA-derived AEA and 2-AG, whereas concentrations of DHEA and EPEA increase.^{50-51,}

^{53, 58-60} This profile shift remained present after an acute inflammatory stimulus with

lipopolysaccharide (LPS) in mice.⁵¹ Interestingly, when comparing the immune-modulating properties of DHEA and EPEA with those of their fatty acid precursors and other ethanolamides in an *in vitro* study, it was shown that especially DHEA has more potent anti-inflammatory properties compared to, *e.g.*, its precursor DHA and its *n*-6 congener AEA⁶¹. These findings suggest that a shift in endocannabinoid profile is one of the mechanisms behind the proposed, and sometimes observed, health effects of *n*-3 fatty acids (**Figure 2-2**).

2.4 *n*-3 Fatty acid-derived endocannabinoids: a new mechanistic link between dietary n-3 fatty acids and anti-inflammatory effects

The two most-studied *n*-3 fatty acid-derivatives to date are DHEA and EPEA (**Figure 2-3**). DHEA was first identified in bovine retina⁶² and later also in human plasma⁴⁸ and other tissues.^{50, 53, 63} Interestingly, this compound has potent anti-inflammatory properties in a variety of models, including stimulated 1) murine RAW264.7 and primary macrophages,⁶⁴ 2) murine 3T3-L1 adipocytes,⁵² and 3) murine BV2 and rat primary microglial cells.⁶⁵ DHEA reduces the release of various pro-inflammatory signaling molecules, including nitric oxide (NO), interleukin-6 (IL-6), monocyte chemotactic protein-1 (MCP-1), and tumor necrosis factor-alpha (TNF- α), although differences exist between different *in vitro* models. Additionally, it was found that DHEA promotes neurogenesis, neuron development, and synaptogenesis.⁶⁶⁻⁶⁸ Because of these properties, DHEA is also referred to as synaptamide.⁶⁶⁻⁶⁷ In a recent study, the G protein-coupled orphan receptor (GPR110) was found to play a key role in this neuro-protective activity of DHEA by activating a cAMP dependent pathway.⁶⁸⁻⁶⁹ Moreover, DHEA displays pro-apoptotic and anti-proliferating activity in human prostate cancer cells with considerably increased potency compared to its precursor fatty acid DHA. Less information is available for EPEA, but this conjugate was also found to possess anti-proliferating and pro-apoptotic effects, although with a distinct underlying mechanism compared to DHEA.⁵⁵ EPEA also displayed anti-inflammatory properties in macrophages and adipocytes, although with less potency compared to DHEA in macrophages.^{52, 64} Both DHEA and EPEA are agonists of the CB receptors and of PPAR- γ , which may mediate the observed anti-inflammatory effects.^{55-56, 70} To better understand the mechanisms through which DHEA exerts its anti-inflammatory effects in macrophages, detailed *in vitro* studies were performed, which provided evidence for a direct interaction between DHEA and the cyclooxygenase-2 (COX-2) enzyme.⁶¹ Using a targeted metabolomics approach that quantified various lipid oxygenation metabolites, it was concluded that DHEA specifically reduced the formation of COX-2 derived oxylipins, such as PGD₂ and PGE₂, whereas other pathways (*e.g.*, 5-lipoxygenase (5-LOX) or cytochrome P450 (CYP450)) were unaffected. These

findings suggested that DHEA might act as a direct competitive inhibitor of COX-2 activity. Interestingly, it was previously shown for, *e.g.*, AEA and 2-AG that they are COX-2 substrates,⁷¹⁻⁷² demonstrating that COX-2 has the capability to metabolize neutral lipids. COX-2 metabolized AEA and 2-AG to oxygenated fatty acid metabolites, such as prostaglandin E₂-ethanolamide (PGE₂-EA) and prostaglandin E₂-glycerol (PGE₂-G), respectively, which have potent anti-inflammatory properties *in vitro*.⁷³⁻⁷⁴ In addition to COX-2, other oxidative enzymes such as those belonging to lipoxygenases (LOX) and CYP450s can metabolize various fatty acid ethanolamides,⁷⁵ including DHEA,⁷⁶⁻⁷⁸ into oxygenated species which display biological activity themselves (see **section 2.5** and **Figure 2-2**). It is thus clear that the biological activity of endocannabinoids and related compounds is not only terminated by their enzymatic hydrolysis via fatty acid amide hydrolase (FAAH) or *N*-acylethanolamine-hydrolyzing acid amidase (NAAA),⁷⁹ but that these signaling molecules can also be metabolized by COX-2, LOX and CYP450s to yield new oxygenated fatty acid metabolites, likely displaying different biological roles.

2.5 Oxygenation of endocannabinoids: the first evidence of oxygenation of endocannabinoids by CYP450's, LOX, and COX-2 and the anti-inflammatory effects of their metabolites

The first evidence of oxygenation of the prototypical endocannabinoid AEA stems from 1995, showing that anandamide is metabolized by CYP450s in both mouse brain and liver microsomes.⁸⁰ Although an accurate product analysis was not performed, it was hypothesized that the CYP450 containing microsomes produced various mono-, di-hydroxylated, and epoxidized metabolites of AEA. More recent studies identified all four possible regioisomeric epoxyeicosatrienoic ethanolamides (EET-EAs) and a terminal hydroxylated epoxyeicosatrienoic ethanolamide 20-HETE-EA metabolite of AEA after conversion by various human CYP450s.⁸¹⁻⁸² Additionally, it was shown that at least 14,15-EET-EA was produced in bovine and porcine heart microsomes.⁸¹ Similar to the EET-EA production by CYP450 enzymes, it was reported in 1995 that 12-LOX from the rat pineal brain converts AEA into 12-HETE-EA, and that soybean 15-LOX produces 15-HETE-EA.⁸³ In 1999, COX-2, was also shown to oxygenate AEA, yielding prostamides (PG-EA's) and the mono-hydroxylated metabolites 11-HETE-EA and 15-HETE-EA.⁸⁴⁻⁸⁵ For the synthesis of the various prostamides known to date, the COX-2 intermediate PGH₂-EA is sequentially metabolized by specific prostaglandin synthases to form the biologically active PGE₂-EA, PGD₂-EA, PGI₂-EA,^{73-74, 86} and PGF₂α-EA (**Figure 2-4**).^{73-74, 87} Studies to assess the biological role of some of these prostamides have revealed several potent anti-inflammatory characteristics, specifically for the prostamides PGF₂α-EA and PGE₂-EA. For example, PGF₂α-EA was found to reduce crypt and mucosal tissue damage in a

colitis model,⁸⁸ and was found to specifically activate the heterodimers of the natural PGF receptor, and one of its splice variants FP-FPalt4.^{74, 89} PGE₂-EA reduces the TNF α production in a cAMP-dependent pathway in LPS-stimulated human peripheral blood mononuclear cell monocytes,⁵⁴ and inhibits the activity of the IL-12p40 promotor in LPS and INF γ stimulated microglia cells (**Figure 2-4**).⁹⁰

Studies investigating receptor affinities of epoxidated AEA metabolites suggested that EET-EAs are potent CB agonists.⁹¹ Specifically, 5,6-EET-EA has a 300-fold selectivity for CB₂ activation over CB₁ activation, and a 1000 times increased affinity for CB₂ when compared to AEA. Moreover, 5,6-EET-EA was shown to be an agonist of the human CB₂ receptor.⁹² In contrast to the EET-EAs, HETE-EAs display varying affinities towards the CB receptors. For example, 11-HETE-EA does not interact with CB₁ and CB₂, whereas 12-HETE-EA is an agonist for both receptors with affinities comparable to AEA.⁹³ 15-HETE-EA activated CB₁ receptors only slightly, but showed strong TRPV1 binding affinity. In view of this TRPV1 activation, it was suggested that 15-HETE-EA caused reduced nociception in a neuropathic pain model.⁹⁴ Whether the other HETE-EA are also strong agonists for TRPV1, and also affect neuropathic pain is currently unknown. At the same time, 15-HETE-EA enhanced AEA biosynthesis by NAPE-PLD, and reduced DAGL and FAAH activity. As a result, 15-HETE-EA thus increased AEA tone in mouse brain homogenates (**Figure 2-4**).⁹⁵ Like 15-HETE-EA, all other HETE-EAs are also known to be inhibitors of FAAH, although with different potencies.⁹³ Flamand and coworkers speculated that the HETE-EAs mainly exert their biological effect via the vanilloid receptors,⁹¹ although some HETE-EAs are also able to selectively interact with the CBs. Following the findings that AEA is a substrate for COX-2, LOX and CYP450 enzymes, it was discovered that other arachidonoyl derivatives are also converted by COX-2, LOX, and CYP450 enzymes.^{73, 86, 96-98} The substrate class now ranges from classical endocannabinoids like 2-AG and AEA to various amino acid derivatives, like AA-Gly, and different vanilloid derivatives, like NADA. Studies towards the biological activity of some of these other secondary AA metabolites showed that PGD₂-G, for example, has strong anti-inflammatory effects by reducing the formation of the pro-inflammatory cytokines in LPS administrated mice,⁹⁹ and by reducing DSS induced murine colitis.¹⁰⁰ The 12/15-LOX derived 15-HETE-G was identified as a PPAR α agonist,¹⁰¹ was found to be a moderate agonist of CB₂ and has no affinity with CB₁.^{93, 102} The CYP450 metabolites 11,12-EET-G, and 14,15-EET-G were found to promote vasodilation in rat mesenteric arteries suggesting that they can act as antihypertensive mediators.^{91, 102-103} Despite these limited data on the physiological role of secondary AA-derived metabolites, there are still many open questions and the extend of this knowledge gap is as yet undefined. More work is needed to fully characterize the metabolism of AA metabolites and to understand their biological roles. Identification of the secondary metabolites of AA and the characterization of their

biological activities changed paradigms in the understanding of endocannabinoid biology. Not only the endocannabinoids themselves, but also their oxygenated products must be taken into account when studying the endocannabinoidome,⁴³ resulting in an additional layer of complexity in the lipid biochemistry field.

2.6 Oxygenation of n-3 PUFA derived endocannabinoids: a new class of endogenous potent anti-inflammatory mediators

In addition to oxygenated metabolites of AA-derived endocannabinoids, evidence is accumulating that DHA and EPA-derived ethanolamides are also substrates for COX-2, LOX and CYP450 enzymes. In this section, we will focus on the formation and inflammatory modulation of recently discovered oxygenated metabolites of DHEA and EPEA.

The first data that demonstrated that DHEA is a substrate for oxidative enzymes was published in 2011 by the group of Serhan and coworkers.⁷⁶ In an enzymatic assay with 15-LOX and DHEA they showed that 17-HDHEA was produced as a specific 15-LOX metabolite. In addition, four major 15-LOX derived metabolites, 7,17-diHDHEA, 4,17-diHDHEA, 10,17-diHDHEA and 15-HEDPEA, were identified in brain tissue,^{76, 104} of which 10,17-diHDHEA and 15-HEDPEA significantly reduced leukocyte chemotaxis. In addition, 10,17-diHDHEA was observed to block platelet-activator factor (PAF)-stimulated platelet-leukocyte aggregation and to stop PMN chemotaxis. 15-HEDPEA was found to stop chemotactic polymorphonuclear leukocyte (PMN) transmigration, to block the PAF-stimulated platelet-leukocyte aggregation, and to significantly reduce PMN accumulation in 6-8 weeks old male mice with hind limb ischemia and second organ reperfusion injuries. Both 10,17-diHDHEA and 15-HEDPEA were found to activate CB₂ receptors. Concluding, both 10,17-diHDHEA and 15-HEDPEA are biologically active anti-inflammatory compounds derived from DHEA (**Figure 2-5, Table 2-1**).^{76, 104}

A cell proliferation study showed that DHEA has anti-proliferating properties in head and neck squamous cell carcinoma (HNSCC) cells, dependent on the activity of 5-LOX.¹⁰⁵ By blocking or silencing 5-LOX, the HNSCC cells displayed increased proliferative activity, suggesting that 5-LOX mediates the anti-proliferating effects of DHEA. Additionally, data was provided that supported the notion that 5-LOX derived products of DHEA are not directly involved in the mediation of the anti-cancerous effect, and that the anti-cancerous effects are mainly induced by reactive oxygen species (ROS) formed by 5-LOX. Interestingly, blocking or silencing of COX-2 did not show a COX-2 mediated anti-proliferating effect of DHEA, suggesting that the anti-proliferative effects of DHEA

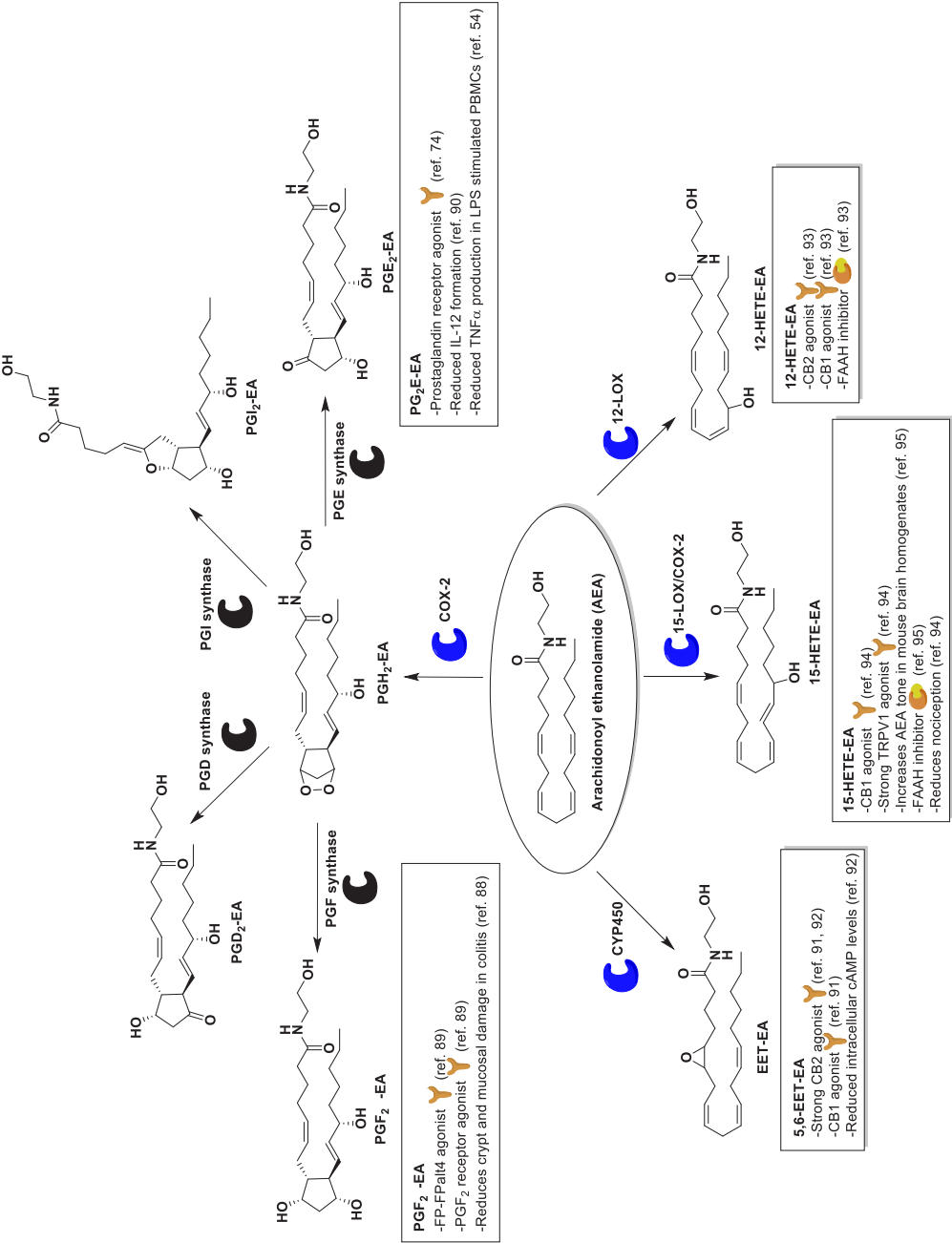


Figure 2-4 Known metabolites of arachidonoyl ethanolamide by COX, LOX and CYP450 enzymes, their main receptor affinities, and biological effects.

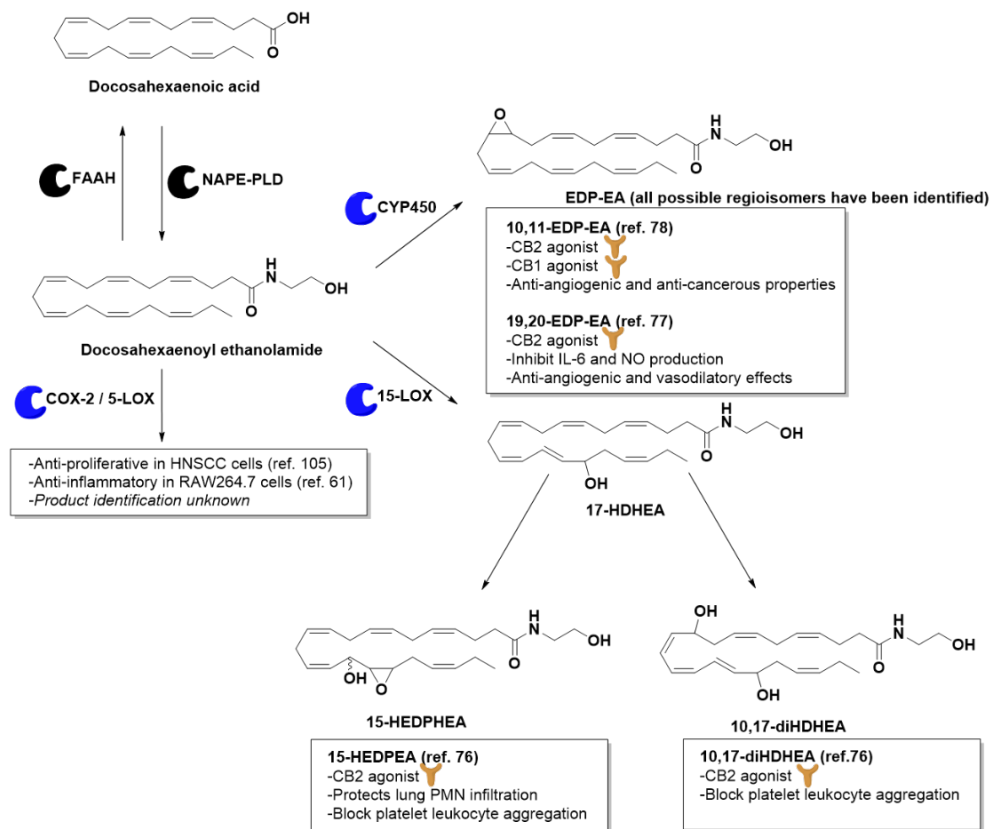


Figure 2-5 Metabolism of docosahexaenoic acid into docosahexaenoyl ethanolamide and subsequent metabolism by CYP450 and 15-LOX into various hydroxylated or epoxidated metabolites.

on HNCSS cells are independent of COX-2. On the other hand, results from our group suggested that DHEA might be a substrate for COX-2 in LPS-stimulated RAW 264.7 macrophages (see above).⁶¹

Das and co-workers demonstrated that both EPEA and DHEA could also be epoxidated by CYP450 to form epoxyeicosatetraenoic acid ethanolamide (EEQ-EA) and epoxydocosapentaenoic acid ethanolamide (EDP-EA), respectively (**Figure 2-5**, **Figure 2-6**, and **Table 2-1**).⁷⁷ The direct *in vitro* production of these structures was proven in rat brain microsomes, activated BV-2 microglia cells, and by recombinant human CYP2J2 that were incorporated into nanodiscs, which are nanoscale lipid bilayers that are surrounded by a membrane scaffold protein as a model system for membrane proteins.¹⁰⁶ It was found that epoxidation of EPEA and DHEA resulted in the formation

of all possible regioisomers, with a preference for the terminal olefin (17,18-EEQ-EA and 19,20-EDP-EA). The terminal regioisomers were tested for their anti-inflammatory properties in BV-2 microglia cells, showing that both 17,18-EEQ-EA and 19,20-EDP-EA inhibit NO and IL-6 production, and induce the production of the anti-inflammatory cytokine IL-10. A selective PPAR- γ antagonist and CB₂ selective antagonist partially reversed the anti-inflammatory effects of the epoxide metabolites, indicating that both receptors are involved in the mediation of the anti-inflammatory response. In comparison with EPEA and DHEA, it was found that the epoxide metabolites had increased preferences for CB₂ receptor activation. Moreover, 17,18-EEQ-EA was found to inhibit platelet aggregation, whereas 19,20-EDP-EA showed pro-aggregation effects. Finally, it was found that both 17,18-EEQ-EA and 19,20-EDP-EA have strong anti-angiogenic effects when compared to 17,18-EEQ and 19,20-EDP (**Figure 2-5**, **Figure 2-6**, and **Table 2-1**).⁷⁷

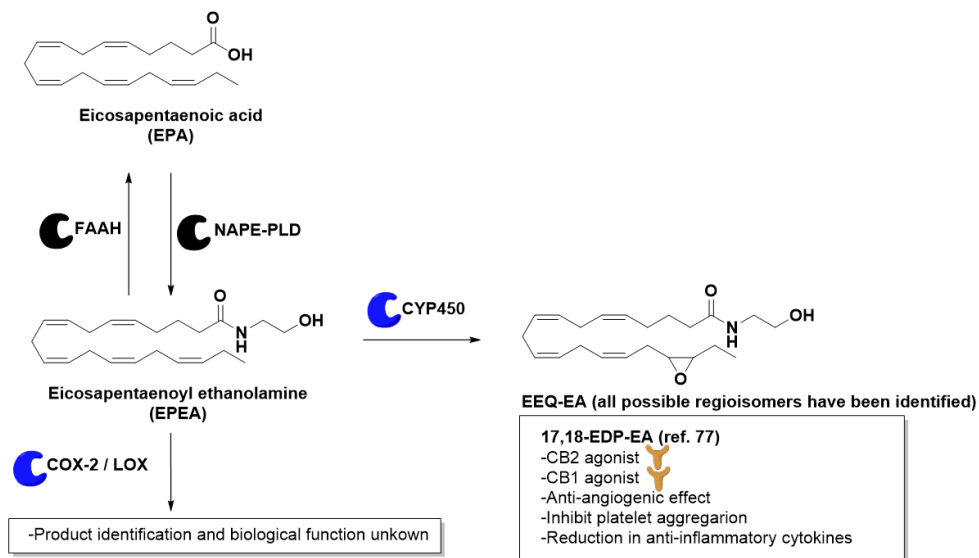


Figure 2-6 Metabolism of eicosapentaenoic acid into eicosapentaenoyl ethanolamide and subsequent metabolism by CYP450 into various epoxidated metabolites.

To study the anti-tumorigenic properties of the EDP-EA structures in more detail, the EDP-EAs were screened for their endogenous synthesis and anti-tumorigenic properties in an osteosarcoma model.⁷⁸ Various DHEA epoxide derivatives were quantified in metastatic lungs of mice, showing that there was a significant increase of all epoxide metabolites in tumorigenic lungs. Of all EDP-EAs tested, only the 13,14-, 10,11-, and 7,8-EDP-EA regioisomers reduced cell viability and migration behavior of tumors. In all

tests 10,11-EDP-EA was found to be the most promising anti-tumorigenic metabolite, and was thus selected for more in depth studies. These showed that 10,11-EDP-EA did not affect the cell cycle of the osteosarcoma cells, but strongly prevented angiogenesis in a human umbilical vein endothelial cell (HUVEC) cell model. Furthermore, 10,11-EDP-EA was found to activate both the CB₁ and CB₂ receptor, although it was demonstrated that its anti-tumorigenic properties are not completely mediated by these CB receptors alone (**Figure 2-5** and **Table 2-1**).

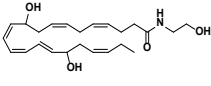
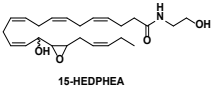
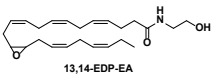
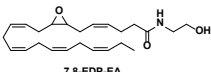
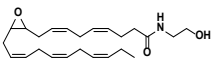
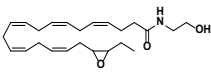
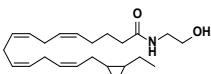
In summary, EEQ-EAs and EDP-EAs have diverse properties when comparing their effects on platelet aggregation and angiogenesis. When concerning their anti-cancerous properties 10,11-EDP-EA thus far shows the most promising results against osteosarcoma. Although evidence suggests that oxidized metabolites of DHEA and EPEA have interesting anti-inflammatory and anti-proliferative effects, these effects were only shown in a limited number of *in vitro* studies. As yet, most publications focus on DHEA and their metabolites, and EPEA received less attention. In addition, no reports described whether glycerol conjugates of DHA and/or EPA can be metabolized by COX-2. More work is needed to better understand the metabolism of DHEA, EPEA and related congeners by oxidative enzymes, and to evaluate their effectiveness as potential anti-inflammatory and anti-tumorigenic compounds in comparable *in vitro* and *in vivo* models.

2.7 Chemical PUFA and endocannabinoid probes: Development of new chemical tools to study the biological role of endocannabinoids and their anti-inflammatory mechanisms

2.7.1 Use of chemical PUFA and endocannabinoid probes

In the previous paragraphs we showed that the endocannabinoidome constitutes a complex interplay between various endocannabinoids, enzymes, and receptors. To better understand the biochemical pathways in the endocannabinoidome and to discover novel therapeutic targets, chemical probes have been particularly useful. Chemical probes consist of a particular binding or recognition unit, by which the probe mimics its natural biological activity. In addition, the probes contain a specific chemical handle, which could be a label (for detection) or a 'clickable' group (for click chemistry based detection, visualization or purification).¹⁰⁷ Sometimes probes also contain a crosslinking group, like a diazirine group, that covalently reacts with biomolecules in close proximity after photo-activation.¹⁰⁸⁻¹⁰⁹

Table 2-1 Recently identified oxidized metabolites of EPEA and DHEA, including the enzyme associated with the conversion, receptor affinities and biological effects (N.D. means not determined).

Compound name and structure	Enzymatic product	Binding to CB ₁ and CB ₂	Biological activity	Ref.
 10,17-diHDHEA	15-LOX metabolite of DHEA (in isolated human PMN cells and mouse brain tissue)	CB ₂ agonist, weak CB ₁ agonist	Stop PMN chemotaxis. Block PAF stimulated formation of platelet-leukocyte aggregates.	76
 15-HEDPHEA	15-LOX metabolite of DHEA (in isolated human PMN cells)	CB ₂ agonist, weak CB ₁ agonist	Block PMN transmigration. Block PAF stimulated formation of platelet-leukocyte aggregates. Protects ischemia/reperfusion second order injuries from PMN infiltration.	76
 13,14-EDP-EA	CYP450 metabolite of DHEA (isolated from lung tissue in mice injected K7M2 osteosarcoma cells)	N.D.	Reduce cell viability and induce apoptosis and anti-migrational activities in tumor cells.	78
 7,8-EDP-EA	CYP450 metabolite of DHEA (isolated from lung tissue in mice injected K7M2 osteosarcoma cells)	N.D.	Reduce cell viability and induce apoptosis and anti-migrational activities in tumor cells.	78
 10,11-EDP-EA	CYP450 metabolite of DHEA (isolated from lung tissue in mice injected K7M2 osteosarcoma cells)	CB ₁ and CB ₂ agonist	Reduce cell viability and induce apoptosis and anti-migrational activities in tumor cells. Anti-angiogenic effects.	78
 19,20-EDP-EA	CYP450 metabolite of DHEA (CYP2J2, main CYP in human brain and heart)	CB ₁ and CB ₂ agonist (higher preference for CB ₂)	Inhibit IL-6 cytokine and NO production, and stimulate IL-10 production in LPS stimulated BV-2 microglia, anti-angiogenic and vasodilatory effects	77
 17,18-EEQ-EA	CYP450 metabolite of EPEA (CYP2J2, main CYP in human brain and heart)	Highly potent CB ₁ and CB ₂ agonist	Inhibit IL-6 cytokine and NO production, and stimulate IL-10 production in LPS stimulated BV-2 microglia, anti-angiogenic effects, reduced platelet aggregation	77

Here we provide some examples of PUFA- and endocannabinoid-derived chemical probes that were used to study their molecular interaction targets. All probes have a distinct PUFA or endocannabinoid structure that serves as the basis of the probe. We recognize that next to these PUFA and endocannabinoid derived probes, many groups have focused

on the development of chemical probes for CB receptors¹⁰⁹⁻¹¹¹ and endocannabinoid-related enzymes (like FAAH, NAAA, COX, and LOX, for example).¹¹²⁻¹¹⁵ These probes are designed to have specific and high binding interactions with their protein target, and do therefore not contain a clear PUFA or endocannabinoid related structure.

Probing of endocannabinoid related enzymes is often performed using activity-based profiling, of which the profiling of 15-LOX, as discussed in Chapter 1, is an excellent example of such a probing methodology.¹¹⁴ Enzymatic inhibitors are often investigated or screened for by performing a competitive study in the presence of an activity-based probe, resulting in the loss of a specific and detectable interaction between the inhibitor and the enzyme in the cell incubation studies.¹¹²

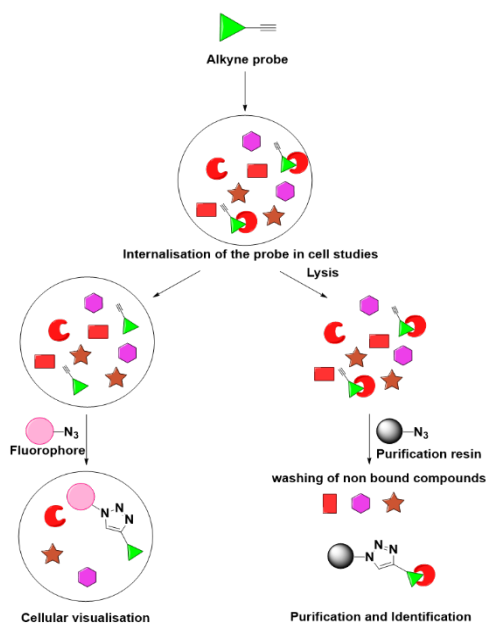


Figure 2-7 Overview of two uses of alkyne probes to study the localization of the molecule of interest with a detectable marker (often a fluorophore), or to study the molecular targets (mostly proteins) of the molecule of interest by clicking the probe to purification resins.

2.7.2 Alkyne probes

The most commonly applied functional group in probes is the terminal alkyne group ($\text{-C}\equiv\text{CH}$). For PUFAs, this yields PUFA or endocannabinoid structures with a terminal alkyne that can be coupled to azide-containing tags via a copper-catalyzed 1,3-dipolar cycloaddition. This is a very rapid and high-yielding reaction that became known as one of the first and best described ‘click’ reactions.^{107, 116} This alkyne-azide reaction is often invoked for the visualization of the probe or for the purification and identification of molecular targets of the probe, such as receptors and enzymes (**Figure 2-7**).

A recent study towards the role of lipid-derived electrophiles derived from 12/15-LOX made use of such a 19-alkyne-AA probe (**aAA** **Figure 2-8**) to show that 12/15-LOX is mainly involved in the regulation of the central metabolic pathway. By converting aAA to lipid-derived electrophilic products in peritoneal macrophages, the alkynes could be coupled to biotinylated azide tags, which were subsequently enriched using streptavidin-coated beads. Proteomic screening then revealed that the lipid-derived electrophiles had strong interactions with proteins from the central metabolic pathway, *e.g.*, glycolysis pathway, citric acid cycle, long chain fatty acid beta-oxidation. Additional knockout studies and control experiments showed that 12/15-LOX indeed plays a particular role in the energy metabolism of peritoneal macrophages, like involvement in glycolysis and mitochondrial respiration.¹¹⁷ A similar study was performed to study the protein targets of stearoyl, palmitoyl, oleoyl, and arachidonoyl ethanolamine derivatives in human embryonic kidney 293 cells (HEK293T), with diazirine and alkyne containing probe molecules (**AEA-DA**, **AA-DA**, **Figure 2-8**).¹⁰⁸ Again, proteomic analysis was performed after clicking the alkynes to azide-functionalized biotinylated tags. The diazirine photo-activation was used to crosslink the probes in a controlled way to the proteome of the cells. This dual activity of the photo-activation followed by the selective clicking of the endocannabinoid probes, showed the power to target also unannotated lipid binding proteins, which could be useful in the characterization of novel (anti-) inflammatory pathways.

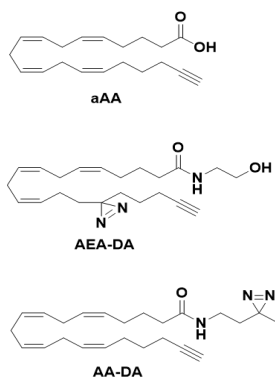


Figure 2-8 Alkyne probes of arachidonic acid (AA) and anandamide (AEA). aAA is a 19-alkyne arachidonic acid probe,¹¹⁸ AEA-DA is a 19-alkyne arachidonoyl ethanolamide probe with a diazirine photo-crosslinker at C16,¹⁰⁹ and AA-DA is a 19-alkyne arachidonoyl probe with a diazirine conjugate group resembling the ethanolamine.¹⁰⁹

Although alkyne probes are powerful handles to study and isolate the fatty acid and endocannabinoid compounds, it should be noted that the alkyne probes not always display identical biological effects compared to the parent compound of interest. For example, when comparing aAA with regular AA it was found that only half of the alkyne compound was taken up by Jurkat cells. Platelets were found to synthesize significantly less LOX and COX-derived products in the presence 19-alkyne-AA compared to AA. Ionophore-stimulated neutrophils produced significantly more 5-LOX products in the presence of the alkyne probe, and one of the AA-derived products leukotriene B₄

(LTB₄) is 12-fold less potent at stimulating neutrophil migration as a terminal alkyne.¹¹⁸ Concluding, this study showed that the use of alkyne-derived analogues can result in lower activities and even in mechanistic changes.

2.7.3 Other probes

To aid in the identification of novel receptors of the prostamide PGE₂-EA and PGE₂-G, both endocannabinoids were synthesized with a terminal azide group or an electrophilic isothiocyanate group, in the laboratory of Makryannis and co-workers. The isothiocyanate surrogate of PGE₂-EA was found to reduce the infiltration of leukocytes in murine peritonitis, thus showing to have retained its expected anti-inflammatory properties (**Figure 2-9**).¹¹⁹ A simultaneous study by the same group showed that chemical modifications of PGE₂-EA in both the head and tail group did not alter the biological interactions of the prostamide with the CB receptors and endocannabinoid enzymes. All chemically derived prostamides did not interact with prostaglandin EP receptors or other endocannabinoid-related proteins, which is also true for PGE₂-EA itself.¹²⁰ This indicates that these synthetic derivatives could play a role in the identification of novel prostamide receptors or prostamide-related proteins in the future. Another study investigated the interaction and binding mode of 2-AG and AEA towards the CB receptors by developing tail and head group-modified endocannabinoids. A biotin moiety was introduced at the terminal end of AEA, or biotin, benzophenone or alkyne moieties were introduced at the ethanolamine end of AEA. All modifications resulted in a complete loss of CB receptor activation. Nonetheless, head group biotinylated 2-AG and 2-arachidonyl glyceryl ether (2-AG-E) did activate CB receptors. Since the biotinylated 2-AG-E probe did show the highest CB₁ receptor activation, this probe was subsequently used to visualize CB₁ receptors in CB₁ transfected mouse hippocampal neuronal cell line HT-22 cells (**Figure 2-9**).¹²¹

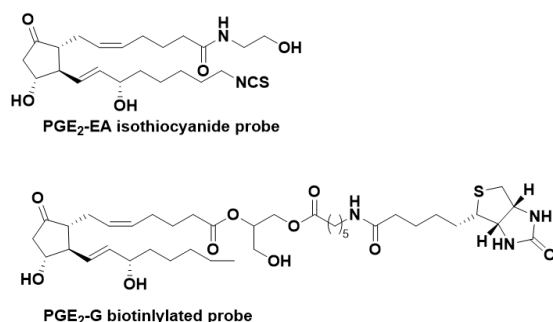


Figure 2-9 PGE₂-EA¹¹⁹ and PGE₂-G¹²¹ probes used to study the interactions of PGE₂-EA and PGE₂-G with CB receptors.

Introduction of labels directly into the structure of PUFAs and endocannabinoids has also been used, in particular for *in vivo* experiments. For example, radiolabeled DHEA was synthesized to study the metabolic fate of DHEA in the brain. From this study it

became clear that in mouse brain homogenates DHEA is almost exclusively converted into more polar phospholipids by FAAH. The study also allowed for quantification of DHEA distribution in specific brain areas, showing the highest concentrations in midbrain, brain stem and hypothalamus, and the lowest in striatum, thalamus and hippocampus.¹²² Next to the use of radiolabels, deuterium labels have also been introduced in PUFAs, mainly to probe enzymatic reactions. Deuterium labelling was used to determine the mechanistic details of the COX-2 enzyme.¹²³⁻¹²⁴

Although chemically derived PUFAs are powerful tools to explore the complexity of their biological fate, their application should not be used without care due to the delicate tuning of the metabolic pathways for differently structured PUFAs and their derivatives. Therefore, their application should always be accompanied with a complete set of control experiments, that should show statistically relevant results.

2.8 Conclusion & future perspective

As outlined in this review, the endocannabinoidome displays a highly complex interplay between dietary lipids, various enzymes and metabolites, and receptors which play an important role in inflammation. It has become clear that *n*-3 fatty acids can be metabolized by enzymes similar to AA, but yielding distinct '*n*-3' molecules with unique biological properties and receptor affinities. To date, it has been shown that COX-2, LOX and CYP450s are capable of metabolizing DHEA and EPEA, yielding oxygenated molecules with interesting biological properties. As these *n*-3 metabolites are discovered and characterized, our understanding of lipid biochemistry has increased. At the same time, with every newly discovered and characterized metabolite, it is becoming increasingly clear that lipid biology is more complex than previously understood. Future work needs to contribute to a better understanding of lipid metabolism, biological mechanisms, and activities of various lipids, particularly *n*-3 LC PUFA-derived structures. In this work, there is a great need for "bio-inert" chemical probes that allow for *in vitro* and *in vivo* identification and screening of cellular targets. This should lead to a mechanistic explanation of the biological roles of *n*-3 lipid metabolites, and a resolution of the controversies that are currently still surrounding human dietary intervention studies with *n*-3 LC PUFA.

2.9 Acknowledgements

We thank the VLAG Graduate School of Wageningen University and Research for financial support.

2.10 References

1. Brenna, J. T.; Salem Jr, N.; Sinclair, A. J.; Cunnane, S. C., α -Linolenic acid supplementation and conversion to n-3 long-chain polyunsaturated fatty acids in humans. *Prostaglandins Leukot. Essent. Fatty Acids* **2009**, 80 (2–3), 85–91.
2. Calder, P. C., Omega-3 fatty acids and inflammatory processes: from molecules to man. *Biochem. Soc. Trans.* **2017**, 45 (5), 1105–1115.
3. Calder, P. C., Very long-chain n-3 fatty acids and human health: fact, fiction and the future. *Proceedings of the Nutrition Society* **2018**, 77 (1), 52–72.
4. Baker, E. J.; Yusof, M. H.; Yaqoob, P.; Miles, E. A.; Calder, P. C., Omega-3 fatty acids and leukocyte-endothelium adhesion: Novel anti-atherosclerotic actions. *Mol. Aspects Med.* **2018**, 64, 169–181.
5. Zehr, K. R.; Walker, M. K., Omega-3 polyunsaturated fatty acids improve endothelial function in humans at risk for atherosclerosis: A review. *Prostaglandins Other Lipid Mediat.* **2018**, 134, 131–140.
6. Bays, H. E.; Ballantyne, C. M.; Kastelein, J. J.; Isaacsohn, J. L.; Braeckman, R. A.; Soni, P. N., Eicosapentaenoic acid ethyl ester (AMR101) therapy in patients with very high triglyceride levels (from the Multi-center, pLAcebo-controlled, Randomized, double-blINd, 12-week study with an open-label Extension [MARINE] trial). *Am. J. Cardiol.* **2011**, 108 (5), 682–90.
7. Hengeveld, L. M.; Praagman, J.; Beulens, J. W. J.; Brouwer, I. A.; van der Schouw, Y. T.; Sluijs, I., Fish consumption and risk of stroke, coronary heart disease, and cardiovascular mortality in a Dutch population with low fish intake. *Eur. J. Clin. Nutr.* **2018**, 72 (7), 942–950.
8. Larrieu, T.; Layé, S., Food for Mood: Relevance of Nutritional Omega-3 Fatty Acids for Depression and Anxiety. *Front. Psychol.* **2018**, 9 (1047), 1–15.
9. Layé, S.; Nadjar, A.; Joffre, C.; Bazinet, R. P., Anti-Inflammatory Effects of Omega-3 Fatty Acids in the Brain: Physiological Mechanisms and Relevance to Pharmacology. *Pharmacol. Rev.* **2018**, 70 (1), 12–38.
10. Cederholm, T., Fish consumption and omega-3 fatty acid supplementation for prevention or treatment of cognitive decline, dementia or Alzheimer's disease in older adults – any news? *Curr. Opin. Clin. Nutr. Metab. Care* **2017**, 20 (2), 104–109.
11. Gioxari, A.; Kaliora, A. C.; Marantidou, F.; Panagiotakos, D. P., Intake of ω -3 polyunsaturated fatty acids in patients with rheumatoid arthritis: A systematic review and meta-analysis. *Nutrition* **2018**, 45 (Supplement C), 114–124.e4.
12. Navarini, L.; Afeltra, A.; Gallo Afflitto, G.; Margiotta, D. P. E., Polyunsaturated fatty acids: any role in rheumatoid arthritis? *Lipids Health Dis.* **2017**, 16 (1), 197.
13. Proudman, S. M.; James, M. J.; Spargo, L. D.; Metcalf, R. G.; Sullivan, T. R.; Rischmueller, M.; Flabouris, K.; Wechalekar, M. D.; Lee, A. T.; Cleland, L. G., Fish oil in recent onset rheumatoid arthritis: a randomised, double-blind controlled trial within algorithm-based drug use. *Ann. Rheum. Dis.* **2015**, 74 (1), 89–95.

14. Khadge, S.; Sharp, J. G.; Thiele, G. M.; McGuire, T. R.; Klassen, L. W.; Duryee, M. J.; Britton, H. C.; Dafferner, A. J.; Beck, J.; Black, P. N.; et al., Dietary omega-3 and omega-6 polyunsaturated fatty acids modulate hepatic pathology. *J. Nutr. Biochem.* **2018**, *52*, 92-102.
15. Nakamoto, K.; Shimada, K.; Harada, S.; Morimoto, Y.; Hirasawa, A.; Tokuyama, S., DHA supplementation prevent the progression of NASH via GPR120 signaling. *Eur. J. Pharmacol.* **2018**, *820*, 31-38.
16. Scorletti, E.; Byrne, C. D., Omega-3 fatty acids and non-alcoholic fatty liver disease: Evidence of efficacy and mechanism of action. *Mol. Aspects Med.* **2018**, *64*, 135-146.
17. Spahis, S.; Alvarez, F.; Ahmed, N.; Dubois, J.; Jalbout, R.; Paganelli, M.; Grzywacz, K.; Delvin, E.; Peretti, N.; Levy, E., Non-alcoholic fatty liver disease severity and metabolic complications in obese children: impact of omega-3 fatty acids. *J. Nutr. Biochem.* **2018**, *58*, 28-36.
18. Witkamp, R. F.; van Norren, K., Let thy food be thy medicine....when possible. *Eur. J. Pharmacol.* **2018**, *836*, 102-114.
19. Fuentes, N. R.; Kim, E.; Fan, Y.-Y.; Chapkin, R. S., Omega-3 fatty acids, membrane remodeling and cancer prevention. *Mol. Aspects Med.* **2018**, *64*, 79-91.
20. Song, M.; Zhang, X.; Meyerhardt, J. A.; Giovannucci, E. L.; Ogino, S.; Fuchs, C. S.; Chan, A. T., Marine ω -3 polyunsaturated fatty acid intake and survival after colorectal cancer diagnosis. *Gut* **2017**, *66* (10), 1790-1796.
21. Borghi, C.; Pareo, I., Omega-3 in Antiarrhythmic Therapy. *High Blood Press. Cardiovasc. Prev.* **2012**, *19* (4), 207-211.
22. Aung, T.; Halsey, J.; Kromhout, D.; Gerstein, H. C.; Marchioli, R.; Tavazzi, L.; Geleijnse, J. M.; Rauch, B.; Ness, A.; Galan, P.; et al., Associations of omega-3 fatty acid supplement use with cardiovascular disease risks: Meta-analysis of 10 trials involving 77 917 individuals. *JAMA Cardiology* **2018**, *3* (3), 225-233.
23. Abdelhamid, A. S.; Brown, T. J.; Brainard, J. S.; Biswas, P.; Thorpe, G. C.; Moore, H. J.; Deane, K. H. O.; AlAbdulghafoor, F. K.; Summerbell, C. D.; Worthington, H. V.; et al., Omega-3 fatty acids for the primary and secondary prevention of cardiovascular disease. *Cochrane Database Syst. Rev.* **2018**, *11* (11), CD003177.
24. Johnsen, S. H.; Jacobsen, B. K.; Brækkan, S. K.; Hansen, J.-B.; Mathiesen, E. B., Fish consumption, fish oil supplements and risk of atherosclerosis in the Tromsø study. *Nutr. J.* **2018**, *17* (1), 56.
25. ASCEND Study Collaborative Group; Bowman, L.; Mafham, M.; Wallendszus, K.; Stevens, W.; Buck, G.; Barton, J.; Murphy, K.; Aung, T.; Haynes, R.; et al., Effects of n-3 Fatty Acid Supplements in Diabetes Mellitus. *N. Engl. J. Med.* **2018**, *379* (16), 1540-1550.
26. Bäck, M.; Hansson, G. K., Omega-3 fatty acids, cardiovascular risk, and the resolution of inflammation. *FASEB J.* **2019**, *33* (2), 1536-1539.
27. Manson, J. E.; Cook, N. R.; Lee, I. M.; Christen, W.; Bassuk, S. S.; Mora, S.; Gibson, H.; Albert, C. M.; Gordon, D.; Copeland, T.; et al., Marine n-3 Fatty Acids and Prevention of

- Cardiovascular Disease and Cancer. *N. Engl. J. Med.* **2018**, *380*, 23-32.
28. Bhatt, D. L.; Steg, P. G.; Miller, M.; Brinton, E. A.; Jacobson, T. A.; Ketchum, S. B.; Doyle, R. T., Jr.; Juliano, R. A.; Jiao, L.; Granowitz, C.; et al., Cardiovascular Risk Reduction with Icosapent Ethyl for Hypertriglyceridemia. *N Engl J Med* **2018**, *380* (1), 11-22.
 29. Budoff, M.; Brent Muhlestein, J.; Le, V. T.; May, H. T.; Roy, S.; Nelson, J. R., Effect of Vascepa (icosapent ethyl) on progression of coronary atherosclerosis in patients with elevated triglycerides (200-499 mg/dL) on statin therapy: Rationale and design of the EVAPORATE study. *Clin. Cardiol.* **2018**, *41* (1), 13-19.
 30. McManus, S.; Tejera, N.; Awwad, K.; Vauzour, D.; Rigby, N.; Fleming, I.; Cassidy, A.; Minihane, A. M., Differential effects of EPA versus DHA on postprandial vascular function and the plasma oxylipin profile in men. *J. Lipid Res.* **2016**, *57* (9), 1720-7.
 31. Thota, R. N.; Ferguson, J. J. A.; Abbott, K. A.; Dias, C. B.; Garg, M. L., Science behind the cardio-metabolic benefits of omega-3 polyunsaturated fatty acids: biochemical effects vs. clinical outcomes. *Food Funct.* **2018**, *9* (7), 3576-3596.
 32. Zhuang, P.; Wang, W.; Wang, J.; Zhang, Y.; Jiao, J., Polyunsaturated fatty acids intake, omega-6/omega-3 ratio and mortality: Findings from two independent nationwide cohorts. *Clin. Nutr.* **2018**, *38* (2), 848-855 .
 33. Tan, J. K.; McKenzie, C.; Mariño, E.; Macia, L.; Mackay, C. R., Metabolite-Sensing G Protein-Coupled Receptors—Facilitators of Diet-Related Immune Regulation. *Annu. Rev. Immunol.* **2017**, *35* (1), 371-402.
 34. Oh, D. Y.; Talukdar, S.; Bae, E. J.; Imamura, T.; Morinaga, H.; Fan, W.; Li, P.; Lu, W. J.; Watkins, S. M.; Olefsky, J. M., GPR120 Is an Omega-3 Fatty Acid Receptor Mediating Potent Anti-inflammatory and Insulin-Sensitizing Effects. *Cell* **2010**, *142* (5), 687-698.
 35. Calder, P. C., n-3 Polyunsaturated fatty acids, inflammation, and inflammatory diseases. *Am. J. Clin. Nutr.* **2006**, *83* (6), S1505-S1519S.
 36. Calder, P. C., Marine omega-3 fatty acids and inflammatory processes: Effects, mechanisms and clinical relevance. *Biochim. Biophys. Acta Mol. Cell Biol. Lipids* **2015**, *1851* (4), 469-484.
 37. Serhan, C.; Arita, M.; Hong, S.; Gotlinger, K., Resolvins, docosatrienes, and neuroprotectins, novel omega-3-derived mediators, and their endogenous aspirin-triggered epimers. *Lipids* **2004**, *39* (11), 1125-1132.
 38. Calder, P. C., Polyunsaturated fatty acids and inflammatory processes: New twists in an old tale. *Biochimie* **2009**, *91* (6), 791-795.
 39. Calder, P. C., The relationship between the fatty acid composition of immune cells and their function. *Prostaglandins Leukot. Essent. Fatty Acids* **2009**, *79* (3-5), 101-108.
 40. Schmitz, G.; Ecker, J., The opposing effects of n-3 and n-6 fatty acids. **2008**, *47* (2), 147-155.
 41. Bagga, D.; Wang, L.; Farias-Eisner, R.; Glaspy, J. A.; Reddy, S. T., Differential effects of prostaglandin derived from w -6 and w -3 polyunsaturated fatty acids on COX-2 expression and IL-6 secretion. *Proc. Natl. Acad. Sci. U.S.A.* **2003**, *100* (4), 1751-1756.
 42. Pertwee, R. G.; Howlett, A. C.; Abood, M. E.; Alexander, S. P. H.; Di Marzo, V.; Elphick, M. R.;

- Greasley, P. J.; Hansen, H. S.; Kunos, G.; Mackie, K.; et al., International Union of Basic and Clinical Pharmacology. LXXIX. Cannabinoid Receptors and Their Ligands: Beyond CB1 and CB2. *Pharmacol. Rev.* **2010**, 62 (4), 588-631.
43. Witkamp, R., Fatty acids, endocannabinoids and inflammation. *Eur. J. Pharmacol.* **2016**, 785, 96-107.
44. Devane, W. A.; Hanus, L.; Breuer, A.; Pertwee, R. G.; Stevenson, L. A.; Griffin, G.; Gibson, D.; Mandelbaum, A.; Etinger, A.; Mechoulam, R., Isolation and Structure of a Brain Constituent That Binds to the Cannabinoid Receptor. *Science* **1992**, 258 (5090), 1946-1949.
45. Fukuda, H.; Muromoto, R.; Takakura, Y.; Ishimura, K.; Kanada, R.; Fushihara, D.; Tanabe, M.; Matsubara, K.; Hirao, T.; Hirashima, K.; et al., Design and Synthesis of Cyclopropane Congeners of Resolvin E2, an Endogenous Proresolving Lipid Mediator, as Its Stable Equivalents. *Org. Lett.* **2016**, 18 (24), 6224-6227.
46. Balvers, M. G. J.; Verhoeckx, K. C. M.; Witkamp, R. F., Development and validation of a quantitative method for the determination of 12 endocannabinoids and related compounds in human plasma using liquid chromatography-tandem mass spectrometry. *J. Chromatogr. B* **2009**, 877 (14-15), 1583-1590.
47. Bradshaw, H. B.; Rimmerman, N.; Krey, J. F.; Walker, J. M., Sex and hormonal cycle differences in rat brain levels of pain-related cannabimimetic lipid mediators. *Am. J. Physiol. Regul. Integr. Comp. Physiol.* **2006**, 291 (2), R349-R358.
48. Wood, J. T.; Williams, J. S.; Pandarinathan, L.; Courville, A.; Keplinger, M. R.; Janero, D. R.; Vouros, P.; Makriyannis, A.; Lammi-Keefe, C. J., Comprehensive profiling of the human circulating endocannabinoid metabolome: clinical sampling and sample storage parameters. *Clin. Chem. Lab. Med.* **2008**, 46 (9), 1289-1295.
49. Zoerner, A. A.; Gutzki, F. M.; Suchy, M. T.; Beckmann, B.; Engeli, S.; Jordan, J.; Tsikas, D., Targeted stable-isotope dilution GC-MS/MS analysis of the endocannabinoid anandamide and other fatty acid ethanol amides in human plasma. *J. Chromatogr. B* **2009**, 877 (26), 2909-2923.
50. Artmann, A.; Petersen, G.; Hellgren, L. I.; Boberg, J.; Skonberg, C.; Nellemann, C.; Hansen, S. H.; Hansen, H. S., Influence of dietary fatty acids on endocannabinoid and N-acyl ethanolamine levels in rat brain, liver and small intestine. *Biochim. Biophys. Acta Mol. Cell Biol. Lipids* **2008**, 1781 (4), 200-212.
51. Balvers, M. G. J.; Verhoeckx, K. C. M.; Bijlsma, S.; Rubingh, C. M.; Meijerink, J.; Wortelboer, H. M.; Witkamp, R. F., Fish oil and inflammatory status alter the n-3 to n-6 balance of the endocannabinoid and oxylipin metabolomes in mouse plasma and tissues. *Metabolomics* **2012**, 8 (6), 1130-1147.
52. Balvers, M. G. J.; Verhoeckx, K. C. M.; Plastina, P.; Wortelboer, H. M.; Meijerink, J.; Witkamp, R. F., Docosahexaenoic acid and eicosapentaenoic acid are converted by 3T3-L1 adipocytes to N-acyl ethanolamines with anti-inflammatory properties. *Biochim. Biophys. Acta Mol. Cell Biol. Lipids* **2010**, 1801 (10), 1107-1114.

53. Wood, J. T.; Williams, J. S.; Pandarinathan, L.; Janero, D. R.; Lammi-Keefe, C. J.; Makriyannis, A., Dietary docosahexaenoic acid supplementation alters select physiological endocannabinoid-system metabolites in brain and plasma. *J. Lipid Res.* **2010**, 51 (6), 1416-1423.
54. Brown, K. L.; Davidson, J.; Rotondo, D., Characterisation of the prostaglandin E₂-ethanolamide suppression of tumour necrosis factor- α production in human monocytic cells. *Biochim. Biophys. Acta Mol. Cell Biol. Lipids* **2013**, 1831 (6), 1098-1107.
55. Brown, I.; Cascio, M. G.; Rotondo, D.; Pertwee, R. G.; Heys, S. D.; Wahle, K. W. J., Cannabinoids and omega-3/6 endocannabinoids as cell death and anticancer modulators. *Prog. Lipid Res.* **2013**, 52 (1), 80-109.
56. Alharthi, N.; Christensen, P.; Hourani, W.; Otori, C.; Barrett, D. A.; Bennett, A. J.; Chapman, V.; Alexander, S. P. H., n-3 polyunsaturated N-acylethanolamines are CB₂ cannabinoid receptor-preferring endocannabinoids. *Biochim. Biophys. Acta Mol. Cell Biol. Lipids* **2018**, 1863 (11), 1433-1440.
57. Hansen, H. S.; Artmann, A., Endocannabinoids and Nutrition. *J. Neuroendocrinol.* **2008**, 20 (1), 94-99.
58. Berger, A.; Crozier, G.; Bisogno, T.; Cavaliere, P.; Innis, S.; Di Marzo, V., Anandamide and diet: Inclusion of dietary arachidonate and docosahexaenoate leads to increased brain levels of the corresponding N-acylethanolamines in piglets. *Proc. Natl. Acad. Sci. U.S.A.* **2001**, 98 (11), 6402-6406.
59. Matias, I.; Carta, G.; Murru, E.; Petrosino, S.; Banni, S.; Di Marzo, V., Effect of polyunsaturated fatty acids on endocannabinoid and N-acyl-ethanolamine levels in mouse adipocytes. *Biochim. Biophys. Acta Mol. Cell Biol. Lipids* **2008**, 1781 (1-2), 52-60.
60. Watanabe, S.; Doshi, M.; Hamazaki, T., n-3 Polyunsaturated fatty acid (PUFA) deficiency elevates and n-3 PUFA enrichment reduces brain 2-arachidonoylglycerol level in mice. *Prostaglandins Leukot. Essent. Fatty Acids* **2003**, 69 (1), 51-59.
61. Meijerink, J.; Poland, M.; Balvers, M. G. J.; Plastina, P.; Lute, C.; Dwarkasing, J.; van Norren, K.; Witkamp, R. F., Inhibition of COX-2-mediated eicosanoid production plays a major role in the anti-inflammatory effects of the endocannabinoid N-docosahexaenoylethanolamine (DHEA) in macrophages. *Br. J. Pharmacol.* **2015**, 172 (1), 24-37.
62. Bisogno, T.; Delton-Vandenbroucke, I.; Milone, A.; Lagarde, M.; Di Marzo, V., Biosynthesis and Inactivation of N-Arachidonoylethanolamine (Anandamide) and N-Docosahexaenoylethanolamine in Bovine Retina. *Arch. Biochem. Biophys.* **1999**, 370 (2), 300-307.
63. Balvers, M. G. J.; Verhoeckx, K. C. M.; Meijerink, J.; Bijlsma, S.; Rubingh, C. M.; Wortelboer, H. M.; Witkamp, R. F., Time-dependent effect of in vivo inflammation on eicosanoid and endocannabinoid levels in plasma, liver, ileum and adipose tissue in C57BL/6 mice fed a fish-oil diet. *Int. Immunopharmacol.* **2012**, 13 (2), 204-214.
64. Meijerink, J.; Plastina, P.; Vincken, J.-P.; Poland, M.; Attya, M.; Balvers, M.; Gruppen, H.; Gabriele,

- B.; Witkamp, R. F., The ethanolamide metabolite of DHA, docosahexaenoylethanolamine, shows immunomodulating effects in mouse peritoneal and RAW264.7 macrophages: evidence for a new link between fish oil and inflammation. *Br. J. Nutr.* **2011**, 105 (12), 1798-1807.
65. Park, T.; Chen, H.; Kevala, K.; Lee, J.-W.; Kim, H.-Y., N-Docosahexaenoylethanolamine ameliorates LPS-induced neuroinflammation via cAMP/PKA-dependent signaling. *J. Neuroinflammation* **2016**, 13 (1), 284.
66. Kim, H.-Y.; Spector, A. A.; Xiong, Z.-M., Asynaptogenicamide N-docosahexaenoylethanolamide promotes hippocampal development. *Prostaglandins Other Lipid Mediat.* **2011**, 96 (1), 114-120.
67. Kim, H.-Y.; Spector, A. A., Synaptamide, endocannabinoid-like derivative of docosahexaenoic acid with cannabinoid-independent function. *Prostaglandins Leukot. Essent. Fatty Acids* **2013**, 88 (1), 121-125.
68. Kim, H.-Y.; Spector, A. A., N-Docosahexaenoylethanolamine: A neurotrophic and neuroprotective metabolite of docosahexaenoic acid. *Mol. Aspects Med.* **2018**, 64, 34-44.
69. Lee, J.-W.; Huang, B. X.; Kwon, H.; Rashid, M. A.; Kharebava, G.; Desai, A.; Patnaik, S.; Marugan, J.; Kim, H.-Y., Orphan GPR110 (ADGRF1) targeted by N-docosahexaenoylethanolamine in development of neurons and cognitive function. *Nat. Commun.* **2016**, 7, 13123.
70. Rovito, D.; Giordano, C.; Vizza, D.; Plastina, P.; Barone, I.; Casaburi, I.; Lanzino, M.; De Amicis, F.; Sisci, D.; Mauro, L.; et al., Omega-3 PUFA ethanolamides DHEA and EPEA induce autophagy through PPAR γ activation in MCF-7 breast cancer cells. *J. Cell. Physiol.* **2013**, 228 (6), 1314-1322.
71. Rouzer, C. A.; Marnett, L. J., Structural and functional differences between cyclooxygenases: Fatty acid oxygenases with a critical role in cell signaling. *Biochem. Biophys. Res. Commun.* **2005**, 338 (1), 34-44.
72. Rouzer, C. A.; Marnett, L. J., Non-redundant Functions of Cyclooxygenases: Oxygenation of Endocannabinoids. *J. Biol. Chem.* **2008**, 283 (13), 8065-8069.
73. Urquhart, P.; Nicolaou, A.; Woodward, D. F., Endocannabinoids and their oxygenation by cyclo-oxygenases, lipoxygenases and other oxygenases. *Biochim. Biophys. Acta Mol. Cell Biol. Lipids* **2015**, 1851 (4), 366-376.
74. Alhouayek, M.; Muccioli, G. G., COX-2-derived endocannabinoid metabolites as novel inflammatory mediators. *Trends Pharmacol.* **2014**, 35 (6), 284-292.
75. Rouzer, C. A.; Marnett, L. J., Endocannabinoid Oxygenation by Cyclooxygenases, Lipoxygenases, and Cytochromes P450: Cross-Talk between the Eicosanoid and Endocannabinoid Signaling Pathways. *Chem. Rev.* **2011**, 111 (10), 5899-5921.
76. Yang, R.; Fredman, G.; Krishnamoorthy, S.; Agrawal, N.; Irimia, D.; Piomelli, D.; Serhan, C. N., Decoding Functional Metabolomics with Docosahexaenoyl Ethanolamide (DHEA) Identifies Novel Bioactive Signals. *J. Biol. Chem.* **2011**, 286 (36), 31532-31541.
77. McDougle, D. R.; Watson, J. E.; Abdeen, A. A.; Adili, R.; Caputo, M. P.; Krapf, J. E.; Johnson, R.

- W.; Kilian, K. A.; Holinstat, M.; Das, A., Anti-inflammatory ω -3 endocannabinoid epoxides. *Proc. Natl. Acad. Sci. U.S.A.* **2017**, *114* (30), E6034-E6043.
78. Roy, J.; Watson, J. E.; Hong, I. S.; Fan, T. M.; Das, A., Antitumorigenic Properties of Omega-3 Endocannabinoid Epoxides. *J. Med. Chem.* **2018**, *61* (13), 5569–5579.
 79. Ueda, N.; Tsuboi, K.; Uyama, T., Enzymological studies on the biosynthesis of N-acyl ethanolamines. *Biochim. Biophys. Acta Mol. Cell Biol. Lipids* **2010**, *1801* (12), 1274–1285.
 80. Bornheim, L. M.; Kim, K. Y.; Chen, B.; Correia, M. A., Microsomal cytochrome P450-mediated liver and brain anandamide metabolism. *Biochem. Pharmacol.* **1995**, *50* (5), 677–686.
 81. McDougale, D. R.; Kambalyal, A.; Meling, D. D.; Das, A., Endocannabinoids Anandamide and 2-Arachidonoylglycerol Are Substrates for Human CYP2J2 Epoxigenase. *J. Pharmacol. Exp. Ther.* **2014**, *351* (3), 616.
 82. Snider, N. T.; Kornilov, A. M.; Kent, U. M.; Hollenberg, P. F., Anandamide Metabolism by Human Liver and Kidney Microsomal Cytochrome P450 Enzymes to Form Hydroxyeicosatetraenoic and Epoxyeicosatrienoic Acid Ethanolamides. *J. Pharmacol. Exp. Ther.* **2007**, *321* (2), 590–597.
 83. Hampson, A. J.; Hill, W. A. G.; Zan-Phillips, M.; Makriyannis, A.; Leung, E.; Eglen, R. M.; Bornheim, L. M., Anandamide hydroxylation by brain lipoxygenase: metabolite structures and potencies at the cannabinoid receptor. *Biochim. Biophys. Acta, Lipids Lipid Metab.* **1995**, *1259* (2), 173–179.
 84. Kozak, K. R.; Prusakiewicz, J. J.; Rowlinson, S. W.; Prudhomme, D. R.; Marnett, L. J., Amino Acid Determinants in Cyclooxygenase-2 Oxygenation of the Endocannabinoid Anandamide. *Biochemistry* **2003**, *42* (30), 9041–9049.
 85. Yu, M.; Ives, D.; Ramesha, C. S., Synthesis of Prostaglandin E2 Ethanolamide from Anandamide by Cyclooxygenase-2. *J. Biol. Chem.* **1997**, *272* (34), 21181–21186.
 86. Kozak, K. R.; Crews, B. C.; Morrow, J. D.; Wang, L.-H.; Ma, Y. H.; Weinander, R.; Jakobsson, P.-J.; Marnett, L. J., Metabolism of the Endocannabinoids, 2-Arachidonoylglycerol and Anandamide, into Prostaglandin, Thromboxane, and Prostacyclin Glycerol Esters and Ethanolamides. *J. Biol. Chem.* **2002**, *277* (47), 44877–44885.
 87. Koda, N.; Tsutsui, Y.; Niwa, H.; Ito, S.; Woodward, D. F.; Watanabe, K., Synthesis of prostaglandin F ethanolamide by prostaglandin F synthase and identification of Bimatoprost as a potent inhibitor of the enzyme: new enzyme assay method using LC/ESI/MS. *Arch. Biochem. Biophys.* **2004**, *424* (2), 128–136.
 88. Nicotra, L. L.; Vu, M.; Harvey, B. S.; Smid, S. D., Prostaglandin ethanolamides attenuate damage in a human explant colitis model. *Prostaglandins Other Lipid Mediat.* **2013**, *100*–101, 22–29.
 89. Woodward, D. F.; Wang, J. W.; Poloso, N. J., Recent Progress in Prostaglandin F₂ α Ethanolamide (Prostamide F₂ α) Research and Therapeutics. *Pharmacol. Rev.* **2013**, *65* (4), 1135–1147.

90. Correa, F.; Docagne, F.; Clemente, D.; Mestre, L.; Becker, C.; Guaza, C., Anandamide inhibits IL-12p40 production by acting on the promoter repressor element GA-12: possible involvement of the COX-2 metabolite prostamide E2. *Biochem. J.* **2008**, 409 (3), 761.
91. Turcotte, C.; Chouinard, F.; Lefebvre, J. S.; Flamand, N., Regulation of inflammation by cannabinoids, the endocannabinoids 2-arachidonoyl-glycerol and arachidonoyl-ethanolamide, and their metabolites. *J. Leukoc. Biol.* **2015**, 97 (6), 1049-1070.
92. Snider, N. T.; Nast, J. A.; Tesmer, L. A.; Hollenberg, P. F., A cytochrome P450-derived epoxygenated metabolite of anandamide is a potent cannabinoid receptor 2-selective agonist. *Mol. Pharmacol.* **2009**, 75 (4), 965-972.
93. van der Stelt, M.; van Kuik, J. A.; Bari, M.; van Zadelhoff, G.; Leeftang, B. R.; Veldink, G. A.; Finazzi-Agrò, A.; Vliegthart, J. F. G.; Maccarrone, M., Oxygenated Metabolites of Anandamide and 2-Arachidonoylglycerol: Conformational Analysis and Interaction with Cannabinoid Receptors, Membrane Transporter, and Fatty Acid Amide Hydrolase. *J. Med. Chem.* **2002**, 45 (17), 3709-3720.
94. Starowicz, K.; Makuch, W.; Korostynski, M.; Malek, N.; Slezak, M.; Zychowska, M.; Petrosino, S.; De Petrocellis, L.; Cristino, L.; Przewlocka, B.; Di Marzo, V., Full Inhibition of Spinal FAAH Leads to TRPV1-Mediated Analgesic Effects in Neuropathic Rats and Possible Lipoxygenase-Mediated Remodeling of Anandamide Metabolism. *PLoS ONE* **2013**, 8 (4), e60040.
95. Amadio, D.; Fezza, F.; Catanzaro, G.; Incani, O.; van Zadelhoff, G.; Finazzi Agrò, A.; Maccarrone, M., Methylation and acetylation of 15-hydroxyanandamide modulate its interaction with the endocannabinoid system. *Biochimie* **2010**, 92 (4), 378-387.
96. Kozak, K. R.; Rowlinson, S. W.; Marnett, L. J., Oxygenation of the Endocannabinoid, 2-Arachidonoylglycerol, to Glyceryl Prostaglandins by Cyclooxygenase-2. *J. Biol. Chem.* **2000**, 275 (43), 33744-33749.
97. Prusakiewicz, J. J.; Turman, M. V.; Vila, A.; Ball, H. L.; Al-Mestarihi, A. H.; Marzo, V. D.; Marnett, L. J., Oxidative metabolism of lipoamino acids and vanilloids by lipoxygenases and cyclooxygenases. *Arch. Biochem. Biophys.* **2007**, 464 (2), 260-268.
98. Moody, J. S.; Kozak, K. R.; Ji, C.; Marnett, L. J., Selective Oxygenation of the Endocannabinoid 2-Arachidonoylglycerol by Leukocyte-Type 12-Lipoxygenase. *Biochemistry* **2001**, 40 (4), 861-866.
99. Alhouayek, M.; Masquelier, J.; Cani, P. D.; Lambert, D. M.; Muccioli, G. G., Implication of the anti-inflammatory bioactive lipid prostaglandin D2-glycerol ester in the control of macrophage activation and inflammation by ABHD6. *Proc. Natl. Acad. Sci. U.S.A.* **2013**, 110 (43), 17558-17563.
100. Alhouayek, M.; Buisseret, B.; Paquot, A.; Guillemot-Legris, O.; Muccioli, G. G., The endogenous bioactive lipid prostaglandin D2-glycerol ester reduces murine colitis via DP1 and PPAR γ receptors. *FASEB J.* **2018**, 32 (9), 5000-5011.
101. Kozak, K. R.; Gupta, R. A.; Moody, J. S.; Ji, C.; Boeglin, W. E.; DuBois, R. N.; Brash, A. R.;

- Marnett, L. J., 15-Lipoxygenase Metabolism of 2-Arachidonylglycerol: generation of a peroxisome proliferator-activated receptor α agonist. *J. Biol. Chem.* **2002**, 277 (26), 23278-23286.
102. Baggelaar, M. P.; Maccarrone, M.; van der Stelt, M., 2-Arachidonoylglycerol: A signaling lipid with manifold actions in the brain. *Prog. Lipid Res.* **2018**, 71, 1-17.
 103. Awumey, E. M.; Hill, S. K.; Diz, D. I.; Bukoski, R. D., Cytochrome P-450 metabolites of 2-arachidonoylglycerol play a role in Ca^{2+} -induced relaxation of rat mesenteric arteries. *Am. J. Physiol. Heart Circ. Physiol.* **2008**, 294 (5), H2363-H2370.
 104. Shinohara, M.; Mirakaj, V.; Serhan, C. N., Functional Metabolomics Reveals Novel Active Products in the DHA Metabolome. *Front. Immunol.* **2012**, 3, 81.
 105. Park, S.-W.; Hah, J. H.; Oh, S.-M.; Jeong, W.-J.; Sung, M.-W., 5-lipoxygenase mediates docosahexaenoyl ethanolamide and N-arachidonoyl-L-alanine-induced reactive oxygen species production and inhibition of proliferation of head and neck squamous cell carcinoma cells. *BMC Cancer* **2016**, 16 (1), 1-14.
 106. McDougale, D. R.; Palaria, A.; Magnetta, E.; Meling, D. D.; Das, A., Functional studies of N-terminally modified CYP2J2 epoxigenase in model lipid bilayers. *Protein Sci.* **2013**, 22 (7), 964-979.
 107. Best, M. D., Click Chemistry and Bioorthogonal Reactions: Unprecedented Selectivity in the Labeling of Biological Molecules. *Biochemistry* **2009**, 48 (28), 6571-6584.
 108. Niphakis, M. J.; Lum, K. M.; Cognetta III, A. B.; Correia, B. E.; Ichu, T.-A.; Olucha, J.; Brown, S. J.; Kundu, S.; Piscitelli, F.; Rosen, H.; et al., A Global Map of Lipid-Binding Proteins and Their Ligandability in Cells. *Cell* **2015**, 161 (7), 1668-1680.
 109. Soethoudt, M.; Stolze, S. C.; Westphal, M. V.; van Stralen, L.; Martella, A.; van Rooden, E. J.; Guba, W.; Varga, Z. V.; Deng, H.; van Kasteren, S. I.; et al., Selective Photoaffinity Probe That Enables Assessment of Cannabinoid CB2 Receptor Expression and Ligand Engagement in Human Cells. *J. Am. Chem. Soc.* **2018**, 140 (19), 6067-6075.
 110. Soethoudt, M.; Grether, U.; Fingerle, J.; Grim, T. W.; Fezza, F.; de Petrocellis, L.; Ullmer, C.; Rothenhäusler, B.; Perret, C.; van Gils, N.; et al., Cannabinoid CB2 receptor ligand profiling reveals biased signalling and off-target activity. *Nat. Commun.* **2017**, 8, 13958.
 111. Martín-Couce, L.; Martín-Fontecha, M.; Palomares, Ó.; Mestre, L.; Cordoní, A.; Hernangomez, M.; Palma, S.; Pardo, L.; Guaza, C.; López-Rodríguez, M. L.; et al., Chemical Probes for the Recognition of Cannabinoid Receptors in Native Systems. *Angew. Chem. Int. Ed.* **2012**, 51 (28), 6896-6899.
 112. Blankman, J. L.; Cravatt, B. F., Chemical Probes of Endocannabinoid Metabolism. *Pharmacol. Rev.* **2013**, 65 (2), 849-871.
 113. Petracca, R.; Romeo, E.; Baggelaar, M. P.; Artola, M.; Pontis, S.; Ponzano, S.; Overkleeft, H. S.; van der Stelt, M.; Piomelli, D., Novel activity-based probes for N-acylethanolamine acid amidase. *Chemical Communications* **2017**, 53 (86), 11810-11813.
 114. Eleftheriadis, N.; Thee, S. A.; Zwinderman, M. R. H.; Leus, N. G. J.; Dekker, F. J., Activity-

- Based Probes for 15-Lipoxygenase-1. *Angew. Chem. Int. Ed.* **2016**, 55 (40), 12300-5.
115. Marnett, L. J., Inflammation and Cancer: Chemical Approaches to Mechanisms, Imaging, and Treatment. *J. Org. Chem.* **2012**, 77 (12), 5224-5238.
116. Kolb, H. C.; Finn, M. G.; Sharpless, K. B., Click Chemistry: Diverse Chemical Function from a Few Good Reactions. *Angew. Chem. Int. Ed.* **2001**, 40 (11), 2004-2021.
117. Isobe, Y.; Kawashima, Y.; Ishihara, T.; Watanabe, K.; Ohara, O.; Arita, M., Identification of Protein Targets of 12/15-Lipoxygenase-Derived Lipid Electrophiles in Mouse Peritoneal Macrophages Using Omega-Alkynyl Fatty Acid. *ACS Chem. Biol.* **2018**, 13 (4), 887-893.
118. Robichaud, P. P.; Poirier, S. J.; Boudreau, L. H.; Doiron, J. A.; Barnett, D. A.; Boilard, E.; Surette, M. E., On the cellular metabolism of the click chemistry probe 19-alkyne arachidonic acid. *J. Lipid Res.* **2016**, 57 (10), 1821-1830.
119. Shelnut, E. L.; Nikas, S. P.; Finnegan, D. F.; Chiang, N.; Serhan, C. N.; Makriyannis, A., Design and synthesis of novel prostaglandin E2 ethanolamide and glycerol ester probes for the putative prostamide receptor(s). *Tetrahedron Lett.* **2015**, 56 (11), 1411-1415.
120. Finnegan, D. F.; Shelnut, E. L.; Nikas, S. P.; Chiang, N.; Serhan, C. N.; Makriyannis, A., Novel tail and head group prostamide probes. *Bioorganic Med. Chem. Lett.* **2015**, 25 (6), 1228-1231.
121. Martín-Couce, L.; Martín-Fontecha, M.; Capolicchio, S.; López-Rodríguez, M. L.; Ortega-Gutiérrez, S., Development of Endocannabinoid-Based Chemical Probes for the Study of Cannabinoid Receptors. *J. Med. Chem.* **2011**, 54 (14), 5265-5269.
122. Sonti, S.; Duclos, R. I.; Tolia, M.; Gatley, S. J., N-Docosahexaenoyl ethanolamine (synaptamide): Carbon-14 radiolabeling and metabolic studies. *Chem. Phys. Lipids* **2018**, 210, 90-97.
123. Peng, S.; Okeley, N. M.; Tsai, A.-L.; Wu, G.; Kulmacz, R. J.; van der Donk, W. A., Synthesis of Isotopically Labeled Arachidonic Acids To Probe the Reaction Mechanism of Prostaglandin H Synthase. *J. Am. Chem. Soc.* **2002**, 124 (36), 10785-10796.
124. van der Donk, W. A.; Tsai, A.-L.; Kulmacz, R. J., The Cyclooxygenase Reaction Mechanism. *Biochemistry* **2002**, 41 (52), 15451-15458.

Chapter 3

**Bi-functional probes of PUFA-derived *N*-acyl amines
identify peroxiredoxins and small GTPase-signaling
proteins as their molecular targets in LPS-stimulated
RAW264.7 macrophages**

This chapter was adapted from:

Ian de Bus,
Antoine H.P. America,
Norbert de Ruijter,
Milena Lam,
Renger F. Witkamp,
Han Zuilhof,
Michiel G.J. Balvers,
Bauke Albada

(Manuscript submitted)

3.1 Abstract

We studied the mechanistic and biological origins of anti-inflammatory poly-unsaturated fatty acid-derived (PUFA-derived) *N*-acylethanolamines using synthetic bi-functional chemical probes of docosahexaenoyl ethanolamide (DHEA) and arachidonoyl ethanolamide (AEA) in RAW264.7 macrophages stimulated with 1.0 µg/mL lipopolysaccharide (LPS). Using a photoreactive diazirine, probes were covalently attached to their target proteins, which were further studied by introducing a fluorescent probe or biotin-based affinity purification. Fluorescence confocal microscopy showed that DHEA and AEA probes localized in the cytosol, specifically in structures that point towards the endoplasmic reticulum and in membrane vesicles. Affinity purification followed by proteomic analysis revealed peroxiredoxin-1 (Prdx1) as most significant binding interactor of both DHEA and AEA probes. In addition, Prdx4, endosomal related proteins, small GTPase-signaling proteins, and prostaglandin synthase 2 (Ptgs2, also known as cyclooxygenase 2 or COX-2) were identified. Lastly, confocal fluorescence microscopy revealed colocalization of Ptgs2 and Rac1 with DHEA and AEA probes. These data identified new molecular targets suggesting that DHEA and AEA may be involved in ROS regulation, cell migration, cytoskeletal remodeling, endosomal trafficking, and support endocytosis as uptake mechanism.

3.2 Introduction

Poly-unsaturated fatty acids (PUFAs) are essential lipids for human development and functioning, where they support important roles such as immune regulation.¹ Next to PUFAs, their corresponding amides, esters, and ethers also possess immunoregulatory activities.¹⁻³ At the moment, the prototypical endocannabinoid arachidonoyl ethanolamide (AEA, also known as anandamide), the ethanolamine conjugate of arachidonic acid (AA) (20:4*n*-6), has well-described interactions with cannabinoid (CB) and other receptors^{1, 4-7} and is known to be converted to inflammatory regulating prostamides.^{1, 5} Nevertheless, the full spectrum of its uptake and biological mechanisms underlying its effects are not yet fully understood.^{1, 8} An important structural analogue of AEA is the *n*-3 PUFA amide docosahexaenoyl ethanolamide (DHEA), the ethanolamine conjugate of docosahexaenoic acid (DHA) (22:6*n*-3). Studies in lipopolysaccharide (LPS)-stimulated mouse-derived RAW264.7 macrophages and microglia cell lines showed that DHEA reduced formation of nitric oxide (NO), COX-2-derived prostaglandins and thromboxanes, and also lowered expression and production of various inflammatory regulating cytokines like monocyte chemoattractant protein-1 (MCP-1), interleukin-6 (IL-6), tumor necrosis factor alpha (TNFα), and IL-1β.⁹⁻¹⁰ Next to cytokine regulation in macrophages, DHEA exerted synaptogenic and neuroprotective effects in neural cells,¹⁰⁻¹¹ stimulated ROS production in head and neck squamous cell carcinoma (HNSCC) cells,¹² and reduced inflammatory and nociceptive pain-related behavior in mice.¹³ Additionally, DHEA and AEA are metabolized by COX-2, 15-LOX and CYP450 to yield compounds with distinct anti-inflammatory and anti-tumorigenic properties.^{1-2, 14-18} Other studies reported interactions between DHEA and the cannabinoid receptors CB₁/CB₂, transient receptor potential V1 (TRPV-1), and peroxisome proliferator-activated receptors (PPARs), although the obtained agonistic effects seem to depend on the model that was used.^{1, 9, 14, 16, 19-21} Our previous studies on LPS-stimulated RAW264.7 macrophages did not show DHEA agonism with CB₁/CB₂ or PPARs, but rather indicated an important role in reducing COX-2-derived prostaglandins.^{9, 17} Clearly, many open questions persist about DHEA signaling in LPS-stimulated macrophages.

In the current study we aim to elucidate underlying mechanisms of the anti-inflammatory effects of AEA and DHEA in 1.0 µg/mL LPS-stimulated murine RAW264.7 macrophages by applying novel bi-functional PUFA-derived probes (**Figure 3-1**). These probes contain a 366 nm UV-active diazirine moiety to covalently attach to their interaction targets, and contain a terminal alkyne to selectively purify or visualize the chemical probes using a copper-mediated alkyne-azide click reaction (CuAAC) with biotin or a fluorescent probe, respectively (**Figure 3-1**).^{1, 22-23} Previously, similar methodological setups identified protein interactions with arachidonoyl-, oleoyl-,

palmitoyl-, and stearoyl probes in human HEK293T and mouse Neuro2a cells, which led to new druggable sites in the endocannabinoid system.⁶ Similarly, non-steroidal anti-inflammatory drug (NSAID) probes²⁴ were used to unravel the interaction of celecoxib with prostaglandin E synthase.²⁵

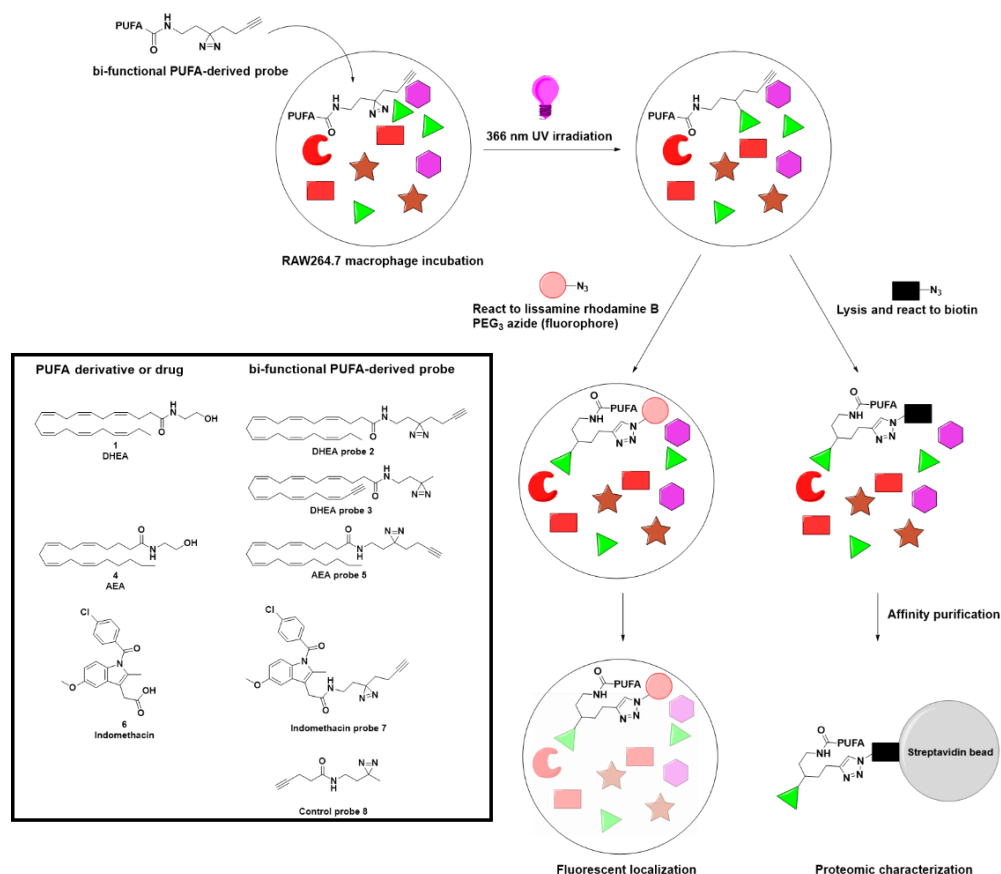


Figure 3-1 Schematic application of bi-functional PUFA derived probes for cellular visualization and proteomic characterization. First the diazine group is covalently linked to the molecular (protein) interaction partner(s) when exposed to 366 nm UV irradiation. Then the PUFA derived probes are either (i) visualized using CuAAC coupling to a fluorophore, or (ii) purified by affinity purification with streptavidin beads and biotinylated probes. Affinity based purification is followed by tryptic digestion and MS/MS-based characterization. Chemical structures of the natural PUFA derivatives or drugs, and their synthetic derived bifunctional probes, are shown in the frame.

To characterize new protein interaction partners of DHEA and AEA in LPS-stimulated RAW264.7 macrophages, we first assessed whether our probes displayed comparable biological effects as their parent compounds. Subsequently, we studied their localization in the macrophages by confocal fluorescence microscopy. Affinity purification followed by proteomic analysis enabled analysis of the protein interactome and provided insight in the molecular interaction partners and underlying pathways. Our data confirms previously proposed roles of both AEA and DHEA in the regulation of ROS production, cytoskeletal remodeling, and migration, which we attribute to newly uncovered interactions with peroxiredoxins, and small GTPase-signaling proteins.

3.3 Materials and Methods

3.3.1 Materials

DHEA ($\geq 98\%$) was purchased from Cayman Chemical and supplied by Sanbio B.V. (Uden, NL). AEA (100% HPLC purity) was obtained from Tocris Chemicals (Abingdon, UK). Ammonium bicarbonate ($\geq 99\%$), azide-PEG3-biotin, dimethyl sulfoxide (DMSO) (BioUltra, for molecular biology, $\geq 99.5\%$), lipopolysaccharides (LPS) from *E. coli* O111:B4 (L3024), saponin (from *Quillaja bark*), sodium L-ascorbate ($\geq 99\%$, BioXtra), tris(3-hydroxypropyltriazolylmethyl)amine (THPTA) ($\geq 95\%$), triton-X100, tween® 20 (for molecular biology), and tetrakis(acetonitrile)copper(I) hexafluorophosphate ($\geq 97\%$) were purchased from Sigma Aldrich (Zwijndrecht, NL). Copper(II)sulfate pentahydrate ($\geq 99\%$, for analysis), D,L-1,4-dithiothreitol (DTT) ($\geq 99\%$, for biochemistry), indomethacin ($\geq 98\%$), iodoacetamide (IAA) ($\geq 98\%$), Pierce™ BCA protein assay kit, protein LowBind tubes, Pierce™ C18 tips, Pierce™ streptavidin magnetic beads were purchased from Fisher Scientific (Landsmeer, NL). Ethylenediaminetetraacetic acid (EDTA) disodium salt dihydrate, Pharmapur® grade, was obtained from Scharlab (Barcelona, ES). Trypsin Gold (mass spectrometry grade) was obtained from Promega Benelux B.V. (Leiden, NL). Formic acid ($\geq 99\%$, ULC/MS grade), trifluoroacetic acid ($\geq 99.95\%$, HPLC grade) were obtained from Biosolve B.V. (Valkenswaard, NL). 1x PBS (pH 7.4), Dulbecco's Modified Eagle's Medium (DMEM), and penicillin and streptomycin were purchased from Corning (supplied by Fisher Scientific, Landsmeer, NL). Fetal calf serum (FCS) was obtained from Biowest and supplied by VWR International B.V. (Amsterdam, NL). Methanol ($\geq 99.9\%$, HiPerSolv CHROMANORM®, ULTRA for LC-MS, suitable for UPLC/UHPLC-MS instruments), acetonitrile (ACN) ($\geq 99.9\%$, HiPerSolv CHROMANORM® for LC-MS, suitable for UPLC/UHPLC instruments), HEPES (2-[4-(2-hydroxyethyl)-1-piperazinyl]-ethane sulfonic acid free acid) high purity ($\geq 99\%$), and sodium dodecyl sulphate (SDS) ($\geq 99\%$), biotechnology grade were obtained from VWR International B.V. (Amsterdam, NL). Urea ($\geq 99\%$, molecular biology grade) was purchased from SERVA Electrophoresis GmbH

(Heidelberg, Germany). 1x cOmplete™ protease inhibitor, and LDH cytotoxicity kit were purchased from Roche (Woerden, NL). Ammonium acetate, and gelatine powder EMPROVE® (≥99%) were obtained from Merck (Darmstadt, Germany). Ethanol (absolute for analysis EMSURE®), and Probumin® BSA were purchased from Merck (Zwijndrecht, NL). Lissamine rhodamine B PEG3 azide (≥95%) was purchased from Tenova Pharma (San Diego, US). Anti-alpha tubulin antibody - microtubule marker (rabbit polyclonal ab18251), recombinant anti-COX2/cyclooxygenase 2 antibody [EPR18376-119], C-terminal (rabbit monoclonal ab188184), goat anti-rabbit IgG H&L (Alexa Fluor® 488) (ab150077) were purchased from Abcam (Cambridge, UK). RAC1 rabbit polyclonal antibody (PA1-091), RAB5C rabbit polyclonal antibody (PA5-39408), and Invitrogen™ DAPI (4',6-diamidino-2-phenylindole, dihydrochloride salt) were obtained from Invitrogen (Thermo Fisher Scientific, Landsmeer, NL). PBS citifluor (AF3), and glycerol citifluor (AF4) were purchased from Citifluor (Hatfield, US). Ultrapure water was filtered by a MilliQ integral 3 system from Millipore (Molsheim, FR).

3.3.2 Cell culture and incubations

All cell experiments were performed in RAW264.7 macrophages (American Type Culture Collection, Teddington, UK) cultured in DMEM containing 10% FCS and 1% penicillin and streptomycin (P/S). Cells were incubated at 37 °C and 5% CO₂ in a humidified incubator.

3.3.3 Analysis of cytotoxic and anti-inflammatory effects

Cytotoxic and anti-inflammatory effects of the probes were evaluated using LDH assay and by measuring effects on IL-6, PGE₂ release, respectively. Macrophages were seeded at 2.5·10⁵ cells/mL and incubated overnight in 24-wells plates (Corning Life Sciences, Amsterdam, NL) containing 0.5 mL medium per well. The medium of the adherent cells was discarded and replaced by new fresh medium containing 5 or 10 μM of the compounds (in EtOH for PUFA conjugates, in DMSO for indomethacin, organic solvent final concentration 0.1% v/v) or a vehicle (0.1% v/v EtOH or 0.1% v/v DMSO) control. The cells were pre-incubated with the compounds for 30 min before stimulation with 1.0 μg/mL LPS in 0.1% PBS or 0.1% PBS control. After addition of the LPS, incubations were performed for 24 h in the dark (aluminum foil covered) to protect the probe from incidental UV exposure. Finally, the medium was collected and IL-6, PGE₂ and LDH concentrations were quantified (*vide infra*).

Cytotoxicity assay

To evaluate the cytotoxicity of the added compounds and probes, an LDH cytotoxicity kit (Roche, Woerden, NL) was used to measure LDH leakage. Extracellular LDH was determined by adding 100 μL of a reagent solution (1:45 (v/v) of LDH reagent 1:LDH reagent 2) to 100 μL of sample medium. Plates were incubated for 30 min followed by

quenching the reaction with 50 μ L of 1.0 M HCl. The absorbance was read using a plate reader at 492 nm. As a positive control for maximum cytotoxicity, cells were incubated with 1% Triton-X100.

Prostaglandin E₂ ELISA

To assess medium concentrations of PGE₂ in incubated medium samples, a prostaglandin E₂ ELISA Kit – Monoclonal (Cayman chemical, Ann Arbor, US) was used. The ELISA was performed according to the recommendations of the manufacturer on 5 or 50x diluted medium samples.

IL-6 ELISA

To assess medium concentrations of IL-6 in incubated RAW264.7 macrophages, a mouse IL-6 DuoSet ELISA from R&D systems (Abingdon, UK) was used. The ELISA was performed according to the recommendations of the manufacturer on 100x diluted medium samples.

3.3.4 Probe incubation

In 100 mm culture dishes (Corning Life Sciences, Amsterdam, NL), RAW264.7 macrophages were seeded at a density of $(0.5-1.0) \cdot 10^6$ cells/mL in 15 mL medium. After overnight culture, cells were stimulated with 5 mL fresh medium containing 1.0 μ g/mL LPS in 0.1% PBS. After 4 h of LPS stimulation, cells were incubated with 5 mL of fresh medium containing 1.0 μ g/mL LPS in 0.1% PBS and 10 μ M of the synthetic probes in 0.1% EtOH or DMSO. The probe-treated macrophages were incubated for 4 h in the dark (aluminum foil covered). Following incubation, medium and non-adherent cells were removed, after which the samples were placed on ice. Illumination with UV light was performed during 10 min at 366 nm and 1 mJ/cm² with an UVP-C1000 crosslinker equipped with five 8W light bulbs (**Figure 3-S1** shows spectral output of the lamp light), or under normal lamp light as control.

After light treatment, cells were scraped in 5 mL ice cold 1x PBS, and centrifuged at 3180 rcf for 5 min at 4 °C. Then cells were washed with 1 mL of ice cold 1x PBS containing 1x cOmplete™ protease inhibitor, followed by centrifugation at 3180 rcf for 5 min at 4°C. The cell pellet was washed with ice cold 1 mL, and 0.5 mL 1x PBS containing 1x cOmplete™ protease inhibitor, before sonicating for 3x 10 s at 10% amplitude with a Branson Digital Sonifier 450 cell disruptor (Branson Ultrasonics Corporation, Danbury, US). The sonicated suspension was transferred to low protein binding tubes and centrifuged at 16000 rcf for 20 min at 4 °C. The protein containing supernatant was stored at -20 °C, and the protein concentration was determined using a BCA assay.

3.3.5 Proteomic workup

Proteomes were diluted to 500 μL of 2 mg/mL protein and allowed to react for 1 h at RT with 10 μL THPTA (100 mM in H_2O), 10 μL CuSO_4 pentahydrate (20 mM in H_2O), 10 μL sodium L-ascorbate (300 mM in H_2O), and 10 μL azide-PEG3-Biotin (5 mM in DMSO). After this click reaction, 1 mL of ice cold MeOH was added to precipitate the proteins at -80°C for 1 h. The precipitated proteins were centrifuged at 15000 rcf for 10 min, dried in the air for 15 min, and subsequently dissolved in 500 μL 1x PBS containing 1x cOmplete™ protease inhibitor, and 0.4% SDS. Subsequently, the biotinylated proteins were incubated overnight with 50 μL of Pierce™ Streptavidin Magnetic Beads at 4°C in an end-over-end shaker. Next day, the beads were washed three times with 250 μL wash buffer 1 (ice cold 1x PBS containing 1x cOmplete™ protease inhibitor), three times with 250 μL wash buffer 2 (4M Urea, 0.4% SDS in ice cold 1x PBS containing 1x cOmplete™ protease inhibitor), and finally again three times with 250 μL wash buffer 1. Washed beads were suspended in 25 μL 8M urea, followed by 75 μL 50 mM ammonium bicarbonate. Then 10 μL of 50 mM DTT was added to achieve cleavage of disulfide bridges during 30 min at 37°C . After cooling bead suspensions, 10 μL of 100 mM IAA was added to alkylate the free thiols. Alkylation was followed by addition of 1 μL of 0.5 $\mu\text{g}/\mu\text{L}$ trypsin, and samples were subsequently incubated for 16 h at 37°C to digest the proteins. After this, the peptide solution was transferred to new low protein binding tubes while magnetically removing the Pierce™ Streptavidin Magnetic Beads. To the resulting peptide solution 6 μL of 10% TFA was added. Peptides were cleaned using Pierce™ C18 tips according to the description of the manufacturer and eluted using 100 μL of 50% ACN and 0.1% FA in ultrapure water. The purified samples were evaporated in a Speedyvac concentrator at 30°C (Salm and Kipp, Breukelen, NL).

3.3.6 Proteomic LC-MS analysis

Dried protein fragments were dissolved in 20 μL 2% ACN in 0.1% FA and 5 μL was injected on a nanoLC-MS system (EASY-LCII connected to Q-exactive^{PLUS}, ThermoScientific, US). Peptides were trapped on a 2 cm x 0.1 mm C18 trap column, and separated on an 8 cm x 0.75 mm C18 analytical column (PepSep, DK) using a flow rate of 300 nL/min. Sample loading and trapping was performed in buffer A (0.1% FA in ultrapure water), and elution was performed with a 20 min gradient going from 2% to 30% buffer B (0.1% FA in ACN), followed by column regeneration at 80% buffer B and re-equilibration at 2 % buffer B. The nanoLC eluate was directly sprayed into the source of the Q-exactive by Flex-ion nanospray, using a PepSep nanospray needle at 2.3 kV ESI potential. MS acquisition was performed using a DDA method with alternating MS1 scan at resolution 70000 profile mode, AGC target $3 \cdot 10^6$, maxIT 50 ms, scan range 500–1400 m/z , and subsequently 8 MS2 scans centroid mode, resolution 17500, AGC target $5 \cdot 10^4$, maxIT 100 ms, with isolation window 1.6 m/z at NCE=28 with preferred peptide match ions of charges 2, 3 or 4 and a

dynamic exclusion window of 30 s.

3.3.7 Proteomic data analysis

Proteomic LC-MS data analysis from triplicate incubations was performed using Maxquant software version 1.6.17.0 matching to the Uniprot reference protein database of *Mus musculus* (taxon 10090) from October 2019. Annotation was performed using peptide spectral matching (PSM) with FDR 0.01, and protein FDR 0.01. Intensity-based absolute quantification (iBAQ) scores were calculated for each annotated protein, allowing match between runs. The iBAQ score is defined as the sum of peak intensities of all peptides matching with a specific protein, divided by the number of theoretically observable peptides of that protein (based on trypsin cleavage sites).¹⁴⁸ Data filtering was performed using Perseus software version 1.6.13.0. Only annotated proteins with MS/MS counts (=number of MS/MS spectra of a protein that are matched with a peptide of that protein) >2 were taken into account. All iBAQ scores were log2 transformed, and only proteins with annotations in all replicates of at least one group were taken into account. All missing values were randomly replaced with normally distributed values containing a downshift of 2 and a width of 0.2. Filtering of the data was performed, continuing only with significant proteins ($P < 0.05$) after a two-sample Student's t-test against the UV-treated vehicle (0.1% EtOH). Subsequently, filtering against the UV-treated control probe **8** was performed using a second two sample Student's t-test, continuing only with proteins that significantly ($P < 0.05$) interacted with the PUFA-derived and indomethacin probes. For analytical purpose the resulting dataset was compared to that of the UV-vehicle (0.1% EtOH) in all data analyses. The significantly interacting proteins observed after sequential filtering were analyzed using Uniprot Knowledgebase (<https://www.uniprot.org/>) and using Ingenuity Pathway Analysis (IPA®) (<http://www.ingenuity.com/science/knowledgebase>) from Qiagen Benelux B.V. (Venlo, NL) in December 2020. The Uniprot Knowledgebase is a free online database containing sequences and annotations extracted from literature.¹⁴⁹ The Ingenuity Knowledge Base is a knowledge repository that houses biological and chemical relationships extracted from the scientific literature. Using IPA, interconnected pathways, protein interactions, and clustering of protein functionality and cellular localization was performed for the extracted proteins.

3.3.8 Fluorescence and immunostaining

Immunostaining and additional fluorescent click labelling were based on a protocol from Gaebler *et al.*¹⁵⁰ In short, RAW264.7 macrophages were seeded in Ibidi μ -Slide 8 Well IbiTreated polymer coverslips (Ibidi GmbH, München, Germany) with a density of $2.5 \cdot 10^5$ cells/mL, containing 300 μ L of cell suspension per well. Cells were allowed to grow overnight. The next day, cells were pre-stimulated for 4 h with 1.0 μ g/mL LPS,

after which they were incubated with 10 μ M probe or 0.1% EtOH (vehicle) and 1.0 μ g/mL LPS (LPS pre-stimulation). Alternatively, the cells were directly incubated with 1.0 μ g/mL LPS and the probes or vehicle for 4 h (no LPS pre-stimulation). After incubation, the medium of the adherent cells was discarded and the cells were irradiated at 366 nm for 5 min on ice (lamp conditions as described in *probe incubation*), or placed on ice under 'control' (normal lamp light) conditions. The cells were subsequently washed 3 x 300 μ L 1x PBS, and fixed in 300 μ L 4% paraformaldehyde in PBS for 10 min at room temperature. After 10 min fixation, cells were washed with 3x 300 μ L 1x PBS. Cells were permeabilized for 15 min. in permeabilization buffer consisting of 1x PBS/1% gelatine/0.01% saponin. This was followed by overnight incubation with the primary antibody in PBS/1% gelatine/0.01% saponin at 4 °C, or in PBS/1% gelatine/0.01% saponin without the primary antibody at 4 °C for the control labelling. The next day, the cells were washed three times with 300 μ L PBS, applying 5 min per wash step. The samples were then treated with the GaR-IgG-Alexa Fluor® 488 secondary antibody in PBS/1% gelatin/0.01% saponin for 1h in the dark, after which the samples were again washed with 3x 300 μ L 1x PBS.

The immunostaining protocol was followed by a lissamine rhodamine B staining protocol using Cu(I)-mediated azide alkyne click reaction. The samples were pre-washed with 300 μ L 100 mM HEPES/KOH pH 7.4 (click buffer). Then 300 μ L of click buffer containing 13 μ M lissamine rhodamine B-PEG3-azide was added, to which 6 μ L of 100 mM CuTFP in acetonitrile was added or 6 μ L of acetonitrile for the control incubations. The reaction was allowed to stand for 1 h at RT in the dark. Hereafter, the samples were washed with 300 μ L click buffer, 20 mM EDTA solution, 155 mM ammonium acetate, and 1x PBS. Samples were washed again in 300 μ L citifluor PBS and thin mounted in citifluor glycerol containing 1.43 μ M DAPI. Next, they were stored at 4 °C.

Microscopy was performed using a Zeiss LSM 510-META Confocal laser scanning Zeiss microscope (Oberkochen, DE), equipped with a Plan-Apochromat 63x/NA1.4 oil DIC lens. Representative images were recorded using 2 individual tracks for one sample: in the first track DAPI was excited with a 405 nm laser line and emission recorded at wavelength 420-490 nm; and lissamine rhodamine B was excited with a 543 nm laser line and emission recorded at wavelength above 560 nm using a long pass filter. In the second track Alexafluor 488 was excited using 488 nm laser line and emission recorded between 505-570 nm. Cells were focused at the midplane and represent signal of an optical slice of 1.0 μ m z-thickness. Optical settings were identical for all images and master gain settings were optimized for each individual image, in which control pictures were always imaged with identical or higher master gain settings than the experimental pictures (**Table 3-S1**).

3.3.9 Statistical analysis

LDH cytotoxicity, PGE₂ ELISA, and IL-6 ELISA samples were measured in three separate experiments applying two technical replicates in each experiment. Cytotoxicity values were presented as percentages normalized to 1% Triton X-100 (100% toxicity) and vehicle (0.1% EtOH or DMSO) control (0% toxicity). Cytotoxicity values, PGE₂ concentrations, and IL-6 concentrations are presented as mean with SD.

Graphical presentation and statistical analysis with one-way ANOVA using Dunnett's multiple comparison *post-hoc*, or one-way ANOVA using Tukey multiple comparison *post-hoc* was performed in GraphPad Prism v 5.0 (GraphPad Software, San Diego, US).

3.4 Results and Discussion

The bi-functional PUFA amide-derived probes (**Figure 3-1**) contain a photo-activatable diazirine for covalent attachment after 366 nm UV-light treatment, and a terminal alkyne for CuAAC based affinity purification or labelling with a fluorescent group. The diazirine was introduced at the *N*-acyl end of the PUFA probe, where it likely not interfered with the biological activity of PUFA-derived amides.⁶ Probe **2** and **3** are synthetic derivatives of DHEA **1**, in which probe **2** has the alkyne at the *N*-acyl end, and probe **3** has the alkyne at the PUFA tail. Probe **5** is a synthetic mimic of the *n*-6 PUFA derivative AEA **4**, having the alkyne and diazirine at the *N*-acyl end of the molecule, probe **7** is a previously reported NSAID probe of indomethacin **6**,²⁴ and was used as a positive control,²⁴ and probe **8** is a short pentynoyl-derived negative control probe lacking immunological effects. Identified interactions with control probe **8** are used to filter out non-specific PUFA-derived probe interactions in the data analysis of the proteomics. Following earlier studies of anti-inflammatory effects of DHEA and AEA,^{9, 12, 14-15, 17-18, 21, 26} probe concentration of 10 μM were used, which is equivalent or below comparable studies with similar lipid probes.^{6, 27-28} Lastly, applying 10 μM of probe counters the attrition that is associated with different steps in the methodology (*i.e.*, uptake of probes by the macrophages, non-quantitative yield of photolabeling,²² loss during enrichment), to obtain sufficient levels of labeled protein above the detection limit of the LC-MS/MS.

3.4.1 Probes reduce PGE₂ and IL-6 concentrations

We verified that our probes have similar biological effects as their parent compounds by measuring the production of PGE₂ and IL-6 as well as the cytotoxicity of the chemical probes in 1.0 μg/mL LPS-stimulated RAW264.7. No significant cytotoxicity was observed for the PUFA-derived probes, and only for indomethacin probe **7** limited cytotoxicity

was observed when compared to the vehicle control (**Figure 3-S2, Table 3-S2**).

Incubation with 10 μ M DHEA reduced PGE₂ levels in the medium with 89% compared to the vehicle control (from 3.62 ± 1.26 ng/mL to 0.40 ± 0.10 ng/mL ($P < 0.001$)), and incubation with 10 μ M of synthetic DHEA probes **2** or **3** reduced PGE₂ levels with 96% (0.16 ± 0.03 ng/mL ($P < 0.001$)) or with 93% (0.27 ± 0.05 ng/mL ($P < 0.001$)), respectively (**Figure 3-2A, Table 3-S2**). Similarly, incubation with 10 μ M indomethacin or indomethacin probe **7** reduced PGE₂ concentrations in the medium to levels below accurately quantifiable concentrations, indicating almost complete inhibition in COX-2 activity (**Table 3-S2**). Strong COX-2 inhibition by indomethacin and indomethacin probe **7** was reported previously.²⁴ Incubation with 10 μ M of the negative control probe **8** resulted in slightly reduced PGE₂ levels in the medium (**Table 3-S2**).

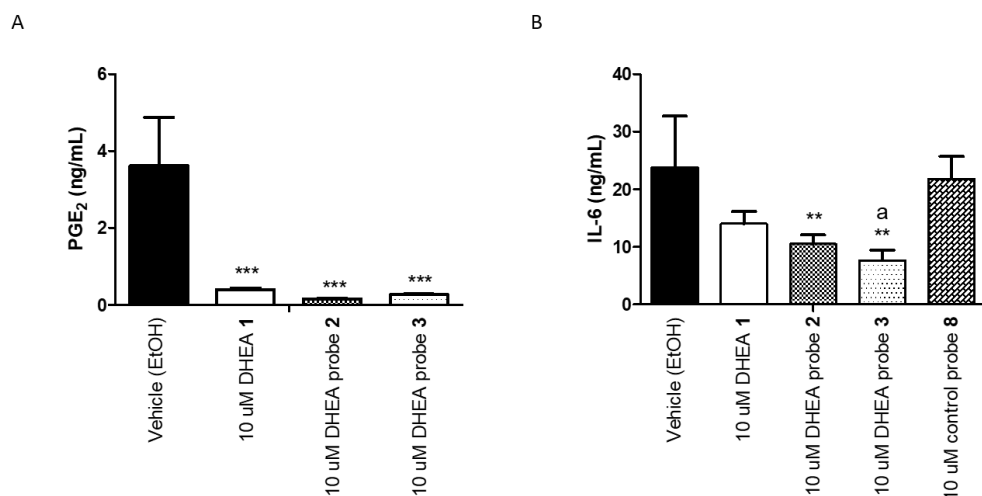


Figure 3-2 Medium concentration of inflammatory regulators released from 1.0 μ g/mL LPS-stimulated RAW264.7 macrophages, incubated with 10 μ M of DHEA **1**, 10 μ M of DHEA derived synthetic probes **2** or **3**, or 10 μ M negative control probe **8**. A) Medium concentrations of PGE₂. B) Medium concentrations of IL-6. Bars represent mean with SD (N=3, technical duplicates). Asterisks indicate significant differences from vehicle (EtOH) control (one-way ANOVA, Dunnett's multiple comparison *post-hoc*; * $P < 0.05$, ** $P < 0.01$, *** $P < 0.001$). 'a' indicates significance between 10 μ M DHEA **1** and 10 μ M DHEA probe **3** incubation (one-way ANOVA, Tukey multiple comparison *post-hoc*; $P < 0.05$).

Similar to PGE₂, medium IL-6 levels were reduced by DHEA in 1.0 μ g/mL LPS-stimulated macrophages.⁹ After 24 h of incubation with 10 μ M DHEA, reduction of 41% in IL-6 medium levels (from 23.7 ± 8.9 ng/mL to 14.0 ± 5.3 ng/mL) was observed, not

reaching significance. Incubations with 10 μ M of the synthetic DHEA probes **2** and **3** did, however, significantly reduced IL-6 concentrations in the medium with 56% (10.5 ± 3.9 ng/mL ($P < 0.01$)) and 68% (7.6 ± 4.3 ng/mL ($P < 0.01$)), respectively. Statistical analysis using Tukey's multiple comparison test indicated that incubation with 10 μ M DHEA probe **3** was significantly more effective ($P < 0.05$) in reducing IL-6 production than 10 μ M DHEA. Control probe **8** (**Figure 3-2B**), indomethacin **6**, and indomethacin probe **7** did not significantly affect IL-6 production (**Table 3-S2**). IL-6 production was also not significantly affected by AEA or AEA probe **5** when compared to vehicle incubation. Remarkably, incubation with 10 μ M AEA probe **5** reduced IL-6 levels with 49% (12.2 ± 9.7 ng/mL), whereas 10 μ M AEA increased IL-6 levels to 122% (29.2 ± 10.9 ng/mL), which corresponds to a significant ($P < 0.05$) difference between 10 μ M AEA and 10 μ M AEA probe **5** incubations using Tukey's multiple comparison test (**Table 3-S2**). Although this outcome might suggest a distinct immunological effect of AEA and its corresponding probe **5** on IL-6, contradicting literature reports lead us to conclude that IL-6 is probably not a suitable marker for the immunological effects of AEA.²⁹⁻³¹

In conclusion, we showed that the synthesized DHEA and indomethacin probes mimic the expected anti-inflammatory effects of the parent compounds in 1.0 μ g/mL LPS-stimulated RAW264.7 macrophages, which was not the case for our negative control probe **8**.

3.4.2 Synthetic probes localize around ER and in membrane vesicles

To better understand the biological functionality of our compounds, we first analyzed the *in vitro* localization of 4 h incubated 10 μ M of the synthetic probes in 1.0 μ g/mL LPS-stimulated RAW264.7 macrophages. The probes were visualized with lissamine rhodamine B PEG3 azide using tetrakis(acetonitrile)copper(I) hexafluorophosphate, in chemically fixed cells that were immunostained with alpha-tubulin Alexafluor488, and nuclear DAPI dsDNA staining (**Figure 3-3**). Control samples showed no non-specific labelling of lissamine rhodamine B and Alexafluor488 (**Figure 3-S3**, **Figure 3-S4**).

DHEA probe **2** was taken up by LPS-stimulated RAW264.7 macrophages in 4 h, and localized around the nuclear periphery in the cytosol, suggesting agglomeration in the ER and Golgi system (**Figure 3-3A1**). In addition, DHEA probe **2** clustered in spherical membrane domains. As the slightly different DHEA probe **3** showed similar intracellular localization as DHEA probe **2** (**Figure 3-3A2**), we conclude that the observations relate to localization of intact DHEA probes. Similarly, AEA probe **5** showed cytoplasmatic staining and an apparent high level of spherical domain compartmentalization (**Figure 3-3A3**). Therefore, PUFA-derived amides tend to localize around the ER where they are generally catabolized by enzymes like COX-2.³² Although metabolic breakdown

of the probes cannot be ruled out completely, we previously showed that intracellular DHEA concentrations in LPS-stimulated RAW264.7 macrophages remained stable for 48 h,¹⁷ and that DHEA exposure did not lead to measurable DHA levels in the medium of LPS-stimulated RAW264.7 macrophages,⁹ likely associated with low expression levels of FAAH in LPS-stimulated RAW264.7 macrophages.⁹ More detailed assessment of the metabolic fate of our probes could be studied by metabolic tracing as described by Thiele and coworkers,³³⁻³⁴ *e.g.*, to quantify probe levels in phospholipids.

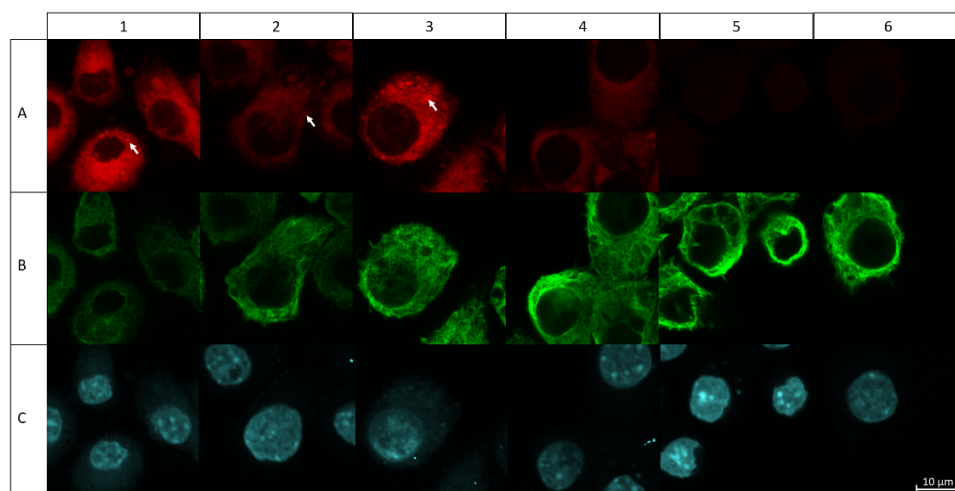


Figure 3-3 Confocal fluorescent images of 1.0 $\mu\text{g/mL}$ LPS stimulated RAW264.7 macrophages. Rows: A) Lissamine rhodamine B channel after CuAAC to lissamine rhodamine B. B) Immunostained tubulin. C) DAPI staining. Columns: 1) 10 μM DHEA probe 2. 2) 10 μM DHEA probe 3. 3) 10 μM AEA probe 5. 4) 10 μM indomethacin probe 7. 5) 10 μM probe 8. 6) 0.1% EtOH vehicle. Arrows highlight vesicle compartmentalization. Scale bar applies to all images in the figure.

Indomethacin probe 7 labeling was weaker than with PUFA derivatives and was also localized inside the cytoplasm (**Figure 3-3A4**). For control probe 8 we observed almost no fluorescent labeling, suggesting its limited uptake or rapid breakdown (**Figure 3-3A5**). Control incubations with the vehicle (0.1% EtOH) showed no background fluorescence from the lissamine rhodamine B (**Figure 3-3A6**).

Specific counterstaining of alpha-tubulin resulted in AlexaFluor488-stained cytoskeleton (**Figure 3-3B**), proving that fixation and immunofluorescence are successfully combined with click labelling of lipids, as reported previously.³⁵ Z-stack projection of tubulin staining additionally showed fine tubulin structures indicating no or limited fixation damage during the preparation of the slides (**Figure 3-S5**, **Video 3-S1**). DAPI staining of

nuclei clearly showed more intense labeling of condensed heterochromatic segments and less intense signals of euchromatic segments in the nucleus (**Figure 3-3C**). Our confocal fluorescent analysis provided evidence for the uptake of our PUFA probes **2** and **3** as well as indomethacin probe **7** in LPS-stimulated macrophages over a period of 4 h, resulting in localization around the ER and in membrane vesicles.

3.4.3 Characterization of PUFA-derived probe interactome

Molecular interaction partners of our probes were identified by proteomic characterization of the interactome in 8 h LPS-stimulated and 4 h probe incubated macrophages. Data-analysis using iBAQ scores enabled identification of relative abundances of proteins.³⁶⁻³⁷ After filtering out non-specific background interactions using signals from the vehicle (0.1% EtOH) incubations and statistical evaluation using a two-sample Student's t-test ($p < 0.05$, and t-test difference > 1.0), 101 significantly enriched proteins were found for DHEA probe **2**, 198 proteins for DHEA probe **3**, 273 proteins for AEA probe **5**, and 55 proteins for indomethacin probe **7**. Sequential filtering using the randomly interacting control probe **8** and a second two-sample Student's t-test ($p < 0.05$, and t-test difference > 1.0) resulted in 6 significantly enriched proteins for DHEA probe **2**, 62 proteins for DHEA probe **3**, 114 proteins for AEA probe **5**, and 4 proteins for indomethacin probe **7**. Significantly enriched proteins resulting from the sequential filtering were displayed against the vehicle (0.1% EtOH) treatment (**Figure 3-4A,B, Table 3-S3**). Despite sequential filtering, also with probe **8**, we identified targets such as ribosomal and cytoskeletal proteins, which are likely non-specific protein targets. Notwithstanding, comparison of enriched proteins with previous chemical proteomic enrichment studies revealed that 52 of the 114 AEA probe **5** targets were also enriched by A-DA and/or AEA-DA, two AEA-based chemical probes, in HEK293T/Neuro2a cells.⁶ Moreover, DHEA probe **3** and AEA probe **5** were found to interact with Ptg2 (also known as COX-2), of which we and others previously demonstrated that this enzyme is involved in the oxygenation of AEA and DHEA (**Figure 3-4A,B**).^{5,17}

Uniprot database and Ingenuity Pathway Analysis (IPA®) were used to identify cellular domain(s) and functional annotation of the protein targets (**Figure 3-4C,D**). Most proteins localized in the cytoplasm (**Figure 3-4C**), confirming our observed cytoplasmatic localization (**Figure 3-3**). In addition to enzymes, we identified transcription and translation regulators, as well as transporters (**Figure 3-4D**). Comparison of the enriched proteins for DHEA probe **2** and **3**, and AEA probe **5** revealed that only three proteins interacted with all three PUFA amide probes (**Figure 3-4E**). In total 38 shared targets were found for DHEA probe **3** and AEA probe **5**, whereas 20 proteins were specific targets of DHEA probe **3**, and 72 proteins were specific targets of AEA probe **5**.

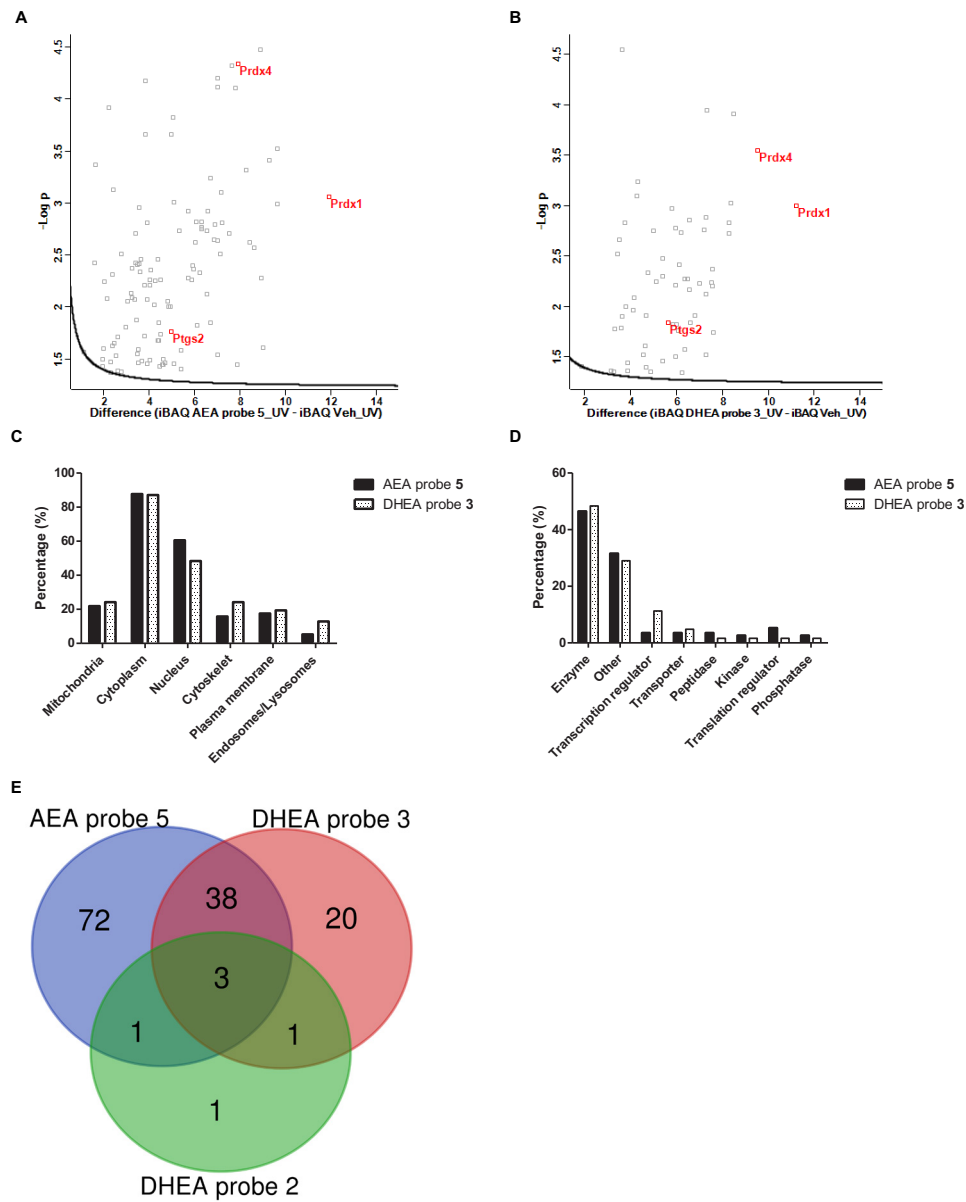


Figure 3-4 Proteomics analyses of DHEA probe 2, 3, and AEA probe 5 (N=3). A) Volcano plot (FDR 0.05, S0 0.1) of AEA probe 5. B) Volcano plot (FDR 0.05, S0 0.1) of DHEA probe 3. Both A and B show sequentially filtered data against the vehicle (0.1% EtOH control). X-axis represents 2log[iBAQ] values (probe – vehicle) differences, and y-axis represents -log p values. C) Protein ontology of AEA probe 5 and DHEA probe 3 targets according to Uniprot. D) Cellular function of AEA probe 5 and DHEA probe 3 targets according to IPA analysis. E) Venn diagram of DHEA probe 2, 3, and AEA probe 5 targets.

Both DHEA probe **3** and AEA probe **5** showed strongest specific interaction with peroxiredoxin 1 (Prdx1) (**Figure 3-4A,B**, **Table 3-1**, **Table 3-2**). Also, Prdx4 labelling was significant for both PUFA derived amide probes (**Figure 3-4A,B**). Peroxiredoxins convert hydrogen peroxide to water and lipid hydroperoxides to alcohols, protecting the cells from ROS toxicity.³⁸⁻³⁹ Although many studies described the anti-inflammatory and protective effects of peroxiredoxins, Prdx1 knockdown decreased inflammatory cytokine production and increased anti-inflammatory IL-10 production in LPS-stimulated RAW264.7 macrophages.⁴⁰ Selective binding of our PUFA amides to Prdx1 could therefore be linked with blockage of the Prdx1-induced inflammation in RAW264.7 cells. Previous proteomic screening with AA, the PUFA precursor of AEA, also showed interaction of AA with ROS regulators in RAW264.7 macrophages, which was ascribed to the induction of lipid electrophile-driven coupling upon stimulation of the macrophages with the LPS mimetic Kdo₂-lipid A.²⁸ Although our methodology used diazirine cross-linking, lipid electrophile coupling to ROS scavengers could not be ruled out as possible interaction mechanism between AEA, DHEA, and peroxiredoxins. Interestingly, both DHEA and AEA were reported to induce ROS production in HNSCC cells,^{12, 26} and in 0.1 µg/mL LPS-stimulated mouse macrophages, 10 nM DHEA was found to reduce ROS production.¹⁰ Next to Prdxs, we found ribosomal proteins, Acat1 (Acetyl-CoA acetyltransferase, mitochondrial), and the signaling regulator Rhoc in the top 10 of AEA probe **5** interactors (**Table 3-1**).⁴¹

The top 10 of DHEA probe **3** interactors showed two intracellular membrane trafficking proteins: Rab1a and Rab5c (**Table 3-2**). Rab1a regulates cell adhesion and cell migration via β 1 integrin recycling, and is localized in the ER and intracellular vesicle domains where DHEA was localized (**Figure 3-3**).⁴² Rab5c is a key regulator in early endosome trafficking and is involved in cell migration via β 1 integrin recycling.⁴³ Interestingly, these observations add to the ongoing debate concerning the uptake mechanism of PUFA derivatives, occurring via a currently unidentified membrane transporter or via passive diffusion.^{8, 44} Characterization of endosomal proteins interacting with DHEA probe **3** and AEA probe **5** might indicate that lipid raft and caveolae-dependent endocytosis is an uptake route for those PUFA-derivatives, as was previously suggested for AEA by McFarland and coworkers.⁴⁵ This hypothesis is further supported by identification of the DHEA probe **3** interactor Dnm2, which has important functions in endosomal formation (**Table 3-S3**).⁴⁶ Clearly, focused studies should be aimed at unravelling the uptake mechanisms of AEA and DHEA to support an endocytosis-dependent uptake mechanism. The transcription regulator Pa2g4, and the pro-inflammatory immune regulator Ifit1 were also significantly bound by DHEA probe **3**. Recently, we reported that expression of Ifit1 was reduced as a result of incubation with 5 µM of 13-HDHEA and 16-HDHEA, products of the interaction between DHEA and COX-2.¹⁸ As significant

Ifit1 interaction with AEA probe 5 was not observed here, it appears that Ifit1 is only involved in signaling of DHEA or its metabolites. Interestingly, previously described endocannabinoid interacting proteins, *e.g.*, CB1, CB2, GPR55, but also TRPV1 and PPAR,^{1, 3-4, 7-8, 19, 21} are not identified in our model, likely due to poor expression of those proteins in LPS-stimulated RAW264.7 macrophages.⁹

Table 3-1 Protein targets AEA probe 5. Only the 10 most different proteins between the vehicle (0.1% EtOH) and 10 μ M AEA probe 5 incubation are reported as 2log[iBAQ] values (probe – vehicle). Protein differences and p-values were determined using a two-sample Student's t-test ($p < 0.05$).

Protein IDs	Protein names	Gene names	-Log Student's T-test p-value iBAQ AEA probe 5 vs. iBAQ vehicle (0.1% EtOH)	Student's T-test difference iBAQ AEA probe 5 vs. iBAQ vehicle (0.1% EtOH)
P35700	Peroxiredoxin-1	Prdx1	3.06	11.93
Q9JJ18	60S ribosomal protein L38	Rpl38	3.52	9.64
Q62159; P62746	Rho-related GTP-binding protein Rhoc	Rhoc	2.99	9.64
Q9Z1N5	Spliceosome RNA helicase Ddx39b	Ddx39b	3.41	9.31
Q8BFZ3	Beta-actin-like protein 2	Actbl2	1.61	9.02
P47915	60S ribosomal protein L29	Rpl29	2.28	8.94
P62245	40S ribosomal protein S15a	Rps15a	4.47	8.90
Q8BP67	60S ribosomal protein L24	Rpl24	2.57	8.63
O09167	60S ribosomal protein L21	Rpl21	2.62	8.42
Q8QZT1	Acetyl-CoA acetyltransferase, mitochondrial	Acat1	3.31	8.27

In conclusion, we observed Prdx-1, Prdx-4, Rhoc, and Acat1 as important AEA probe interactors in LPS-stimulated RAW264.7 macrophages. From these targets only Prdx-1 was already characterized as potential AEA target.⁶ Next to these AEA targets, Prdx1, Rab1a, Rab5c, Pa2g4, and Ifit1 were identified as most important DHEA interacting proteins. Our chemical biological high-throughput method enabled identification of novel PUFA-amide targets that could not have been revealed with classical endocannabinoid receptor binding studies.

Table 3-2 Protein targets DHEA probe 3. Only the 10 most different proteins between the vehicle (0.1% EtOH) and 10 μ M DHEA probe 3 incubation are reported as $2\log[\text{iBAQ}]$ values (probe – vehicle). Protein differences and p-values were determined using a two-sample Student's t-test ($p < 0.05$).

Protein IDs	Protein names	Gene names	-Log Student's T-test p-value iBAQ DHEA probe 3 vs. iBAQ vehicle (0.1% EtOH)	Student's T-test difference iBAQ DHEA probe 3 vs. iBAQ vehicle (0.1% EtOH)
P35700	Peroxiredoxin-1	Prdx1	2.99	11.24
O08807	Peroxiredoxin-4	Prdx4	3.54	9.52
P47911	60S ribosomal protein L6	Rpl6	3.91	8.47
Q60605; Q8CI43	Myosin light polypeptide 6	Myl6	3.02	8.38
P47738	Aldehyde dehydrogenase, mitochondrial	Aldh2	2.72	8.30
P62821; Q9D1G1	Ras-related protein Rab-1A; Ras-related protein Rab-1B	Rab1A; Rab1b	2.83	8.28
P35278	Ras-related protein Rab-5C	Rab5c	1.74	7.63
P50580	Proliferation-associated protein 2G4	Pa2g4	2.20	7.59
P45376	Aldose reductase	Akr1b1	2.37	7.56
Q64282	Interferon-induced protein with tetratricopeptide repeats 1	Ifit1	2.24	7.55

3.4.4 IPA® analysis indicates involvement of GTPase-signaling

Functional IPA® analysis revealed that enriched protein targets of DHEA probe 3 and AEA probe 5 are mainly involved in Rho family GTPase-signaling and actin regulation. A notable protein in the regulation of this pathway is Rac1, which was identified as significant interactor with DHEA probe 3 and AEA probe 5, but did suffer from relatively weak spectral matching scores and should therefore be interpreted with care. Notwithstanding, 21 of the 62 protein hits from DHEA probe 3 and 48 of the 114 protein hits from AEA probe 5 (including Rac1 itself) were identified as (putative) Rac1 interacting proteins to further support the potential role of Rac1 in PUFA-derived amide mediated GTPase-signaling.⁴⁷⁻⁴⁸ Rho GTPase-signaling plays an important role in ROS signaling, cell migration, cytoskeletal remodeling, and actin regulation.⁴⁸⁻⁵⁰ Indeed, these phenotypic effects can be related to previously reported functions of DHEA and AEA. The effects of DHEA and AEA on ROS regulation were already described above, and other studies reported anti-migratory properties of AEA^{3-4, 10} and DHEA,¹⁰ including its oxidized metabolites.^{15-16, 18} In addition to small GTPase-signaling several actin and myosin-related proteins were also significantly affected by DHEA probe 3 and AEA probe 5 to suggest cytoskeletal remodeling as prerequisite for migration.

Disease and function analysis in IPA® found indications for a response similar to viral infections for DHEA probe **3** proteins, and cellular organization, response to viral infections, and reduced cell death for AEA probe **5** proteins. However, as IPA® analysis uses experimental results from literature reports, it is suboptimal for our current methodology, which was aimed at unravelling novel interactions. In conclusion, links to ROS signaling, actin remodeling, and cell migration were obtained using IPA® analysis, but additional research is required to prove that these effects are mediated by GTPase-signaling via DHEA and AEA interactions.

3.4.5 Colocalization support DHEA and AEA interactions with Rac1 and Ptgs2

To support a suggested role in endosomal trafficking, Rho GTPase-signaling, and lipid metabolism, we performed fluorescent confocal imaging studies staining DHEA probe **3** and AEA probe **5** with lissamine rhodamine B, and Rab5c, Rac1, and Ptgs2 with Alexafluor488 immunostaining (**Figure 3-5**). RAW264.7 macrophages were pre-stimulated for 4 h with 1.0 µg/mL LPS and subsequently exposed to 10 µM DHEA probe **3** or 10 µM AEA probe **5** and 1.0 µg/mL LPS for 4 h, mimicking conditions of the proteomic experiment to allow correlations. In addition to midplane images (**Figure 3-5**), Z-stack series were recorded, showing that midplane images are representative for the fluorescence localization (**Video 3-S2-7**). Cytoplasmatic localization was observed for the green Rac1 channel that often colocalized with the spectrally well-separated red PUFA-derived probes in the cell (**Figure 3-5A1**, **Figure 3-5B1**), indicating potential interaction of Rac1 with the PUFA probes. Nonetheless, areas that contained only a signal corresponding to Rac1 or to the PUFA-derived probes were also obtained. Rab5c immunostaining resulted in localization of small vesicles possibly representing late endosomes, but showed no clear colocalization with our probes (**Figure 3-5A2**, **Figure 3-5B2**). Ptgs2 staining showed main Ptgs2 signals at the cytoplasmic face of nuclear periphery, known to be rich in ER where Ptgs2 synthesis takes place (**Figure 3-5A3**, **Figure 3-5B3**).⁵¹ Interestingly, the fluorescent signal of the PUFA amide probes was also relatively strong in the nuclear periphery. Although areas of colocalizing Ptgs2 and PUFA derived amide probes were observed, the signal from Ptgs2 and the probes did not fully colocalize. Even though colocalization within the same voxel (~270x270x1000 nm) does not directly proof molecular interaction, this is a prerequisite. Nevertheless, our observations further support that PUFA derived amides could interact with multiple partners including Rac1 and Ptgs2. Direct proof for the interaction between the PUFA amides and Ptgs2 was indeed previously demonstrated by the Ptgs2 mediated catabolic conversion of AEA and DHEA.^{1, 5, 17} Controls without primary Rac1, Rab5c, and Ptgs2 antibodies showed no immunofluorescence, indicating specificity of the antibodies and immunostaining protocol (**Figure 3-S6**). In conclusion, confocal fluorescence microscopy showed colocalization between the PUFA-derived probes and Rac1

and Ptgs2 as a prerequisite for molecular interaction. Together with the previously characterized biochemical interaction in the proteomic setup and the reported metabolic interaction between the PUFA amides and Ptgs2, these data strongly support a functional interaction.

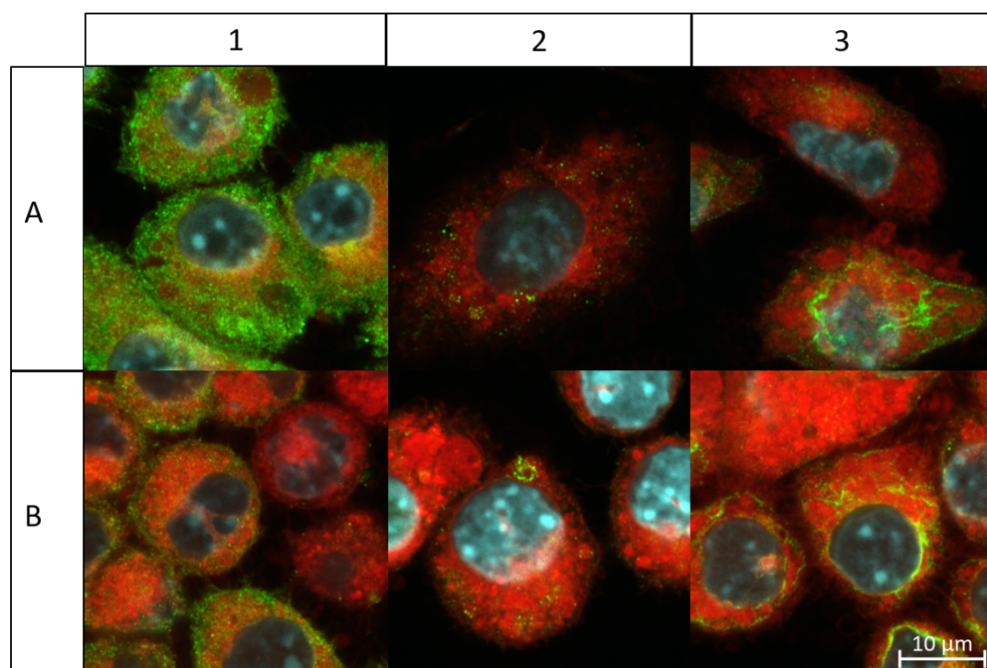


Figure 3-5 Confocal fluorescent images of probe incubated RAW264.7 macrophages pre-stimulated for 4 h with 1.0 µg/mL LPS. A) Cells incubated with fresh 1.0 µg/mL LPS and 10 µM DHEA probe **3** for an additional 4 h. B) Cells incubated with fresh 1.0 µg/mL LPS and 10 µM AEA probe **5** for an additional 4 h. Color overlays represent lissamine rhodamine B (red), Alexafluor488 antibody (green), and DAPI staining (blue). 1) Visualizes Rac1 labelling, 2) visualizes Rab5c labelling, 3) visualizes Ptgs2 labelling. Scale bar applies to all images in the figure.

3.5 Conclusion

Chemical probes of DHEA and AEA containing two specific tagging functionalities showed that PUFA amides interact with Prdx1, Prdx4, endosomal proteins like Rab1 and Rab5c, and proteins of the GTPase-signaling pathway in LPS-stimulated RAW264.7 macrophages, rather than only with Ptgs2. In addition, fluorescence labelling of our probes indicated localization in the cytosol, and seemingly the ER and Golgi system, next to compartmentalization in membrane vesicles. Colocalization experiments

using confocal fluorescent microscopy supported interactions between PUFA-derived probes and the small GTPase-regulating protein Rac1 as well as Ptg2. Together, these observations provide novel insights in cellular PUFA amide interactions and their effects on cytoskeletal remodeling, cell migration, and ROS regulation. In addition, our results provide evidence for passive endosomal uptake mediated by lipid rafts.

In view of the unnaturally high lipid probe concentrations used in our and similar studies, future research should strengthen the interactome data sets by reducing non-specific binding or potential metabolism of probes. Additional details regarding PUFA amide-protein interactions that regulate ROS formation, cytoskeletal remodeling and cell migration may also be obtained, as well as support of a lipid raft-dependent uptake mechanism of PUFA-derived amides. This might enable translation of *in vitro* effects of DHEA and AEA to *in vivo* models, and ultimately to human metabolism.

3.6 Acknowledgements

The authors thank Daan Boogers for his help in the optimization of the proteomics workup, Mieke Poland for her assistance with the cell incubations and biological assays, Barend van Lagen for his assistance with the NMR measurements, and Frank Claassen for his assistance with mass spectrometry measurements, and VLAG graduate school of Wageningen University for their financial support..

3.7 References

1. de Bus, I.; Witkamp, R.; Zuilhof, H.; Albada, B.; Balvers, M., The role of n-3 PUFA-derived fatty acid derivatives and their oxygenated metabolites in the modulation of inflammation. *Prostaglandins Other Lipid Mediat.* **2019**, *144*, 106351.
2. Watson, J. E.; Kim, J. S.; Das, A., Emerging class of omega-3 fatty acid endocannabinoids & their derivatives. *Prostaglandins Other Lipid Mediat.* **2019**, *143*, 106337.
3. Chiurchiù, V.; Battistini, L.; Maccarrone, M., Endocannabinoid signalling in innate and adaptive immunity. *Immunology* **2015**, *144*, 352-364.
4. Turcotte, C.; Chouinard, F.; Lefebvre, J. S.; Flamand, N., Regulation of inflammation by cannabinoids, the endocannabinoids 2-arachidonoyl-glycerol and arachidonoyl-ethanolamide, and their metabolites. *J. Leukoc. Biol.* **2015**, *97*, 1049-1070.
5. Alhouayek, M.; Muccioli, G. G., COX-2-derived endocannabinoid metabolites as novel inflammatory mediators. *Trends Pharmacol.* **2014**, *35*, 284-292.
6. Niphakis, M. J.; Lum, K. M.; Cognetta III, A. B.; Correia, B. E.; Ichu, T.-A.; Olucha, J.; Brown, S. J.; Kundu, S.; Piscitelli, F.; Rosen, H.; Cravatt, B. F., A Global Map of Lipid-Binding Proteins and Their Ligandability in Cells. *Cell* **2015**, *161*, 1668-1680.
7. Pertwee, R. G.; Howlett, A. C.; Abood, M. E.; Alexander, S. P. H.; Di Marzo, V.; Elphick, M. R.; Greasley, P. J.; Hansen, H. S.; Kunos, G.; Mackie, K.; et al., International Union of Basic and Clinical Pharmacology. LXXIX. Cannabinoid Receptors and Their Ligands: Beyond CB1 and CB2. *Pharmacol. Rev.* **2010**, *62*, 588-631.
8. Maccarrone, M., Metabolism of the Endocannabinoid Anandamide: Open Questions after 25 Years. *Front. Mol. Neurosci.* **2017**, *10*, 166.
9. Meijerink, J.; Poland, M.; Balvers, M. G. J.; Plastina, P.; Lute, C.; Dwarkasing, J.; van Norren, K.; Witkamp, R. F., Inhibition of COX-2-mediated eicosanoid production plays a major role in the anti-inflammatory effects of the endocannabinoid N-docosahexaenoylethanolamine (DHEA) in macrophages. *Br. J. Pharmacol.* **2015**, *172*, 24-37.
10. Park, T.; Chen, H.; Kim, H.-Y., GPR110 (ADGRF1) mediates anti-inflammatory effects of N-docosahexaenoylethanolamine. *J. Neuroinflammation* **2019**, *16*, 225.
11. Lee, J.-W.; Huang, B. X.; Kwon, H.; Rashid, M. A.; Kharebava, G.; Desai, A.; Patnaik, S.; Marugan, J.; Kim, H.-Y., Orphan GPR110 (ADGRF1) targeted by N-docosahexaenoylethanolamine in development of neurons and cognitive function. *Nat. Commun.* **2016**, *7*, 13123.
12. Park, S.-W.; Hah, J. H.; Oh, S.-M.; Jeong, W.-J.; Sung, M.-W., 5-lipoxygenase mediates docosahexaenoyl ethanolamide and N-arachidonoyl-L-alanine-induced reactive oxygen species production and inhibition of proliferation of head and neck squamous cell carcinoma cells. *BMC Cancer* **2016**, *16*, 1-14.
13. Paton, K. F.; Shirazi, R.; Vyssotski, M.; Kivell, B. M., N-docosahexaenoyl ethanolamine (synaptamide) has antinociceptive effects in male mice. *Eur. J. Pain* **2020**, *24*, 1990-1998.
14. McDougale, D. R.; Watson, J. E.; Abdeen, A. A.; Adili, R.; Caputo, M. P.; Krapf, J. E.; Johnson, R.

- W.; Kilian, K. A.; Holinstat, M.; Das, A., Anti-inflammatory ω -3 endocannabinoid epoxides. *Proc. Natl. Acad. Sci. U.S.A.* **2017**, *114*, E6034-E6043.
15. Roy, J.; Watson, J. E.; Hong, I. S.; Fan, T. M.; Das, A., Antitumorigenic Properties of Omega-3 Endocannabinoid Epoxides. *J. Med. Chem.* **2018**, *61*, 5569–5579.
16. Yang, R.; Fredman, G.; Krishnamoorthy, S.; Agrawal, N.; Irimia, D.; Piomelli, D.; Serhan, C. N., Decoding Functional Metabolomics with Docosahexaenoyl Ethanolamide (DHEA) Identifies Novel Bioactive Signals. *J. Biol. Chem.* **2011**, *286*, 31532-31541.
17. de Bus, I.; Zuilhof, H.; Witkamp, R.; Balvers, M.; Albada, B., Novel COX-2 products of n-3 polyunsaturated fatty acid-ethanolamine-conjugates identified in RAW 264.7 macrophages. *J. Lipid Res.* **2019**, *60*, 1829-1840.
18. de Bus, I.; van Krimpen, S.; Hooiveld, G. J.; Boekschoten, M. V.; Poland, M.; Witkamp, R.; Albada, B.; Balvers, M., Immunomodulating effects of 13- and 16-hydroxylated docosahexaenoyl ethanolamide in LPS stimulated RAW264.7 macrophages. *Biochim. Biophys. Acta Mol. Cell Biol. Lipids* **2021**, *1866*, 158908.
19. Alharthi, N.; Christensen, P.; Hourani, W.; Otori, C.; Barrett, D. A.; Bennett, A. J.; Chapman, V.; Alexander, S. P. H., n-3 polyunsaturated N-acylethanolamines are CB2 cannabinoid receptor-preferring endocannabinoids. *Biochim. Biophys. Acta Mol. Cell Biol. Lipids* **2018**, *1863*, 1433-1440.
20. Brown, I.; Lee, J.; Sneddon, A. A.; Cascio, M. G.; Pertwee, R. G.; Wahle, K. W. J.; Rotondo, D.; Heys, S. D., Anticancer effects of n-3 EPA and DHA and their endocannabinoid derivatives on breast cancer cell growth and invasion. *Prostaglandins Leukot Essent Fatty Acids* **2020**, *156*, 102024.
21. Rovito, D.; Giordano, C.; Vizza, D.; Plastina, P.; Barone, I.; Casaburi, I.; Lanzino, M.; De Amicis, F.; Sisci, D.; Mauro, L.; et al., Omega-3 PUFA ethanolamides DHEA and EPEA induce autophagy through PPAR γ activation in MCF-7 breast cancer cells. *J. Cell. Physiol.* **2013**, *228*, 1314-1322.
22. Dubinsky, L.; Krom, B. P.; Meijler, M. M., Diazirine based photoaffinity labeling. *Bioorg. Med. Chem.* **2012**, *20*, 554-570.
23. Wright, M. H.; Sieber, S. A., Chemical proteomics approaches for identifying the cellular targets of natural products. *Nat. Prod. Rep.* **2016**, *33*, 681-708.
24. Gao, J.; Mfuh, A.; Amako, Y.; Woo, C. M., Small Molecule Interactome Mapping by Photoaffinity Labeling Reveals Binding Site Hotspots for the NSAIDs. *J. Am. Chem. Soc.* **2018**, *140*, 4259-4268.
25. Miyamoto, D. K.; Flaxman, H. A.; Wu, H.-Y.; Gao, J.; Woo, C. M., Discovery of a Celecoxib Binding Site on Prostaglandin E Synthase (PTGES) with a Cleavable Chelation-Assisted Biotin Probe. *ACS Chem. Biol.* **2019**, *14* (12), 2527-2532.
26. Park, S.-W.; Kim, J.-E.; Oh, S.-M.; Cha, W.-J.; Hah, J.-H.; Sung, M.-W., Anticancer effects of anandamide on head and neck squamous cell carcinoma cells via the production of receptor-independent reactive oxygen species. *Head Neck* **2015**, *37*, 1187-1192.

27. Isobe, Y.; Kawashima, Y.; Ishihara, T.; Watanabe, K.; Ohara, O.; Arita, M., Identification of Protein Targets of 12/15-Lipoxygenase-Derived Lipid Electrophiles in Mouse Peritoneal Macrophages Using Omega-Alkynyl Fatty Acid. *ACS Chem. Biol.* **2018**, *13*, 887-893.
28. Beavers, W. N.; Rose, K. L.; Galligan, J. J.; Mitchener, M. M.; Rouzer, C. A.; Tallman, K. A.; Lamberson, C. R.; Wang, X.; Hill, S.; Ivanova, P. T.; et al., Protein Modification by Endogenously Generated Lipid Electrophiles: Mitochondria as the Source and Target. *ACS Chem. Biol.* **2017**, *12* (8), 2062-2069.
29. Alhouayek, M.; Bottemanne, P.; Makriyannis, A.; Muccioli, G. G., N-acylethanolamine-hydrolyzing acid amidase and fatty acid amide hydrolase inhibition differentially affect N-acylethanolamine levels and macrophage activation. *Biochim. Biophys. Acta Mol. Cell Biol. Lipids* **2017**, *1862*, 474-484.
30. Ortega-Gutiérrez, S.; Molina-Holgado, E.; Guaza, C., Effect of anandamide uptake inhibition in the production of nitric oxide and in the release of cytokines in astrocyte cultures. *Glia* **2005**, *52*, 163-8.
31. Molina-Holgado, F.; Molina-Holgado, E.; Guaza, C., The endogenous cannabinoid anandamide potentiates interleukin-6 production by astrocytes infected with Theiler's murine encephalomyelitis virus by a receptor-mediated pathway. *FEBS Lett.* **1998**, *433*, 139-142.
32. Giordano, C.; Plastina, P.; Barone, I.; Catalano, S.; Bonofiglio, D., n-3 Polyunsaturated Fatty Acid Amides: New Avenues in the Prevention and Treatment of Breast Cancer. *Int. J. Mol. Sci.* **2020**, *21*, 2279.
33. Thiele, C.; Papan, C.; Hoelper, D.; Kusserow, K.; Gaebler, A.; Schoene, M.; Piotrowitz, K.; Lohmann, D.; Spandl, J.; Stevanovic, A.; et al., Tracing Fatty Acid Metabolism by Click Chemistry. *ACS Chem. Biol.* **2012**, *7*, 2004-2011.
34. Thiele, C.; Wunderling, K.; Leyendecker, P., Multiplexed and single cell tracing of lipid metabolism. *Nature Methods* **2019**, *16*, 1123-1130.
35. Gaebler, A.; Penno, A.; Kuerschner, L.; Thiele, C., A highly sensitive protocol for microscopy of alkyne lipids and fluorescently tagged or immunostained proteins. *J. Lipid Res.* **2016**, *57*, 1934-1947.
36. Schwanhäusser, B.; Busse, D.; Li, N.; Dittmar, G.; Schuchhardt, J.; Wolf, J.; Chen, W.; Selbach, M., Global quantification of mammalian gene expression control. *Nature* **2011**, *473*, 337-342.
37. Dandela, R.; Mantin, D.; Cravatt, B. F.; Rayo, J.; Meijler, M. M., Proteome-wide mapping of PQS-interacting proteins in *Pseudomonas aeruginosa*. *Chem. Sci.* **2018**, *9*, 2290-2294.
38. Heo, S.; Kim, S.; Kang, D., The Role of Hydrogen Peroxide and Peroxiredoxins throughout the Cell Cycle. *Antioxidants* **2020**, *9*, 280.
39. Knoop, B.; Argyropoulou, V.; Becker, S.; Ferte, L.; Kuznetsova, O., Multiple Roles of Peroxiredoxins in Inflammation. *Mol Cells* **2016**, *39*, 60-64.
40. Tae Lim, Y.; Sup Song, D.; Joon Won, T.; Lee, Y. J.; Yoo, J. S.; Eun Hyung, K.; Won Yoon, J.;

- Park, S. Y.; Woo Hwang, K., Peroxiredoxin-1, a possible target in modulating inflammatory cytokine production in macrophage like cell line RAW264.7. *Microbiology and immunology* **2012**, *56*, 411-419.
41. Phuyal, S.; Farhan, H., Multifaceted Rho GTPase Signaling at the Endomembranes. *Front. Cell Dev. Biol.* **2019**, *7*, 127.
42. Wang, C.; Yoo, Y.; Fan, H.; Kim, E.; Guan, K.-L.; Guan, J.-L., Regulation of Integrin $\beta 1$ Recycling to Lipid Rafts by Rab1a to Promote Cell Migration. *J. Biol. Chem.* **2010**, *285*, 29398-29405.
43. Barbera, S.; Nardi, F.; Elia, I.; Realini, G.; Lugano, R.; Santucci, A.; Tosi, G. M.; Dimberg, A.; Galvagni, F.; Orlandini, M., The small GTPase Rab5c is a key regulator of trafficking of the CD93/Multimerin-2/ $\beta 1$ integrin complex in endothelial cell adhesion and migration. *Cell Commun. Signal.* **2019**, *17*, 55.
44. Fowler, C. J., Transport of endocannabinoids across the plasma membrane and within the cell. *FASEB J.* **2013**, *280*, 1895-1904.
45. McFarland, M. J.; Porter, A. C.; Rakhshan, F. R.; Rawat, D. S.; Gibbs, R. A.; Barker, E. L., A Role for Caveolae/Lipid Rafts in the Uptake and Recycling of the Endogenous Cannabinoid Anandamide. *J. Biol. Chem.* **2004**, *279*, 41991-41997.
46. Brown, F. C.; Collett, M.; Tremblay, C. S.; Rank, G.; De Camilli, P.; Booth, C. J.; Bitoun, M.; Robinson, P. J.; Kile, B. T.; Jane, S. M.; Curtis, D. J., Loss of Dynamin 2 GTPase function results in microcytic anaemia. *Br. J. Haematol.* **2017**, *178*, 616-628.
47. Marei, H.; Carpy, A.; Macek, B.; Malliri, A., Proteomic analysis of Rac1 signaling regulation by guanine nucleotide exchange factors. *Cell Cycle* **2016**, *15*, 1961-1974.
48. Marei, H.; Carpy, A.; Woroniuk, A.; Vennin, C.; White, G.; Timpson, P.; Macek, B.; Malliri, A., Differential Rac1 signalling by guanine nucleotide exchange factors implicates FLN1 in regulating Rac1-driven cell migration. *Nat. Commun.* **2016**, *7*, 10664.
49. Acevedo, A.; González-Billault, C., Crosstalk between Rac1-mediated actin regulation and ROS production. *Free Radic. Biol. Med.* **2018**, *116*, 101-113.
50. Sadok, A.; Marshall, C. J., Rho GTPases. *Small GTPases* **2014**, *5*, e983878.
51. Patel, R.; Attur, M. G.; Dave, M.; Abramson, S. B.; Amin, A. R., Regulation of Cytosolic COX-2 and Prostaglandin E2 Production by Nitric Oxide in Activated Murine Macrophages. *J. Immunol.* **1999**, *162*, 4191.

Supporting information belonging to Chapter 3

Supplemental figures

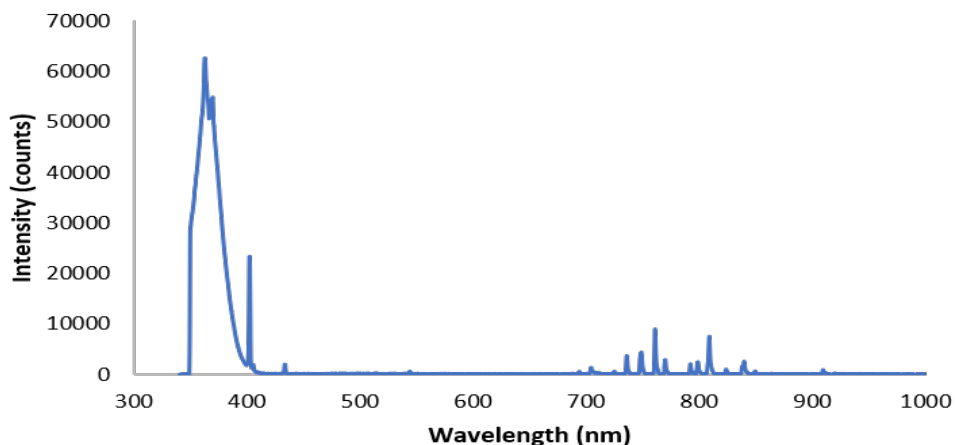


Figure 3-S1 Spectral output of UVP-C1000 crosslinker equipped with 5x 8W light bulbs of 366 nm. Spectral output was analyzed, using a Flame Miniature Spectrometer from Ocean Optics.

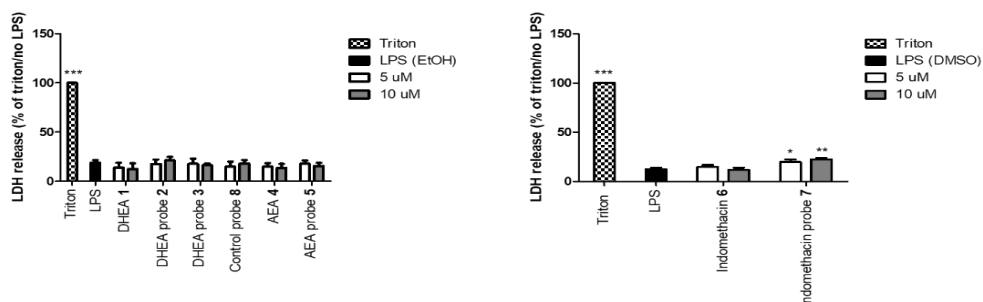


Figure 3-S2 LDH release of 1.0 $\mu\text{g/mL}$ LPS-stimulated RAW264.7 macrophages incubated with 5 and 10 μM of PUFA-derivatives or indomethacin. A) LDH release of DHEA, AEA, and their respective synthetic bi-functional chemical probes. B) LDH release of indomethacin and its respective synthetic bi-functional chemical probe (B). The LDH release is expressed as percentage compared to 1.0% Triton X-100 treated positive control (set as 100% cytotoxicity), and non LPS-stimulated macrophages (set as 0% cytotoxicity). All samples were measured in triplicate containing technical duplicates. Asterisks indicate significant differences from the vehicle with 1.0 $\mu\text{g/mL}$ LPS control (One-way ANOVA, Dunnett's multiple comparison test post hoc; * $P < 0.05$, ** $P < 0.01$, *** $P < 0.001$).

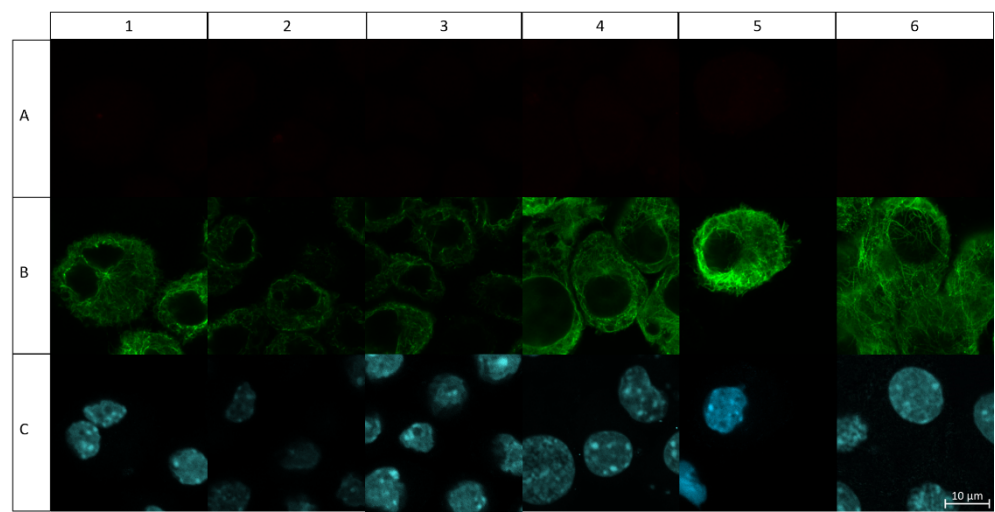


Figure 3-S3 Confocal microscopy images of 1.0 $\mu\text{g}/\text{mL}$ LPS-stimulated RAW264.7 macrophages. A) shows the lissamine rhodamine B channel without tetrakis(acetonitrile)copper(I) hexafluorophosphate. B) shows immunostaining of alpha tubulin. C) shows DAPI staining in nuclei. 1) 10 μM DHEA probe 2. 2) 10 μM DHEA probe 3. 3) 10 μM AEA probe 5. 4) 10 μM indomethacin probe 7. 5) 10 μM probe 8. 6) 0.1% EtOH vehicle. Scale bar applies to all images in the figure.

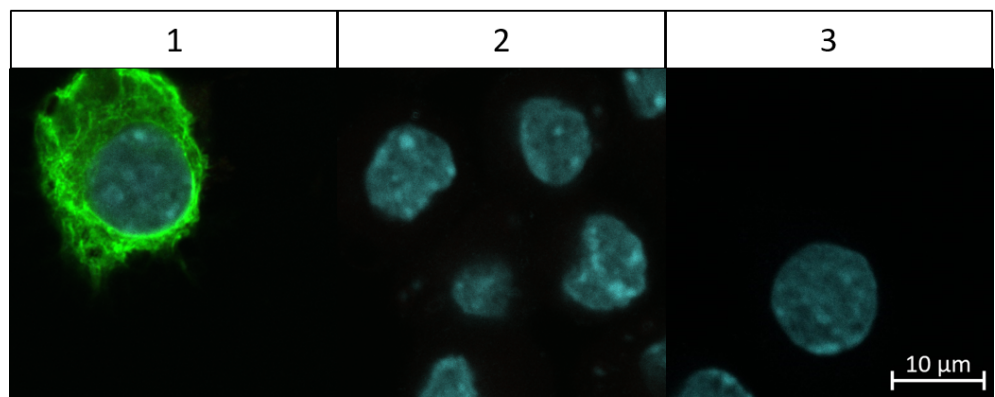


Figure 3-S4 Fluorescent microscopy pictures of 1.0 $\mu\text{g}/\text{mL}$ LPS-stimulated RAW264.7 macrophages. Shown are overlays of the lissamine rhodamine B channel with the addition of tetrakis(acetonitrile)copper(I) hexafluorophosphate (red), Alexafluor 488 immunostaining of tubulin (green), and DAPI staining of the nuclei (blue). 1) EtOH vehicle with primary tubulin antibody. 2) 1 EtOH vehicle without primary tubulin antibody. 3) LPS stimulated cells only. Scale bar applies to all images in the figure.

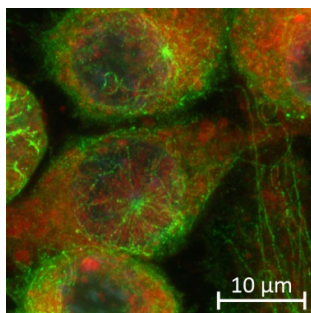


Figure 3-S5 Confocal fluorescent maximum intensity Z-stack projection of 1.0 $\mu\text{g/mL}$ LPS-stimulated RAW264.7 macrophages incubated with 10 μM indomethacin probe 7. Overlay shows the lissamine rhodamine B channel after the addition of tetrakis(acetonitrile)copper(I) hexafluorophosphate (red), Alexafluor 488 (AF488) immunostaining of tubulin (green), and DAPI staining of the nuclei (blue).

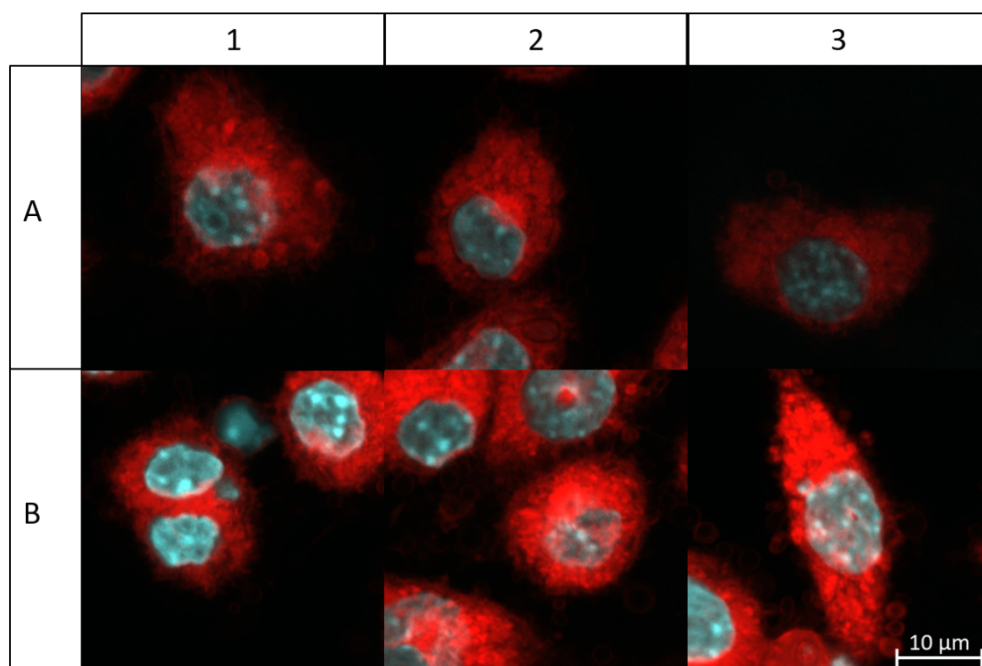


Figure 3-S6 Fluorescent microscopy pictures of 1.0 $\mu\text{g/mL}$ LPS-stimulated RAW264.7 probe incubated macrophages. A) Shows 4 h incubation with 10 μM DHEA probe 3, B) shows 4 h incubation with 10 μM AEA probe 5. Overlays represent lissamine rhodamine B (red), Alexafluor488 antibody (green), and DAPI staining (blue). Cells were stained with 1) secondary AF488 antibody without primary Rac1 antibody, 2) Rab5c antibody, or 3) Ptgs2 antibody. Scale bar applies to all images in the figure.

Supplemental Tables

Table 3-S1 Overview of master gain settings during confocal imaging of the fluorophores.

Figure 3	1	2	3	4	5	6
A (Rhodamine)	380	450	420	450	550	550
B (AF488)	500	500	480	480	500	480
C (DAPI)	600	590	650	600	600	600

Figure S3	1	2	3	4	5	6
A (Rhodamine)	550	550	550	550	550	550
B (AF488)	500	460	480	480	500	480
C (DAPI)	600	600	650	600	640	600

Figure S4	1	2	3
Rhodamine	550	550	550
AF488	480	480	500
DAPI	600	600	600

Figure 5	1	2	3
A Rhodamine	500	500	500
AF488	600	600	600
DAPI	600	600	600
B Rhodamine	450	450	450
AF488	600	600	600
DAPI	550	550	550

Figure S5	
A Rhodamine	600
AF488	500
DAPI	507

Figure S6	1	2	3
A Rhodamine	500	500	500
AF488	600	600	600
DAPI	600	600	600
B Rhodamine	450	450	430
AF488	600	600	600
DAPI	550	550	530

Table 3-S2 Medium concentrations of the inflammatory markers PGE₂, IL-6, and cytotoxicity marker LDH in 1.0 µg/mL LPS-stimulated RAW264.7 macrophages incubated with 5 µM and 10 µM of DHEA, AEA, indomethacin, or their respective synthetic bi-functional chemical probe. LDH concentration is expressed as percentage compared to 1.0% Triton X-100 treated positive control (set as 100% cytotoxicity), and non LPS-stimulated macrophages (set as 0% cytotoxicity). All samples were measured in triplicate containing technical duplicates. Asterisks indicate significant differences from the 1.0 µg/mL LPS-stimulated vehicle incubation (One-way ANOVA, Dunnett's multiple comparison test post hoc; * P<0.05, ** P<0.01, *** P<0.001). † Value represented is an estimation of PGE₂ concentration, because absolute absorbance values were too low to be accurately determined. <LOD represent values below the calibration.

	PGE ₂ (ng/mL)	IL-6 (ng/mL)	LDH activity (%)
Vehicle (0.1% EtOH)	3.62 ± 1.26	23.77 ± 8.94	18.9 ± 2.5
DHEA 1 (5.0 µM)		16.71 ± 8.56	13.8 ± 5.0
DHEA 1 (10.0 µM)	0.40 ± 0.10***	14.00 ± 5.30	12.4 ± 5.8
DHEA probe 2 (5.0 µM)		10.64 ± 4.27	17.6 ± 4.5
DHEA probe 2 (10.0 µM)	0.16 ± 0.03 ***	10.53 ± 3.85	21.2 ± 3.6
DHEA probe 3 (5.0 µM)		13.47 ± 7.87	17.7 ± 5.2
DHEA probe 3 (10.0 µM)	0.27 ± 0.05 ***	7.66 ± 4.31 *	16.2 ± 1.8
AEA 4 (5.0 µM)		27.11 ± 10.26	14.9 ± 3.4
AEA 4 (10.0 µM)		29.19 ± 10.90	13.6 ± 4.1
AEA probe 5 (5.0 µM)		15.01 ± 14.32	17.8 ± 3.3
AEA probe 5 (10.0 µM)		12.18 ± 9.65	15.5 ± 3.2
Control probe 8 (5.0 µM)		21.51 ± 6.83	14.9 ± 5.2
Control probe 8 (10.0 µM)	2.6 ± 0.8†	21.84 ± 9.43	18.1 ± 3.5
Vehicle (0.1% EtOH) without LPS	< LOD ***	< LOD ***	0
	PGE ₂ (ng/mL)	IL-6 (ng/mL)	LDH activity (%)
Vehicle (0.1% DMSO)	2.95 ± 0.72	18.65 ± 6.84	12.3 ± 4.3
Indomethacin 6 (5.0 µM)		16.49 ± 8.73	14.8 ± 4.4
Indomethacin 6 (10.0 µM)	< LOD ***	14.96 ± 6.94	11.9 ± 5.3
Indomethacin probe 7 (5.0 µM)		14.23 ± 5.47	19.7 ± 6.4 *
Indomethacin probe 7 (10.0 µM)	< LOD ***	15.15 ± 6.66	22.6 ± 3.7**
Vehicle (0.1% DMSO) without LPS	< LOD ***	< LOD ***	0



Table 3-S3

To access this supplemental table please scan the QR-code below.



Supplemental videos

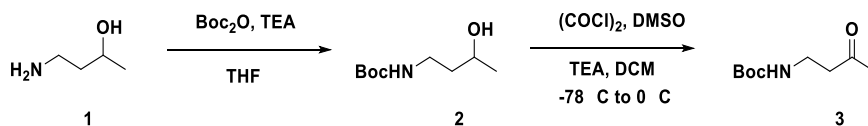
To access the supplemental videos please scan the QR-code below.

Synthesis of chemical probes

Materials

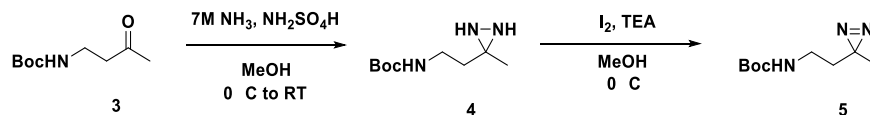
Ammonia (ca. 7N solution in MeOH), 2-(3-(but-3-yn-1-yl)-3H-diazirin-3-yl)ethan-1-amine ($\geq 95\%$), celite® 545, chloroform-*d* (≥ 99.8 atom % *D*, contains 0.5 wt-% silver foil as stabiliser, 0.03% (v/v) TMS), distilled triethylamine (TEA) ($>99.5\%$), hydroxylamine-O-sulfonic acid ($\geq 97\%$), iodine ($\geq 99\%$), propargyl-*N*-hydroxysuccinimidyl ester, ammonium bicarbonate ($\geq 99\%$), 1,2,4,5-tetrachloro-3-nitrobenzene (Standard for quantitative NMR, TraceCERT®) were purchased from Sigma-Aldrich (Zwijndrecht, The Netherlands). 4-Amino-2-butanol ($\geq 98\%$), bis(2-oxo-3-oxazolidinyl)phosphinic chloride (BOP-Cl) ($\geq 97\%$), di-*tert*-butyl dicarbonate ($\geq 97\%$), isobutyl chloroformate ($\geq 98\%$), methanol Extra Dry over Molecular Sieves ($\geq 99.8\%$), oxalyl chloride ($\geq 98\%$), sodium sulphate ($\geq 99\%$), sodium thiosulphate ($\geq 98.5\%$) were purchased from Fisher Scientific (Landsmeer, The Netherlands). Dimethyl sulfoxide (DMSO) ($\geq 98\%$) was purchased from TCI Chemicals (Zwijndrecht, Belgium). Acetonitrile ($\geq 99.9\%$, HiPerSolv CHROMANORM® for LC-MS), ethyl acetate (EtOAc) (technical grade) heptane (technical grade), silica gel 40-63 μm for flash chromatography, sodium dodecyl sulfate (SDS) ($\geq 99\%$, Biotechnology grade) were purchased from VWR Chemicals (Amsterdam, The Netherlands). Formic acid ($\geq 99\%$, ULC/MS grade, and trifluoroacetic acid ($\geq 99.95\%$, HPLC grade) were obtained from Biosolve B.V. (Valkenswaard, The Netherlands). Ethanol (absolute for analysis EMSURE®), was obtained from Merck (Amsterdam, The Netherlands). Pure chloroform-*d* (100.0 atom% *D*) was obtained from Janssen Chimica (Beerse, Belgium). Anhydrous DCM and THF were obtained using a Pure Solv 400 solvent purification system from Innovative Technology (Amesbury, USA). Ultrapure water was filtered by a MilliQ integral 3 system from Millipore (Molsheim, France).

Synthesis of *tert*-butyl 3-oxobutylcarbamate (3)



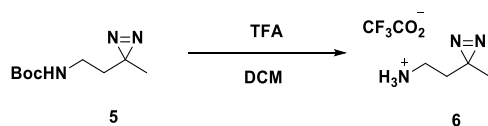
An oven-dried round bottom flask (RBF) containing 40 mL anhydrous tetrahydrofuran (THF) was placed under argon, and 1.7 mL (13 mmol, 1.2 eq.) freshly distilled Et_3N and 1.0 mL (10 mmol, 1.0 eq.) 4-amino-2-butanol (**1**) were added. While stirring the solution continuously at room temperature, 2.5 g (12 mmol, 1.1 eq.) of Boc_2O was added in small portions over a time span of 10 min. After stirring the mixture for 1 h at room temperature the reaction was quenched by pouring the mixture in 50 mL ice cold 0.5 M HCl. Extraction of the product with 3 x 100 mL EtOAc was performed, the organic layers were combined and dried with anhydrous Na_2SO_4 to obtain *tert*-butyl (3-hydroxybutyl) carbamate (**2**).

An oven-dried three-necked RBF containing 200 mL of anhydrous dichloromethane (DCM) was placed under argon atmosphere and cooled to -78°C . Then, 1.8 mL (21 mmol, 2 equiv.) oxalyl chloride was added, followed by drop-wise addition of 3.0 mL (42 mmol, 4 eq.) dimethyl sulfoxide (DMSO). The reaction was stirred for 30 min at -78°C . *Tert*-butyl (3-hydroxybutyl)carbamate (**2**) was dissolved in 20 mL anhydrous DCM and subsequently added to the reaction over a period of 30 min. After stirring the reaction at -78°C for 2 h, 5.8 mL (42 mmol, 4 eq.) of freshly distilled Et_3N was added and the mixture was stirred for another 2 h at -78°C . Then, the temperature was brought to 0°C by placing the RBF in an ice-bath for 30 min, and was then warmed to room temperature. Hereafter, the mixture was diluted with 220 mL Et_2O and passed through a silica plug. The remaining mixture was concentrated under reduced pressure, providing a yellow oil. The final product was obtained by purification of the residue by SiO_2 flash chromatography, using 50% EtOAc/heptane, providing the title compound (**3**) as a slightly yellowish oil (1.6 g, 81%). ^1H NMR (400 MHz, CDCl_3) δ 4.99 (s, 1H), 3.34 (q, J = 6.0 Hz, 2H), 2.66 (t, J = 5.8 Hz, 2H), 2.15 (d, J = 1.0 Hz, 3H), 1.42 (s, 9H). ^{13}C NMR (101 MHz, CDCl_3) δ 208.5, 156.1, 79.5, 43.8, 35.4, 30.4, 28.7. MS (ESI+) m/z calculated for $\text{C}_9\text{H}_{17}\text{NO}_3$ $[\text{M}+\text{H}]^+$ 188.12812, found 188.12766, and for $[\text{M}+\text{Na}]^+$ 210.11006, found 210.10978.

Synthesis of *tert*-butyl (2-(3-methyl-3H-diazirin-3-yl)ethyl)carbamate (5)

In a three-necked RBF 1.56 g (8.33 mmol, 1 eq.) *tert*-butyl(3-oxobutyl)carbamate (**3**) was dissolved in 18.8 mL 7.0 N NH_3 in methanol at 0 °C under argon. This mixture was stirred at 0 °C for 3 h, after which a solution of hydroxylamine-*O*-sulfonic acid 1.09 g (9.58 mmol, 1.15 eq.) in 18.8 mL anhydrous MeOH was added drop-wise in the course of 20 min. After allowing the reaction to slowly warm to room temperature overnight, the mixture was concentrated under a stream of nitrogen. The residue was re-dissolved in 18.8 mL Et_2O and passed through a celite pad. The filtrate was concentrated under reduced pressure and re-dissolved in 9.4 mL anhydrous MeOH in an amberized RBF. The RBF was placed under argon and the mixture was cooled to 0 °C. While stirring, 1.7 mL (13 mmol, 1.5 eq.) freshly distilled Et_3N was added after which the reaction was allowed to stir for 5 min. Following, 2.35 g I_2 (9.16 mmol, 1.1 eq.) was slowly added in small portions over a period of 30 min until a red-brown color persisted, which was checked by taking a small droplet from the mixture with a pipette and visually inspecting the color. After this the mixture was stirred for 30 min at 0 °C and the reaction was quenched with 94 mL of a saturated $\text{Na}_2\text{S}_2\text{O}_3$ solution. The quenched reaction mixture was vigorously mixed for 10 min and 188 mL EtOAc was added. The product was extracted with 3 x 100 mL EtOAc and the combined organic layers were dried using anhydrous Na_2SO_4 . The remaining mixture was concentrated under reduced pressure. The title product (**5**) was purified by SiO_2 flash chromatography using 35% EtOAc/heptane, providing the final product as a yellow oil (0.45 g, 27%); ^1H NMR (400 MHz, CDCl_3) δ 4.56 (s, 1H), 3.05 (q, J = 6.7 Hz, 2H), 1.56 (t, J = 6.9 Hz, 2H), 1.45 (s, 9H), 1.05 (s, 3H). ^{13}C NMR (101 MHz, CDCl_3) δ 79.7, 35.9, 34.8, 29.2, 28.5, 20.0. MS (ESI+) m/z calculated for $[\text{M}+\text{H}]^+$ $\text{C}_9\text{H}_{17}\text{O}_2\text{N}_3$ 200.13902, found 200.13898, and for $[\text{M}+\text{Na}]^+$ 222.12130, found 222.12087.

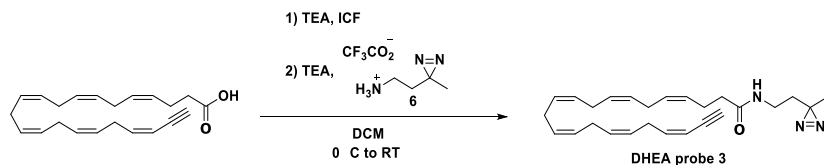
Synthesis of diazine amine (6)



Note: Deprotection of the amine was performed immediately before coupling to the docosahexaenoic acid alkyne.

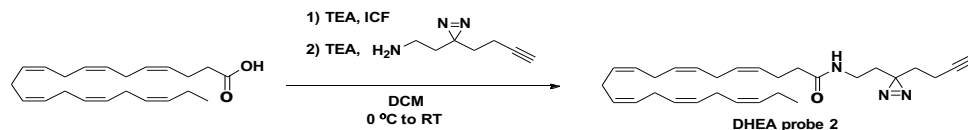
In an amberized glass vial 80 mg (0.38 mmol, 1 eq.) *tert*-butyl(2-(3-methyl-3H-diazirin-3-yl)ethyl)carbamate (**5**) was dissolved in 0.8 mL anhydrous DCM. The solution was cooled to 0 °C while stirring, and subsequently 0.2 mL (2.6 mmol, 6.4 eq.) TFA was added to the mixture. After 1 h the reaction mixture was concentrated under a stream of N₂. The residue was dissolved in 5 mL anhydrous DCM and concentrated again. This procedure was repeated three times, after which the residue was put under high vacuum for 1 h. The remaining residue was used in the subsequent coupling reaction without further purification. TLC and ¹H-NMR analysis were used to confirm deprotection.

Synthesis of DHEA probe 3



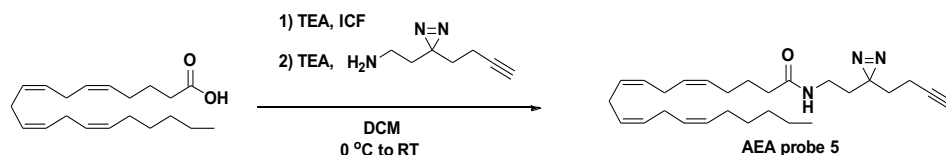
In a 3 mL glass vial, 1.0 mg (3.1 μmol, 1.0 eq.) DHA-alkyne in EtOH was evaporated to dryness using co-evaporation with DCM. After this, the glass vial was placed under argon atmosphere in 1 mL anhydrous DCM and protected from light by aluminum foil. Then 6.0 μL of freshly distilled Et₃N (43 μmol, 14 eq.) was added, followed by 4.8 μL isobutyl chloroformate (37 μmol, 12 eq.) in anhydrous DCM. The reaction was allowed to stir for 1 h at room temperature after which the reaction mixture was cooled in an ice bath. Hereafter, 3.4 mg of 2-(3-methyl-3H-diazirin-3-yl)ethan-1-amine (**6**) (34 μmol, 11 eq.) was dissolved in 1 mL of dry DCM in an amberized glass vial together with 4.7 μL freshly distilled Et₃N (34 μmol, 11 eq.), and added to the reaction mixture. The reaction was stirred overnight on ice before the solvent was evaporated under a stream of nitrogen. The residue was re-dissolved in 1 mL Water/ACN (2:8, v/v) and purified by semi-preparative HPLC (*vide infra*). Quantification was performed by quantitative NMR analysis. The title compound was obtained as 245 μg (20% yield) pure product. ¹H NMR (600 MHz, CDCl₃) δ 5.98 (dt, *J* = 10.8, 7.4 Hz, 1H), 5.62 – 5.31 (m, 12H), 3.19 (q, *J* = 6.6 Hz, 3H, theor. 2H), 3.17 – 3.12 (m, 3H), 2.89 (dt, *J* = 21.5, 6.1 Hz, 8H), 2.44 (p, *J* = 6.9 Hz, 2H), 2.27 (t, *J* = 7.5 Hz, 2H), 1.62 (t, *J* = 6.8 Hz, 3H, theor. 2H), 1.07 (s, 3H). MS (ESI+) *m/z* calculated for C₂₆H₃₅N₃O [M+H]⁺ 406.28529, found 406.28473 and for [M+Na]⁺ 428.26723, found 428.26592.

Synthesis of DHEA probe 2



20 mg (61 μ mol, 1.0 eq.) DHA in EtOH was pipetted into a 5 mL glass vial, evaporated to dryness using co-evaporation with DCM, and placed under argon atmosphere. This DHA was dissolved in 2 mL of anhydrous DCM, and treated with 11.8 μ L freshly distilled Et₃N (84.7 μ mol, 1.4 eq.) and 9.7 μ L of isobutyl chloroformate (75 μ mol, 1.2 eq.) for 1 h at room temperature. After this, the reaction was cooled in an ice bath and protected from light by aluminum foil. To the mixture 0.5 mL of anhydrous DCM containing 9.4 μ L freshly distilled Et₃N (67 μ mol, 1.1 eq.) and 9.2 mg of 2-(3-(but-3-yn-1-yl)-3H-diazirin-3-yl)ethan-1-amine (67 μ mol, 1.1 eq.) was added. The reaction was stirred on ice for overnight. The next day the mixture was concentrated to dryness under a stream of nitrogen and dissolved in 2.0 mL water/ACN (2:8, v/v). The title product was purified by preparative-HPLC *vide infra*, and finally obtained as 16.0 mg (59% yield) of pure oil. ¹H NMR (400 MHz, CDCl₃) δ 5.55 (s, 1H), 5.48 – 5.23 (m, 12H), 3.10 (q, *J* = 6.5 Hz, 2H), 2.84 (q, *J* = 8.0, 6.7 Hz, 10H), 2.42 (q, *J* = 7.1 Hz, 2H), 2.23 (t, *J* = 7.5 Hz, 2H), 2.17 – 1.93 (m, 5H), 1.67 (dt, *J* = 17.9, 7.0 Hz, 4H), 0.97 (t, *J* = 7.6 Hz, 3H). ¹³C NMR (101 MHz, CDCl₃) δ 172.5, 134.1 – 125.6 (m), 82.8, 77.4, 69.5, 36.6, 34.4, 32.7, 32.3, 27.0, 25.8, 23.5, 20.7, 14.4, 13.4. MS (ESI+) *m/z* calculated for C₂₉H₄₁N₃O [M+H]⁺ 448.33224, found 448.33154 and for [M+Na]⁺ 470.31418, found 470.31285.

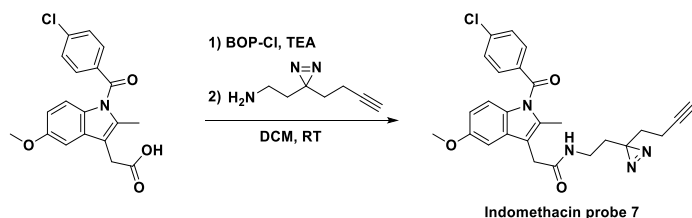
Synthesis of AEA probe 5



20 mg arachidonic acid in EtOH (66 μ mol, 1.0 eq.) was pipetted into a 5 mL glass vial, evaporated to dryness using co-evaporation with DCM, and placed under argon atmosphere. The arachidonic acid was dissolved in 2 mL of anhydrous DCM, and reacted with 12.8 μ L freshly distilled Et₃N (91.8 μ mol, 1.4 eq.) and 10.2 μ L of isobutyl chloroformate (78.6 μ mol, 1.2 eq.) for 1 h at room temperature. After this, the mixture was cooled in an ice bath and protected from light by aluminum foil. To the mixture 0.5 mL of anhydrous DCM containing 10.1 μ L freshly distilled Et₃N (72.5 μ mol, 1.1 eq.) and 9.9 mg of 2-(3-(but-3-yn-1-yl)-3H-diazirin-3-yl)ethan-1-amine (73 μ mol, 1.1 eq.) was added. After overnight stirring on ice, the reaction mixture was evaporated to dryness under a

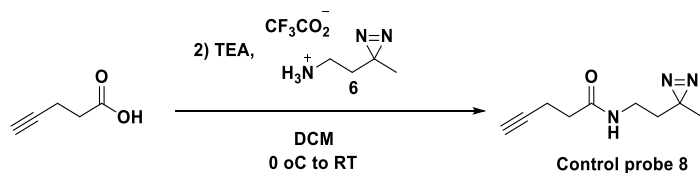
stream of nitrogen and dissolved in 2.0 mL water/ACN (2/8, v/v). The title product was purified by preparative-HPLC (*vide infra*), and finally obtained as 13.2 mg (47% yield) of pure oil. ^1H NMR (400 MHz, CDCl_3) δ 5.51 (d, J = 6.4 Hz, 1H), 5.46 – 5.27 (m, 7H, theor. 8H), 3.11 (q, J = 6.4 Hz, 2H), 2.83 (dt, J = 11.3, 5.6 Hz, 6H), 2.24 – 1.98 (m, 9H), 1.78 – 1.59 (m, 6H), 1.42 – 1.23 (m, 6H), 0.89 (t, J = 6.8 Hz, 3H). ^{13}C NMR (101 MHz, CDCl_3) δ 173.3, 132.0–126.2 (m), 83.1, 69.9, 36.5, 34.7, 33.0, 32.6, 29.8, 27.7, 27.3, 27.1, 26.1, 25.9, 23.0, 14.5, 13.7. MS (ESI+) m/z calculated for $\text{C}_{27}\text{H}_{41}\text{N}_3\text{O}$ $[\text{M}+\text{H}]^+$ 424.33224, found 424.33248 and for $[\text{M}+\text{Na}]^+$ 446.31418, found 446.31461.

Synthesis of Indomethacin probe 7



For the synthesis of an alkyne and diazirine based indomethacin probe, 100 mg of indomethacin (0.28 mmol, 2.6 eq.) and 71 mg (0.28 mmol, 2.6 eq.) BOP-Cl were dissolved in 5 mL anhydrous DCM in an argon filled dry amberized RBF. To the reaction 78 μL (0.56 mmol, 5.2 eq.) of freshly distilled Et_3N was added, and the reaction was stirred at room temperature. After 10 min, 15 mg 2-(3-(but-3-yn-1-yl)-3H-diazirin-3-yl)ethan-1-amine (0.11 mmol, 1 eq.) was added and stirred for over the weekend. The crude mixture was concentrated by reduced pressure and purified by SiO_2 flash chromatography using 50% EtOAc in hexanes, providing the final product as a yellow solid (14.9 mg, 29%). ^1H NMR (400 MHz, CDCl_3) δ 7.82 – 7.57 (m, 2H), 7.56 – 7.39 (m, 2H), 6.96 – 6.80 (m, 2H), 6.70 (dd, J = 9.0, 2.3 Hz, 1H), 5.73 (d, J = 6.2 Hz, 1H), 3.83 (s, 3H), 3.65 (s, 2H), 3.10 (q, J = 6.2 Hz, 2H), 2.42 (s, 3H), 1.95 – 1.77 (m, 3H), 1.57 (dt, J = 33.9, 6.8 Hz, 4H). ^{13}C NMR (101 MHz, CDCl_3) δ 168.3, 156.3, 139.6, 136.6, 133.6, 131.2, 131.0, 130.3, 129.2, 115.2, 112.5, 112.3, 100.9, 82.6, 69.3, 55.8, 34.7, 32.5, 32.3, 31.9, 26.8, 13.3, 13.0. MS (ESI+) m/z calculated for $\text{C}_{26}\text{H}_{25}\text{ClN}_4\text{O}_3$ $[\text{M}+\text{H}]^+$ 477.16879, found 477.16917 and for $[\text{M}+\text{Na}]^+$ 499.15074, found 499.15114.

Synthesis of control probe 8



20 mg 4-pentynoic acid (0.20 mmol, 1.0 eq.) was weighted and placed under argon in an amberized 3-necked RBF. The 4-pentynoic acid was dissolved in 10 mL anhydrous DCM, and subsequently 40 μ L freshly distilled Et₃N (0.29 mmol, 1.4 eq.) and 32 μ L isobutyl chloroformate (0.25 mmol, 1.2 eq.) were added. The reaction was stirred at room temperature for 1 h and then cooled on ice. To the cooled reaction mixture, 31 μ L (0.22 mmol, 1.1 eq.) of freshly distilled Et₃N and 22 mg (0.22 mmol, 1.1 eq.) of 2-(3-methyl-3H-diazirin-3-yl)ethan-1-amine **f** were added. The reaction was stirred on ice for overnight. Next day 20 mL water was added and the resulting mixture was stirred for 10 min, after which the phases were separated. The water layer was extracted with extra 3x 25 mL EtOAc, and the combined organic layers were finally extracted with brine and dried using Na₂SO₄. The mixture was evaporated to dryness and dissolved in 3 mL water:ACN (1:2, v/v). Purification was performed using preparative HPLC (*vide infra*) and the title compound was finally obtained as 6.9 mg (19% yield) of pure oil. ¹H NMR (400 MHz, CDCl₃) δ 5.65 (s, 1H), 3.20 (qd, *J* = 6.8, 1.8 Hz, 2H), 2.54 (td, *J* = 7.1, 2.6 Hz, 2H), 2.46 – 2.29 (m, 2H), 2.01 (q, *J* = 2.4 Hz, 1H), 1.62 (td, *J* = 6.8, 1.7 Hz, 2H), 1.06 (d, *J* = 1.7 Hz, 3H). ¹³C NMR (101 MHz, CDCl₃) δ 171.0, 82.9, 69.5, 35.4, 34.7, 34.1, 24.4, 19.8, 14.8. MS (ESI+) *m/z* calculated for C₉H₁₃N₃O [M+H]⁺ 180.11314, found 180.11284, and for [M+Na]⁺ 202.09508, found 202.09460.

Purification and quantification of chemical probes

Preparative HPLC purification of DHEA probe 2 and AEA probe 5

The desired DHEA probe **2** & AEA probe **5** were purified by preparative-HPLC on an Agilent 1260 Preparative HPLC with DAD and MSD using a PrepHT XDB-C18 21.2x250 mm, 7 μ column (Agilent Technologies, Amstelveen, The Netherlands). Purification was performed using a flow rate of 20 mL/min with solvent A being water containing 0.1% FA and solvent B being ACN containing 0.1% FA. The gradient profile started with 5 min of 80% B in A, followed by a linear increase to 100% B at min 13. The run was continued isocratically at 100% B until min 18, after which the gradient was switched back to 80% B in A in 0.5 min. The run was continued at 80% B in A until min 23. The collected fractions were evaporated using speedyvac concentrator (Salm and Kipp, Breukelen, The Netherlands).

Semi-Preparative HPLC purification of DHEA probe 3

The desired DHEA probe **3** was purified by semi-preparative-HPLC on an Agilent 1260 Preparative HPLC with DAD and MSD using a Semi-Prep Zorbax Eclipse XDB-C18 9.4 x 250 mm, 5 μ column (Agilent Technologies, Amstelveen, The Netherlands). The purification was performed using an isocratic run of 20% water in ACN with 0.1% FA at a flowrate of 4.0 mL/min. After purification the title molecule was concentrated under a stream of nitrogen followed by lyophilization.

Preparative HPLC purification of control probe 8

The desired control probe **8** was purified by preparative-HPLC on an Agilent 1260 Preparative HPLC with DAD and MSD (Agilent Technologies, Amstelveen, The Netherlands) using a Grace Alltima C18 5 μ 250 mm x 22 mm column (Fisher Scientific, Landsmeer, The Netherlands). The sample was dissolved in 3 mL (2:1 ACN:MQ +0.1%FA), and filtered through a syringe filter to remove insoluble precipitates. Then the product was purified by HPLC purification using gradient elution. Gradient elution was performed using a flow rate of 20 mL/min with solvent A being water containing 0.1% FA and solvent B being ACN containing 0.1% FA. The gradient started with 5 min of 5% B in A, followed by a linear increase to 95% B in A which was achieved at min 20. The gradient was kept at 95% B in A until min 23, before the gradient was returned to 5% B in A in 0.5 min. The column was re-equilibrated for until min 26 at 5% solvent B in solvent A. After purification the title molecule was concentrated under a stream of nitrogen followed by lyophilization.

Quantification of DHEA probe 3

Quantification of DHEA probe **3** was performed using quantitative NMR. Deuterated chloroform containing 0.03% TMS was used as internal standard being placed in Wilmad® coaxial insert (Sigma Aldrich, Zwijndrecht, The Netherlands). Calibration of the signal was performed using 1,2,4,5-tetrachloro-3-nitrobenzene (standard for quantitative NMR, TraceCERT®) in concentrations ranging from 3.8-0.9 mM. DHEA probe **3** was quantified based on the calibration of 1,2,4,5-tetrachloro-3-nitrobenzene (**Figure S3-7**).

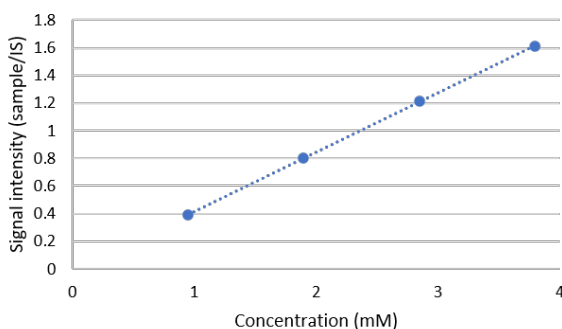


Figure 3-S7 Calibration curve of 1,2,4,5-tetrachloro-3-nitrobenzene, used for the quantification of DHEA probe **3**.

Chapter 4

**Novel COX-2 products of *n*-3 polyunsaturated
fatty acid-ethanolamine conjugates identified in
RAW264.7 macrophages**

This chapter was adapted from:

**Ian de Bus,
Han Zuilhof,
Renger F. Witkamp,
Michiel G.J. Balvers,
Bauke Albada**

Journal of Lipid Research, **2019**, 60, 1829-1840; doi: 10.1194/jlr.M094235

4.1 Abstract

Cyclooxygenase 2 (COX-2) plays a key role in the regulation of inflammation by catalyzing the oxygenation of PUFAs to prostaglandins (PGs) and hydroperoxides. Next to this, COX-2 can metabolize neutral lipids, including endocannabinoid-like esters and amides. We developed an LC-HRMS-based human recombinant (h)COX-2 screening assay to examine its ability to also convert *n*-3 PUFA-derived *N*-acylethanolamines. Our assay yields known hCOX-2-derived products from established PUFAs and anandamide. Importantly, we provide evidence that eicosapentaenoyl ethanolamide (EPEA), the *N*-acylethanolamine derivative of EPA is converted into PGE₃-ethanolamide (PGE₃-EA), and into 11-, 14-, and 18-hydroxyeicosapentaenoyl-EA (11-, 14-, and 18-HEPE-EA, respectively). Interestingly, we demonstrated that docosahexaenoyl ethanolamide (DHEA) is converted by hCOX-2 into the previously unknown metabolites, 13- and 16-hydroxy-DHEA (13- and 16-HDHEA, respectively). These products were also produced by lipopolysaccharide-stimulated RAW264.7 macrophages incubated with DHEA. No oxygenated DHEA metabolites were detected when the selective COX-2 inhibitor, celecoxib, was added to the cells, further underlining the role of COX-2 in the formation of the novel hydroxylated products. This work demonstrates for the first time that DHEA and EPEA are converted by COX-2 into previously unknown hydroxylated metabolites and invites future studies towards the biological effects of these metabolites.

4.2 Introduction

Cyclooxygenase-2 (COX-2) is a non-constitutional enzyme that is upregulated upon inflammation in order to generate inflammatory regulators.¹⁻³ It is known to convert arachidonic acid (AA) into prostaglandin (PG)_{H₂}, the precursor of various inflammation-regulating PGs and thromboxanes (TXs).^{1-2, 4} Although AA is considered the prototypical COX-2 substrate, the enzyme has a broad substrate specificity that includes other PUFAs and their derivatives, such as the endocannabinoid arachidonoyl ethanolamide (AEA; also known as anandamide).^{2, 5-11} Previous studies revealed that COX-2 converts AEA into PG ethanolamides (EAs), also called prostamides, and potent anti-inflammatory mono-hydroxylated AEAs.^{5-6, 11-14} Although various amide-, and ester- bound derivatives of AA are converted by COX-2,^{5-6, 13-17} the interaction between COX-2 and endocannabinoid-like molecules derived from PUFAs other than AA is barely investigated. Previous work revealed that docosahexaenoyl ethanolamide (DHEA), an *n*-3 PUFA endocannabinoid-like metabolite, has potent anti-inflammatory properties *in vitro*.¹⁸ DHEA is present in human blood and a variety of animal tissues in a concentration that depends on the dietary intake of *n*-3 PUFAs as present in fish oil.¹⁹⁻²² Several studies showed interesting biological properties of DHEA. For example, DHEA is able to inhibit head and neck squamous cell carcinoma proliferation, the formation of pro-inflammatory cytokines such as interleukin (IL)-6, and to induce the production of the anti-inflammatory cytokine IL-10, which all results in strong anti-inflammatory effects.²³⁻²⁶ In addition, DHEA stimulates neurite growth, hippocampal development, and synaptogenesis in developing neurons in the central nervous system,²⁷⁻³¹ hence the alternative name synaptamide for DHEA.^{29, 32} Recently, it was suggested that the neural and hippocampal stimulating roles are at least partly caused by the interaction of DHEA with the G-protein coupled receptor 110, stimulating a cAMP-dependent signal transduction pathway.^{28, 30} Previously, our group has demonstrated that DHEA reduces the production of the pro-inflammatory mediator PGE₂ in lipopolysaccharide (LPS)-stimulated RAW264.7 macrophages, which could not be fully explained by the modest reduction of COX-2 protein expression.¹⁸ This observation suggests that DHEA may act as a COX-2 substrate, which reduces PG formation through competitive inhibition.

Several studies aimed at unravelling the metabolic fate of DHEA. Although the interactions of DHEA and 15-lipoxygenase (15-LOX) or cytochrome P450 (CYP450) were reported,^{21, 24, 26, 28} the possible interaction between COX-2 and DHEA is poorly understood. For instance, Serhan and coworkers reported that 15-LOX yields di-hydroxylated and epoxidated DHEA products. Two of these, *i.e.*, 10,17-diHDHEA and 15-HEDPEA, were found to reduce platelet leukocyte aggregation, and 15-HEDPEA was even shown to be protective *in vivo* in murine hind limb ischemia and second organ reperfusion injury.²⁶

Similarly, several CYP450-derived epoxide products of DHEA increased the formation of anti-inflammatory cytokines and exerted anti-angiogenic effects in human microvascular endothelial cells, vasodilatory actions on bovine coronary arteries and reciprocally regulated platelet aggregation in washed human platelets.²⁴ In view of the prominent role of COX-2 in inflammation regulation, we studied the interaction between DHEA and COX-2.

To this end, *n*-3 PUFA-ethanolamine-conjugates were applied in a cell-free enzymatic human recombinant (h)COX-2 assay, and a LC separation coupled to a high-resolution (HR) MS (LC-HRMS) method was used to identify yet unidentified COX-2 metabolites of eicosapentaenoyl ethanolamide (EPEA), *i.e.*, PGE₃-EA and 11-HEPE-EA (and the postulated products 14- and 18-HEPE-EA), and DHEA, *i.e.*, 13- and 16-HDHEA. Then, we developed an ultrahigh performance (UP)LC-MS/MS-based method to quantify the products and studied the role of COX-2 metabolism of DHEA in cells by measuring the COX-2-related production of 13- and 16-HDHEA in LPS-stimulated RAW264.7 macrophages. We show that formation of these products is inhibited upon addition of the selective COX-2 inhibitor, celecoxib, proving a COX-2-dependent metabolism.

4.3 Experimental section

4.3.1 Materials

COX-2 (human recombinant, hCOX-2), arachidonic acid ($\geq 98\%$ purity), eicosapentaenoic acid ($\geq 98\%$ purity), docosahexaenoic acid ($\geq 98\%$ purity), eicosapentaenoyl ethanolamide ($\geq 98\%$ purity), docosahexaenoyl ethanolamide ($\geq 98\%$ purity), (\pm)11-HEPE ($\geq 98\%$ purity), (\pm)13-HDHA ($\geq 98\%$ purity), (\pm)16-HDHA ($\geq 98\%$ purity), prostaglandin E₃ ($\geq 98\%$ purity), prostaglandin E₂ ethanolamide-*d*₄ ($\geq 98\%$ PGE₂-EA, $\geq 99\%$ deuterated forms *d*₁-*d*₄), docosahexaenoyl ethanolamide ($\geq 98\%$ purity, $\geq 99\%$ deuterated forms *d*₁-*d*₄), and celecoxib (CBX) ($\geq 98\%$ purity) were purchased at Cayman Chemical (supplied by Sanbio B.V., Uden, The Netherlands). The lactate dehydrogenase (LDH) cytotoxicity kit was purchased at Roche Applied Science (Almere, The Netherlands). Anandamide (100% purity from HPLC) was obtained from Tocris Chemicals (Abingdon, UK). DMEM was purchased from Corning (supplied by VWR, Amsterdam, The Netherlands), fetal bovine serum (FBS), streptomycin and penicillin were obtained from Lonza (Verviers, Belgium). Hematin porcine, Triton™ X-100, lipopolysaccharide (LPS), butylated hydroxytoluene (BHT) (99%), isobutyl chloroformate (98%), triethylamine (99.5%), ethanolamine ($\geq 98\%$), ethanol-1,1,2,2-*d*₄-amine (98 atom % D), and ethanol (EtOH absolute for analysis) were purchased at Sigma-Aldrich (Zwijndrecht, The Netherlands). Ethyl acetate and *n*-heptane were acquired from VWR Chemicals (Amsterdam, The Netherlands). Trizma

base (99%), phenol (>99%, for biochemistry), DMSO (>99.7%), and methanol (99.99%, LC/MS grade) were obtained from Fisher Scientific (Landsmeer, The Netherlands). Formic acid (99%, ULC/MS-CC/SFC) and acetonitrile (ACN) (ULC/MS-CC/SFC) were purchased at Biosolve Chemicals (Valkenswaard, The Netherlands). The HLB solid phase extraction columns (Oasis, 60 mg, 3cc) were obtained from Waters (Etten-Leur, The Netherlands). Ultrapure water was filtered by a MilliQ Integral 3 system from Millipore (Molsheim, France). DCM for the synthetic procedure of the standards was purified using a Pure Solv 400 solvent purification system (Innovative Technology, Amesbury, USA).

4.3.2 Enzymatic cell free COX-2 assay

A cell-free enzymatic hCOX-2 assay was performed, based on previously reported protocols.³³⁻³⁵ A 0.1 M Tris/HCl buffer pH 8.0 was prepared containing 50 μM Na_2EDTA to stabilize the enzyme in solution. For the enzymatic incubations, 179 μL buffer was mixed with 2 μL of 100 μM hematin solution in DMSO, 10 μL of 25 mM phenol solution in buffer and 5 μL hCOX-2 in buffer giving a total amount of 1.0 μg enzyme per reaction. In the negative control, 5 μL buffer was added instead of 5 μL hCOX-2 solution. The mixtures were pre-incubated for 2 min at room temperature, before adding 4 μL of a 1 mM substrate solution in ethanol, giving a final substrate concentration of 20 μM . The reaction mixture was heated at 37 °C for 20 min, before quenching the reaction with 5 μL of formic acid. 800 μL of EtOAc:Heptane (1:1, v/v) was used to extract the substrates and metabolites, after which the organic solvent was evaporated under reduced pressure at 40 °C. The dried extract was reconstituted with 200 μL EtOH and analyzed on the LC-HRMS system (*vide infra*). For the UPLC-MS/MS-based quantifications of the EPEA and DHEA metabolites, the reactions were quenched with 5 μL of formic acid followed by the addition of 2 mL of MeOH containing 806 pg/mL product (11-HEPE-EA- d_4 or PGE₂-EA- d_4 or 13-HDHEA- d_4) and 1000 pg/mL starting material (DHEA- d_4) as internal standards. Thereafter, the metabolites were collected by SPE using HLB columns (*vide infra*).

4.3.3 LC-HRMS analysis

LC-HRMS analyses were performed using a Finnigan Surveyor Plus HPLC from Thermo Fischer Scientific (Breda, The Netherlands) coupled to a Q-Exactive Focus Quadrupole Orbitrap high-resolution mass spectrometer equipped with a higher-energy collisional dissociation chamber, also from Thermo Fischer Scientific. The machine was operated at a mass resolution of 70,000 to allow the chemical characterization of the products. Ionization was performed using a heated electrospray ionization source applying a spray voltage of 3.2 kV and a capillary temperature of 300 °C using polarity switching (1 s for a cycle of one positive and one negative scan). For the fragmentation analysis, the collision energies were optimized per ion. Chromatography was performed on

a Reprosil Gold 120 C8, 3 μm column of 250 x 3 mm (Dr. Maisch GmbH, Germany), using the following eluents and gradient. Eluent A consisted of water/ACN (95/5) with 0.1% FA; eluent B consisted of 100% ACN with 0.1% FA. For elution of the various lipids and oxylipins, the program started isocratically with 50% B in A. From min 3 to 8 the concentration was linearly increased to 100% B, and the run was continued with 100% B until min 15. Then the gradient was decreased to 50% B in A in 2 min, and run with 50% B in A until min 21. During the run column temperature was kept at 30 °C and the sample tray was cooled to 4 °C, to limit auto-oxidation. For the runs 25 μL or 10 μL of sample was injected.

Data analysis of the mass spectra and the extracted ion chromatograms were performed using Thermo Xcalibur software version 3.0 from Thermo Fischer Scientific (Breda, The Netherlands). All extracted ion chromatograms displayed are within a range of 0.03 Da. All chromatograms were processed with peak smoothing using boxcar smoothing to give representative peaks, unless stated otherwise. The displayed fragmentation spectra were obtained after background subtraction and were reproducible in multiple experiments.

4.3.4 *In vitro* RAW264.7 macrophage incubations

To verify whether DHEA is also metabolized in COX-2-expressing cells, RAW264.7 macrophages (American Type Culture Collection, Teddington, UK) were cultured in DMEM containing 10% FCS and 1% penicillin and streptomycin (P/S) at 37 °C in a 5% CO₂ humidified incubator. For the *in vitro* experiments 2 mL of 250.000 cells/mL were seeded and incubated for 24 h in 6-well plates. The medium of the adherent cells was discarded and replaced by new fresh medium, and the various compounds were subsequently added for the experiments. To investigate COX-2-mediated conversion of DHEA, RAW macrophages were pre-incubated for 30 min. with 10 μM DHEA, followed by stimulation with 1.0 $\mu\text{g/mL}$ LPS. In the celecoxib control experiments the RAW macrophages were pre-incubated with 0.3 μM CXB before DHEA incubation. After 24 h the lipids were extracted for metabolite identification (*vide infra*).

4.3.5 Cell viability, cytotoxicity and PGE₂ quantification determination

To assess the viability of the macrophages after the various treatments, microscopic evaluation of the wells was performed after incubation. Pictures were taken with a LEICA DFS450C microscope from Leica Microsystems (Amsterdam, The Netherlands), and white balancing was applied to optimize the color brightness of each picture. Cell cytotoxicity was tested in the medium, based on the LDH concentration. The LDH assay was performed according to the manufacturer's instructions.

PGE₂ quantification was performed using a PGE₂ EIA assay. A PGE₂ ELISA kit (Monoclonal) was purchased at Cayman Chemical and supplied by Sanbio B.V. (Uden, The Netherlands) and the ELISA was performed according to the manufacturer's instructions.

4.3.6 Intracellular lipid extraction from LPS-stimulated RAW264.7 cells

Extraction of intracellular lipids from incubated RAW264.7 macrophages was performed using an adapted version of a previously described oxylipin extraction protocol, which was optimized for adherent cells.¹⁹ In short, the medium was replaced by 1 mL of fresh medium and the macrophages were scraped from the culture plates in order to suspend them in the fresh medium. The cells were centrifuged (330 *g* at 4 °C) for 5 min and the supernatant was discarded. Subsequently, the macrophages were extracted with 1 mL MeOH, containing 806 pg/mL 13-HDHEA-*d*₄ as an internal standard. This suspension was sonicated for 5 min and centrifuged (330 *g* at 4 °C) for 5 min, after which the supernatant was stored in a clean 15 mL falcon tube. The pellet was treated a second time with 1 mL of fresh MeOH containing 806 pg/mL 13-HDHEA-*d*₄. After 5 min sonication and 5 min centrifugation (330 *g* at 4 °C), this supernatant was also transferred to the 15 mL falcon tube containing the supernatant of the first extraction. The combined extracts were diluted with 8 mL of ultrapure water containing 0.125% FA before solid-phase extraction on HLB columns. The columns were preactivated using 2 mL of MeOH and 2 mL of ultrapure water containing 0.1% FA, respectively. Then the columns were loaded with the extract and rinsed using 2 mL of 20% MeOH in ultrapure water containing 0.1% FA. The lipids were eluted using 1 mL of MeOH containing 0.1% FA, and collected in tubes filled with 20 µL of 10% glycerol and 500 µM of BHT in EtOH (BHT was present to prevent auto-oxidation of the products). The samples were evaporated to dryness using a speedyvac concentrator (Salm and Kipp, Breukelen, The Netherlands) and were re-dissolved in 100 µL EtOH. The samples were directly analyzed by UPLC-MS/MS or stored at -80 °C and used at a later time point.

4.3.7 UPLC-MS/MS analysis and quantification

For improved chromatographic separation and sensitivity, an UPLC-MS/MS method was developed to quantify the hydroxylated fatty acid-ethanolamine-conjugates. The standards used for the quantification were either commercially available or synthesized as described in the supporting information. The analyses were performed on an I-class fixed-loop UPLC coupled to a Xevo TQ-S triple-quadrupole mass spectrometer (Waters, Etten-Leur, The Netherlands). The electron spray interface was operated with a capillary voltage of 4.50 kV, a cone voltage of 50 V, and a desolvation temperature of 600 °C. The mass spectrometer was operated in Multiple Reaction Mode (MRM), with mass transitions and collision energies that were optimized per component. Chromatographic separation was performed on a Zorbax Eclipse Plus C18 Rapid

Resolution HD, 1.8 μ column of 2.1 x 150 mm (Agilent, Amstelveen, The Netherlands), using an elution profile identical to a method reported by Balvers *et al.*¹⁹ In short, eluent A consisted of water/ACN (95/5) with 0.1% formic acid (FA); eluent B consisted of 100% ACN with 0.1% FA. The program started with 5% B in A followed by a linear increase to 30% B in A, which was achieved after 5 min. This was followed by a linear increase towards 50 % B in A, which was achieved at 11.25 min and maintained until 13.25 min. The system was subsequently switched to 100% B, which was achieved at 15.75 min and maintained until 16.75 min, after which the column was left to equilibrate at 5% B in A for approximately 3 min. During the run column temperature was kept at 60 °C and the sample tray was cooled to 4 °C, to limit auto-oxidation. For each run 3 μ L of sample was injected.

The results were analyzed using MassLynx 4.1 software (Waters, Etten-Leur, The Netherlands). Quantification of the HDHEA levels were performed using linear regression of the response ratios (peak area HDHEA/peak area internal standard) from the calibration curve as a function of the corresponding HDHEA concentration. Depending on experiment, the data were weighted 1/x or 1/x² to obtain high accuracy of the back-calculated concentrations throughout the calibrated range. The accuracy and precision of the method were determined by quality control samples.

4.4 Results

4.4.1 Validation of hCOX-2 assay using AA, EPA, DHA, and AEA

The validity of our developed cell free hCOX-2 assay was shown using the COX-2-dependent oxidation of the PUFAs, AA, EPA, DHA, and AEA. As expected AA was converted into PGE₂ and PGD₂ (**Figure 4-S1**).^{2, 35-36} In addition, mono-hydroxylation on C11 or C15 was proven using mass fragmentation, resulting in 11- and 15-HETE (**Figure 4-S2**).^{2, 35-36} a non-specific auto-oxidation product was also observed which is a common feature for PUFAs.³⁷ Similarly, EPA oxidized to PGE₃, PGD₃, 11-HEPE, and 14-HEPE, which is in line with COX-2 products reported in the literature (**Figure 4-S3, 4-S4**).^{35, 38} Lastly, our assay and mass fragmentation confirmed that DHA was converted into 13-HDHA (**Figure 4-S5**).^{35, 39-40}

When the neutral endocannabinoid derivative, AEA, was added to our assay, we found that it was converted into PGE₂-EA and PGD₂-EA. These structures are consistent with other reports,^{5, 11, 13-16} demonstrating that our *in vitro* hCOX-2 assay is capable of identifying these metabolites. Specifically, PGE₂-EA and PGD₂-EA were found as [M+H]⁺ with *m/z* = 396.2741, and with lesser intensity as [M+Na]⁺ with *m/z* = 418.2559. Fragmentation of

the $[M+H]^+$ ion of the prostamides using a collision energy of 20.0 electronvolts (eV) in the higher-energy collisional dissociation chamber showed identical fragmentation products as reported in the literature (**Figure 4-S6**).^{13-14, 36} In addition to the prostamides, we also observed mono-hydroxylated HETE-EAs as the sodium adduct $[M+Na]^+$ at $m/z = 386.2663$ and, in the negative mode, as the formate adduct $[M+HCO_2]^-$ at $m/z = 408.2757$.¹⁴ Mass fragmentation on both species provided evidence for the formation of 11- and 15-HETE-EA (**Figure 4-S7, Table 4-1**).⁷ After validation of our hCOX-2 assay we studied EPEA and DHEA as two potentially new substrates for COX-2.

4.4.2 hCOX-2-derived metabolites of the *n*-3 fatty acid EAs, EPEA and DHEA

Incubation of hCOX-2 with EPEA led to the formation of PG_3 -EA and HEPE-EA products. Fragmentation of the $m/z = 394.25880$ $[M+H]^+$ parent mass of the prostamide product of EPEA showed a fragmentation pattern corresponding with prostamide structures (**Figure 4-1**). The elution profile suggested production of at least two different PG_3 -EA products, most likely PGE_3 -EA and PGD_3 -EA.

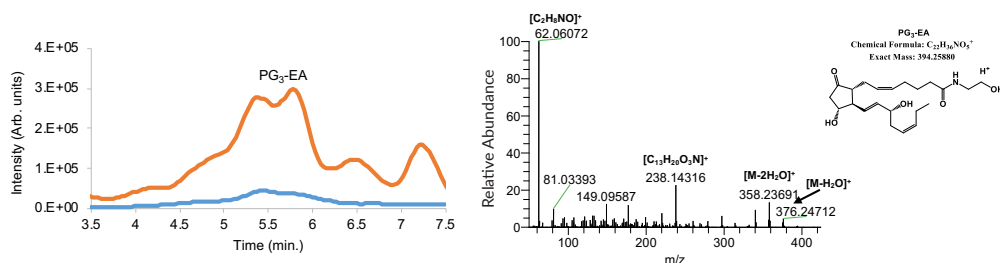


Figure 4-1 Extracted ion chromatogram of $m/z = 394.24$ - 394.27 of PGE_3 -EA $[M+H]^+$. The orange trace in the chromatogram depicts the products of EPEA formed by hCOX-2; the blue trace shows the control assay without hCOX-2. The mass fragmentation spectrum corresponds to the product eluting at min 5.10-5.42 using 20.0 eV collision energy.

Evidence for the formation of three mono-hydroxylated products of EPEA was also found, *i.e.*, 11-, 14-, and 18-HEPE-EA formation. As was observed for the AEA-derived products, the $[M+H-H_2O]^+$ ion with $m/z = 344.26808$ was most abundant in the positive ionization mode, together with $[M+Na]^+$ with $m/z = 384.26236$. In the negative ionization mode, $[M+HCO_2]^-$ was detected at $m/z = 406.25990$.^{7, 36} Based on the fragmentation pattern of the formate adduct or the sodium adduct, we postulated formation of 11-, 14-, and 18-HEPE-EA (**Figure 4-2, Table 4-1**). Of these products, 18-HEPE-EA eluted earlier than 14-HEPE-EA and 11-HEPE-EA, which is analogous to the elution of HEPE products described by Smith and coworkers.³⁵ Fragmentation of the formate adduct resulted in a mass fragment of $m/z = 215.17966$ (chemical composition of $C_{16}H_{23}$). This product

is most likely the result of a β -ene rearrangement leading to the formation of one of the main fragments of 18-HEPE.^{35, 41} The sodium adduct of 14-HEPE-EA fragmented between C13 and C14, resulting in a mass ion of $m/z = 274.18165$ (chemical composition of $C_{15}H_{25}NNaO_2$) that most likely resulted from a γ -ene rearrangement. Fragmentation of 11-HEPE-EA resulted in a fragment ion of $m/z = 234.14837$ (chemical composition of $C_{12}H_{21}NNaO_2$), which resulted from a γ -ene rearranged cleavage between C10 and C11.⁴¹ The 11- and 14-HEPE-EA fragments were found to undergo a sequential neutral loss of C_3H_6 (**Figure 4-2**), as was also observed for 11-HETE-EA (**Figure 4-S6**). Fragmentation analysis on the formate adduct of the two latter products again showed bond fission between C10-C11 and C13-C14, supporting the formation of 11- and 14-HEPE-EA. Further evidence was obtained using a chemically synthesised 11-HEPE-EA product that showed identical retention time and mass fragmentation pattern as the postulated 11-HEPE-EA product (**Figure 4-S8**).

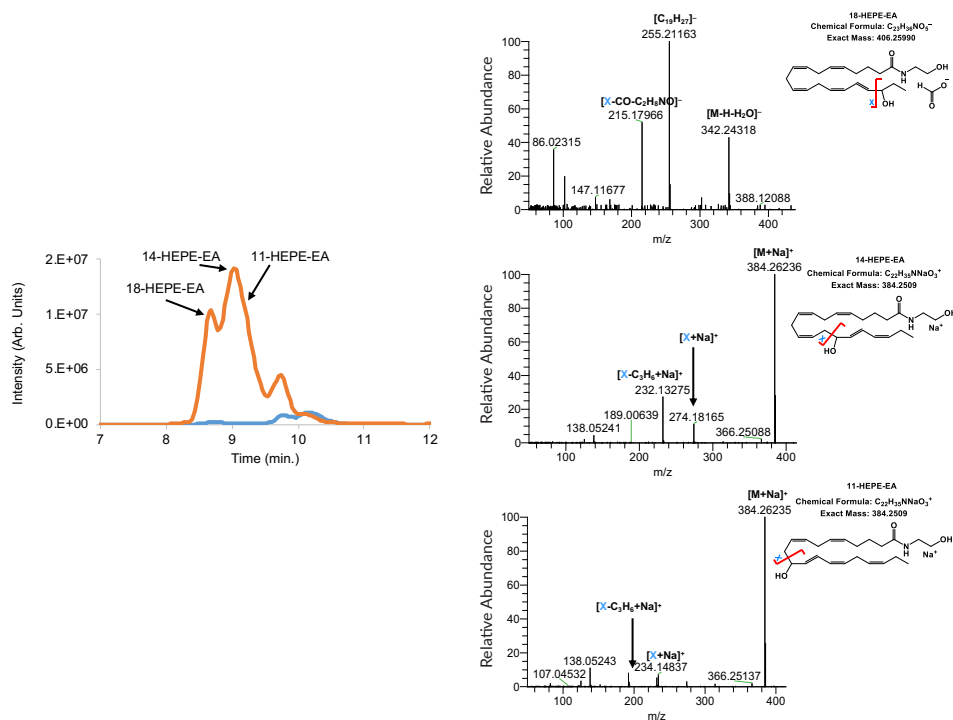


Figure 4-2 Extracted ion chromatogram of $m/z = 344.25$ - 344.27 of HEPE-EAs $[M+H-H_2O]^+$. The orange trace in the chromatogram depicts the products of EPEA formed by hCOX-2; the blue trace shows the control assay without hCOX-2. Mass fragmentation spectra of hCOX-2 products were obtained by fragmenting the $[H+HCO_2]^+$ adduct using 20.0 eV and/or the $[M+Na]^+$ adduct using 30.0 eV. The fragmentation spectra of the postulated 18-HEPE-EA is averaged from 8.43-8.82 min, 14-HEPE-EA from 8.81-9.01 min, and 11-HEPE-EA from 9.04-9.41 min.

Table 4-1 Overview of COX-2 derived monohydroxylated products of *N*-acyl ethanolamides derived from PUFAs and their observed ions in the mass spectrometer. For the $[M+Na]^+$ and $[M+CHO_2]^-$ adducts the obtained fragment ions and proposed rearrangements are given.

Product	$[M+H-H_2O]^+$	$[M+Na]^+$	$[M+CHO_2]^-$
11-HETE-EA	$m/z =$ 346.27432	$m/z = 386.26657$ 243.14639 $[M+Na-C_{10}H_{16}O]^+$ (γ -ene rearrangement) 192.09961 $[M+Na-C_{13}H_{22}O]^+$	$m/z = 408.27555$ 362.27007 $[M-H]^-$ 344.25950 $[M-H-H_2O]^-$ 210.15049 $[M-H-C_{10}H_{16}O]^+$ (γ -ene rearrangement)
15-HETE-EA	$m/z =$ 346.27432	$m/z = 386.26657$ 286.17900 $[M+Na-C_6H_{12}O]^+$ (β -ene rearrangement)	$m/z = 408.27555$ 362.27007 $[M-H]^-$ 344.25950 $[M-H-H_2O]^-$ 262.18112 $[M-H-C_6H_{12}O]^-$ (β -ene rearrangement)
11-HEPE-EA	$m/z =$ 344.25888	$m/z = 384.25092$ 234.14672 $[M+Na-C_{10}H_{14}O]^+$ (γ -ene rearrangement) 192.09949 $[M+Na-C_{13}H_{20}O]^+$	$m/z = 406.25990$ 360.25442 $[M-H]^-$ 342.24385 $[M-H-H_2O]^-$ 238.14494 $[M-H-C_9H_{14}]^-$ (β -ene rearrangement) 210.14999 $[M-H-C_{10}H_{14}O]^-$ (γ -ene rearrangement)
14-HEPE-EA	$m/z =$ 344.25888	$m/z = 384.25092$ 274.17776 $[M+Na-C_7H_{10}O]^+$ (γ -ene rearrangement) 232.13076 $[M+Na-C_{10}H_{16}O]^+$	$m/z = 406.25990$ 360.25442 $[M-H]^-$ 342.24385 $[M-H-H_2O]^-$ 250.18129 $[M-H-C_7H_{10}O]^-$ (γ -ene rearrangement)
13-HDHEA	$m/z =$ 370.27433	$m/z = 410.26657$ 392.25476 $[M+Na-H_2O]^+$ 260.16127 $[M+Na-C_{10}H_{14}O]^+$ (γ -ene rearrangement) 218.11452 $[M+Na-C_{13}H_{20}O]^+$	$m/z = 432.27555$ 368.25919 $[M-H-H_2O]^-$ 264.16033 $[M-H-C_9H_{14}]^-$ (β -ene rearrangement) 236.16555 $[M-H-C_{10}H_{14}O]^-$ (γ -ene rearrangement)
16-HDHEA	$m/z =$ 370.27433	$m/z = 410.26657$ 392.25485 $[M+Na-H_2O]^+$ 300.19255 $[M+Na-C_7H_{10}O]^+$ (γ -ene rearrangement) 258.14571 $[M+Na-C_{10}H_{16}O]^+$	$m/z = 432.27555$ 368.25919 $[M-H-H_2O]^-$ 276.19660 $[M-H-C_7H_{10}O]^-$ (γ -ene rearrangement)

For DHEA, only mono-hydroxylated products and no cyclooxygenated products were identified. Again, an in-source fragment with the loss of water of $m/z = 370.27433$ and a sodium adduct of $m/z = 410.26642$ for 13-HDHEA and $m/z = 410.26657$ for 16-HDHEA were observed for the hydroxylated products in the positive ionization mode. The negative ionization mode showed a formate adduct of $m/z = 432.27553$. Based on the fragmentation spectra of the $[M+Na]^+$ ion, using a collision energy of 30.0 eV, it was concluded that 13-HDHEA and 16-HDHEA are the main enzymatic products of DHEA (Figure 4-3). Both products were not chromatographically resolved. Mass fragmentation resulted in a fragment ion of $m/z = 260.16186$ corresponding to a chemical structure of

$C_{14}H_{23}NNaO_2^+$. This fragment matched with the proposed γ -ene rearranged product of 13-HDHEA. A second fragment of $m/z = 300.19316$ corresponded to a chemical structure of $C_{17}H_{27}NNaO_2^+$, which matched with the γ -ene rearranged product of 16-HDHEA. Again, the HDHEA fragments were prone to a neutral loss of C_3H_6 (**Figure 4-3**). Also, in the negative ionization mode, the fragmentation performed on the formate adduct gave rise to the expected loss of a water fragment ($m/z = 368.25959$), a γ -ene rearranged fragment ($m/z = 236.16560$), and a β -ene rearranged fragment ($m/z = 264.16037$) for 13-HDHEA. Similarly, the expected loss of a water fragment ($m/z = 368.25904$), and a γ -ene rearranged fragment ($m/z = 276.19677$) were observed for 16-HDHEA (**Table 4-1**). To confirm our observations, we synthesized 13- and 16-HDHEA as analytical standards and observed that these standards eluted, ionized, and fragmented identically (**Figure 4-S9, 4-S10**).

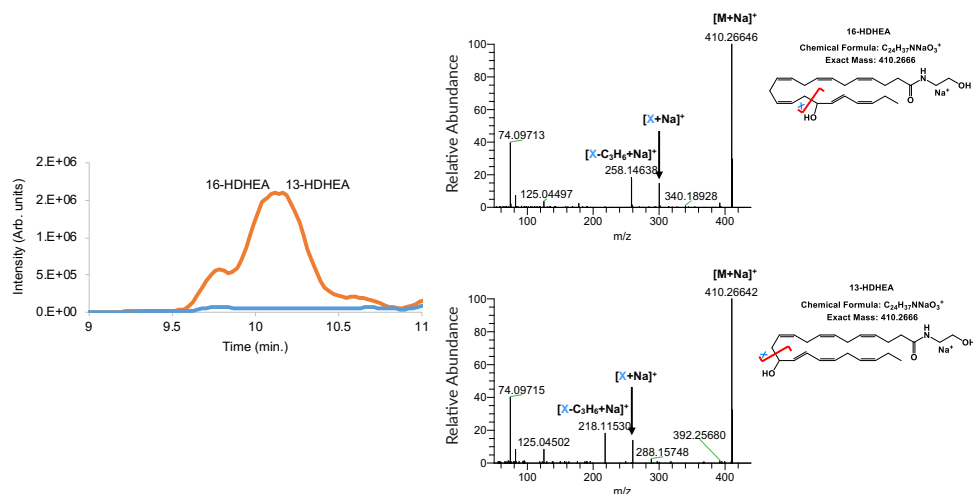


Figure 4-3 Extracted ion chromatogram of $m/z = 370.26$ - 370.28 HDHEAs $[M+H-H_2O]^+$. The orange trace in the chromatogram depicts the products of DHEA formed by hCOX-2; the blue trace shows the control assay without hCOX-2. Mass fragmentation spectra of both hCOX-2 products were obtained by fragmenting the $[M+Na]^+$ adduct from 9.91-10.04 min for 16-HDHEA and from 10.19-10.24 min for 13-HDHEA using 30.0 eV collision energy.

4.4.3 UPLC-MS/MS analysis of hCOX-2 enzymatic incubation of DHEA and EPEA

For further investigation into the metabolism of EPEA and DHEA and to quantify the hCOX-2-derived products of EPEA and DHEA, we developed an analytical method with sufficient chromatographic separation and increased analytical sensitivity. For this, we synthesized appropriate analytical standards by coupling ethanolamine or

ethanolamine- d_4 to commercially available monohydroxylated fatty acid precursors. Thereafter, a targeted UPLC-MS/MS method was developed for the quantification of PGE₃-EA, HEPE-EAs, and 13- and 16-HDHEA. We successfully quantified PGE₃-EA formation at 28.5 (\pm 1.1) pmol (\sim 0.7% conversion) (**Figure 4-4, Table 4-2**). Although exact quantification of HEPE-EAs was not successful due to substantial interfering auto-oxidation of EPEA, we estimate that HEPE-EAs were formed in the same order of magnitude as the PGE₃-EA product, *i.e.*, with \sim 1% conversion, because the peak areas were of the same order of magnitude. The 13- and 16-HDHEA were baseline separated by our UPLC-MS/MS method, and we were able to quantify both mono-oxygenated products: 55.9 (\pm 9.1) pmol (\sim 1.4% of DHEA) for 13-HDHEA and 52.1 (\pm 6.5) pmol (\sim 1.3% of DHEA) for 16-HDHEA (**Figure 4-5, Table 4-2**).

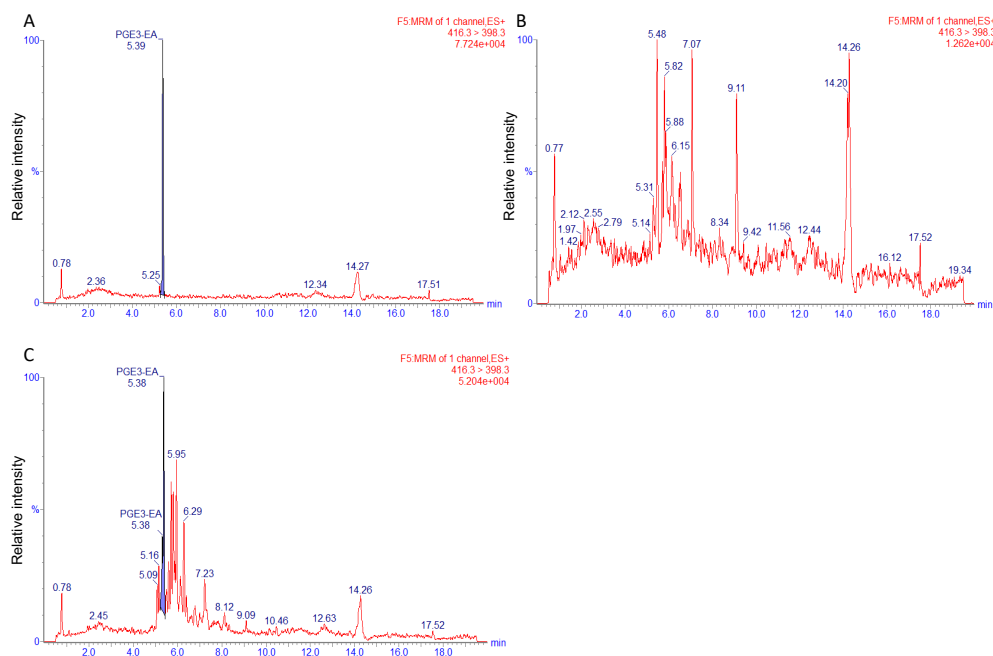


Figure 4-4 MRM chromatograms of $m/z = 416 > 398$ for the 10 ng spiked PGE₃-EA standard (A), control incubation of EPEA without hCOX-2 (B), and hCOX-2 incubation of EPEA (C).

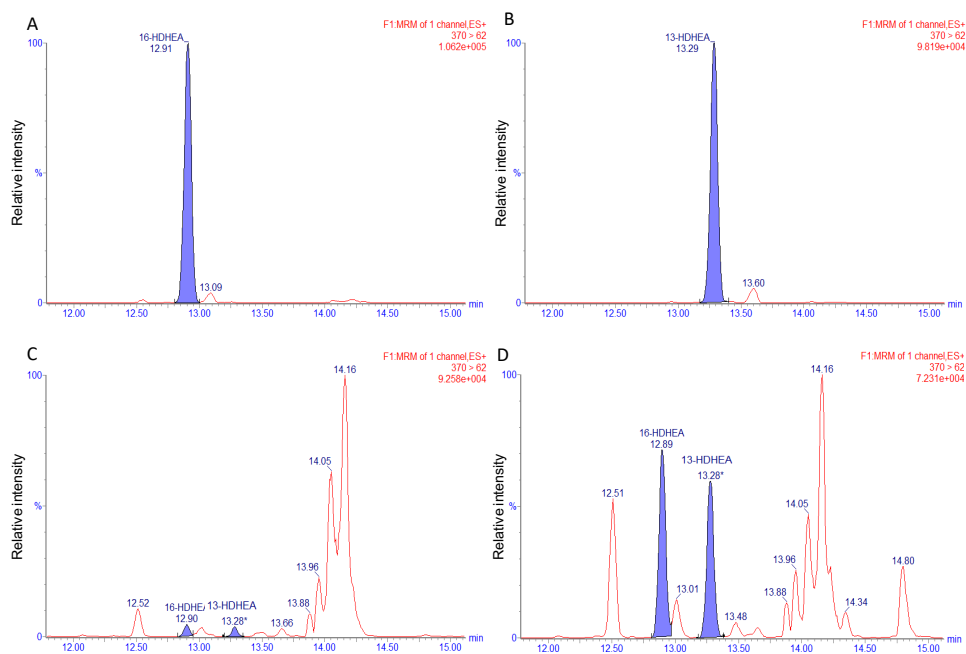


Figure 4-5 MRM chromatograms of $m/z = 370 > 62$ for the synthetic standards 16-HDHEA (A), 13-HDHEA (B), control incubation of DHEA without hCOX-2 (C), and hCOX-2 incubation of DHEA (D).

Table 4-2 Identified products and yields of the enzymatic conversion of EPEA to PGE₃-EA and DHEA to 13- and 16-HDHEA by hCOX-2 as quantified by UPLC-MS/MS. Data are presented as the mean from three independent experiments containing technical duplicates containing standard deviation

Substrate	hCOX-2 product	Amount of product formed (pmol)	Yield (%)
EPEA (4 nmol)	PGE ₃ -EA	28.5 ± 1.1	0.7 ± 0.02
DHEA (4 nmol)	13-HDHEA	55.9 ± 9.1	1.4 ± 0.05
DHEA (4 nmol)	16-HDHEA	52.1 ± 6.5	1.3 ± 0.03

4.4.4 13-HDHEA and 16-HDHEA are formed from DHEA in LPS-stimulated RAW264.7 macrophages by a COX-2 dependent process

To investigate whether our findings from the hCOX-2 assay were also relevant in a murine cell-based system, we exposed LPS-stimulated RAW264.7 macrophages to DHEA and analyzed the cell lysates using our optimized UPLC-MS/MS method. After 30 min

of incubation with 10 μ M of DHEA and 24 h of stimulation with 1.0 μ g/mL LPS, 13- and 16-HDHEA were detected as the main products in the cell extracts but not in the cell media. The products were quantified to be 43.2 (\pm 17.5) pmol/mL for 13-HDHEA and 36.3 (\pm 11.6) pmol/mL for 16-HDHEA (**Table 4-3**). No product was detected in the control incubations in which LPS and/or DHEA were not added (**Figure 4-8, Table 4-3**). Additionally, to explore a potential time-dependent effect of LPS stimulation, we showed that the formation of 13- and 16-HDHEA was not significantly affected when the cells were first stimulated by LPS to upregulate COX-2 expression before the incubation with DHEA (**Figure 4-S11**). We also quantified the amount of DHEA that was present in the cell extracts at various time points, showing that only a limited amount of the 10 μ M of DHEA was taken up by the cells but was chemically stable in medium without cells (**Figure 4-S12**) and that the highest amount of 13- and 16-HDHEA were found after 24 h (**Figure 4-S13**).

Table 4-3 Concentrations of 13- and 16-HDHEA in 100 μ L of the RAW264.7 macrophage extracts, and concentrations of PGE₂ in cell medium. Data are presented as the mean from three independent experiments containing technical duplicates, with standard error of the mean. N.D. is not detected.

Incubation condition	16-HDHEA (pmol/mL)	13-HDHEA (pmol/mL)	PGE ₂ (pmol/mL)
Vehicle control	N.D.	N.D.	0.0513 \pm 0.0147
DHEA (10 μ M)	0.8 \pm 0.4	0.4 \pm 0.4	0.0899 \pm 0.0126
LPS (1.0 μ g/mL)	N.D.	N.D.	2.0717 \pm 0.0325
DHEA (10 μ M) and LPS (1.0 μ g/mL)	43.2 \pm 17.5	36.3 \pm 11.6	0.9229 \pm 0.2111
DHEA (10 μ M), and LPS (1.0 μ g/mL), and celecoxib (0.3 μ M)	1.7 \pm 0.4	1.0 \pm 0.5	0.1245 \pm 0.0244

Clearly, 13- and 16-HDHEA formation in our macrophage model was caused by the combined incubation with 10 μ M of DHEA and stimulation with 1.0 μ g/mL LPS, suggesting that these products originated from a COX-2 dependent mechanism. Further evidence was provided by blocking the catalytic activity of COX-2 using 0.3 μ M of the specific COX-2 inhibitor, celecoxib (IC₅₀ 0.07 μ M).^{33, 42-44} The addition of celecoxib resulted in the complete loss of intracellular 13- and 16-HDHEA and of PGE₂ (**Figure 4-6, Table 4-3**). Interestingly, PGE₂ formation was decreased when LPS-stimulated cells were treated with DHEA, confirming previously published data from our laboratory.¹⁸

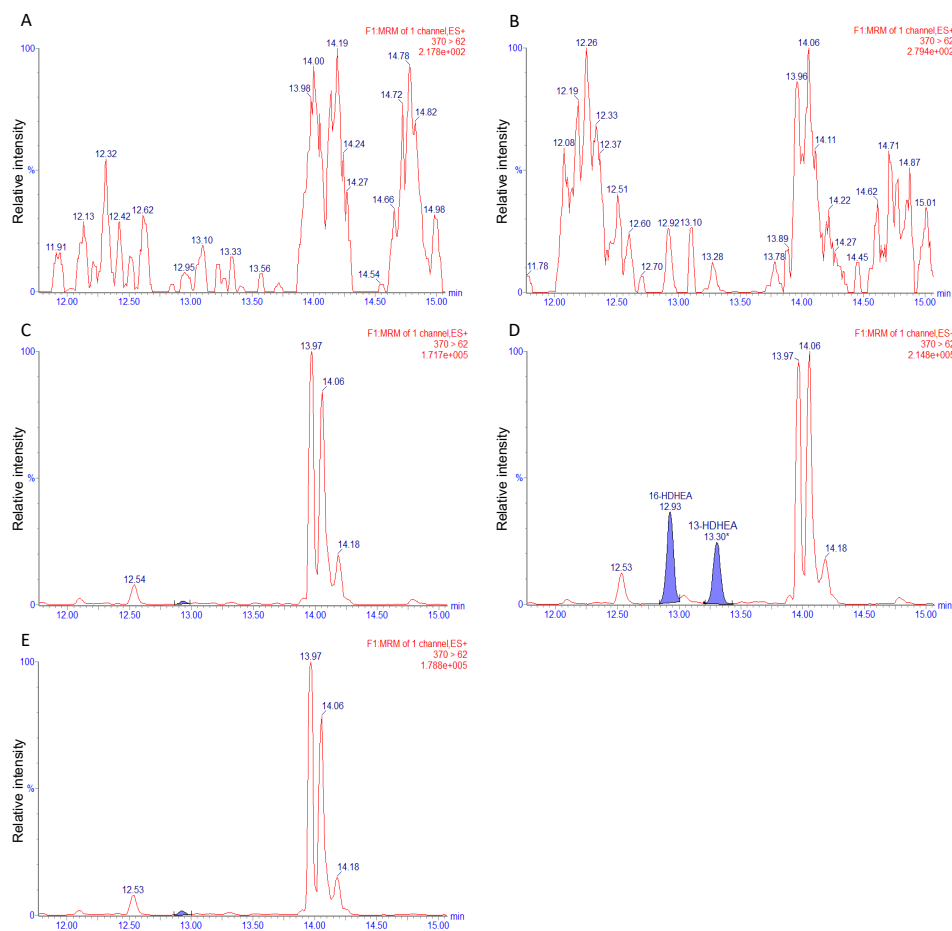


Figure 4-6 MRM chromatograms of $m/z = 370 > 62$ for the RAW264.7 macrophage extracts after 24 h of incubation. The macrophage cells were treated with a vehicle control (EtOH, PBS, and DMSO) (A), 1.0 $\mu\text{g/mL}$ LPS (B), 10 μM of DHEA (C), 1.0 $\mu\text{g/mL}$ LPS and 10 μM of DHEA (D), or 0.3 μM celecoxib, 1.0 $\mu\text{g/mL}$ LPS, and 10 μM of DHEA (E).

4.5 Discussion

In this study, we have developed an LC-HRMS assay to identify novel hCOX-2 products, which we validated using three different PUFAs.^{35-36, 40-41, 45-46} Next, we demonstrated enzymatic conversion of neutral lipids, including the endocannabinoid, anandamide, and identified $\text{PGE}_2\text{-EA}$, $\text{PGD}_2\text{-EA}$, and 11- and 15-HETE-EA to further validate our methodology.^{2, 5, 10-11, 13-14} Interestingly, LC-HRMS data showed that hCOX-2 also oxygenates EPEA and DHEA. To the best of our knowledge, the present study is the first to report that DHEA and EPEA serve as COX-2 substrates, also providing evidence for a set of

previously unknown lipid metabolites such as PGE_3 -EA, 11-, 14-, and 18-HEPE-EA, and 13- and 16-HDHEA. The newly detected compounds were identified based on the mass fragmentation pattern and the isotopic ratio, which were in correspondence with the proposed structure. The formation of PGE_3 -EA, 11-HEPE-EA, and 13- and 16-HDHEA was confirmed using synthetically derived congeners that displayed identical LC retention and mass fragmentation.

During validation of our LC-HRMS method, we found that both PUFA and endocannabinoid structures have the tendency to easily lose water during ionization, leading to a high abundance of $[\text{M}+\text{H}-\text{H}_2\text{O}]^+$ ions for the hydroxylated endocannabinoid-like products. This was found to be an inherent property associated with PUFA and endocannabinoid structures, and has been obtained in many studies before,^{7, 13, 36, 39, 41} especially for mono-hydroxylated products of the *N*-acylethanolamine derivatives. In those cases, no $[\text{M}+\text{H}]^+$ ion peak was observed. Decreasing the temperature of the ion source did not decrease in-source fragmentation of the hydroxylated endocannabinoid-like products. Alternatively, a sodium adduct $[\text{M}+\text{Na}]^+$ was detected in the positive ionization mode, and a formate adduct $[\text{M}+\text{CHO}_2]^-$ in the negative ionization mode. These ions allowed us to perform fragmentation experiments on the hydroxylated AEA, EPEA, and DHEA products.

In the LC-HRMS measurement of the hCOX-2-treated EPEA, we found three hydroxylated HEPE-EA products, *i.e.*, 11-, 14-, and 18-HEPE-EA, whereas only two hydroxylated products of EPA were observed, *i.e.*, 11- and 14-HEPE.³⁵ Similarly, two DHEA-derived products were found, *i.e.*, 13- and 16-HDHEA, whereas only one hydroxylated product of DHA was observed, *i.e.*, 13-HDHA.³⁵ The origin of these extra hydroxylated products in the *N*-acylethanolamine-derived PUFAs needs to be further investigated.

Next, we developed an UPLC-MS/MS method for the quantitative analysis of PGE_3 -EA, HEPE-EAs, and 13- and 16-HDHEA. Whereas our HPLC combined with Orbitrap HR-MS analysis proved to be a powerful tool to identify new COX-2-derived products, it was insufficient in achieving chromatographic separation to quantitatively analyze the products. After achieving baseline separation of the products using UPLC, we were able to accurately quantify the enzymatic production of PGE_3 -EA, and 13- and 16-HDHEA to be 0.5-1.5%. Although exact quantification of the HEPE-EAs was prohibited by the auto-oxidation of EPEA, we estimate the production of the HEPE-EAs to be in the same order as the formation of the other products. In summary it was concluded that only a small fraction of the DHEA or EPEA is metabolized to 13- and 16-HDHEA or PGE_3 -EA, respectively. Various earlier studies showed anti-inflammatory and anti-cancerous properties of 15-LOX or CYP450 metabolites of DHEA.^{24, 26, 47} Additionally, evidence was found that

DHEA interacts with COX-2, resulting in interesting anti-inflammatory effects *in vitro*.^{18, 23} Therefore, we investigated whether the COX-2-mediated conversion of DHEA also occurs in cells. Here RAW264.7 macrophages were only stimulated with 1.0 µg/mL LPS, only incubated with 10 µM of DHEA, or incubated with 10 µM of DHEA 30 min prior to stimulation with 1.0 µg/mL LPS. In short, LPS activation stimulates the expression of COX-2 and induces an inflammatory response in the macrophages.^{18, 48-50} We used a DHEA preincubation of 30 min on the macrophages before the addition of LPS, which is similar to the incubation methodology described in Meijerink *et al.*¹⁸ These conditions were chosen to ensure an identical incubation methodology compared with our previous study where we posed the hypothesis that DHEA could be a potential COX-2 substrate. To explore the time effect of LPS stimulation, control studies were performed, which showed that stimulation with 1.0 µg/mL LPS prior to the 24 h incubation with 10 µM of DHEA does not lead to higher concentrations of the products (**Figure 4-S11**). Similarly, product formation was shown to be the highest 24.5 h after DHEA incubation (which equals to 24 h after LPS stimulation) (**Figure 4-S13**).

We showed that 13- and 16-HDHEA products were formed when incubating the macrophages with both DHEA and LPS, and showed that there was no product formation when only one of the two compounds was added to the cells. In addition, when the selective COX-2 inhibitor, celecoxib, was added, no HDHEAs were detected, which further proved that 13- and 16-HDHEA are formed by a COX-2-dependent mechanism (**Figure 4-8, Table 4-3**). Finally, a decrease in PGE₂ formation was observed when treating the stimulated macrophages with 10 µM of DHEA; that PGD₂ also decreases was already shown earlier.¹⁸ This observation indicates that the conversion of DHEA by COX-2 at least partly competes with the conversion of endogenous AA into PGs, and further supports the anti-inflammatory behavior linked to DHEA.

In the macrophage incubation experiment, we found that, after 24 h incubation, the macrophages produced 36.3 ± 11.6 pmol/mL of 13-HDHEA and 43.2 ± 17.5 pmol/mL of 16-HDHEA (**Table 4-3**). This is comparable to the amount of epoxidated products of DHEA formed by CYP450 in BV-2 microglia cells.²⁴ Specifically, CYP450 forms between 3 and 10 pmol per 10⁶ BV-2 microglia cells of the various epoxidated isomers,²⁴ and we find 7.3 ± 2.3 pmol of 13-HDHEA per 10⁶ RAW macrophage cells and 8.6 ± 3.5 pmol of 16-HDHEA per 10⁶ RAW macrophage cells. Although obtained by different laboratories and using different models, these apparent comparable amounts indicate that the products are formed in the same order of magnitude.

Furthermore, it must be taken into account that only 1-2% of the added 10 µM of DHEA was detected in the macrophages (**Figure 4-S12**). This is most likely due to limited

uptake of the DHEA, degradation via NAAA and FAAH, and conversion into novel metabolites via various lipoxygenases and CYP450s. Studies with radiolabeled DHEA in immortalized fetal mesencephalic cells also showed that the uptake of DHEA was limited, and that the uptake of DHEA is driven by its FAAH-dependent hydrolysis.⁵¹ Therefore, we expect that the reported values of 13- and 16-HDHEA most likely are an underestimation of the biosynthetic capacity of the macrophage model used. In addition to this, it must be pointed out that DHEA itself can also modulate several specific anti-inflammatory activities during incubation. For example, it has been shown that DHEA inhibits PG formation^{18, 25} and is able to bind several endocannabinoid-related receptors, like CB₂, TRPV1,⁵⁰ and GPR110;²⁹ although for GPR110, it is unknown whether this receptor is present in macrophages. Whether these indirect effects of DHEA interfere with the synthesis of 13- and 16-HDHEA in our study is not known.

Finally, the fact that 13- and 16-HDHEA were found in both the hCOX-2 assay and the murine RAW264.7 macrophages suggests that DHEA oxygenation by COX-2 is conserved between both human COX-2 and murine COX-2. Further studies are warranted to reveal the presence of the hydroxylated DHEA and EPEA products in blood and tissues and to investigate the biological effects of the novel oxygenated DHEA products. Based on the strong anti-inflammatory properties of previously identified epoxidated and hydroxylated DHEA-derived products,^{24, 26, 47} it is tempting to speculate that these newly detected compounds play a role in inflammatory processes, in already limited concentrations.

In conclusion, we have developed a new cell-free hCOX-2 metabolite identification and quantification method. Using this method, we have identified previously unknown COX-2 metabolites of DHEA and EPEA in hCOX-2 incubations and extended these findings to LPS-stimulated RAW264.7 macrophages. Future work in our laboratory will investigate the biological effects of these new DHEA and EPEA metabolites, characterize the binding properties of DHEA to COX-2, and further focus on the uptake and metabolism of DHEA.

4.6 Acknowledgements

The authors acknowledge Mieke Poland and Frank Claassen for their technical assistance, Carolina Tabares Mafla for conducting part of the incubation studies, Floor Leurs for help with the UPLC-MS/MS measurements, Niels de Roo for his help with the NMR measurements, and prof. Michel Nielen for fruitful discussions. The authors thank the VLAG Graduate School of Wageningen University and Research for their financial support.

4.7 References

1. Ricciotti, E.; FitzGerald, G. A., Prostaglandins and Inflammation. *Arterioscler. Thromb. Vasc. Biol.* **2011**, *31* (5), 986-1000.
2. Rouzer, C. A.; Marnett, L. J., Endocannabinoid Oxygenation by Cyclooxygenases, Lipoxygenases, and Cytochromes P450: Cross-Talk between the Eicosanoid and Endocannabinoid Signaling Pathways. *Chem. Rev.* **2011**, *111* (10), 5899-5921.
3. Smith, W. L.; DeWitt, D. L.; Garavito, R. M., Cyclooxygenases: Structural, Cellular, and Molecular Biology. *Annu. Rev. Biochem.* **2000**, *69*(1), 145-182.
4. Serhan, C. N.; Chiang, N.; Van Dyke, T. E., Resolving inflammation: dual anti-inflammatory and pro-resolution lipid mediators. *Nat. Rev. Immunol.* **2008**, *8* (5), 349-361.
5. Alhouayek, M.; Muccioli, G. G., COX-2-derived endocannabinoid metabolites as novel inflammatory mediators. *Trends Pharmacol.* **2014**, *35* (6), 284-292.
6. Fowler, C. J., The contribution of cyclooxygenase-2 to endocannabinoid metabolism and action. *Br. J. Pharmacol.* **2007**, *152* (5), 594-601.
7. Kozak, K. R.; Prusakiewicz, J. J.; Rowlinson, S. W.; Prudhomme, D. R.; Marnett, L. J., Amino Acid Determinants in Cyclooxygenase-2 Oxygenation of the Endocannabinoid Anandamide. *Biochemistry* **2003**, *42* (30), 9041-9049.
8. Prusakiewicz, J. J.; Kingsley, P. J.; Kozak, K. R.; Marnett, L. J., Selective oxygenation of N-arachidonylglycine by cyclooxygenase-2. *Biochem. Biophys. Res. Commun.* **2002**, *296* (3), 612-617.
9. Prusakiewicz, J. J.; Turman, M. V.; Vila, A.; Ball, H. L.; Al-Mestarihi, A. H.; Marzo, V. D.; Marnett, L. J., Oxidative metabolism of lipoamino acids and vanilloids by lipoxygenases and cyclooxygenases. *Arch. Biochem. Biophys.* **2007**, *464* (2), 260-268.
10. Rouzer, C. A.; Marnett, L. J., Non-redundant Functions of Cyclooxygenases: Oxygenation of Endocannabinoids. *J. Biol. Chem.* **2008**, *283* (13), 8065-8069.
11. Urquhart, P.; Nicolaou, A.; Woodward, D. F., Endocannabinoids and their oxygenation by cyclo-oxygenases, lipoxygenases and other oxygenases. *Biochim. Biophys. Acta Mol. Cell Biol. Lipids* **2015**, *1851* (4), 366-376.
12. Alhouayek, M.; Masquelier, J.; Cani, P. D.; Lambert, D. M.; Muccioli, G. G., Implication of the anti-inflammatory bioactive lipid prostaglandin D2-glycerol ester in the control of macrophage activation and inflammation by ABHD6. *Proc. Natl. Acad. Sci. U.S.A.* **2013**, *110* (43), 17558-17563.
13. Urquhart, P.; Wang, J.; Woodward, D. F.; Nicolaou, A., Identification of prostamides, fatty acyl ethanolamines, and their biosynthetic precursors in rabbit cornea. *J. Lipid Res.* **2015**, *56* (8), 1419-1433.
14. Yu, M.; Ives, D.; Ramesha, C. S., Synthesis of Prostaglandin E2 Ethanolamide from Anandamide by Cyclooxygenase-2. *J. Biol. Chem.* **1997**, *272* (34), 21181-21186.
15. Kozak, K. R.; Crews, B. C.; Morrow, J. D.; Wang, L.-H.; Ma, Y. H.; Weinander, R.; Jakobsson,

- P.-J.; Marnett, L. J., Metabolism of the Endocannabinoids, 2-Arachidonylglycerol and Anandamide, into Prostaglandin, Thromboxane, and Prostacyclin Glycerol Esters and Ethanolamides. *J. Biol. Chem.* **2002**, *277* (47), 44877-44885.
16. Kozak, K. R.; Crews, B. C.; Ray, J. L.; Tai, H.-H.; Morrow, J. D.; Marnett, L. J., Metabolism of Prostaglandin Glycerol Esters and Prostaglandin Ethanolamides in Vitro and in Vivo. *J. Biol. Chem.* **2001**, *276* (40), 36993-36998.
 17. Kozak, K. R.; Rowlinson, S. W.; Marnett, L. J., Oxygenation of the Endocannabinoid, 2-Arachidonylglycerol, to Glyceryl Prostaglandins by Cyclooxygenase-2. *J. Biol. Chem.* **2000**, *275* (43), 33744-33749.
 18. Meijerink, J.; Poland, M.; Balvers, M. G. J.; Plastina, P.; Lute, C.; Dwarkasing, J.; van Norren, K.; Witkamp, R. F., Inhibition of COX-2-mediated eicosanoid production plays a major role in the anti-inflammatory effects of the endocannabinoid N-docosahexaenoylethanolamine (DHEA) in macrophages. *Br. J. Pharmacol.* **2015**, *172* (1), 24-37.
 19. Balvers, M. G. J.; Verhoeckx, K. C. M.; Bijlsma, S.; Rubingh, C. M.; Meijerink, J.; Wortelboer, H. M.; Witkamp, R. F., Fish oil and inflammatory status alter the n-3 to n-6 balance of the endocannabinoid and oxylipin metabolomes in mouse plasma and tissues. *Metabolomics* **2012**, *8* (6), 1130-1147.
 20. Balvers, M. G. J.; Wortelboer, H. M.; Witkamp, R. F.; Verhoeckx, K. C. M., Liquid chromatography-tandem mass spectrometry analysis of free and esterified fatty acid N-acyl ethanolamines in plasma and blood cells. *Anal. Biochem.* **2013**, *434* (2), 275-283.
 21. de Bus, I.; Witkamp, R.; Zuilhof, H.; Albada, B.; Balvers, M., The role of n-3 PUFA-derived fatty acid derivatives and their oxygenated metabolites in the modulation of inflammation. *Prostaglandins Other Lipid Mediat.* **2019**, *144*, 106351.
 22. Meijerink, J.; Balvers, M. G. J.; Witkamp, R. F., N-acyl amines of docosahexaenoic acid and other n-3 polyunsaturated fatty acids – from fishy endocannabinoids to potential leads. *Br. J. Pharmacol.* **2013**, *169* (4), 772-783.
 23. Alhouayek, M.; Bottemanne, P.; Makriyannis, A.; Muccioli, G. G., N-acylethanolamine-hydrolyzing acid amidase and fatty acid amide hydrolase inhibition differentially affect N-acylethanolamine levels and macrophage activation. *Biochim. Biophys. Acta Mol. Cell Biol. Lipids* **2017**, *1862* (5), 474-484.
 24. McDougale, D. R.; Watson, J. E.; Abdeen, A. A.; Adili, R.; Caputo, M. P.; Krapf, J. E.; Johnson, R. W.; Kilian, K. A.; Holinstat, M.; Das, A., Anti-inflammatory ω -3 endocannabinoid epoxides. *Proc. Natl. Acad. Sci. U.S.A.* **2017**, *114* (30), E6034-E6043.
 25. Park, S.-W.; Hah, J. H.; Oh, S.-M.; Jeong, W.-J.; Sung, M.-W., 5-lipoxygenase mediates docosahexaenoyl ethanolamide and N-arachidonoyl-L-alanine-induced reactive oxygen species production and inhibition of proliferation of head and neck squamous cell carcinoma cells. *BMC Cancer* **2016**, *16* (1), 1-14.
 26. Yang, R.; Fredman, G.; Krishnamoorthy, S.; Agrawal, N.; Irimia, D.; Piomelli, D.; Serhan, C. N., Decoding Functional Metabolomics with Docosahexaenoyl Ethanolamide (DHEA) Identifies

- Novel Bioactive Signals. *J. Biol. Chem.* **2011**, *286* (36), 31532-31541.
27. Kim, H.-Y.; Moon, H.-S.; Cao, D.; Lee, J.; Kevala, K.; Jun, S. B.; Lovinger, D. M.; Akbar, M.; Huang, B. X., N-Docosahexaenoylethanolamide promotes development of hippocampal neurons. *Biochem.* **2011**, *435* (2), 327-336.
 28. Kim, H.-Y.; Spector, A. A., N-Docosahexaenoylethanolamine: A neurotrophic and neuroprotective metabolite of docosahexaenoic acid. *Mol. Aspects Med.* **2018**, *64*, 34-44.
 29. Kim, H.-Y.; Spector, A. A.; Xiong, Z.-M., Asynaptogenicamide N-docosahexaenoylethanolamide promotes hippocampal development. *Prostaglandins Other Lipid Mediat.* **2011**, *96* (1), 114-120.
 30. Lee, J.-W.; Huang, B. X.; Kwon, H.; Rashid, M. A.; Kharebava, G.; Desai, A.; Patnaik, S.; Marugan, J.; Kim, H.-Y., Orphan GPR110 (ADGRF1) targeted by N-docosahexaenoylethanolamine in development of neurons and cognitive function. *Nat. Commun.* **2016**, *7*, 13123.
 31. Park, T.; Chen, H.; Kevala, K.; Lee, J.-W.; Kim, H.-Y., N-Docosahexaenoylethanolamine ameliorates LPS-induced neuroinflammation via cAMP/PKA-dependent signaling. *J. Neuroinflammation* **2016**, *13* (1), 284.
 32. Kim, H.-Y.; Spector, A. A., Synaptamide, endocannabinoid-like derivative of docosahexaenoic acid with cannabinoid-independent function. *Prostaglandins Leukot. Essent. Fatty Acids* **2013**, *88* (1), 121-125.
 33. Cao, H.; Yu, R.; Tao, Y.; Nikolic, D.; van Breemen, R. B., Measurement of cyclooxygenase inhibition using liquid chromatography-tandem mass spectrometry. *J. Pharm. Biomed. Anal.* **2011**, *54* (1), 230-235.
 34. Reininger, E. A.; Bauer, R., Prostaglandin-H-synthase (PGHS)-1 and -2 microtiter assays for the testing of herbal drugs and in vitro inhibition of PGHS-isoenzymes by polyunsaturated fatty acids from *Platycodi radix*. *Phytomedicine* **2006**, *13* (3), 164-169.
 35. Sharma, N. P.; Dong, L.; Yuan, C.; Noon, K. R.; Smith, W. L., Asymmetric acetylation of the cyclooxygenase-2 homodimer by aspirin and its effects on the oxygenation of arachidonic, eicosapentaenoic, and docosahexaenoic acids. *Mol. Pharmacol.* **2010**, *77* (6), 979-986.
 36. Murphy, R. C.; Barkley, R. M.; Zemski Berry, K.; Hankin, J.; Harrison, K.; Johnson, C.; Krank, J.; McAnoy, A.; Uhlson, C.; Zarini, S., Electrospray ionization and tandem mass spectrometry of eicosanoids. *Anal. Biochem.* **2005**, *346* (1), 1-42.
 37. Porter, N. A., A Perspective on Free Radical Autoxidation: The Physical Organic Chemistry of Polyunsaturated Fatty Acid and Sterol Peroxidation. *J. Org. Chem.* **2013**, *78* (8), 3511-3524.
 38. Tanaka, N.; Yamaguchi, H.; Furugen, A.; Ogura, J.; Kobayashi, M.; Yamada, T.; Mano, N.; Iseki, K., Quantification of intracellular and extracellular eicosapentaenoic acid-derived 3-series prostanoids by liquid chromatography/electrospray ionization tandem mass spectrometry. *Prostaglandins Leukot. Essent. Fatty Acids* **2014**, *91* (3), 61-71.
 39. Derogis, P. B. M. C.; Freitas, F. P.; Marques, A. S. F.; Cunha, D.; Appolinário, P. P.; de Paula, F.; Lourenço, T. C.; Murgu, M.; Di Mascio, P.; Medeiros, et al., The Development of a Specific

- and Sensitive LC-MS-Based Method for the Detection and Quantification of Hydroperoxy- and Hydroxydocosahexaenoic Acids as a Tool for Lipidomic Analysis. *PLoS ONE* **2013**, *8* (10), e77561.
40. Serhan, C. N.; Hong, S.; Gronert, K.; Colgan, S. P.; Devchand, P. R.; Mirick, G.; Moussignac, R.-L., Resolvins: A Family of Bioactive Products of Omega-3 Fatty Acid Transformation Circuits Initiated by Aspirin Treatment that Counter Proinflammation Signals. *J. Exp. Med* **2002**, *196* (8), 1025-1037.
 41. Hong, S.; Lu, Y.; Yang, R.; Gotlinger, K. H.; Petasis, N. A.; Serhan, C. N., Resolvin D1, protectin D1, and related docosahexaenoic acid-derived products: Analysis via electrospray/low energy tandem mass spectrometry based on spectra and fragmentation mechanisms. *J. Am. Soc. Mass Spectrom.* **2007**, *18* (1), 128-144.
 42. Goldenberg, M. M., Celecoxib, a selective cyclooxygenase-2 inhibitor for the treatment of rheumatoid arthritis and osteoarthritis. *Clin. Ther.* **1999**, *21* (9), 1497-1513.
 43. Kim, K. J.; Choi, M. J.; Shin, J.-S.; Kim, M.; Choi, H.-E.; Kang, S. M.; Jin, J. H.; Lee, K.-T.; Lee, J. Y., Synthesis, biological evaluation, and docking analysis of a novel family of 1-methyl-1H-pyrrole-2,5-diones as highly potent and selective cyclooxygenase-2 (COX-2) inhibitors. *Bioorganic Med. Chem. Lett.* **2014**, *24* (8), 1958-1962.
 44. Zarghi, A.; Arfaei, S., Selective COX-2 Inhibitors: A Review of Their Structure-Activity Relationships. *Iran. J. Pharm. Res.* **2011**, *10* (4), 655-683.
 45. Brose, S. A.; Thuen, B. T.; Golovko, M. Y., LC/MS/MS method for analysis of E(2) series prostaglandins and isoprostanes. *J. Lipid Res.* **2011**, *52* (4), 850-859.
 46. Vecchio, A. J.; Simmons, D. M.; Malkowski, M. G., Structural Basis of Fatty Acid Substrate Binding to Cyclooxygenase-2. *J. Biol. Chem.* **2010**, *285* (29), 22152-22163.
 47. Roy, J.; Watson, J. E.; Hong, I. S.; Fan, T. M.; Das, A., Antitumorigenic Properties of Omega-3 Endocannabinoid Epoxides. *J. Med. Chem.* **2018**, *61* (13), 5569-5579.
 48. Gabrielsson, L.; Gouveia-Figueira, S.; Häggström, J.; Alhouayek, M.; Fowler, C. J., The anti-inflammatory compound palmitoylethanolamide inhibits prostaglandin and hydroxyeicosatetraenoic acid production by a macrophage cell line. *Pharmacol. Res. Perspect.* **2017**, *5* (2), e00300.
 49. Gdula-Argasińska, J.; Bystrowska, B., Docosahexaenoic acid attenuates in endocannabinoid synthesis in RAW 264.7 macrophages activated with benzo(a)pyrene and lipopolysaccharide. *Toxicol. Lett.* **2016**, *258*, 93-100.
 50. Hwang, D.; Jang, B. C.; Yu, G.; Boudreau, M., Expression of mitogen-inducible cyclooxygenase induced by lipopolysaccharide: Mediation through both mitogen-activated protein kinase and nf-kb signaling pathways in macrophages. *Biochem. Pharmacol.* **1997**, *54* (1), 87-96.
 51. Sonti, S.; Tolia, M.; Duclos, R. I.; Loring, R. H.; Gatley, S. J., Metabolic studies of synaptamide in an immortalized dopaminergic cell line. *Prostaglandins Other Lipid Mediat.* **2019**, *141*, 25-33.

Supporting information belonging to Chapter 4

In order to access the synthetic methodology, purification and accompanying data, the reader is referred to the online version of the publication at doi: 10.1194/jlr.M094235.

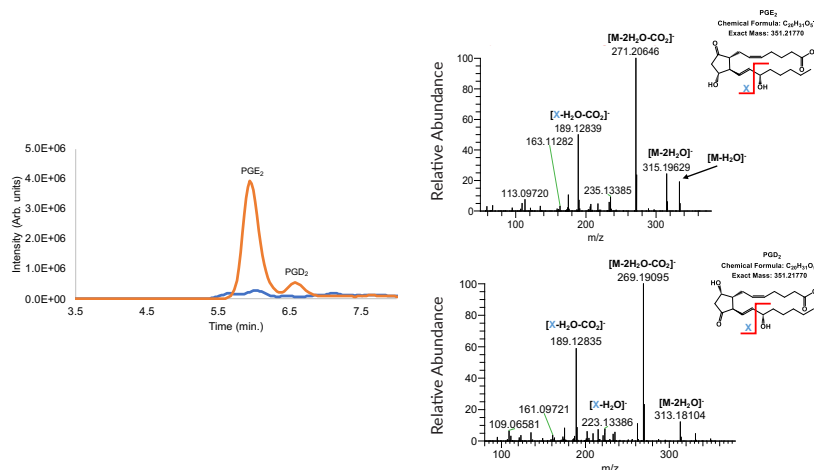


Figure 4-S1 Extracted ion chromatogram of $m/z = 351.21$ – 351.22 assigned to $[M-H]^-$ of PGE₂ and PGD₂. The orange trace in the chromatogram depicts products of the hCOX-2 assay with AA; the blue trace shows the control assay without hCOX-2. Mass fragmentation spectra correspond to PGE₂ eluting at 5.82–6.33 min and PGD₂ eluting at 6.60–7.19 min using 20.0 eV collision energy.

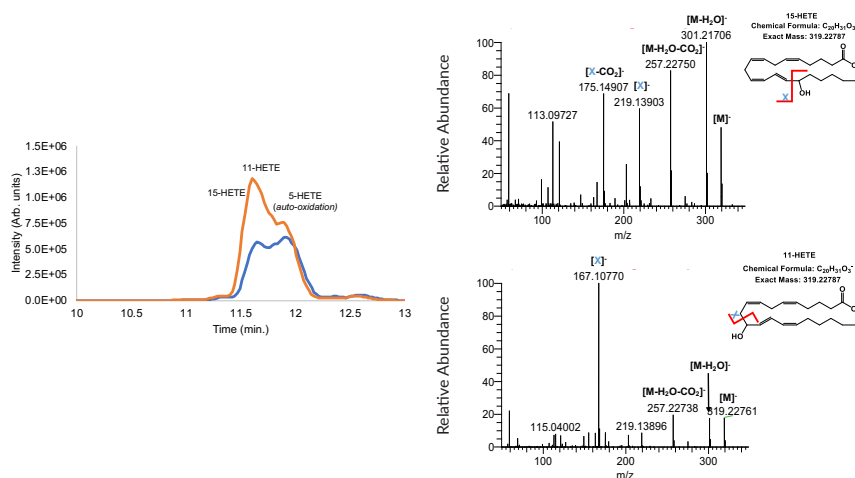


Figure 4-S2 Extracted ion chromatogram of $m/z = 319.21$ – 319.23 assigned to $[M-H]^-$ of HETEs. The orange trace in the chromatogram depicts products of the hCOX-2 assay with AA; the blue trace shows the control assay without hCOX-2. Mass fragmentation spectra correspond to 15-HETE eluting at 11.19–11.33 min and 11-HETE eluting at 11.47–11.97 min using 20 eV collision energy.

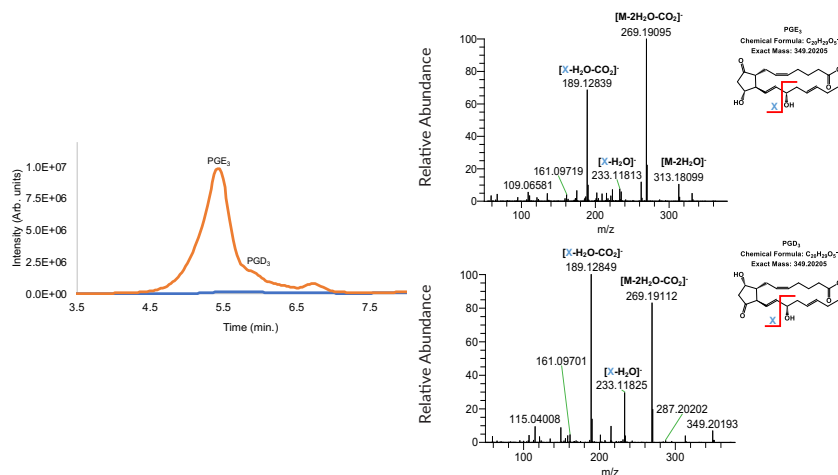


Figure 4-S3 Extracted ion chromatogram of $m/z = 349.19-349.21$ assigned to $[M-H]^-$ of PGE_3 and PGD_3 . The orange trace in the chromatogram depicts products of the hCOX-2 assay with EPA; the blue trace shows the control assay without hCOX-2. Mass fragmentation spectra corresponds to PGE_3 eluting at 5.03–5.52 min and PGD_3 eluting at 5.57–5.78 min using 20.0 eV collision energy.

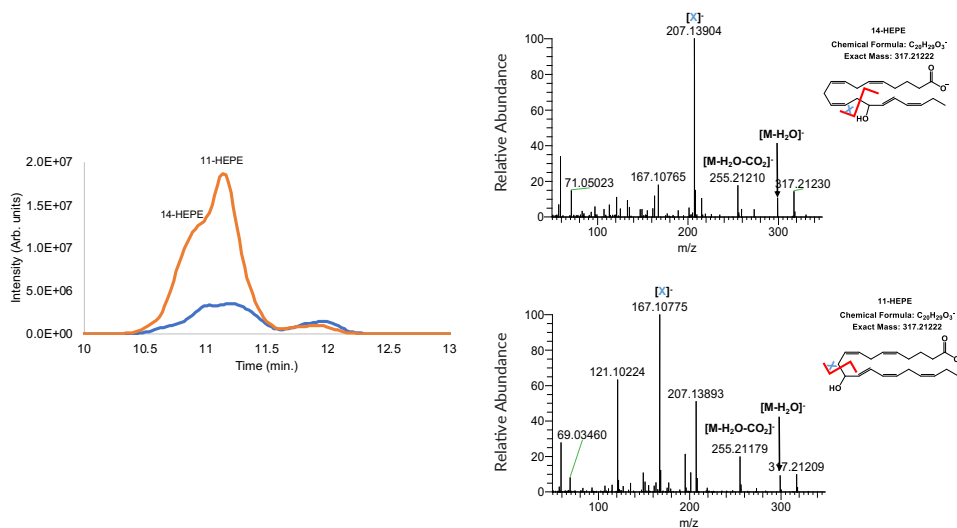


Figure 4-S4 Extracted ion chromatogram of $m/z = 317.21-317.22$ assigned to $[M-H]^-$ of HEPEs. The orange trace in the chromatogram depicts products of the hCOX-2 assay with EPA; the blue trace shows the control assay without hCOX-2. Mass fragmentation spectra corresponds to 14-HEPE eluting at 10.93–10.98 min and 11-HEPE eluting at 11.14–11.28 min using 20.0 eV collision energy.

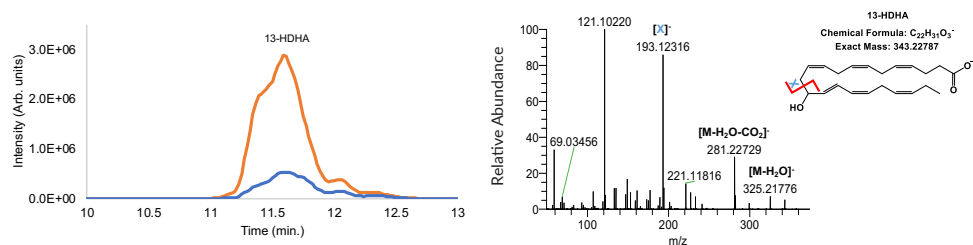


Figure 4-S5 Extracted ion chromatogram of $m/z = 343.22$ – 343.24 assigned to $[M-H]^-$ 13-HDHA. The orange trace in the chromatogram depicts products of the hCOX-2 assay with DHA; the blue trace shows the control assay without hCOX-2. Mass fragmentation spectra corresponds 13-HDHA eluting at 11.43–11.70 min using 20.0 eV collision energy.

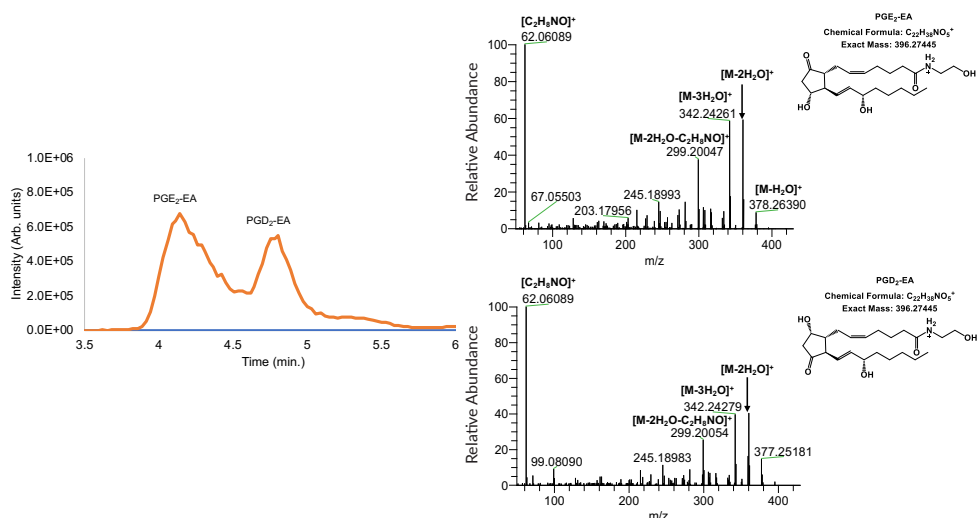


Figure 4-S6 Extracted ion chromatogram of $m/z = 396.26$ – 396.29 , assigned to $[M+H]^+$ of PGE₂-EA and PGD₂-EA. The orange trace in the chromatogram depicts products of the hCOX-2 assay with AEA; the blue trace shows the control assay without hCOX-2. Mass fragmentation spectra corresponds to PGE₂-EA eluting at 4.02–4.47 min and PGD₂-EA eluting at 4.80 min using 20.0 eV collision energy.

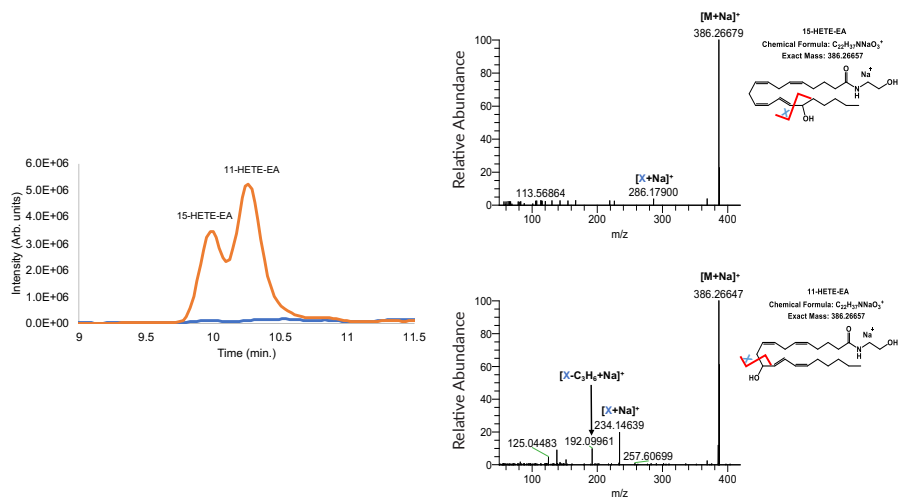


Figure 4-S7 Extracted ion chromatogram of $m/z = 346.26\text{--}346.29$, which is assigned to $[M+H-H_2O]^+$ of HETE-EAs. The orange trace in the chromatogram depicts products of the hCOX-2 assay with AEA; the blue trace shows the control assay without hCOX-2. Mass fragmentation correspond to 15-HETE-EA eluting at 9.97 min and 11-HETE-EA eluting at 10.17-10.35 min using a collision energy of 30.0 eV on the $[M+Na]^+$ adduct ions.

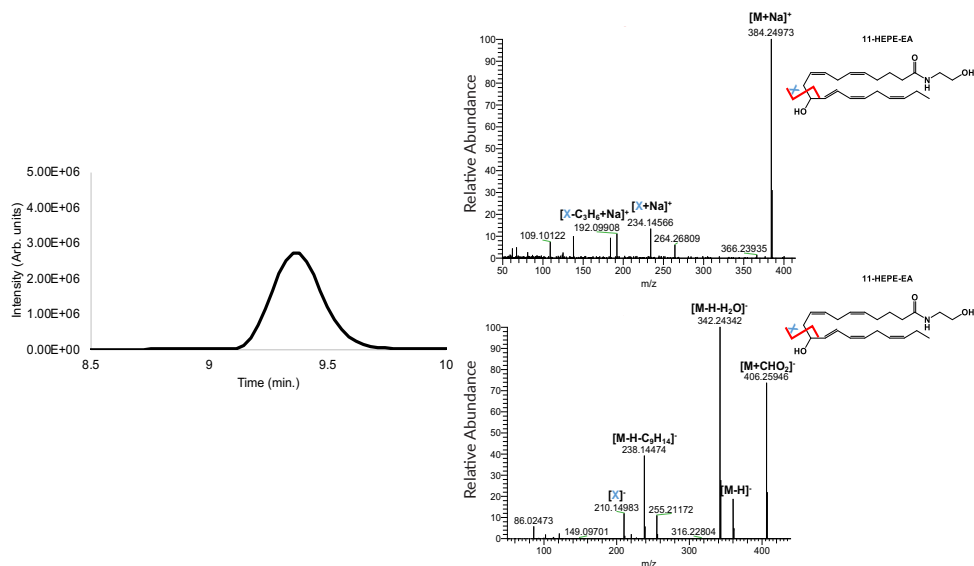


Figure 4-S8 Extracted ion chromatogram of $m/z = 344.25\text{--}344.27$ of the $[M+H-H_2O]^+$ ion of the chemically synthesized 11-HEPE-EA. Mass fragmentation spectra of both the $[M+Na]^+$ adduct ion using a collision energy of 30.0 eV (top), and the $[M+HCO_2]^+$ using a collision energy of 10.0 eV (bottom) are depicted.

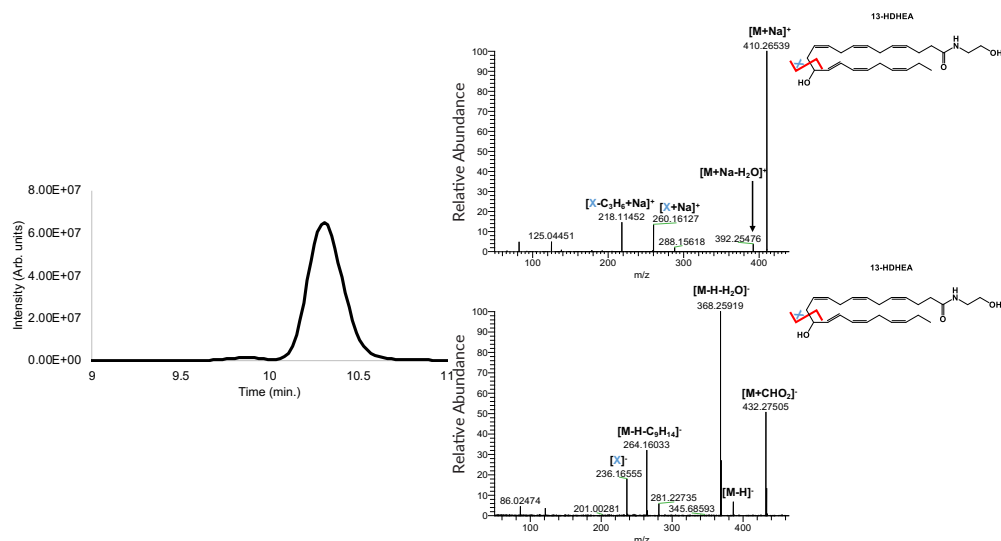


Figure 4-S9 Extracted ion chromatogram of $m/z = 370.26$ – 370.28 of the $[M+H-H_2O]^+$ ion of the chemically synthesized 13-HDHEA. Mass fragmentation spectra of both the $[M+Na]^+$ adduct ion using a collision energy of 30.0 eV (*top*), and the $[M+HCO_2]^-$ using a collision energy of 10.0 (*bottom*) are depicted.

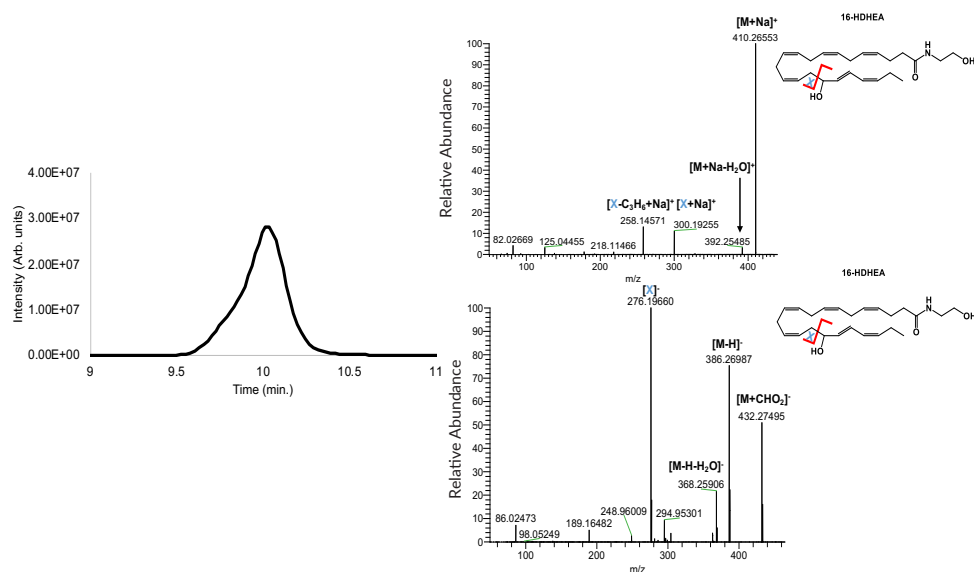


Figure 4-S10 Extracted ion chromatogram of $m/z = 370.26$ – 370.28 of the $[M+H-H_2O]^+$ ion of the chemically synthesized 16-HDHEA. Mass fragmentation spectra of both the $[M+Na]^+$ adduct ion using a collision energy of 30.0 eV (*top*), and the $[M+HCO_2]^-$ using a collision energy of 10.0 (*bottom*) are depicted.

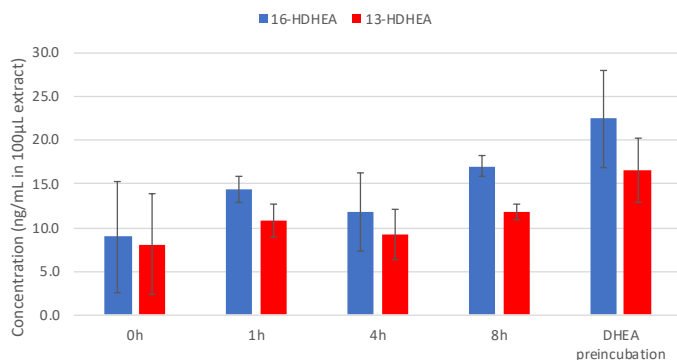


Figure 4-S11 Production of 13- and 16-HDHEA by RAW264.7 macrophages 24 h after incubation with 10 μ M DHEA. Stimulation was performed by adding 1.0 μ g/mL LPS 0 h, 1 h, 4 h or 8 h to the cells prior to the DHEA incubation, or 30 min after DHEA incubation for the DHEA pre-incubation experiment. Standard error bars obtained from biological duplicates.

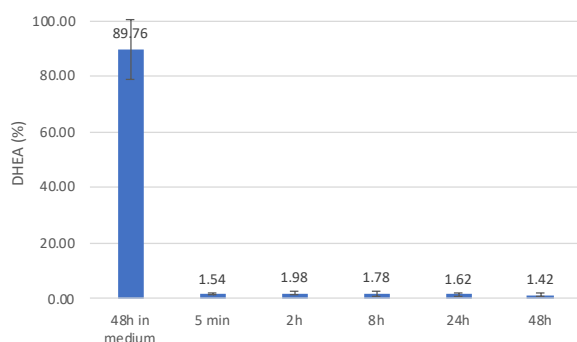


Figure 4-S12 Quantification of DHEA (in % relative to the 10 μ M DHEA that was added) in the RAW264.7 macrophage extracts at various time points. As control 10 μ M DHEA was incubated for 48 h in medium without cells. All the cells were incubated with 10 μ M DHEA 30 min. before stimulation with 1.0 μ g/mL LPS. Standard error bars obtained from biological duplicates.

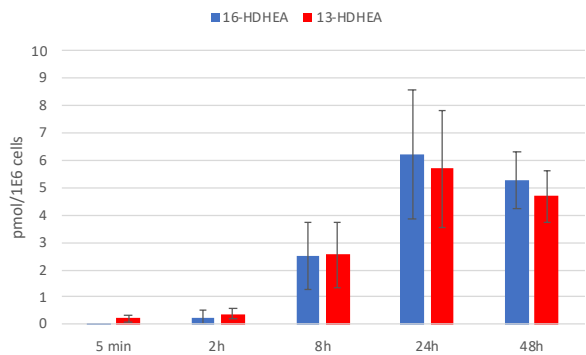


Figure 4-S13 Production of 13- and 16-HDHEA by RAW264.7 macrophages as function of time. The cells were incubated with 10 μ M DHEA 30 min before the stimulation with 1.0 μ g/mL LPS. 13- and 16- HDHEA were quantified at various times. Standard error bars obtained from biological duplicates.

Chapter 5

Immunomodulating effects of 13- and 16-hydroxylated docosahexaenoyl ethanolamide in LPS stimulated RAW264.7 macrophages

This chapter was adapted from:

Ian de Bus,
Sandra van Krimpen,
Guido J. Hooiveld,
Mark V. Boekschoten,
Mieke Poland,
Renger F. Witkamp,
Bauke Albada,
Michiel G.J. Balvers

Biochimica et Biophysica Acta (BBA) - Molecular and Cell Biology of Lipids, **2021**, 1866,
158908; doi: 10.1016/j.bbalip.2021.158908.

5.1 Abstract

Docosahexaenoyl ethanolamide (DHEA), the ethanolamine conjugate of the *n*-3 long chain polyunsaturated fatty acid docosahexaenoic acid, is endogenously present in human circulation and in tissues. Its immunomodulating properties have been (partly) attributed to an interaction with the cyclooxygenase-2 (COX-2) enzyme. We discovered recently that COX-2 converts DHEA into two oxygenated metabolites, 13- and 16-hydroxylated-DHEA (abbreviated as 13- and 16-HDHEA, respectively). It remained unclear whether these oxygenated metabolites also display immunomodulating properties as was known for their parent DHEA. In this study we investigated the immunomodulating properties of 13- and 16-HDHEA in lipopolysaccharide (LPS)-stimulated RAW264.7 macrophages. The compounds reduced production of tumor necrosis factor alpha (TNF α), interleukin (IL)-1 β and IL-1Ra, but did not affect nitric oxide (NO) and IL-6 release. Transcriptome analysis showed that the compounds inhibited LPS-mediated induction of pro-inflammatory genes (InhbA, Ifit1) and suggested potential inhibition of regulators such as toll-like receptor 4 (TLR4), MyD88, and interferon regulatory factor 3 (IRF3), whereas anti-inflammatory genes (SerpB2) and potential regulators IL-10, sirtuin 1 (Sirt-1), fluticasone propionate were induced. Additionally, transcriptome analysis of 13-HDHEA suggests a potential anti-angiogenic role. In contrast to known oxylipin-lowering effects of DHEA, liquid chromatography coupled to tandem mass spectrometry (LC-MS/MS) analyses revealed that 13- and 16-HDHEA did not affect oxylipin formation. Overall, the anti-inflammatory effects of 13-HDHEA and 16-HDHEA are less pronounced compared to their parent molecule DHEA. Therefore, we propose that COX-2 metabolism of DHEA acts as a regulatory mechanism to limit the anti-inflammatory properties of DHEA.

5.2 Introduction

Long chain *n*-3 polyunsaturated fatty acids (LC-PUFAs) are essential for neural development and functioning, and have been linked to certain beneficial health effects. For example, *n*-3 LC-PUFAs have been associated with neuroprotective and anti-depressant effects, improved endothelial functioning, lowered triglyceride levels, functional fetal and infant development, and proper cardiovascular and immune functioning.¹⁻³ Moreover, *n*-3 LC-PUFAs are described to inhibit propagation of many (chronic) inflammatory diseases like inflammatory bowel disease,⁴ cardiovascular disease,⁵⁻⁶ rheumatoid arthritis,⁷⁻⁹ and asthma.¹⁰ Notwithstanding this, the potential health effects of *n*-3 LC-PUFAs are continuously being challenged by new studies. Suggested explanations for these apparent discrepancies are differences in the level of intake or administered dose, and the study population.¹

One of the most studied *n*-3 LC-PUFAs is docosahexaenoic acid (DHA; C22:6-*n*3). DHA exerts immunomodulating effects through various mechanisms.¹ First, DHA can directly bind to receptors or key regulators of inflammatory processes,¹¹ such as peroxisome proliferator-activated receptor gamma (PPAR γ)¹² or the G-protein coupled receptor 120 (GPR120).¹³⁻¹⁴ Second, increased dietary DHA intake alters the cell membrane composition leading to a higher *n*-3 content. This change in membrane composition leads to a decreased production of pro-inflammatory *n*-6 oxylipins and increases the production of potent inflammation resolving *n*-3 oxylipins including resolvins, protectins, and maresins.^{1, 11, 15-19} Third, DHA is converted to the endocannabinoid-like structure docosahexaenoyl ethanolamide (DHEA) (**Figure 5-1**). DHEA is endogenously present in the circulation and tissues in humans and animals,^{15, 20-25} and its levels are generally increased after DHA intake, for example by consumption of *n*-3 fatty acid-containing products such as fatty fish or fish oil supplements.^{15, 20, 22, 26} Although the exact biosynthetic route of DHEA is yet to be determined, evidence suggests the involvement of *N*-acyl transferase and *N*-acyl phosphatidylethanolamine-specific phospholipase D (NAPE-PLD).²⁷⁻²⁸ Breakdown of DHEA is subsequently mediated by fatty acid amide hydrolase (FAAH) (**Figure 5-1**).²⁸ Importantly, DHEA is a potent inhibitor of inflammation in various models.^{1, 28-29} For example, DHEA inhibits neuroinflammation via interaction with the GPR110,^{28, 30} and reduces the production of inflammation markers like monocyte chemoattractant protein 1 (MCP-1), NO, IL-6, and prostaglandin E₂ (PGE₂) in LPS-stimulated RAW264.7 macrophages and 3T3-L1 adipocytes.^{1, 29, 31-33}

DHEA can be oxygenated to form DHEA derived metabolites with novel biological activities.^{1, 34} Previously, 15-lipoxygenase (15-LOX) was shown to metabolize DHEA into 17-hydroxydocosahexaenoyl ethanolamide (17-HDHEA), which is further metabolized

into 10,17-dihydroxydocosahexaenoyl ethanolamide (10,17-diHDHEA), 15-hydroxy-16(17)-epoxy-docosapentaenoyl ethanolamide (15-HEDPEA), and 13-HEDPEA. Of those metabolites, 10,17-diHDHEA and 15-HEDPEA prevented formation of platelet-leukocyte aggregates in human whole blood, and 15-HEDPEA possessed organ protecting roles in mouse reperfusion second organ injury.³⁵ CYP450-derived epoxide metabolites of DHEA were also shown to possess anti-inflammatory, anti-angiogenic, anti-migratory, and antitumorigenic properties.³⁶⁻³⁷ Collectively, these data underline that DHEA is not an end product of DHA and ethanolamine, but that its oxygenated metabolites possess a variety of immunomodulatory properties.

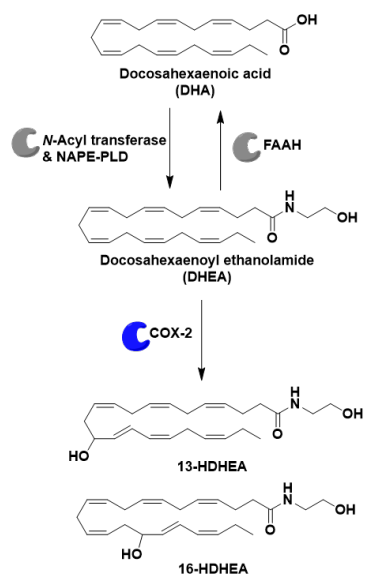


Figure 5-1 Overview of the COX-2 mediated synthesis of 13-HDHEA and 16-HDHEA from DHEA, including the suggested synthesis of DHEA from DHA involving *N*-acyl transferase and NAPE-PLD. Hydrolysis of DHEA to DHA is mediated by FAAH.

Recently, we showed that COX-2 also metabolizes DHEA (Chapter 4).³⁸ Using enzyme assays, we demonstrated that purified COX-2 converts DHEA into 13- and 16-HDHEA, and we confirmed its formation in 1.0 $\mu\text{g/mL}$ LPS-stimulated RAW264.7 macrophages (**Figure 5-1**).³⁸ Because of the observed immunomodulatory properties of the various oxygenated DHEA metabolites, it is tempting to speculate that 13- and 16-HDHEA also exert biological effects. To determine that this is indeed the case, we performed a series of studies to unravel the immunomodulating properties of 13- and 16-HDHEA in comparison to their parent DHEA. In the current work, we analyzed the biological effects of the compounds on the level of individual cytokines using ELISAs. Subsequently, we measured effects on mRNA expression levels in RAW264.7 macrophages using transcriptomic analysis. Finally, we screened the production of lipid mediators from several selected enzymes using targeted metabolomics with LC-MS/MS.

5.3 Materials and methods

5.3.1 Materials

DHEA ($\geq 98\%$), (\pm)13-HDHA ($\geq 98\%$), (\pm)16-HDHA ($\geq 98\%$), 5-HETE ($\geq 5\%$), 5-HETE- d_8 ($\geq 99\%$ deuterated forms (d_1 - d_8)), LTB₄ ($\geq 97\%$), LTC₄ ($\geq 97\%$), LTD₄ ($\geq 97\%$), LTD₄- d_5 ($\geq 99\%$ deuterated forms (d_1 - d_5)), PGE₂ ($\geq 98\%$), PGD₂ ($\geq 98\%$), PGE₂- d_4 ($\geq 99\%$ deuterated forms (d_1 - d_4)), DHA ($\geq 98\%$), and DHA- d_5 ($\geq 99\%$ deuterated forms (d_1 - d_5)) were purchased from Cayman Chemical (supplied by Sanbio B.V., Uden, NL). Isobutyl chloroformate ($\geq 98\%$) was purchased at Fisher Scientific (Landsmeer, NL). Absolute ethanol (EtOH) (for analysis, EMSURE®), ethanolamine ($\geq 99\%$), Distilled Et₃N ($\geq 99.5\%$), Lipopolysaccharides from Escherichia coli O111:B4 (L3024), and Triton X-100 were purchased from Sigma Aldrich (Zwijndrecht, NL). Chloroform- d (100.0 atom% D) was obtained from Janssen Chimica (Beerse, BE). Dichloromethane (DCM) for the synthetic procedure of the standards was purified using a Pure Solv 400 solvent purification system from Innovative Technology (Amesbury, USA). Acetonitrile (ACN) ($\geq 99.9\%$, HiPerSolv CHROMANORM® for LC-MS) was obtained from VWR Chemicals (Amsterdam, NL). Formic acid (FA) (99%, ULC/MS) was purchased from Biosolve B.V. (Valkenswaard, NL). Ultrapure water was filtered by a MilliQ integral 3 system from Millipore (Molsheim, FR). 1x PBS (pH 7.4), Dulbecco's Modified Eagle's Medium (DMEM) and penicillin and streptomycin were purchased from Corning (supplied by Fisher Scientific, Landsmeer, NL). Fetal calf serum (FCS) was obtained from Biowest (supplied by VWR International B.V., Amsterdam, NL), Probumin® BSA was purchased from Merck (Zwijndrecht, NL).

5.3.2 Synthesis of 13-HDHEA or 16-HDHEA

Synthesis of 13-HDHEA and 16-HDHEA was performed according to a previously reported method.³⁸ In short, 500 μ g of 13-HDHA or 16-HDHA dissolved in EtOH (1 eq., 1.45 μ mol) was evaporated to dryness using co-evaporation with DCM, and dissolved in 2 mL dry DCM under argon atmosphere. Then, 100 μ L of a freshly prepared solution of 282 μ L Et₃N in 10 mL dry DCM was added (14 eq., 20.3 μ mol), followed by the addition of 100 μ L of a freshly prepared solution of 226 μ L isobutyl chloroformate in 10 mL dry DCM (12 eq., 17.4 μ mol). The solutions were stirred at room temperature for 1 h under argon atmosphere to form the mixed anhydrides, before the reaction was cooled on ice. To the mixed anhydrides, 100 μ L of a freshly prepared solution of 223 μ L Et₃N (11 eq., 16.0 μ mol) and 96 μ L ethanolamine (11 eq., 16.0 μ mol) in 10 mL dry DCM was added. The reactions were stirred on ice overnight. The next day, the reaction mixtures were evaporated and dissolved in 500 μ L water:ACN (30:70) to purify the product by preparative high pressure reversed phase liquid chromatography (HPLC) (*vide infra*). After purification, 169 μ g of 13-HDHEA and 151 μ g of 16-HDHEA were obtained, which equals an isolated yield of 30% and 27%, respectively. NMR spectra and LC-HRMS chromatograms of the

obtained compounds are provided in the Supporting Information of the original article (available at doi: 10.1016/j.bbalip.2021.158908).

5.3.3 Preparative HPLC

13-HDHEA and 16-HDHEA were purified on a Zorbax Eclipse XDB-C18 column (9.4 × 250 mm, 5 μ) from Agilent Technologies B.V. (Amstelveen, NL). The purification was performed using an isocratic run of 30:70 water:ACN containing 0.1% FA with a flow rate of 4 mL/min. The purified compounds were evaporated to dryness using a rotary evaporator and subsequent freeze drying. The samples were dissolved in absolute EtOH for quantification and use in cell culture experiments.

5.3.4 HPLC quantification

Subsequent quantification of the HDHEA compounds was based on the UV absorption at 240 nm, caused by the conjugated diene structure in the oxidized PUFAs and their ethanolamine derived product; the UV-absorption of DHEA indicated that the amide structure of the endocannabinoid does not contribute to the 240 nm absorption. Calibration curves of 13-HDHA and 16-HDHA were injected in concentrations ranging from 0–100 μg/mL in duplicate, using 10 μL per injection. The chromatography was performed on a Zorbax Eclipse XDB-C18 column (4.6 × 250 mm, 5 μ) from Agilent Technologies B.V. (Amstelveen, NL), using an isocratic run of 30:70 water:ACN containing 0.1% FA with a flow rate of 1 mL/min.

5.3.5 Cell incubations

RAW264.7 macrophages (American Type Culture Collection, Teddington, UK) were cultured in DMEM containing 10% fetal calf serum (FCS) and 1% penicillin and streptomycin (P/S) at 37 °C in a 5% CO₂ humidified incubator. For the incubations 2 mL of 250.000 cells/mL were seeded in 6-wells plates. After 24 h, the medium of the adherent cells was discarded and replaced by fresh medium containing vehicle (0.1% EtOH), DHEA, 13-HDHEA, 16-HDHEA or a combination of 13-HDHEA and 16-HDHEA. During the incubations, the final concentration of EtOH was preserved at 0.1% in DMEM. After 30 min pre-incubation with the compounds, the macrophages were stimulated with 1.0 μg/mL LPS. This was achieved by adding 20 μL of 100 μg/mL LPS (10% PBS in medium) to the cells. Control incubations without LPS were supplied with 20 μL 10% PBS in medium. After 24 h, the medium of the adherent cells was used for biological assays immediately or stored at –80 °C. The cells were lysed using RLT buffer from Qiagen Benelux B.V. (Venlo, NL) to extract the RNA from the macrophages (*vide intra*), which was stored at –80 °C. Experiments were performed three times using technical duplicates.

5.3.6 Cell Cytotoxicity

To evaluate the cytotoxicity of the added compounds an LDH cytotoxicity Kit from Roche (Woerden, NL) was used to measure extracellular lactate dehydrogenase. The LDH assay was measured immediately after collection of the sample medium. In short, 50 μ L of a reagent solution (1:45 LDH reagent 1:LDH reagent 2) was mixed with 50 μ L of sample medium. The plate was then incubated at room temperature until the positive control (cells treated with 1% Triton X-100) colored dark red. The reaction was quenched with 25 μ L of 1.0 M HCl before the absorbance was read with a plate reader at 492 nm.

5.3.7 Determination of NO concentration

Production of NO in LPS-stimulated macrophages was measured using a Griess assay from Cayman Chemical (supplied by Sanbio B.V., Uden, NL). The assay was performed directly after collection of the medium by adding 50 μ L of Griess Reagent 1 and 50 μ L Griess Reagent 2 to 100 μ L of the medium. The samples were mixed at room temperature until the color developed. The samples were compared to a nitrite standard ranging from 0–35 μ M, after blank subtraction. The samples were measured on an ELISA plate reader at 540 nm.

5.3.8 Determination of cytokine concentrations

Concentrations of excreted IL-6, IL-1 β , IL-1Ra, and TNF α in the sample medium of the 24 h treated macrophages were determined by the appropriate ELISA assays [*i.e.*, a mouse IL-6 DuoSet ELISA, mouse IL-1ra/IL-1F3 DuoSet ELISA, mouse IL-1 beta/IL-1F2 DuoSet ELISA, and mouse TNF-alpha DuoSet ELISA were purchased from R&D systems (Abingdon, UK)] according to the description of the manufacturer. IL-1 β concentration was determined in undiluted medium samples; IL-1Ra was determined in 10 \times diluted medium samples; TNF α and IL-6 concentrations were determined in 100 \times diluted medium samples.

5.3.9 Transcriptome analysis

Cellular incubations with the synthesized compounds were performed three times containing technical duplicates. RNA from the technical duplicates were pooled for each separate experiment, thereby obtaining a single RNA sample from each condition for each of the three independent experiments. For the transcriptome analyses we used RNA from 1.0 μ g/mL LPS-stimulated RAW264.7 macrophages that were pre-incubated for 30 mins with vehicle (0.1% EtOH), 5.0 μ M 13-HDHEA, 5.0 μ M 16-HDHEA, or a mixture containing 2.5 μ M 13-HDHEA and 2.5 μ M 16-HDHEA.

RNA from the lysed macrophages was purified according to the description of the manufacturer using a RNeasy[®] Micro kit from Qiagen Benelux B.V. (Venlo, NL). After

purification on the columns, RNA was eluted using 20 μ L of RNase free water. RNA concentration was determined using nanodrop, and RNA quality was assessed using RNA 6000 nanochips on the Agilent 2100 bioanalyzer from Agilent Technologies B.V (Amstelveen, NL). All RNA exceeded an RNA integrity number (RIN) of 9.5. Per sample, 100 ng of purified total RNA was labelled with the Whole-Transcript Sense Target Assay kit from Affymetrix (Life Technologies, Bleiswijk, NL, P/N 902281), which was hybridized to an Affymetrix GeneChip Mouse Gene 2.1 ST arrays (Life Technologies, Bleiswijk, NL). Hybridization, washing, and scanning of the peg arrays were carried out on an Affymetrix GeneTitan instrument according to the recommendations of the manufacturer.

Microarray quality control and data analysis pipeline have been described in detail previously.³⁹ Briefly, normalized expression estimates of probe sets were computed by the robust multiarray analysis (RMA) algorithm⁴⁰ as implemented in the Bioconductor library *oligo*.⁴¹ Probe sets were redefined using current genome information according to Dai *et al.*⁴² based on annotations provided by the Entrez Gene database, which resulted in the profiling of 27381 unique genes (custom CDF v24). Differentially expressed probe sets (genes) compared to the vehicle control were identified by using linear models (library *limma*) and an intensity-based moderated t-statistic.⁴³⁻⁴⁵ The heterogeneity in gene expression profiles that was observed in PCA plots was taken into account by fitting a heteroskedastic model that included relative quality weights that were computed for each sample per experimental group.⁴⁶⁻⁴⁷ Probe sets that satisfied the criterion of moderated P-value <0.01, and average gene expressions (average log2 expression >3.5) were considered to be significantly regulated (**Table 5-S1**). The microarray data set has been submitted to the Gene Expression Omnibus (accession number GSE160086).

5.3.10 IPA® analysis

Functional and Upstream Regulator analysis was performed using Ingenuity Pathway Analysis (IPA®) (<http://www.ingenuity.com/science/knowledgebase>) from Qiagen Benelux B.V. (Venlo, NL) in July 2020. The Ingenuity Knowledge Base is a knowledge repository that houses the biological and chemical relationships extracted from the scientific literature, and this information was used to analyze the effects between transcriptional regulators (from transcription factor, to micro-RNA, kinase, compound or drug, that affects the expression of other molecules) and their target genes. IPA® examines the number of known gene targets for each transcription regulator that is present in the data set, and compares both direction and change (*i.e.*, expression of a gene in the 13- and 16-HDHEA treatment compared to the vehicle) to stored pathways extracted from literature (<http://pages.ingenuity.com/IngenuityUpstreamRegulatorAnalysisWhitepaper.html>). Using this prediction tool, potential upstream regulators and potential cellular processes that may have been affected by 13- and 16-HDHEA are identified.

Differentially expressed genes between vehicle treated LPS-stimulated macrophages and the various HDHEA compounds (*i.e.*, 5.0 μ M 13-HDHEA, 5.0 μ M 16-HDHEA, 2.5 μ M 13-HDHEA and 2.5 μ M 16-HDHEA combined) treated LPS-stimulated macrophages were included in the input of the IPA® analysis. In the output the upstream transcriptional regulators were scored using an activation Z-score. Cut-off values for the activation Z-score are 2.0 for induced upstream regulators or -2.0 for inhibited upstream regulators. Similarly, Z-score cut-offs of 2.0 and -2.0 were used in diseases and functions analysis. Moderated P values give significance of the observed regulator pathways and functions. In the results only significant ($P < 0.01$) pathways and functions are displayed.

5.3.11 LC-MS/MS quantification of oxylipins and PUFAs

LC-MS/MS-based quantification of various eicosanoids and PUFAs was performed by extracting 187.5 μ L sample medium with 1.5 mL MeOH containing 1.33 ng/mL of the internal standards PGE₂-*d*₄, 5-HETE-*d*₈, LTD₄-*d*₅, DHA-*d*₅ on ice for 30 min. The samples were centrifuged at 4 °C at 14000 rpm, after which the supernatant was diluted with 6 mL ultrapure water containing 0.1% formic acid (FA). The samples were purified over HLB oasis SPE columns from Waters Chromatography B.V. (Breda, NL). The columns were activated using 2 mL of MeOH, and equilibrated using 2 mL ultrapure water containing 0.1% FA. Subsequently, the samples were loaded, after which the columns were washed using 2 mL 20% MeOH in ultrapure water containing 0.1% FA. The columns were dried for 15 min and the oxylipins and PUFAs were eluted using 1 mL MeOH. The eluates were collected in borosilicate glass vials containing 20 μ L of 500 μ M butylated hydroxytoluene and 10% glycerol in EtOH to prevent oxidation of the oxylipins and to allow for proper evaporation on a Turbopap evaporator (Biotage; Uppsala, SE). The samples were dissolved in 100 μ L of absolute EtOH, after which 6 μ L of the samples were injected on an ultra-high pressure liquid chromatography (UPLC) coupled to a TQS mass spectrometer from Waters Chromatography B.V. (Breda, NL). The MS settings were optimized and measured in the negative ionization mode using 2.5 kV capillary voltage, 40 V cone voltage, source offset 20, 600 °C desolvation temperature. The chromatographic separation was accomplished on a Zorbax Eclipse Plus C18 column 2.1 \times 150 mm, 1.8 μ from Agilent Technologies B.V. (Amstelveen, NL) using gradient elution with solvent A containing 5% ACN in ultrapure water with 0.1% FA, and solvent B containing 100% ACN with 0.1% FA. The gradient started by applying 5% B in A followed by a linear increase to 30% B, which was achieved after 5 min. This was followed by a linear increase towards 50% B, which was achieved at min 11.25 and maintained until min 13.25. The system was subsequently switched to 100% B which was achieved at min 15.75 and maintained until min 18.75, after which the system was equilibrated at 5% B until min 22. The mass fragmentation settings were optimized per compound (**Table 5-1**). Peak identification and quantification were performed using

TargetLynx version 4.1 software from Waters Chromatography B.V. (Breda, NL). Quality control samples were included to check the quality of the analysis.

Table 5-1 Overview of the parent and fragment ions, including their collision energy, that were used in the LC-MS/MS quantification of the PUFAs and oxylipins.

Molecule	Parent ion (m/z)	Fragment ion (m/z)	Collision energy (eV)
DHA	327.2	229.2	15
DHA- <i>d</i> ₅	332.2	288.2	15
5-HETE	319.2	115.0	15
5-HETE- <i>d</i> ₈	327.1	116.0	15
LTB ₄	335.1	195.0	15
LTC ₄	623.8	271.8	15
LTD ₄	494.9	176.8	15
LTD ₄ - <i>d</i> ₅	499.9	176.8	15
PGD ₂	351.1	271.1	15
PGE ₂	351.1	271.1	15
PGE ₂ - <i>d</i> ₄	355.1	275.1	15

5.3.12 Statistical analyses

Experiments were performed three times containing two technical replicates. Data is expressed as average percentage relative to 1.0 µg/mL LPS treated vehicle control (set as 100%) containing standard deviation or standard error of the mean. Statistical analysis was performed using a non-parametric one-way ANOVA followed by a Dunnet's *t*-test. P-values assigned as statistically relevant are classified as P<0.05, P<0.01, P<0.001. Statistical differences between treatments were shown if an effect was found on 13- and 16-HDHEA (non-parametric one-way ANOVA followed by a Tukey multiple comparison test, *post hoc*).

5.4 Results

5.4.1 Cytotoxicity of test compounds

Cytotoxicity of DHEA, 13-HDHEA and 16-HDHEA was evaluated by measuring the LDH release from 1.0 µg/mL LPS-stimulated and incubated RAW264.7 macrophages. Macrophages were incubated for 24.5h with 2.5 µM and 5.0 µM of the test compounds, or a combination of 2.5 µM 13-HDHEA and 2.5 µM 16-HDHEA. Neither the individual compounds nor the combination showed a significant cytotoxic effect on the macrophages when compared to the vehicle control with 1.0 µg/mL LPS stimulation (**Figure 5-S1**).

5.4.2 13- and 16-HDHEA do not reduce LPS induced NO and IL-6 release

The effects of 13- and 16-HDHEA and DHEA on the release of the inflammatory mediators nitric oxide (NO) and IL-6 were investigated using LPS-stimulated RAW264.7 macrophages. No significant effect was observed for 13-HDHEA and 16-HDHEA on NO release after 24.5h, whereas the parent compound DHEA caused a small but significant inhibition for NO (**Figure 5-2A**). Statistical testing showed that DHEA treatment significantly reduced NO release ($71 \pm 6 \%$ at $2.5 \mu\text{M}$ DHEA ($P < 0.05$); $66 \pm 18 \%$ at $5 \mu\text{M}$ DHEA ($P < 0.05$)).

Similarly, 13-HDHEA and 16-HDHEA did not affect IL-6 production (**Figure 5-2B**). DHEA again showed a significant reduction of IL-6 production, although the levels of $2.5 \mu\text{M}$ and $5 \mu\text{M}$ were the same (*i.e.*, to $75 \pm 6 \%$ at $2.5 \mu\text{M}$ DHEA ($P < 0.01$); and to $77 \pm 11 \%$ at $5 \mu\text{M}$ DHEA ($P < 0.05$)).

5.4.3 13-HDHEA reduces LPS induced production of TNF α and IL-1 β

Incubation of LPS-stimulated cells with $5 \mu\text{M}$ 13-HDHEA resulted in lower TNF α concentrations ($83 \pm 7 \%$ ($P < 0.05$)) compared to the vehicle (**Figure 5-2C**). Incubations with DHEA also caused significant reduction of TNF α production (to $82 \pm 4 \%$ at $2.5 \mu\text{M}$ DHEA ($P < 0.001$); and to $88 \pm 2 \%$ at $5 \mu\text{M}$ DHEA ($P < 0.01$)). Statistical analysis using Tukey's multiple comparison test showed no additional significant differences between the various treatments.

Incubation of LPS-stimulated cells with $5 \mu\text{M}$ 13-HDHEA also significantly reduced IL-1 β cytokine concentrations (to $78 \pm 6 \%$ ($P < 0.05$)) compared to the vehicle (**Figure 5-2D**). In addition, IL-1 β concentration was reduced by the incubation with the mixture of $2.5 \mu\text{M}$ 13-HDHEA and $2.5 \mu\text{M}$ 16-HDHEA (to $80 \pm 8 \%$ ($P < 0.05$)). DHEA also reduced IL-1 β cytokine levels (*i.e.*, to $71 \pm 2 \%$ at $2.5 \mu\text{M}$ DHEA ($P < 0.001$); $59 \pm 9 \%$ at $5 \mu\text{M}$ DHEA ($P < 0.001$)). Statistical analysis using Tukey's multiple comparison test indicated that $5 \mu\text{M}$ DHEA treatment was significantly more effective in reducing IL-1 β compared to $2.5 \mu\text{M}$ 13-HDHEA and 16-HDHEA ($P < 0.05$), but not compared to $5 \mu\text{M}$ 13-HDHEA.

5.4.4 13- and 16-HDHEA reduce LPS induced production of IL-1Ra

Incubation of LPS-stimulated cells with 13-HDHEA and 16-HDHEA displayed inhibiting trends on IL-1Ra production (**Figure 5-2E**). Reduced IL-1Ra production was established when the macrophages were incubated with the mixture of $2.5 \mu\text{M}$ 13-HDHEA and $2.5 \mu\text{M}$ 16-HDHEA (to $66 \pm 9 \%$ ($P < 0.001$)), or with only $5 \mu\text{M}$ 16-HDHEA (to $70 \pm 7 \%$ ($P < 0.01$)). Interestingly, incubations with only 13-HDHEA or DHEA did not result in a significant reduction of IL-1Ra. Statistical analysis using Tukey's multiple comparison test showed no additional significant differences between the various tests.

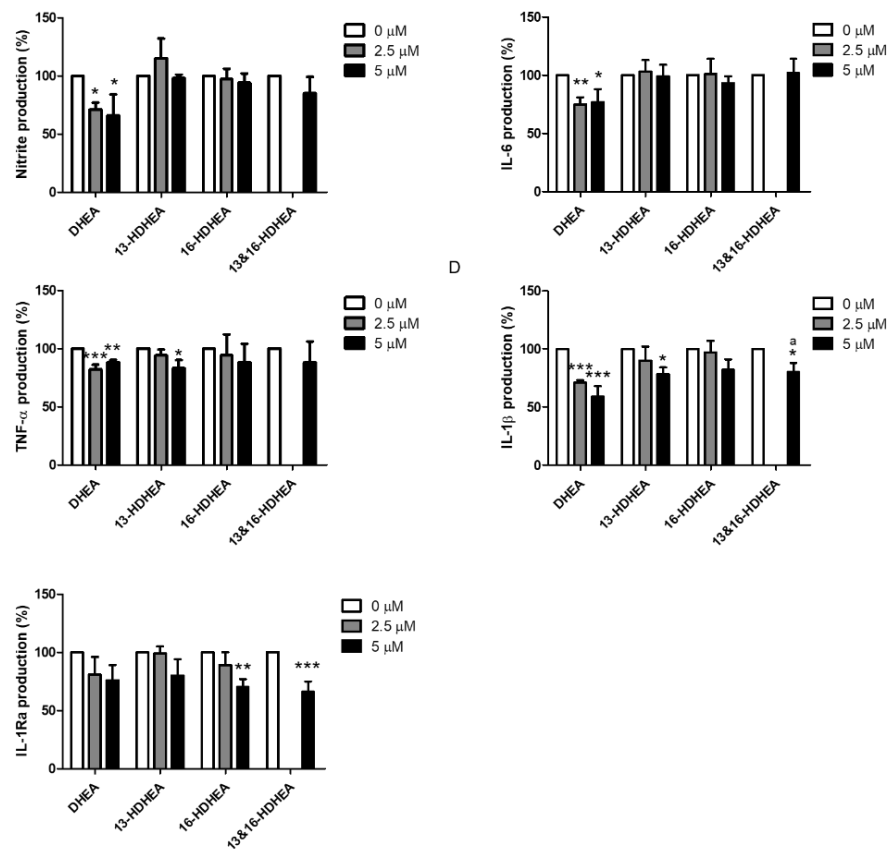


Figure 5-2 Production of NO (a), IL-6 (b), TNF α (c), IL-1 β (d), and IL-1Ra (e) released from 1.0 μ g/mL LPS-stimulated RAW264.7 macrophages, incubated with 2.5 μ M or 5 μ M DHEA, 13-HDHEA, 16-HDHEA and a combined exposure to 2.5 μ M 13-HDHEA and 2.5 μ M 16-HDHEA. Cells were pre-treated with the compounds for 30 min before 1.0 μ g/mL LPS addition and incubation of 24 h. Data are expressed as % relative to the vehicle control with 1.0 μ g/mL LPS (=100%). Bars represent averages with SD from n=3 independent experiments containing technical duplicates. Asterisks indicate significant differences from the vehicle with 1.0 μ g/mL LPS control (one-way ANOVA, Dunnett's *t*-test *post hoc*; * P <0.05, ** P <0.01, *** P <0.001). Statistical testing showed significant effects compared to 5 μ M DHEA treatment (a) (one-way ANOVA, Tukey multiple comparison test *post hoc*; P <0.05).

5.4.5 13- and 16-HDHEA reduce expression of *Inhba* and *Ifit1*, and induce expression of *Serpina2*, *Ptgs1*, *Alox5* and *Ppib*

Because 13-HDHEA and 16-HDHEA showed relatively moderate effects on the production and release of inflammatory mediators NO, IL-6, IL-1Ra, IL-1 β , and TNF- α in LPS-stimulated macrophages, it was decided to continue exploring the effects of

13- and 16-HDHEA by investigating the effects on full gene expression profiles of LPS-stimulated RAW264.7 macrophages. For transcriptome analysis, incubations with 5 μ M 13-HDHEA, 5 μ M 16-HDHEA, and the mixture of 2.5 μ M 13-HDHEA and 2.5 μ M 16-HDHEA were compared to the vehicle control. Transcriptome analysis revealed 203 differentially expressed genes for exposure to 13-HDHEA, 120 differentially expressed genes for incubation with 16-HDHEA, and 165 differentially expressed genes for the combined 13-HDHEA and 16-HDHEA exposure (**Table 5-S1**). For 13-HDHEA exposure the ribosomal protein L23A (Rpl23a) gene was most strongly induced, and the predicted gene 15754 (Gm15754) was most strongly reduced. For 16-HDHEA strongest induction was obtained for melanoma antigen, family A, 2 (Magea2), and highest reduction was obtained for gasdermin C-like 2 (Gsdmcl2). Combined incubation with 13- and 16-HDHEA resulted in strongest induction of the predicted gene 7665 (Gm7665), and highest reduction of an unannotated gene. Twenty of the differentially expressed genes were shared among the various incubations with HDHEA (**Figure 5-3, Table 5-2**). Among these genes, pro-platelet basic protein (Pbbp) was most strongly induced by 13-HDHEA, whereas GM4924 was most strongly induced by 16-HDHEA. Interestingly, the inflammatory resolution related gene serine peptidase inhibitor, clade B, member 2 (Serpina2) was significantly induced by HDHEA exposure.⁴⁸ Next to the induction of resolution related genes, inhibition of the inflammatory regulating genes interferon-induced protein with tetratricopeptide repeats 1 (Ifit1) and inhibin beta-A (Inhba) was observed.⁴⁹⁻⁵⁰ Finally, the oxylipin regulating genes prostaglandin-endoperoxide synthase 1 (Ptgs1) and arachidonate 5-lipoxygenase (Alox5) were also found to be induced in all conditions tested.

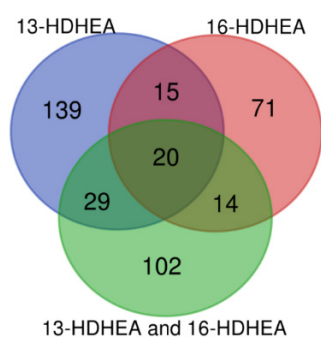


Figure 5-3 Venn diagram showing overlap of significantly expressed genes ($P < 0.01$ and average \log_2 expression value > 3.5) of the 1.0 μ g/mL LPS-stimulated RAW264.7 macrophages, incubated with 5 μ M 13-HDHEA (blue), 5 μ M 16-HDHEA (red), and a combinatorial 2.5 μ M 13-HDHEA and 2.5 μ M 16-HDHEA incubation (green). Cells were incubated for 24 h, and pre-treated with the compounds 30 min before LPS addition. Experiments were performed three times individually with pooled technical duplicates.

The Venn diagram was drawn using the free online Venn diagram drawing tool (<http://bioinformatics.psb.ugent.be/webtools/Venn/>).

Gene Symbol	13-HDHEA vs Vehicle	16-HDHEA vs Vehicle	13- & 16-HDHEA vs Vehicle	Average Expr	Gene Name
Plin2	1.285	1.179	1.242	1796.082	perilipin 2
1110008P14Rik	1.140	1.174	1.138	955.671	RIKEN cDNA 1110008P14 gene
Csf2rb	1.237	1.254	1.243	768.796	colony stimulating factor 2 receptor, beta, low-affinity (granulocyte-macrophage)
Pf4	1.188	1.216	1.187	775.378	platelet factor 4
Smox	1.259	1.242	1.236	452.344	spermine oxidase
Serpinb2	1.276	1.346	1.333	287.437	serine (or cysteine) peptidase inhibitor, clade B, member 2
Lsm3	1.261	1.210	1.224	201.941	LSM3 homolog, U6 small nuclear RNA and mRNA degradation associated
Fcgr3	1.315	1.272	1.269	155.375	Fc receptor, IgG, low affinity III
C130050O18Rik	1.479	1.247	1.239	150.907	RIKEN cDNA C130050O18 gene
Ptgs1	1.314	1.246	1.289	104.593	prostaglandin-endoperoxide synthase 1
Frrmd6	1.267	1.295	1.337	90.337	FERM domain containing 6
Alox5	1.416	1.302	1.425	76.133	arachidonate 5-lipoxygenase
Mir466f-4	1.320	1.344	1.274	86.522	microRNA 466f-4
Mir3075	1.694	1.605	1.551	27.848	microRNA 3075
Gm4924	1.475	1.716	1.515	13.016	predicted gene 4924
Ppbbp	2.069	1.399	1.621	12.278	pro-platelet basic protein
Selenos	-1.149	-1.143	-1.155	412.811	selenoprotein S
Ifit1	-1.358	-1.215	-1.346	376.919	interferon-induced protein with tetratricopeptide repeats 1
Clcn7	-1.157	-1.166	-1.210	375.762	chloride channel, voltage-sensitive 7
Inhba	-1.353	-1.314	-1.428	86.121	inhibin beta-A

Table 5-2 Fold change of significantly induced/reduced genes ($P < 0.01$) between the vehicle exposed LPS-stimulated macrophages and the 5 μM 13-HDHEA, 5 μM 16-HDHEA, and the mixture of 2.5 μM 13-HDHEA and 2.5 μM 16-HDHEA exposed LPS-stimulated macrophages after 24 h incubation. Inhibited genes are displayed in green, induced genes in red (average log2 expression value > 3.5 ; Average Expr > 11.314). LPS stimulation was performed using 1.0 $\mu\text{g/mL}$ LPS 30 min after pre-treatment of the compounds. Data is obtained from three independent pooled technical duplicates.

5.4.6 Upstream regulator pathway analysis reveals an anti-inflammatory signature for 13- and 16-HDHEA

To investigate whether the observed changes in gene expression showed a consistent pattern or relation with known regulators and pathways, Ingenuity Pathway Analysis (IPA[®]) was performed (July, 2020). Identified upstream regulators clearly show an anti-inflammatory signature (**Figure 5-4**). Many of the upstream regulators were classified by IPA[®] as potentially inhibited, like TLR4, MyD88, IRF3, IRF7, STAT1, and several IFNs are involved in LPS signaling through TLR4.⁵¹⁻⁵² Potentially induced regulators like IL-10RA, SIRT-1, and that of the anti-inflammatory drug fluticasone propionate are generally involved in anti-inflammatory processes.⁵³⁻⁵⁵ Analysis of stimulated macrophages incubated with 16-HDHEA at 5 μM did not reveal any significantly affected upstream regulators.

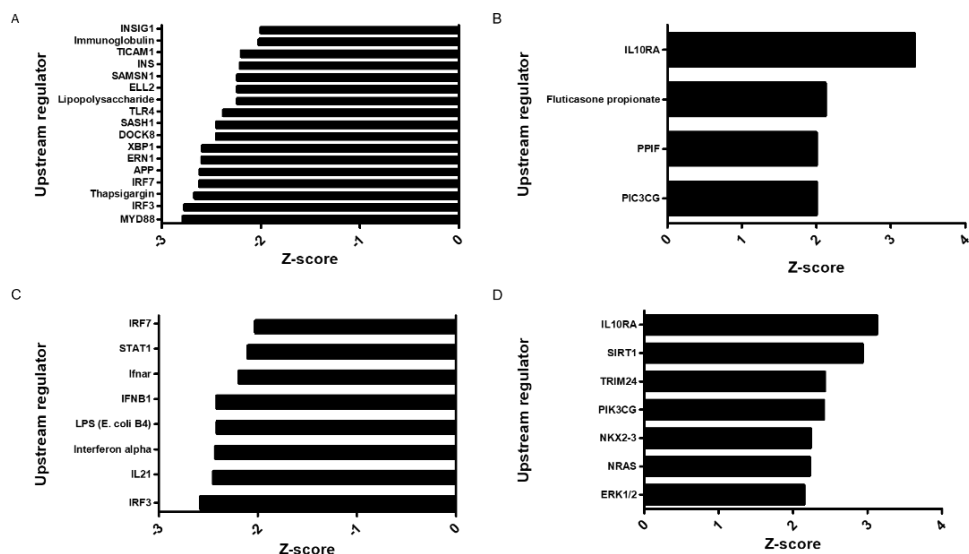


Figure 5-4 Activation Z-scores of affected upstream regulators of 5 μ M 13-HDHEA treated (a and b) and 2.5 μ M 13-HDHEA and 2.5 μ M 16-HDHEA combined treatment (c and d) in 1.0 μ g/mL LPS-stimulated RAW264.7 macrophages. Upstream regulators shown have a Z-score < -2.0 (a and c) or Z-score > 2.0 (b and d), and are significant compared to the vehicle control ($P < 0.01$).

Functional IPA® analysis was performed in order to link the alterations in expression to physiological processes with similar changes. This approach generates hypotheses concerning the functional consequences of the observed changes in gene expression. The functional IPA® analyses suggested that 5 μ M 13-HDHEA changed the expression of gene sets associated with a decrease in angiogenesis, apoptosis of prostate cancer cells, and the development of epithelial tissue (**Figure 5-5A**). Subsequently, gene sets associated with cell movement, adhesion of immune cells, degeneration of connective tissue, and production of radical oxygen species (ROS) for 5 μ M 13-HDHEA were identified as potentially induced (**Figure 5-5B**). Incubation with 5 μ M 16-HDHEA also resulted in regulation of gene sets associated with an increase in cell movement of phagocytes and adhesion of immune cells (**Figure 5-5C**). The combined incubation with 2.5 μ M 13-HDHEA and 2.5 μ M 16-HDHEA only pointed to potential increased inflammatory functions (**Figure 5-5D**).

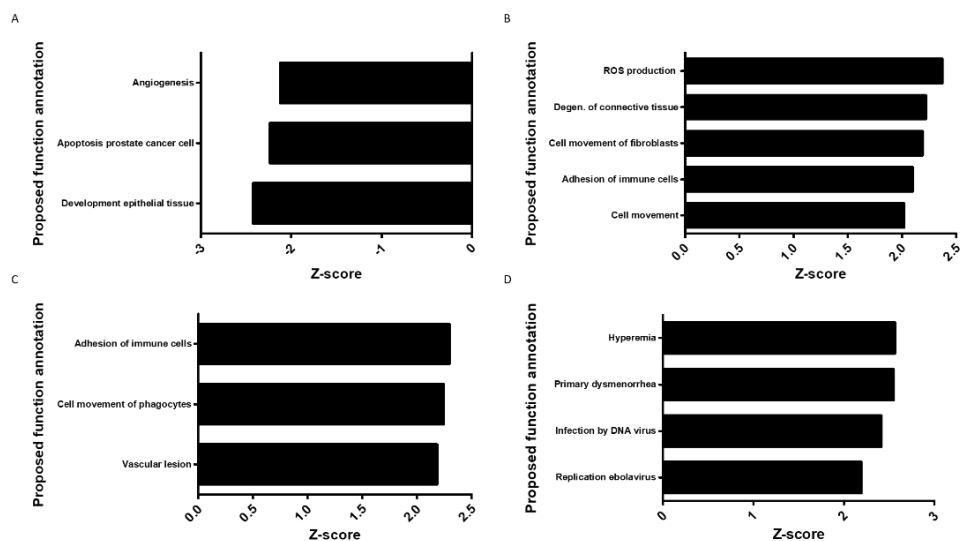


Figure 5-5 Activation Z-scores of disease and function annotations of 5 μM 13-HDHEA treated (a and b), 5 μM 16-HDHEA (c), and 2.5 μM 13-HDHEA and 2.5 μM 16-HDHEA combined treatment (d) of 1.0 $\mu\text{g}/\text{mL}$ LPS-stimulated RAW264.7 macrophages. Inhibited diseases and functions have a Z-score < -2.0 (a), and induced diseases and functions have a Z-score > 2.0 (b-d). All diseases and functions are significantly affected compared to the vehicle control ($P < 0.01$).

5.4.7 13- and 16-HDHEA do not affect oxylipin profiles

Giving the inducing effects of 13-HDHEA and 16-HDHEA on the expression of the lipid metabolizing genes *Ptgs1*, *Alox5* (Table 5-2), and the inducing effect of 13-HDHEA on leukotriene synthase C4 (*Ltc4s*) (Table 5-S1), we continued with lipidomic analyses to further validate the consequences of the altered gene expression levels of these lipoxygenases. To this end, a targeted LC-MS/MS method was developed to detect 5-HETE and LTB_4 as *Alox5* products, LTC_4 and LTD_4 as products of *Ltsc4*, PGE_2 and PGD_2 as *Ptgs1* (also known as COX-1) and *Ptgs2* (also known as COX-2) products, and DHA as DHEA precursor in LPS-stimulated macrophages. PGE_2 excretion was significantly inhibited by DHEA (to $38 \pm 6\%$ at 2.5 μM ($P < 0.001$); and to $21 \pm 10\%$ at 5 μM DHEA ($P < 0.001$)) (Figure 5-6A). With 13-HDHEA and 16-HDHEA exposed cells no significant inhibition of the LPS induced PGE_2 production was obtained. Similarly, PGD_2 excretion was significantly reduced DHEA (to $40 \pm 6\%$ at 2.5 μM ($P < 0.001$); and to $26 \pm 10\%$ at 5 μM DHEA ($P < 0.001$)) (Figure 5-6B), and both 13-HDHEA and 16-HDHEA did not cause a reduction of PGD_2 production. For the combination of 2.5 μM 13- and 16-HDHEA even a small but significant induction of PGD_2 production was obtained. DHA levels were found to be significantly decreased by 13-HDHEA (to $69 \pm 26\%$ at 2.5 μM ($P < 0.05$); and to $70 \pm 14\%$ at 5 μM ($P < 0.05$)), by 5 μM 16-HDHEA (to $64 \pm 34\%$ ($P < 0.05$)), and by the combination

of 2.5 μM 13- and 16-HDHEA (to $73 \pm 32\%$ ($P < 0.05$)). In contrast to a reduction of DHA formation after incubation with HDHEA, DHEA seemed to give an increasing trend on the DHA levels (**Figure 5-6C**). Statistical testing using a one-way ANOVA multiple comparisons test using Tukey's statistics indicated a significant difference in DHA levels between 5 μM DHEA and 5 μM 16-HDHEA ($P < 0.001$), 5 μM 13-HDHEA ($P < 0.01$), and the combination of 2.5 μM 13-HDHEA and 16-HDHEA ($P < 0.01$). Levels of 5-HETE, LTB_4 , LTC_4 , and LTD_4 could not be quantified, because the concentrations were below the LOD.

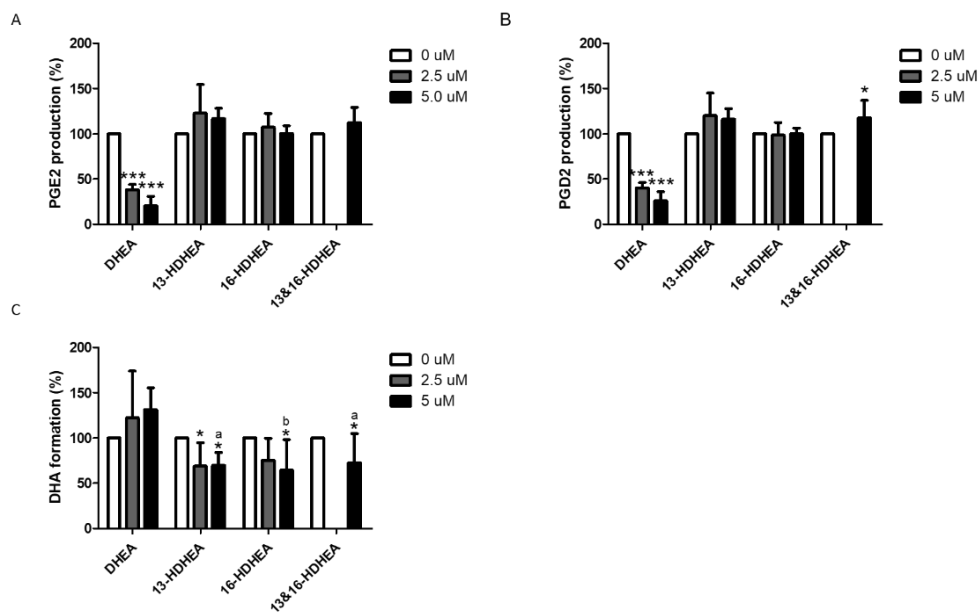


Figure 5-6 Release of PGE₂ (a), PGD₂ (b), and DHA (c) from 1.0 $\mu\text{g/mL}$ LPS-stimulated RAW264.7 macrophages, incubated with 2.5 μM or 5 μM DHEA, 13-HDHEA, 16-HDHEA, and a combined treatment of 2.5 μM 13-HDHEA and 2.5 μM 16-HDHEA as determined by LC-MS/MS. Cells were pre-treated with the compounds for 30 min before 1.0 $\mu\text{g/mL}$ LPS addition and incubation of 24 h. Data are expressed as % relative to the vehicle and 1.0 $\mu\text{g/mL}$ LPS treated control (=100%). Bars represent means with SD from n=3 independent experiments containing technical duplicates. Asterisks indicate significant differences from the vehicle control (one-way ANOVA, Dunnett's *t*-test *post hoc*; * $P < 0.05$, *** $P < 0.001$). Statistical testing showed significant effects compared to 5 μM DHEA treatment $P < 0.01$ (a) or $P < 0.001$ (b) (one-way ANOVA, Tukey multiple comparison test *post hoc*).

5.5 Discussion

In this study we explored the biological effects of the recently discovered DHEA metabolites 13- and 16-HDHEA in LPS-stimulated RAW264.7 macrophages.³⁸ Potential immunomodulating effects of 13- and 16-HDHEA were studied on cytokine release, transcriptome analysis, and via the production of several oxylipin mediators. In short, 13-HDHEA at medium concentrations of 5 μ M significantly reduced production of TNF- α and IL-1 β in LPS-stimulated macrophages, and incubation with 5 μ M 16-HDHEA led to a significant reduction of IL-1Ra production. The combination of 2.5 μ M 13-HDHEA and 2.5 μ M 16-HDHEA in the medium led to a significant decrease in IL-1 β and IL-1Ra production. In contrast to the parent DHEA, 13- and 16-HDHEA did not reduce LPS-induced IL-6 and NO levels. Transcriptome analysis revealed an anti-inflammatory signature for both 13-HDHEA and 16-HDHEA. Incubation with 13-HDHEA and 16-HDHEA induced the resolution related gene *Serpina1*, and was predicted to induce anti-inflammatory regulated pathways, including IL-10, Sirt-1, and those mimicking anti-inflammatory effects of the corticosteroid fluticasone propionate. Additionally, 13-HDHEA and 16-HDHEA inhibited inflammatory regulating genes *Il1b* and *Inhba*, and were predicted to deactivate several downstream regulators of LPS activation. Finally, targeted lipidomic analysis revealed that in contrast to DHEA, 13- and 16-HDHEA do not reduce PGE₂ and PGD₂ production after LPS stimulation, but led to a remarkable decrease of DHA in the cell medium. Even though 13- and 16-HDHEA display anti-inflammatory effects in LPS-stimulated RAW264.7 macrophages, these effects are less pronounced compared to DHEA.

The anti-inflammatory effects of 13- and 16-HDHEA stand out from other known DHEA metabolites that have been previously described in the literature. For instance, 5 μ M of 19(20)-EDP-EA, a predominant metabolite produced by CYP450, showed a significant reduction in NO release and IL-6 production in 25 ng/mL LPS-stimulated BV-2 microglial cells.³⁶ In contrast to these observations, our model revealed that 5 μ M of 13- or 16-HDHEA did not inhibit IL-6 and NO production, which might indicate a distinct anti-inflammatory profile between the CYP450- and COX-2-derived DHEA metabolites. A direct comparison can, however, not be made due to differences in the experimental setup such as a difference cell model and a substantially lower LPS concentration compared to our model. In the current study we specifically chose a relatively strong LPS stimulation of 1.0 μ g/mL to maintain conditions identical to the conditions in which 13- and 16-HDHEA were formed, as well as to conditions in studies on the immuno-modulating effects of DHEA and other DHA-derived endocannabinoids that were previously performed in our laboratory.^{32-33, 38, 56-57}

Additionally, the effects of 13- and 16-HDHEA also seem to stand out from the 15-LOX products 10,17-diHDHEA and 15-HEDPEA. 10,17-diHDHEA and 15-HEDPEA were previously found to reduce platelet-leukocyte aggregation in human whole blood at concentrations as low as 10 pM, whereas DHEA showed no activity up to 100 nM. Moreover, 15-HEDPEA and 10,17-diHDHEA showed increased CB₂ receptor activation when compared to DHEA.³⁵ Consequently, the 15-LOX metabolites seem to have increased anti-inflammatory potential compared to DHEA, whereas 13- and 16-HDHEA generally seem to be less anti-inflammatory than DHEA. Nevertheless, due to differences in the experimental setup, a lack of DHEA control experiment in several other 15-LOX metabolite anti-inflammatory tests, differences in anti-inflammatory markers and mechanisms measured, and the use of different models, a direct and conclusive comparison between the anti-inflammatory potential of 15-LOX metabolites and 13- and 16-HDHEA cannot be made.

Transcriptome analysis was performed to investigate mechanistic immunomodulating effects of 13- and 16-HDHEA, next to the modest anti-inflammatory behavior obtained by cytokine release. Here, expression of *Ifit1* and *InhbA* was significantly reduced by both 13- and 16-HDHEA. *Ifit1* is a key regulator in downstream TLR4 mediated LPS activation.⁴⁹ *InhbA* leads to the production of activin A which induces early-stage activation of RAW264.7 macrophages leading to an inflammatory response⁵⁰. Reduction of expression of these genes therefore suggests anti-inflammatory effects induced by 13-HDHEA and 16-HDHEA. In addition, *Pbbp* and *SerpB2* were found to be induced by both 13- and 16-HDHEA. *Pbbp* is a biomarker for lung cancer, and leads to induced macrophage chemotaxis.⁵⁸ *SerpB2* reduces cell migration and promotes the resolution of inflammation, thus suggesting an anti-inflammatory role for 13- and 16-HDHEA.⁴⁸ Previously, it was observed that incubation of a different DHA derived endocannabinoid, docosahexaenoyl serotonin, reduced *SerpB2* gene expression in LPS stimulated RAW264.7 macrophages, suggesting differential effects.⁵⁶ In addition to the direct effect on these inflammatory regulating genes, several targets linked to inflammasome activation like the IL-1 pathway, *MyD88*, *Mir3075*, *SerpB2*, *Neat*, and *Cmpk2* were significantly affected in macrophages exposed to 13-HDHEA.⁵⁹⁻⁶⁰ These observations suggest that 13- and 16-HDHEA reduce the production of inflammasome regulators. Nonetheless, RAW264.7 cells are unable to produce functional inflammasomes, because they lack the ASC adaptor protein,⁶¹ so this cannot be experimentally verified in our model. Future experiments in different models are required to establish whether 13- and 16-HDHEA do reduce functional inflammasome formation.

Inhibition of upstream regulators involved in LPS signaling was suggested for 5 μ M 13-HDHEA and the combined treatment of 2.5 μ M 13-HDHEA and 2.5 μ M 16-HDHEA

during IPA® analysis. Examples of upstream regulators suggested to be inhibited are TLR4, MyD88, IRF3, IRF7, STAT1, and LPS itself, pointing to an anti-inflammatory effect somewhere in the LPS pathway.^{33, 52, 62} On the other hand, upstream regulators involved in anti-inflammatory responses, like IL-10, Sirt-1, and a fluticasone propionate related pathway were suggested to be induced by 13- and 16-HDHEA.⁵³⁻⁵⁵ Since IPA® analysis is limited by the overlap in gene-expression profiles of connected pathways and the input of studies in the database, it cannot be excluded that 13- and 16-HDHEA can directly interact with TLR4, or adaptor molecules like MyD88 and IRF. Function annotation analysis using IPA® suggested a potential reduction in angiogenesis and an increase in ROS production for the 5 µM 13-HDHEA incubation. The proposed anti-angiogenic effect of 13-HDHEA was further supported by its reducing activity on Ang expression (**Table 5-S1**), which plays an important role in the angiogenic effect of cells.⁶³ Moreover, SerpinB2 was found to decrease cancer metastasis and macrophage migration, which could therefore also be linked to anti-angiogenic effects.⁴⁸ Other oxidized DHEA metabolites like the CYP450-produced derivatives also demonstrated strong anti-angiogenic properties.³⁶⁻³⁷ The proposed ROS production of 13-HDHEA was further supported by previous research showing that the interaction between DHEA and the enzymes COX-2 and 5-LOX resulted in increased ROS production in head and neck squamous cell carcinoma cells.⁶⁴ Moreover, perilipin 2 (Plin2) induction is known to increase ROS formation (**Table 5-2**).⁶⁵ Interestingly, Plin2 is regulated via activation of CB₁, which could directly be targeted by the CYP450 metabolites of DHEA, and the 15-LOX metabolites 10,17-diHDHEA and 15-HEDPEA.^{35-37, 66} Based on these observations it could be speculated that 13- and 16-HDHEA reduce angiogenesis, and increase ROS formation via the interaction with CB₁, ultimately leading to an anti-tumorigenic potential.

Since transcriptomic analysis showed 13- and 16-HDHEA mediated induction on several lipoxygenase genes (like Alox5, Ptgsh1, and Ltc4s) and DHEA itself has interactions with lipoxygenases,¹ we tested the formation of several oxylipins. We found no detectable amounts of leukotrienes and 5-HETE, which corresponds with previous observations in our laboratory.³³ Incubations of the macrophages with 13- and 16-HDHEA decreased DHA levels, whereas DHEA incubations resulted in DHA formation. The latter observation is most likely explained by hydrolysis of DHEA.^{28, 67} Reasons for the reduction of DHA levels in the 13- and 16-HDHEA incubations are unknown. Finally, PGE₂ and PGD₂ production in LPS-stimulated cells was not affected by 13- and 16-HDHEA, whereas DHEA strongly inhibits COX-2 derived prostaglandin formation.^{33, 38} Transcriptome analysis suggested 13- and 16-HDHEA-mediated induction of Ptgsh1, however this remains without consequences at the metabolite level. Apparently, the COX-2 upregulation by 1.0 µg/mL LPS has a stronger effect on prostaglandin formation than the observed additional induction of COX-1. Interestingly, the observations in this study support that the neutral

lipid DHEA competes with arachidonic acid in the substrate binding site of COX-2, whereas its oxidized products 13-HDHEA and 16-HDHEA do not interfere with this binding.^{38, 68}

Comparisons in the anti-inflammatory profile of 13- and 16-HDHEA with DHEA indicated that 13- and 16-HDHEA are less effective in reducing individual mediators like NO, IL-6, TNF α , and IL-1 β , but also show distinct effects on *e.g.* IL-1Ra and DHA. Interestingly, transcriptome analysis from a previously performed experiment using 10 μ M DHEA showed limited overlap in expression profile with 13- and 16-HDHEA (**Figure 5-S2**), further underlining a distinct anti-inflammatory profile between DHEA and its COX-2 derived metabolites.³³ Additionally, in contrast to DHEA, 13- and 16-HDHEA do not inhibit prostaglandin formation. It remains speculative to provide a meaningful interpretation for this, or to speculate whether these differences would also be apparent during *in vivo* inflammation. The modest anti-inflammatory effects of 13-HDHEA and 16-HDHEA could also suggest that 13- and 16-HDHEA are products of an DHEA-inactivation route via COX-2 instead of specifically produced immunomodulating compounds. In addition, the metabolic fate of 13- and 16-HDHEA is unknown. Many other lipoxygenases may be present, that could further metabolize 13- and 16-HDHEA into compounds with yet unknown effects, making biological interpretation more complex.^{1, 19, 34}

Future work should focus on the hypothesized anti-angiogenic and anti-migratory properties of 13- and 16-HDHEA, which seem to be distinct for oxidized DHEA derived metabolites.³⁵⁻³⁷ Secondly, it should be clarified whether 13- and 16-HDHEA are terminal end-products of DHEA or whether they themselves are further metabolized. A further elucidation of the metabolism and functional consequences of 13- and 16-HDHEA could explain more about the physiological relevance of DHEA and its metabolism *in vivo*. Interestingly, epoxide-derived DHEA metabolites have been quantified in Sprague-Dawley rat brain, peripheral organs,³⁶ in metastatic mice lungs,³⁷ and 15-LOX metabolites were found in mice brain,³⁵ demonstrating the presence of DHEA metabolism *in vivo*. Next to the quantification of DHEA derived metabolites, future studies should focus on the immunological effect of these DHEA derived metabolites *in vivo*. Recently, it was shown that 5 mg/kg i.p. injected DHEA exerts inhibitory effects on the pro-inflammatory cytokines IL-1 β and TNF α in 1.0 mg/kg i.p. LPS injected mice.³⁰ It would be interesting to understand the potential role of the various DHEA metabolites in this and similar studies.

In conclusion, 13- and 16-HDHEA differentially inhibit LPS induced inflammation in RAW264.7 macrophages, and the observed immunomodulating effects were typically smaller and distinct from their parent compound DHEA. Future studies should elucidate whether 13- and 16-HDHEA are potential immunomodulating in different

disease models (like tumorigenic and angiogenic models), and identify whether 13- and 16-HDHEA are (terminal) end-products of DHEA or intermediates in a further metabolic route.

5.6 Acknowledgements

The authors like to thank Hans Beijleveld and Frank Claassen for their assistance in the HPLC and mass spectrometry analysis of the 13-HDHEA and 16-HDHEA; Tatiana Nikolaeva and Niels de Roo for their support in NMR analysis; Fay Schrouff for her pioneering work on this project. The authors like to thank the VLAG Graduate School of Wageningen University and Research for their financial support.

5.7 References

1. de Bus, I.; Witkamp, R.; Zuilhof, H.; Albada, B.; Balvers, M., The role of n-3 PUFA-derived fatty acid derivatives and their oxygenated metabolites in the modulation of inflammation. *Prostaglandins Other Lipid Mediat.* **2019**, *144*, 106351.
2. Dunstan, J. A.; Mitoulas, L. R.; Dixon, G.; Doherty, D. A.; Hartmann, P. E.; Simmer, K.; Prescott, S. L., The Effects of Fish Oil Supplementation in Pregnancy on Breast Milk Fatty Acid Composition Over the Course of Lactation: A Randomized Controlled Trial. *Pediatr. Res.* **2007**, *62* (6), 689-694.
3. Swanson, D.; Block, R.; Mousa, S. A., Omega-3 Fatty Acids EPA and DHA: Health Benefits Throughout Life. *Adv. Nutr.* **2012**, *3* (1), 1-7.
4. Marton, L. T.; Goulart, R. d. A.; Carvalho, A. C. A. d.; Barbalho, S. M., Omega Fatty Acids and Inflammatory Bowel Diseases: An Overview. *Int. J. Mol. Sci.* **2019**, *20* (19), 4851.
5. Abdelhamid, A. S.; Brown, T. J.; Brainard, J. S.; Biswas, P.; Thorpe, G. C.; Moore, H. J.; Deane, K. H. O.; AlAbdulghafoor, F. K.; Summerbell, C. D.; Worthington, H. V.; et al., Omega-3 fatty acids for the primary and secondary prevention of cardiovascular disease. *Cochrane Database of Systematic Reviews* **2018**, (7).
6. Manson, J. E.; Cook, N. R.; Lee, I. M.; Christen, W.; Bassuk, S. S.; Mora, S.; Gibson, H.; Albert, C. M.; Gordon, D.; Copeland, T.; et al., f. t. V. R. G., Marine n-3 Fatty Acids and Prevention of Cardiovascular Disease and Cancer. *N. Engl. J. Med.* **2018**, *380*, 23-32.
7. Gioxari, A.; Kaliora, A. C.; Marantidou, F.; Panagiotakos, D. P., Intake of ω -3 polyunsaturated fatty acids in patients with rheumatoid arthritis: A systematic review and meta-analysis. *Nutrition* **2018**, *45* (Supplement C), 114-124.e4.
8. Navarini, L.; Afeltra, A.; Gallo Afflitto, G.; Margiotta, D. P. E., Polyunsaturated fatty acids: any role in rheumatoid arthritis? *Lipids Health Dis.* **2017**, *16* (1), 197.
9. Proudman, S. M.; James, M. J.; Spargo, L. D.; Metcalf, R. G.; Sullivan, T. R.; Rischmueller, M.; Flabouris, K.; Wechalekar, M. D.; Lee, A. T.; Cleland, L. G., Fish oil in recent onset rheumatoid arthritis: a randomised, double-blind controlled trial within algorithm-based drug use. *Ann. Rheum. Dis.* **2015**, *74* (1), 89-95.
10. Adams, S.; Lopata, A. L.; Smuts, C. M.; Baatjies, R.; Jeebhay, M. F., Relationship between Serum Omega-3 Fatty Acid and Asthma Endpoints. *Int. J. Environ. Res. Public Health* **2019**, *16* (1).
11. Calder, P. C., Omega-3 polyunsaturated fatty acids and inflammatory processes: nutrition or pharmacology? *Br. J. Clin. Pharmacol.* **2013**, *75* (3), 645-662.
12. Zapata-Gonzalez, F.; Rueda, F.; Petriz, J.; Domingo, P.; Villarroya, F.; Diaz-Delfin, J.; de Madariaga, M. A.; Domingo, J. C., Human dendritic cell activities are modulated by the omega-3 fatty acid, docosahexaenoic acid, mainly through PPAR γ :RXR heterodimers: comparison with other polyunsaturated fatty acids. *J. Leukoc. Biol.* **2008**, *84* (4), 1172-1182.
13. Nakamoto, K.; Shimada, K.; Harada, S.; Morimoto, Y.; Hirasawa, A.; Tokuyama, S., DHA supplementation prevent the progression of NASH via GPR120 signaling. *Eur. J. Pharmacol.*

2018, 820, 31-38.

14. Oh, D. Y.; Talukdar, S.; Bae, E. J.; Imamura, T.; Morinaga, H.; Fan, W.; Li, P.; Lu, W. J.; Watkins, S. M.; Olefsky, J. M., GPR120 Is an Omega-3 Fatty Acid Receptor Mediating Potent Anti-inflammatory and Insulin-Sensitizing Effects. *Cell* **2010**, *142* (5), 687-698.
15. Balvers, M. G. J.; Verhoeckx, K. C. M.; Bijlsma, S.; Rubingh, C. M.; Meijerink, J.; Wortelboer, H. M.; Witkamp, R. F., Fish oil and inflammatory status alter the n-3 to n-6 balance of the endocannabinoid and oxylipin metabolomes in mouse plasma and tissues. *Metabolomics* **2012**, *8* (6), 1130-1147.
16. Calder, P. C., Marine omega-3 fatty acids and inflammatory processes: Effects, mechanisms and clinical relevance. *Biochim. Biophys. Acta Mol. Cell Biol. Lipids* **2015**, *1851* (4), 469-484.
17. Calder, P. C., Omega-3 fatty acids and inflammatory processes: from molecules to man. *Biochem. Soc. Trans.* **2017**, *45* (5), 1105-1115.
18. Serhan, C. N.; Chiang, N.; Van Dyke, T. E., Resolving inflammation: dual anti-inflammatory and pro-resolution lipid mediators. *Nat. Rev. Immunol.* **2008**, *8* (5), 349-361.
19. Serhan, C. N.; Levy, B. D., Resolvins in inflammation: emergence of the pro-resolving superfamily of mediators. *J. Clin. Invest.* **2018**, *128* (7), 2657-2669.
20. Balvers, M. G. J.; Wortelboer, H. M.; Witkamp, R. F.; Verhoeckx, K. C. M., Liquid chromatography–tandem mass spectrometry analysis of free and esterified fatty acid N-acyl ethanolamines in plasma and blood cells. *Anal. Biochem.* **2013**, *434* (2), 275-283.
21. Bisogno, T.; Delton-Vandenbroucke, I.; Milone, A.; Lagarde, M.; Di Marzo, V., Biosynthesis and Inactivation of N-Arachidonylethanolamine (Anandamide) and N-Docosahexaenylethanolamine in Bovine Retina. *Arch. Biochem. Biophys.* **1999**, *370* (2), 300-307.
22. Wood, J. T.; Williams, J. S.; Pandarinathan, L.; Janero, D. R.; Lammi-Keefe, C. J.; Makriyannis, A., Dietary docosahexaenoic acid supplementation alters select physiological endocannabinoid-system metabolites in brain and plasma. *J. Lipid Res.* **2010**, *51* (6), 1416-1423.
23. Kendall, A. C.; Pilkington, S. M.; Massey, K. A.; Sassano, G.; Rhodes, L. E.; Nicolaou, A., Distribution of Bioactive Lipid Mediators in Human Skin. *J. Invest. Dermatol.* **2015**, *135* (6), 1510-1520.
24. Kantae, V.; Ogino, S.; Noga, M.; Harms, A. C.; van Dongen, R. M.; Onderwater, G. L. J.; van den Maagdenberg, A. M. J. M.; Terwindt, G. M.; van der Stelt, M.; Ferrari, M. D.; et al., Quantitative profiling of endocannabinoids and related N-acylethanolamines in human CSF using nano LC-MS/MS. *J. Lipid Res.* **2017**, *58* (3), 615-624.
25. Czepiel, J.; Gdula-Argasińska, J.; Biesiada, G.; Bystrowska, B.; Jurczynszyn, A.; Perucki, W.; Sroczyńska, K.; Zajac, A.; Librowski, T.; Garlicki, A., Fatty acids and selected endocannabinoids content in cerebrospinal fluids from patients with neuroinfections. *Metab. Brain Dis.* **2019**, *34* (1), 331-339.
26. Balvers, M. G. J.; Verhoeckx, K. C. M.; Meijerink, J.; Bijlsma, S.; Rubingh, C. M.; Wortelboer, H. M.; Witkamp, R. F., Time-dependent effect of in vivo inflammation on eicosanoid and endocannabinoid levels in plasma, liver, ileum and adipose tissue in C57BL/6 mice fed a fish-oil diet. *Int. Immunopharmacol.* **2012**, *13* (2), 204-214.
27. Leishman, E.; Mackie, K.; Luquet, S.; Bradshaw, H. B., Lipidomics profile of a NAPE-PLD KO

- mouse provides evidence of a broader role of this enzyme in lipid metabolism in the brain. *Biochim. Biophys. Acta Mol. Cell Biol. Lipids* **2016**, *1861* (6), 491-500.
28. Kim, H.-Y.; Spector, A. A., N-Docosahexaenoylethanolamine: A neurotrophic and neuroprotective metabolite of docosahexaenoic acid. *Mol. Aspects Med.* **2018**, *64*, 34-44.
 29. Meijerink, J.; Balvers, M. G. J.; Witkamp, R. F., N-acyl amines of docosahexaenoic acid and other n-3 polyunsaturated fatty acids – from fishy endocannabinoids to potential leads. *Br. J. Pharmacol.* **2013**, *169* (4), 772-783.
 30. Park, T.; Chen, H.; Kim, H.-Y., GPR110 (ADGRF1) mediates anti-inflammatory effects of N-docosahexaenoylethanolamine. *J. Neuroinflammation* **2019**, *16* (1), 225.
 31. Balvers, M. G. J.; Verhoeckx, K. C. M.; Plastina, P.; Wortelboer, H. M.; Meijerink, J.; Witkamp, R. F., Docosahexaenoic acid and eicosapentaenoic acid are converted by 3T3-L1 adipocytes to N-acyl ethanolamines with anti-inflammatory properties. *Biochim. Biophys. Acta Mol. Cell Biol. Lipids* **2010**, *1801* (10), 1107-1114.
 32. Meijerink, J.; Plastina, P.; Vincken, J.-P.; Poland, M.; Attya, M.; Balvers, M.; Gruppen, H.; Gabriele, B.; Witkamp, R. F., The ethanolamide metabolite of DHA, docosahexaenoylethanolamine, shows immunomodulating effects in mouse peritoneal and RAW264.7 macrophages: evidence for a new link between fish oil and inflammation. *Br. J. Nutr.* **2011**, *105* (12), 1798-1807.
 33. Meijerink, J.; Poland, M.; Balvers, M. G. J.; Plastina, P.; Lute, C.; Dwarkasing, J.; van Norren, K.; Witkamp, R. F., Inhibition of COX-2-mediated eicosanoid production plays a major role in the anti-inflammatory effects of the endocannabinoid N-docosahexaenoylethanolamine (DHEA) in macrophages. *Br. J. Pharmacol.* **2015**, *172* (1), 24-37.
 34. Witkamp, R., Fatty acids, endocannabinoids and inflammation. *Eur. J. Pharmacol.* **2016**, *785*, 96-107.
 35. Yang, R.; Fredman, G.; Krishnamoorthy, S.; Agrawal, N.; Irimia, D.; Piomelli, D.; Serhan, C. N., Decoding Functional Metabolomics with Docosahexaenoyl Ethanolamide (DHEA) Identifies Novel Bioactive Signals. *J. Biol. Chem.* **2011**, *286* (36), 31532-31541.
 36. McDougale, D. R.; Watson, J. E.; Abdeen, A. A.; Adili, R.; Caputo, M. P.; Krapf, J. E.; Johnson, R. W.; Kilian, K. A.; Holinstat, M.; Das, A., Anti-inflammatory ω -3 endocannabinoid epoxides. *Proc. Natl. Acad. Sci. U.S.A.* **2017**, *114* (30), E6034-E6043.
 37. Roy, J.; Watson, J. E.; Hong, I. S.; Fan, T. M.; Das, A., Antitumorigenic Properties of Omega-3 Endocannabinoid Epoxides. *J. Med. Chem.* **2018**, *61* (13), 5569-5579.
 38. de Bus, I.; Zuilhof, H.; Witkamp, R.; Balvers, M.; Albada, B., Novel COX-2 products of n-3 polyunsaturated fatty acid-ethanolamine-conjugates identified in RAW 264.7 macrophages. *J. Lipid Res.* **2019**, *60* (11), 1829-1840.
 39. Lin, K.; Kools, H.; de Groot, P. J.; Gavai, A. K.; Basnet, R. K.; Cheng, F.; Wu, J.; Wang, X.; Lommen, A.; Hooiveld, G. J.; et al., MADMAX - Management and analysis database for multiple -omics experiments. *J. Integr. Bioinform.* **2011**, *8* (2), 160.
 40. Irizarry, R. A.; Hobbs, B.; Collin, F.; Beazer-Barclay, Y. D.; Antonellis, K. J.; Scherf, U.; Speed, T. P., Exploration, normalization, and summaries of high density oligonucleotide array probe

- level data. *Biostatistics* **2003**, *4* (2), 249-64.
41. Carvalho, B. S.; Irizarry, R. A., A framework for oligonucleotide microarray preprocessing. *Bioinformatics* **2010**, *26* (19), 2363-7.
 42. Dai, M.; Wang, P.; Boyd, A. D.; Kostov, G.; Athey, B.; Jones, E. G.; Bunney, W. E.; Myers, R. M.; Speed, T. P.; Akil, H.; et al., Evolving gene/transcript definitions significantly alter the interpretation of GeneChip data. *Nucleic Acids Res.* **2005**, *33* (20), e175.
 43. Bolstad, B. M.; Irizarry, R. A.; Astrand, M.; Speed, T. P., A comparison of normalization methods for high density oligonucleotide array data based on variance and bias. *Bioinformatics* **2003**, *19* (2), 185-93.
 44. Sartor, M. A.; Tomlinson, C. R.; Wesselkamper, S. C.; Sivaganesan, S.; Leikauf, G. D.; Medvedovic, M., Intensity-based hierarchical Bayes method improves testing for differentially expressed genes in microarray experiments. *BMC Bioinform.* **2006**, *7*, 538.
 45. Smyth, G. K., Linear models and empirical bayes methods for assessing differential expression in microarray experiments. *Stat. Appl. Genet. Mol. Biol.* **2004**, *3* (1), 1-25.
 46. Ritchie, M. E.; Diagnostics, D.; Neilson, J.; van Laar, R.; Dobrovic, A.; Holloway, A.; Smyth, G. K., Empirical array quality weights in the analysis of microarray data. *BMC Bioinform.* **2006**, *7*, 261.
 47. Liu, R.; Holik, A. Z.; Su, S.; Jansz, N.; Chen, K.; Leong, H. S.; Blewitt, M. E.; Asselin-Labat, M. L.; Smyth, G. K.; Ritchie, M. E., Why weight? Modelling sample and observational level variability improves power in RNA-seq analyses. *Nucleic Acids Res.* **2015**, *43* (15), e97.
 48. Schroder, W. A.; Hirata, T. D.; Le, T. T.; Gardner, J.; Boyle, G. M.; Ellis, J.; Nakayama, E.; Pathirana, D.; Nakaya, H. I.; Suhrbier, A., SerpinB2 inhibits migration and promotes a resolution phase signature in large peritoneal macrophages. *Sci. Rep.* **2019**, *9* (1), 12421-12421.
 49. McDermott, J. E.; Vartanian, K. B.; Mitchell, H.; Stevens, S. L.; Sanfilippo, A.; Stenzel-Poore, M. P., Identification and Validation of Ifit1 as an Important Innate Immune Bottleneck. *PLoS ONE* **2012**, *7* (6), e36465.
 50. Ge, J.; Wang, Y.; Feng, Y.; Liu, H.; Cui, X.; Chen, F.; Tai, G.; Liu, Z., Direct effects of activin A on the activation of mouse macrophage RAW264.7 cells. *Cell. Mol. Immunol.* **2009**, *6* (2), 129-133.
 51. Lu, Y.-C.; Yeh, W.-C.; Ohashi, P. S., LPS/TLR4 signal transduction pathway. *Cytokine* **2008**, *42* (2), 145-151.
 52. Schmitz, F.; Mages, J.; Heit, A.; Lang, R.; Wagner, H., Transcriptional activation induced in macrophages by Toll-like receptor (TLR) ligands: from expression profiling to a model of TLR signaling. *Eur. J. Immunol.* **2004**, *34* (10), 2863-2873.
 53. Shouval, D. S.; Ouahed, J.; Biswas, A.; Goettel, J. A.; Horwitz, B. H.; Klein, C.; Muise, A. M.; Snapper, S. B., Interleukin 10 receptor signaling: master regulator of intestinal mucosal homeostasis in mice and humans. *Adv. Immunol.* **2014**, *122*, 177-210.
 54. Ding, R.-B.; Bao, J.; Deng, C.-X., Emerging roles of SIRT1 in fatty liver diseases. *Int. J. Biol. Sci.* **2017**, *13* (7), 852-867.
 55. Johnson, M., The anti-inflammatory profile of fluticasone propionate. *Allergy* **1995**, *50* (23 Suppl), 11-4.

56. Poland, M.; ten Klooster, J. P.; Wang, Z.; Pieters, R.; Boekschoten, M.; Witkamp, R.; Meijerink, J., Docosahexaenoyl serotonin, an endogenously formed n-3 fatty acid-serotonin conjugate has anti-inflammatory properties by attenuating IL-23-IL-17 signaling in macrophages. *Biochim. Biophys. Acta Mol. Cell Biol. Lipids* **2016**, *1861* (12, Part A), 2020-2028.
57. Wang, Y.; Plastina, P.; Vincken, J.-P.; Jansen, R.; Balvers, M.; ten Klooster, J. P.; Gruppen, H.; Witkamp, R.; Meijerink, J., N-Docosahexaenoyl Dopamine, an Endocannabinoid-like Conjugate of Dopamine and the n-3 Fatty Acid Docosahexaenoic Acid, Attenuates Lipopolysaccharide-Induced Activation of Microglia and Macrophages via COX-2. *ACS Chem. Neurosci.* **2017**, *8* (3), 548-557.
58. Unver, N.; Esendagli, G.; Yilmaz, G.; Guc, D., CXCL7-induced macrophage infiltration in lung tumor is independent of CXCR2 expression: CXCL7-induced macrophage chemotaxis in LLC tumors. *Cytokine* **2015**, *75* (2), 330-7.
59. Ojcius, D. M.; Jafari, A.; Yeruva, L.; Schindler, C. W.; Abdul-Sater, A. A., Dicer regulates activation of the NLRP3 inflammasome. *PLoS ONE* **2019**, *14* (4), e0215689-e0215689.
60. Zhong, Z.; Liang, S.; Sanchez-Lopez, E.; He, F.; Shalapour, S.; Lin, X.-j.; Wong, J.; Ding, S.; Seki, E.; Schnabl, B.; et al., New mitochondrial DNA synthesis enables NLRP3 inflammasome activation. *Nature* **2018**, *560* (7717), 198-203.
61. Pelegrin, P.; Barroso-Gutierrez, C.; Surprenant, A., P2X7 Receptor Differentially Couples to Distinct Release Pathways for IL-1 β in Mouse Macrophage. *J. Immunol.* **2008**, *180* (11), 7147-7157.
62. Genard, G.; Lucas, S.; Michiels, C., Reprogramming of Tumor-Associated Macrophages with Anticancer Therapies: Radiotherapy versus Chemo- and Immunotherapies. *Front. Immunol.* **2017**, *8* (828), 1-19.
63. Sheng, J.; Xu, Z., Three decades of research on angiogenin: a review and perspective. *Acta Biochim. Biophys. Sin.* **2015**, *48* (5), 399-410.
64. Park, T.; Chen, H.; Kevala, K.; Lee, J.-W.; Kim, H.-Y., N-Docosahexaenoyl ethanolamine ameliorates LPS-induced neuroinflammation via cAMP/PKA-dependent signaling. *J. Neuroinflammation* **2016**, *13* (1), 284.
65. ten Hove, M.; Pater, L.; Storm, G.; Weiskirchen, S.; Weiskirchen, R.; Lammers, T.; Bansal, R., The hepatic lipidome: From basic science to clinical translation. *Adv. Drug Deliv. Rev.* **2020**, *159*, 180-197.
66. Irunbam, K.; Churin, Y.; Matono, T.; Weglage, J.; Ocker, M.; Glebe, D.; Hardt, M.; Koepfel, A.; Roderfeld, M.; Roeb, E., Cannabinoid receptor 1 knockout alleviates hepatic steatosis by downregulating perilipin 2. *Lab. Investig.* **2020**, *100* (3), 454-465.
67. Alhouayek, M.; Bottemanne, P.; Makriyannis, A.; Muccioli, G. G., N-acyl ethanolamine-hydrolyzing acid amidase and fatty acid amide hydrolase inhibition differentially affect N-acyl ethanolamine levels and macrophage activation. *Biochim. Biophys. Acta Mol. Cell Biol. Lipids* **2017**, *1862* (5), 474-484.
68. Smith, W. L.; Malkowski, M. G., Interactions of fatty acids, nonsteroidal anti-inflammatory drugs, and coxibs with the catalytic and allosteric subunits of cyclooxygenases-1 and -2. *J. Biol. Chem.* **2019**, *294* (5), 1697-1705.

Supporting information belonging to Chapter 5

For the data belonging to the purification and analysis of the synthesized 13-HDHEA and 16-HDHEA, and to access the filtered gene table including probe sets that satisfied the criterion of moderated P-value <0.01, and average gene expressions with average log2 expression >3.5 (**Table 5-S1**), the reader is referred to the online version of the publication at doi: 10.1016/j.bbali.2021.158908.

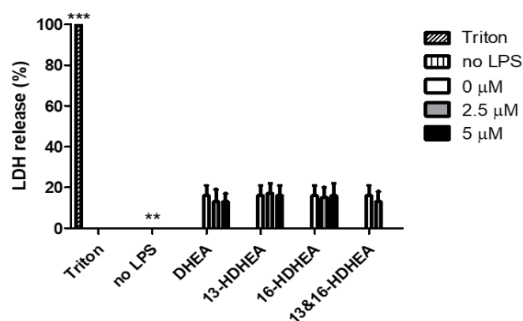


Figure 5-S1 LDH release of 1.0 $\mu\text{g}/\text{mL}$ stimulated RAW264.7 macrophages incubated with 2.5 μM or 5.0 μM 13-HDHEA, 16-HDHEA, a stoichiometric mixture thereof, or DHEA. The LDH release is expressed in percentage compared to Triton X-100 treated positive control (100% cytotoxicity), and no LPS treated macrophages (0% cytotoxicity).

All samples were measured in triplicate containing technical duplicates. Asterisks indicate significant differences from the vehicle with 1.0 µg/mL LPS control (one-way ANOVA, Dunnett's multiple comparison test *post hoc*; * P<0.05, ** P<0.01, *** P<0.001).

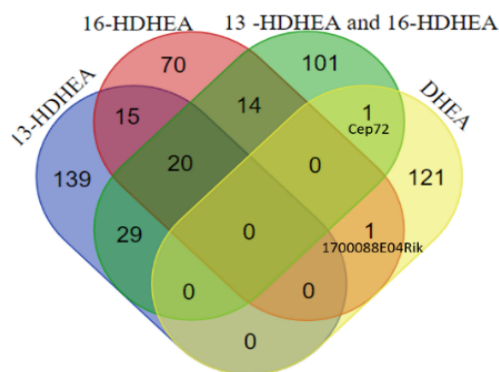


Figure 5-S2 Venn diagram showing overlap of significantly expressed genes ($P < 0.01$ and average \log_2 expression value > 3.5) of $1.0 \mu\text{g/mL}$ LPS stimulated RAW264.7 macrophages, incubated with $5 \mu\text{M}$ 13-HDHEA (blue), $5 \mu\text{M}$ 16-HDHEA (red), and a combinatorial $2.5 \mu\text{M}$ 13-HDHEA and $2.5 \mu\text{M}$ 16-HDHEA incubation (green), and $10 \mu\text{M}$ DHEA ($P < 0.01$, using data from a previous study in our group³³) (yellow).

The Venn diagram was drawn using the free online Venn diagram drawing tool (<http://bioinformatics.psb.ugent.be/webtools/Venn/>).

Chapter 6

**Effects of docosahexaenoyl ethanolamide
on symptoms of colitis, liver inflammatory
markers and hepatic PUFA metabolism
in a model of DSS-induced colitis**

**Ian de Bus,
Pim Koelink,
Aletta Kraneveld,
Mieke Poland,
Renger F. Witkamp,
Bauke Albada,
Michiel G.J. Balvers**

(Unpublished results)

6.1 Abstract

Inflammatory bowel diseases (IBDs) are chronic relapsing inflammatory disorders affecting the gastrointestinal tract. The most common forms are ulcerative colitis and Crohn's disease, which show increasing incident rates in Western and newly industrialized countries. Nutritional intervention, by shifting the *n*-3/*n*-6 PUFA ratio through diet or supplementation has been proposed to reduce risk and development of IBD, which may be partly explained by the protective nature of specific *n*-3 PUFA derived metabolites. Here we study the effects of docosahexaenoyl ethanolamide (DHEA), an *n*-3 PUFA derivative displaying potent anti-inflammatory activity in several *in vitro* studies, in a 5-day 2% DSS-induced C57Bl/6 mice model. Peritoneal injection with DHEA (10 or 15 mg/kg) significantly improved several phenotypic colitis markers such as decreased body weight loss and poor stool quality. However, no histopathological improvements were found in the colon of animals receiving DHEA injections. Liver tissues were analyzed for RNA expression of genes involved in the regulation of inflammatory processes and concentrations of a various PUFA mediators. We found that 2% DSS-induction did not clearly induce a pro-inflammatory status in the liver. Hepatic concentrations of DHEA were increased with increased DHEA dosing, but anandamide levels remained unaltered. Oxygenated DHEA metabolites were not observed in the livers of the mice, potentially explained by the lower expression of specific oxygenases in the liver.

6.2 Introduction

Crohn's disease and ulcerative colitis are the two major forms of inflammatory bowel diseases (IBDs) and are characterized by chronic relapsing inflammation of the gastrointestinal tract.¹ Symptoms of IBD include abdominal pain, diarrhea, and rectal bleeding often accompanied by systemic symptoms such as fever, weight loss, and fatigue.¹⁻³ It is estimated that over 6.8 million people worldwide suffer from IBD. Incident rates are still rising, especially in Western countries and newly industrialized countries in South America, eastern Europe, Asia, and Africa.^{1,4} Notable risk factors include genetic factors, but unhealthy lifestyle and poor nutrition are also important contributors.⁵ An increasing number of studies report that changes from a typical Western type diet, rich in *n*-6 polyunsaturated fatty acids (PUFAs), to healthier alternatives, that are *e.g.* rich in *n*-3 PUFAs, are linked to reduced risk and progression of IBD.⁶⁻⁷ *In vivo*, *n*-3 PUFAs are converted to bio-active mediators like the pro-resolving maresins, protectins, and resolvins, and also to their *N*-acyl conjugates including ethanolamine-, dopamine-, and serotonin derivatives.^{2, 8-12} For example, docosahexaenoyl serotonin (DHA-5HT) was identified in the human colon, and was also shown to possess potential anti-inflammatory effects by attenuating prototypical inflammatory mediators like IL-17, IL-23, and C-C motif chemokine ligand 20 (CCL-20) in ConA-stimulated human PBMCs and LPS-stimulated RAW264.7 macrophages.¹¹ ¹³ Docosahexaenoyl ethanolamide (DHEA) has been identified in human and murine plasma and in tissues such as mouse ileum and liver.¹⁴⁻¹⁵ DHEA showed a variety of immune-regulating properties, such as the reduction of pro-inflammatory cytokines and chemokines in LPS-stimulated macrophages,^{8, 10, 16-17} antinociceptive effects in a formaldehyde pain model,¹⁸ and neuroprotective roles via interaction with G-protein-coupled receptor 110 (GPR110),¹⁹⁻²¹ . Moreover, we and others have shown that DHEA serves as a substrate of oxygenases, leading to its conversion into new compounds which themselves possess potent anti-inflammatory and antitumorigenic properties.^{8, 16, 22-25} Although many studies have investigated the anti-inflammatory effects of DHEA *in vitro*, studies into the kinetics and efficacy of DHEA in disease models of *e.g.* IBD are lacking. Elucidating the mechanisms through which *n*-3 PUFAs and their metabolites might interact with IBD is important, as it may reveal new leads for prevention or targets for treatment.

Over the years, different IBD and colitis models have been developed, including the dextran sodium sulphate (DSS) model. The DSS model closely resembles human IBD and different modifications of the protocol exist to resemble acute, chronic or relapsing inflammation, while being simple, fast, reproducible, controllable and known to respond to anti-IBD treatment.²⁶ Administration of DSS in the drinking

water induces toxicity to the epithelium of the colon, thereby decreasing the epithelial barrier function and inducing inflammation. DSS-induced colitis is characterized by the release of pro-inflammatory cytokines and other factors as well as a progressive inflammation in the GI tract and colon.^{3, 26}

Interestingly, various *n*-3 PUFAs and their metabolites showed potential anti-inflammatory effects on colitis. For example, DHA-5HT showed inhibitory effects on T-helper 17 cell (Th17)-related cytokines like IL-17, IL-23, and CCL-20, considered to be pivotally involved in IBD pathogenesis,^{11, 13} eicosapentaenoic acid monoglyceride (MAG-EPA) reduced colon inflammation in a DSS-induced colitis model in rats,^{24, 27} and docosahexaenoic acid (DHA) itself attenuated DSS-induced colitis in mice.²⁸ Given the immune-modulatory effects of DHEA and the effects of other *n*-3 PUFA metabolites in colitis, we hypothesized that DHEA may reduce symptoms of DSS colitis. In the current study we tested the effects and kinetics of intraperitoneally (i.p.) injected DHEA in DSS-induced colitis in C57Bl/6 mice (**Figure 6-1**). We analyzed phenotypic markers of IBD, including body weight, stool consistency, and rectal bleeding, together with pathophysiological markers in the colon, such as colon length, cellular infiltration, and neutrophil activity. To explore the effects and metabolism of DHEA in the liver, we determined hepatic concentrations of DHEA, its oxidized metabolites, pro-inflammatory lipid regulators, and gene expression levels of inflammatory markers and cytokines. DHEA significantly affected phenotypic manifestations of colitis such as weight loss, stool consistency and blood loss, but had no effects on pathophysiological parameters such as colon inflammation. In the liver, only levels of the parent compound DHEA were significantly influenced following injection.

6.3 Materials and Methods

6.3.1 Materials

PGE₂ (≥98%), PGD₂ (≥98%), TXB₂ (≥98%), (±)13-HDHA (≥98%), (±)16-HDHA (≥98%), (±)10,11-EpDPA (≥98%), (±)19,20-EpDPA (≥98%), EPEA (≥98%), DHEA (≥98%), PGE₂-*d*₄ (≥99% deuterated forms *d*₁-*d*₄), DHEA-*d*₄ (≥99% purity deuterated forms *d*₁-*d*₄) were purchased at Cayman Chemical and supplied by Sanbio B.V. (Uden, The Netherlands). AEA (100% purity according to HPLC) was bought from Tocris (Abingdon, UK). Acetonitrile (≥99.9%, HiPerSolv CHROMANORM® for LC-MS), and methanol (≥99.9%, HiPerSolv CHROMANORM®, ULTRA for LC-MS) were purchased at VWR International B.V. (Amsterdam, The Netherlands). Formic acid (≥99% ULC/MS) was obtained from Biosolve B.V. (Valkenswaard, The Netherlands). Absolute Ethanol (for analysis, EMSURE®) was obtained from Merck Millipore (Zwijndrecht, The Netherlands). Ultrapure water was filtered by a MilliQ Integral 3 system from

Millipore (Molsheim, France). Triethylamine ($\geq 99.5\%$ purity) and ethanolamine ($\geq 98\%$ purity) were purchased at Sigma Aldrich (Zwijndrecht, The Netherlands). Isobutyl chloroformate ($\geq 98\%$ purity) was purchased at Thermo Fisher (Landsmeer, The Netherlands). Ethanolamine- d_4 ($\geq 98\%$ purity, 100.0% isotopic enrichment) was obtained from Cambridge Isotope Laboratories Inc. (Andover, USA). DCM for the synthetic procedure of the standards was purified using a Pure Solv 400 solvent purification system from Innovative Technology (Amesbury, USA). DSS (36–50 kDa) was purchased from MP Biomedicals (Aurora, USA). Sterile arachis oil for i.p. injection was obtained from the pharmacy of the faculty of Veterinary Medicine from Utrecht University.

6.3.2 Animal experiment

The animal experiment was conducted in the animal research study facilities of Utrecht University, using 8–10 weeks old wild type, male C57Bl/6 mice. A schematic overview of the mouse experiment is given in **Figure 6-1**. The mouse study was approved by the Animal Ethics Committee of Utrecht University (2012.II.07.096). Mice were intraperitoneally (i.p.) injected with arachis oil (as vehicle control), or 10 mg/kg DHEA, or 15 mg/kg DHEA (DHEA was dissolved in arachis oil) from day –1 until day 6 of the study. From day 0 until day 5, animals in the DSS group received water containing 2% w/v DSS, which was provided *ad libitum*. Control mice received normal drinking water throughout the experiment. The experiment involved the following treatment groups; vehicle – 2% DSS (n=10), 10 mg/kg DHEA – 2% DSS (n=10), 15 mg/kg DHEA – 2% DSS (n=10), vehicle – no DSS (n=6), 15 mg/kg DHEA – no DSS (n=6). Clinical features of colitis, such as body weight and stool consistency/blood loss, were evaluated each day. The condition of the stool was evaluated by scoring stool consistency and blood. Stool consistency was scored based on the appearance (normal = 0, soft = 1, loose/diarrhea = 2), and stool blood was scored based on the presence of blood (absent = 0, only detected with Colo-Rectal test kit from Axon Lab AG (Reichenbach, Germany) = 1, macroscopically present = 2); a higher score thus indicates a stronger colitis phenotype. On the final day of the experiment (day 7) the mice were anesthetized using isoflurane inhalation after which plasma was collected. Subsequently, the animals were sacrificed using cervical dislocation, and tissues were collected.

6.3.3 Colon length, myeloperoxidase (MPO) activity assay, and histopathological staining

Colons of the sacrificed mice were isolated, and colon lengths determined. Hereafter, the colon was opened longitudinally before cleaning in PBS, and placing on a filter with the luminal side up. The colon was cut in half over the length; one half was fixed in buffered 4% formalin for 24 hours and stored in 70% ethanol at 4 °C, the other half was cut into a proximal and distal end and placed at –70 °C. The proximal and distal

colon parts were weighed and dissolved in PBS giving a concentration of 100 mg colon per mL PBS. The colon parts were homogenized five times for 10 sec. at 6000 rpm in the homogenizer from Bertin Technologies (Montigny-le-Bretonneux, France) and were placed on ice for 2 min between each homogenization step. Vials were centrifuged for 15 min at 13000 rpm at 4 °C. The supernatant was collected and stored at -70 °C. A standard BCA protein assay kit from Thermo Fisher Scientific (Rockford, IL, USA) was used to perform protein quantification in proximal and distal colon supernatants. Afterwards MPO concentrations were determined using a Mouse MPO ELISA kit from Hycult Biotechnology (Uden, The Netherlands). Measured MPO concentrations were corrected for the total amount of protein in the samples.

Fixed colon parts were embedded in paraffin (Swiss roll technique), cut at 5 µm and stained with haematoxylin and eosin, according to standard procedures.²⁹ Sections were graded under the microscope in a blinded fashion by three different researchers for epithelial damage (no damage = 0, minor loss of crypt structure = 1, major loss of crypt structure = 2, loss of upper layer = 3, loss of total epithelium = 4) and cover size of the damage (none = 0, <25% = 1, 25–50% = 2, 50–75% = 3, >75% = 4). Cellular inflammatory infiltration in a range from 0–4 (no infiltration = 0, infiltration between crypts = 1, sub-mucosal infiltration = 2, muscularis infiltration = 3, extensive infiltration = 4) and cover size of the cellular inflammatory infiltration (none = 0, <25% = 1, 25–50% = 2, 50–75% = 3, >75% = 4) were analyzed identically. The cumulative score (of 0–16) represent the DSS-colitis histological colon score.²⁹

6.3.4 Synthesis of 13-HDHEA, 16-HDHEA, 10,11-EDP-EA, 19,20-EDP-EA

100 µg of 13-HDHA, 16-HDHA, 10,11-EDP-EA, and 19,20-EDP-EA (1 eq., 0.29 µmol) in EtOH were evaporated to dryness using co-evaporation with DCM. The compounds were subsequently placed under argon atmosphere and dissolved in 2 mL dry DCM. Then, 100 µL of a freshly prepared solution of 59.3 µL distilled triethylamine in 10 mL dry DCM was added (14 eq., 4.25 µmol), followed by the addition of 100 µL of a freshly prepared solution of 47.3 µL isobutyl chloroformate in 10 mL dry DCM (12 eq., 3.65 µmol). The solution was stirred at room temperature for 1 h under argon atmosphere to form the mixed anhydride, before cooling the reaction on ice. To the mixed anhydride 100 µL of a freshly prepared solution of 46.6 µL distilled triethylamine (11 eq., 3.34 µmol) and 20.2 µL ethanolamine (11 eq., 3.34 µmol) in 10 mL dry DCM was added. The reaction was stirred on ice for overnight. Next day the reaction mixture was evaporated and dissolved in 1 mL ultrapure water:ACN (30:70) to purify the product by preparative HPLC. The yield of the synthesis was determined based on the UV absorption (*vide infra*); for 13-HDHEA (33.8 µg, 30%), 16-HDHEA (49.5 µg, 44%), 10,11-EDP-EA (15.1 µg, 13%), and 19,20-EDP-EA (28.1 µg, 25%) (**Figure S6-1, S6-2**).

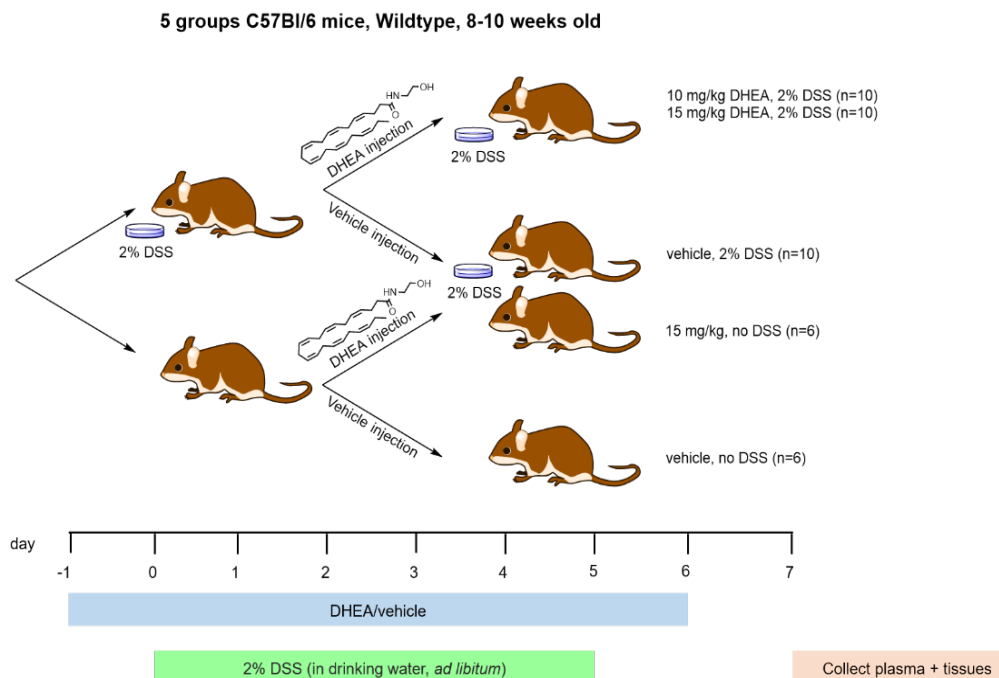


Figure 6-1 Experimental overview of colitis C57Bl/6 mouse study. DHEA 10 mg/kg or 15 mg/kg (dissolved in arachis oil), or vehicle (arachis oil) were i.p. injected each day from day -1 until day 6. From day 0 until day 5 DSS mice received 2% DSS *ab libitum* in the drinking water. At day 7 the plasma of the DSS mice (n=10), and control mice (n=6) was collected and the tissues were harvested.

6.3.5 Synthesis of 13-HDHEA- d_4

100 μ g of 13-HDHA (1 eq., 0.29 μ mol) in EtOH was evaporated to dryness using co-evaporation with DCM, and subsequently placed under argon atmosphere. The 13-HDHA was stirred in 2 mL of dry DCM and then reacted with 100 μ L of a freshly prepared solution of 59.3 μ L distilled triethylamine in 10 mL dry DCM (14 eq., 4.25 μ mol) and 100 μ L of a freshly prepared solution of 47.3 μ L isobutyl chloroformate in 10 mL dry DCM (12 eq., 3.65 μ mol). The solution was stirred at room temperature for 1 h under argon atmosphere to form the mixed anhydride, before cooling the reaction on ice. To the mixed anhydride 100 μ L of a freshly prepared solution of 46.6 μ L distilled triethylamine (11 eq., 3.34 μ mol) and 20.2 μ L ethanolamine- d_4 (11 eq., 3.34 μ mol) in 10 mL dry DCM was added. The reaction was stirred on ice for overnight. Next day the reaction mixture was evaporated and dissolved in 1 mL ultrapure water:ACN (30:70) to purify the product by preparative HPLC. The yield of the synthesis was determined based on the 240 nm UV absorption (*vide infra*) and found to be 2.2 μ g, 2% (**Figure S6-1**).

6.3.6 Preparative HPLC

The products were purified on an Agilent 1260 Preparative HPLC with DAD and MSD from Agilent Technologies B.V. (Amstelveen, The Netherlands). Purification was performed using an isocratic run of 30:70 ultrapure water:ACN containing 0.1% FA using a flow rate of 4 mL/min on a Zorbax Eclipse XDB-C18 5 μ column of 9.4 \times 250 mm from Agilent Technologies B.V. (Amstelveen, the Netherlands). Purified compounds were evaporated to dryness using a rotary evaporator and subsequent freeze drying. The samples were dissolved in absolute EtOH to be quantified and used in the experiments.

6.3.7 Quantitative HPLC

Quantification of the synthesized standards was performed on an Agilent 1220 HPLC Infinity with DAD from Agilent Technologies B.V. (Amstelveen, The Netherlands). The HPLC run was performed using an isocratic run of 30:70 ultrapure water:ACN containing 0.1% FA for 15 or 20 min with a flow rate of 1.00 mL/min on a Zorbax Eclipse XDB-C18 5 μ column 4.6 \times 250 mm from Agilent Technologies B.V. (Amstelveen, The Netherlands). The concentration of the HDHEA standards was determined at 240 nm absorption, by comparing the peak areas of the synthetic compounds to those of 13-HDHA and 16-HDHA standard curves (**Figure S6-3**). EDP-EA standard concentrations were estimated by measuring peak areas at 200 nm absorption of the synthetic compounds to those of 10,11-EpDPA and 19,20-EpDPA standard curves (**Figure S6-4**).

6.3.8 Extraction of metabolites from liver tissue

Approximately 200 mg of wet liver tissue was weighted and extracted with 1 mL MeOH containing 500 pg/mL PGE₂-*d*₄, DHEA-*d*₄ and 403 pg/mL 13-HDHEA-*d*₄ using 3 \times 10 s tip sonication at 30% amplitude using a Branson Digital Sonifier 450 cell disruptor from Branson Ultrasonics Corporation (Danbury, USA). The resulting suspensions were centrifuged at 4 °C for 5 min at 3180 rcf and the supernatants were stored in a clean 15 mL falcon tube. The pellet was extracted once more with 1 mL MeOH containing the internal standards, ultimately resulting in a total of 2 mL tissue extract. The tissue extract was diluted with 8 mL ultrapure water containing 0.125% FA, before the samples were purified using HLB Oasis columns from Waters Chromatography B.V. (Etten-Leur, The Netherlands). Column purification was performed by activating the columns with 2 mL MeOH, followed by equilibrating with 2 mL ultrapure water containing 0.1% FA. Then the samples were loaded, and subsequently washed with 2 mL 20% MeOH in ultrapure water containing 0.1% FA. The columns were dried on the air for 15 min, followed by metabolite elution with 1 mL MeOH. The eluate is collected in borosilicate glass vials containing 20 μ L 500 μ M BHT and 10% glycerol in EtOH to limit auto-oxidation of the metabolites. The eluate was then evaporated using a Turbopap from Biotage (Uppsala, Sweden) and dissolved in 50 μ L EtOH.

6.3.9 UPLC-MS/MS analysis of *N*-acyl PUFA-derived metabolites

An ultra-pressure liquid chromatography coupled to tandem mass spectrometry (UPLC-MS/MS) method was developed to quantify the *N*-acyl PUFA derivatives DHEA, EPEA, AEA, and 13-HDHEA, 16-HDHEA, 10,11-EDP-EA, 19,20-EDP-EA as metabolites of DHEA using electrospray in positive ionization mode (ESI+). Standards used for the quantification were either commercially available or synthesized as described. The analyses were performed on an I-class fixed-loop UPLC coupled to a Xevo TQ-S triple-quadrupole MS from Waters Chromatography B.V. (Etten-Leur, the Netherlands). The electrospray interface was operated with a capillary voltage of 4.0 kV, a cone voltage of 50 V, and a desolvation temperature of 600 °C. The MS was operated in Multiple Reaction Mode (MRM), with mass transitions and collision energies that were optimized per component (**Table 6-1**). Chromatographic separation was performed on a Zorbax Eclipse Plus C18 Rapid Resolution HD, 1.8 μ column of 2.1 \times 150 mm from Agilent Technologies B.V. (Amstelveen, the Netherlands). For separation of the metabolites eluent A consisted of ultrapure water/ACN (95/5) with 0.1% FA; eluent B consisted of 100% ACN with 0.1% FA. The gradient started with 5% B in A followed by a linear increase to 50% B in A, which was achieved at min 5 and continued until min 8. This was followed by a linear increase towards 100 % B, which was achieved at min 13 and maintained until min 16, after which the column was equilibrated at 5% B in A which was maintained until min 21. During the run a flow rate of 0.5 mL/min, and a column temperature of 50 °C was set. The sample tray was cooled to 10 °C to limit auto-oxidation. For the quantification 6.0 μ L of standards and samples was injected. Peak identification and quantification were performed using TargetLynx version 4.1 software from Waters Chromatography B.V. (Breda, The Netherlands). Quality control samples were included to monitor the quality of the extraction and UPLC-MS/MS analysis.

Table 6-1 MS/MS fragmentations used for the targeted analysis of PUFA-derived metabolic compounds.

Compound	MS/MS fragmentation (<i>m/z</i>)	Collision Energy (eV)
DHEA	372.3 \rightarrow 62.2	15
EPEA	346.3 \rightarrow 62.2	15
AEA	348.3 \rightarrow 62.2	15
13-HDHEA	370.3 \rightarrow 62.2	15
16-HDHEA	370.3 \rightarrow 62.2	15
10,11-EDP-EA	370.3 \rightarrow 62.2	15
19,20-EDP-EA	370.3 \rightarrow 62.2	15

6.3.10 UPLC-MS/MS analysis of oxylipins

Quantification of PUFAs and oxylipins was performed using UPLC-MS/MS on an I-class fixed-loop UPLC coupled to a Xevo TQ-S triple-quadrupole MS using electrospray ionization in negative ionization mode (ESI⁻). Standards used for the quantification were commercially available. The electron spray interface was operated with a capillary voltage of 2.5 kV, cone voltage of 40 V, and desolvation temperature of 600 °C. The MS was operated in Multiple Reaction Mode (MRM), with mass transitions and collision energies that were optimized per component (**Table 6-2**).

Table 6-2 MS/MS fragmentations used for the targeted analysis of oxylipins.

Compound	MS/MS fragmentation (m/z)	Collision Energy (eV)
PGE ₂	315.1 → 271.1	15
PGD ₂	315.1 → 271.1	15
TBX ₂	369.2 → 169.1	15

Chromatographic separation was performed on a Zorbax Eclipse Plus C18 Rapid Resolution HD, 1.8μ column of 2.1 × 150 mm using eluent A consisting of ultrapure water/ACN (95/5) with 0.1% FA, and eluent B consisting of 100% ACN with 0.1% FA. The chromatographic method started with 5% B in A followed by a linear increase to 30% B in A, which was achieved at min 5. The gradient was then linearly increased to 50% B, which was achieved at min 11.25 and maintained until min 13.25. Then the gradient was increased to 100% B at min 15.75, which was maintained until min 18.75, after which the column was immediately brought back to 5% B in A and maintained until min 22. During the run a flow rate of 0.5 mL/min, and a column temperature of 50 °C was set. The sample tray was cooled to 10 °C to limit auto-oxidation. For the quantification 6.0 μL of standards and samples was injected. Peak identification and quantification were performed using TargetLynx version 4.1 software from Waters Chromatography B.V. (Breda, The Netherlands).

6.3.11 RNA extraction from mouse livers

A small piece of liver tissue was placed in 1 mL cold Trizol together with a stainless-steel bead (5 mm) from Qiagen Benelux B.V. (Venlo, The Netherlands). The liver was lysed in a tissue lyser for 30 s, while shaking. The tissue lysing was repeated, and 700 μL of Trizol solution was mixed with 140 μL chloroform. The suspension was centrifuged for 15 min at 4 °C at maximum speed to separate the layers, and 250 μL of the water phase was combined with 500 μL of EtOH before purification using a RNeasy® Micro kit from Qiagen Benelux B.V. (Venlo, The Netherlands). RNA purification was performed according to manufacturer's descriptions, and the RNA was eluted using 14 μL of RNase free water. RNA quantity and quality was assessed using nanodrop.

6.3.12 Quantitative reverse-transcription real-time PCR

RNA (1 µg per sample) was converted into complementary DNA (cDNA) using a Promega A3500 reverse transcriptase kit (Leiden, The Netherlands). Subsequently, cDNA was amplified by PCR using Sensimix SYBR mastermix from Bioline Reagents Ltd. (London, UK) on a CFX Real Time System apparatus from Bio-Rad (Veenendaal, The Netherlands). The following primer pairs were used for amplification of COX-2: 5'-TGAGCAAC-TATTCCAAACCAGC-3' (forward) and 5'-GCACGTAGTCTTCGATCACTATC-3' (reverse), IL-6: 5'-CTTCCATCCAGTTGCCTTCTTG-3' (forward) and 5'-AATTAAGCCTCCGACTTGTGAAG-3' (reverse), LPL: 5'-GGGAGTTTGGCTCCAGAGTTT-3' (forward) and 5'-TGTGTCTTCAGGG-GTCCTTAG-3' (reverse), MCP-1: 5'-CCCAATGAGTAGGCTGGAGA-3' (forward) and 5'-TCTG-GACCCATTCTTCTTG-3' (reverse), 36B4: 5'-ATGGGTACAAGCGCGTCCTG-3' (forward) and 5'-GCCTTGACCTTTTCAGTAAG-3' (reverse), ICAM-1: 5'-TGTGCTTTGAGAACTGTGGCA-3' (forward) and 5'-TGGCGGCTCAGTATCTCCTC-3' (reverse), CXCL1: 5'-CTGGGATTACCT-CAAGAACATC-3' (forward) and 5'-CAGGGTCAAGGCAAGCCTC-3' (reverse), TGF-β: 5'-CTC-CCGTGGCTTCTAGTGC-3' (forward) and 5'-CCTTAGTTTGGACAGGATCTG-3' (reverse), CYP450a14: 5'-AGGCAGTCCAATTCTACTTACG-3' (forward) and 5'-GCTCCTTGTCTTCAGAT-GG-3' (reverse). The samples were analyzed in duplicate and the mRNA expression was normalized to 36B4. The mRNA expression levels were expressed as average fold inductions compared to the vehicle non-DSS mice using standard deviation.

6.3.13 Statistical analysis

Phenotypic IBD data, like body weight, stool consistency and blood were measured each day for each individual mouse (vehicle – 2% DSS (n=10), 10 mg/kg DHEA – 2% DSS (n=10), 15 mg/kg DHEA – 2% DSS (n=10), vehicle – no DSS (n=6), 15 mg/kg DHEA – no DSS (n=6)). Measured body weight changes were shown as percentage compared to the initial weight of the mice at day -1. Statistical analysis was performed using linear mixed model with least significant difference (LSD) in SPSS based on the absolute weight values. Stool consistency and stool blood score were reported and analyzed for significance to the vehicle – DSS group using One-way ANOVA, Dunnett's multiple comparison *post-hoc* in Graphpad Prism v5.

At day 7 the colon length of each individual mouse was measured. Pathophysiological data including infiltration and crypt damage of the colon and MPO/protein concentration (pg/µg) to determine neutrophil infiltration in the colon were analyzed for a subset of mice. Significance to the vehicle, DSS group was analyzed using Dunnett's multiple comparison *post-hoc* in Graphpad Prism v5.

UPLC-MS/MS based liver concentrations of lipid derivatives are represented as scatter plots showing mean concentrations with error bars representing SEM. RNA expression

levels in the liver were assessed for each individual mouse and normalized to mean fold induction compared to the vehicle, DSS group. Significance to the vehicle, DSS group was analyzed using Dunnett's multiple comparison *post-hoc* in Graphpad Prism v5.

6.4 Results

6.4.1 DHEA treatment reduces a DSS-induced loss of body weight

All mice gained weight in a similar pattern until day 5, after which differences became apparent (**Figure 6-2**). At day 6 and 7, the DSS mice lost weight whereas the non-DSS groups continued to gain weight. With the DHEA-DSS treated mice the reduction in body weight started later and was less pronounced than with the vehicle-DSS control mice. At the final day of the experiment, day 7, the body weight loss of vehicle-DSS control mice was significantly different ($P<0.001$) compared to the non-DSS treated groups. Injection of 15 mg/kg DHEA ($p<0.05$) and 10 mg/kg DHEA ($p<0.01$) significantly reduced the body weight loss compared to DSS treated vehicle mice. The 10 mg/kg and 15 mg/kg DHEA DSS groups did not significantly differ from each other.

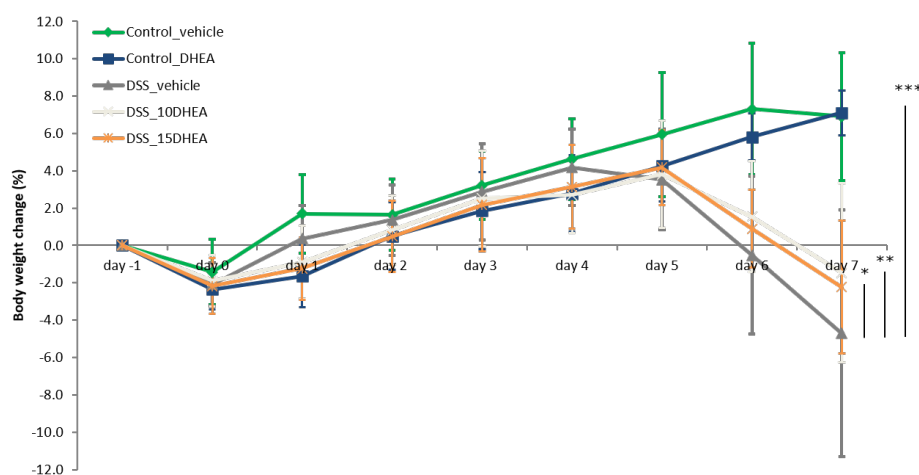


Figure 6-2 Body weight change of mice receiving i.p. injections of vehicle (arachis oil), DHEA (10 mg/kg or 15 mg/kg) in combination with or without 2% DSS in the drinking water, expressed as percentage compared to day -1. Green: vehicle, no DSS; Blue: 15 mg/kg DHEA, no DSS; Dark grey: vehicle, DSS; Light grey: 10 mg/kg DHEA, DSS; Orange: 15 mg/kg DHEA, DSS. Mean values with SD were plotted. Asterisks indicate significant differences from the vehicle DSS mice at day 7 determined using linear mixed model analysis using the actual body weights, LSD; * $P<0.05$, ** $P<0.01$, *** $P<0.001$).

6.4.2 DHEA improves stool consistency and diminishes blood content

Stool consistency and blood loss in the stool of the mice were analyzed, and results from day 5 and day 7 were plotted (**Figure 6-3**). Higher scores indicated a more loose and/or bloody stool. DSS treatment successfully induced colitis-like symptoms as indicated by the presence of loose and bloody stool. Stool consistency improved after 10 mg/kg DHEA ($p < 0.01$) and 15 mg/kg DHEA ($p < 0.01$) injection in DSS mice at day 5, but no difference between the DHEA groups was found (**Figure 6-3A**). The effect of DHEA injection on improvement of the stool consistency score was higher at day 5 than at day 7, as evidenced by the lack of significance at day 7 (**Figure 6-3B**). Again, also no significant differences were observed between the 10 mg/kg DHEA and 15 mg/kg DHEA injection. Scores of occult blood levels were also significantly reduced by 10 mg/kg DHEA and 15 mg/kg DHEA ($p < 0.001$) at day 5. At day 7 differences in blood stool levels of the DHEA-DSS mice and vehicle-DSS control mice were smaller but still significant ($p < 0.05$) (**Figure 6-3C** and **Figure 6-3D**). For occult blood levels also no significant differences were observed between the 10 mg/kg DHEA and 15 mg/kg DHEA injected groups. In general, the effects of DHEA injection on improvement of the stool consistency and reduction of the occult blood levels appeared to be stronger at day 5 than at day 7.

6.4.3 DHEA has limited effects on colon damage, colon length, and neutrophil infiltration

The effects of DHEA on colon tissue were further evaluated by scoring tissue damage, measuring colon length, and neutrophil activity. DSS treatment resulted in colitis-specific features such as the induction of crypt damage (**Figure 6-4A**), shortening of the colon (**Figure 6-4B**), and increased neutrophil activity in the proximal (**Figure 6-4C**) and distal colon (**Figure 6-4D**). In the DHEA injected DSS groups, no significant improvement on cellular inflammatory infiltration and crypt damage, increase of colon length, or reduction in neutrophil activity was observed. In conclusion, pathological analysis of the colon shows that DSS-induced inflammation is not reduced by DHEA treatment at day 7.

6.4.4 Targeted metabolomics reveals that only hepatic DHEA concentrations are affected by i.p. injection of DHEA

Liver DHEA and arachidonoyl ethanolamide (AEA, anandamide) levels were quantified using targeted UPLC-MS/MS analysis to investigate DHEA breakdown and possible effects on the endocannabinoid AEA in DHEA-injected DSS mice. The DSS-treated mice showed an increase in hepatic DHEA levels with increasing DHEA dose, reaching significance ($p < 0.01$) for 15 mg/kg DHEA compared to the vehicle treated mice (**Figure 6-5A**). For the non-DSS mice 15 mg/kg DHEA i.p. injections also resulted in significant increase in DHEA concentrations compared to the vehicle DSS ($p < 0.001$). Hepatic DHEA

concentrations were only affected by the DHEA injections and not by DSS-induced inflammation. For AEA, no significant differences in liver concentrations were observed (Figure 6-5B).

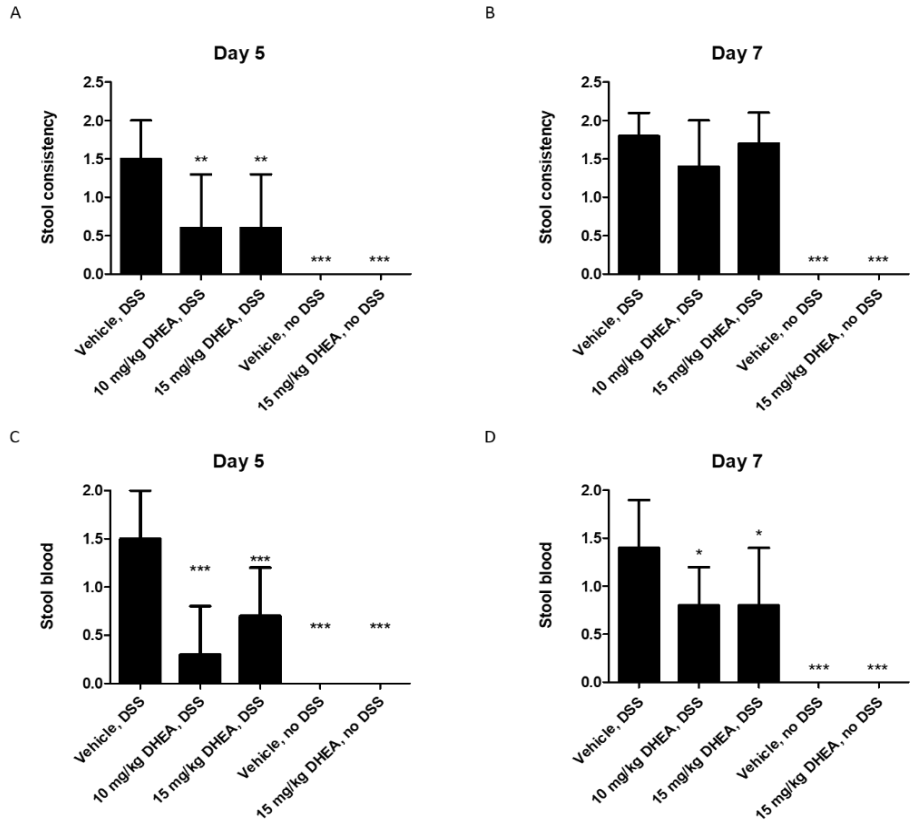


Figure 6-3 Stool consistency scores (A at day 5, B at day 7) and stool blood scores (C at day 5, D at day 7) of mice receiving i.p. injections of vehicle (arachis oil), DHEA (10 mg/kg or 15 mg/kg) in combination with or without 2% DSS in the drinking water. Bars represent means with error bars representing SD. Asterisks indicate significant differences compared to the DSS vehicle (One-way ANOVA, Dunnett's multiple comparison *post-hoc*; * $P < 0.05$, ** $P < 0.01$, *** $P < 0.001$).

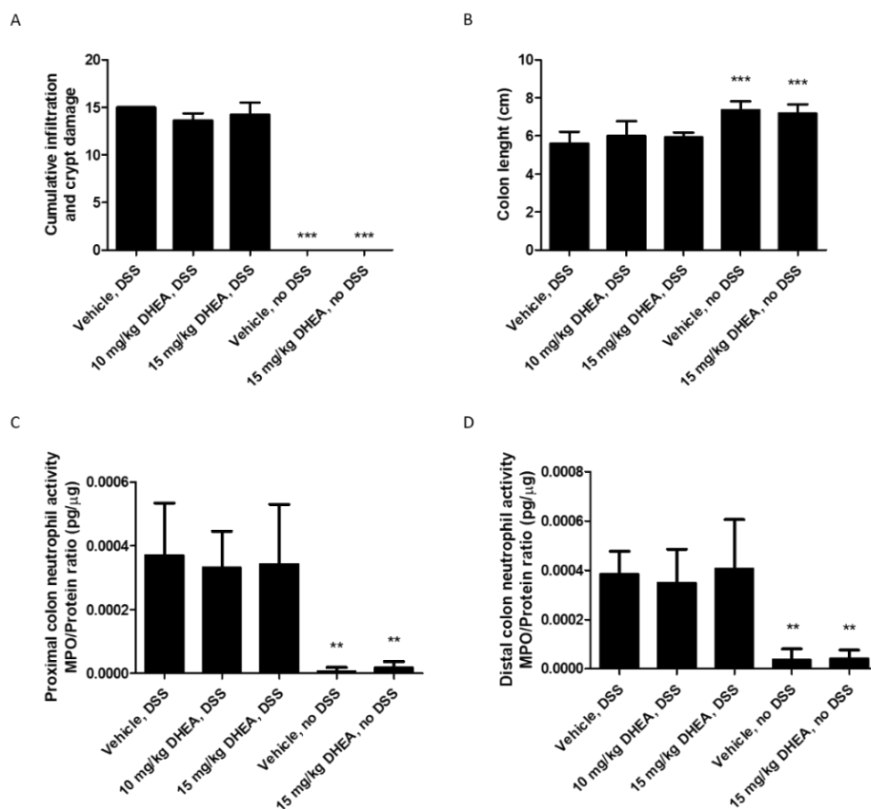


Figure 6-4 Histopathological markers of colon damage from mice receiving i.p. injections of vehicle (arachis oil), DHEA (10 mg/kg or 15 mg/kg) with or without 2% DSS in the drinking water. **A)** Colon damage score assessed by quantification of the cellular infiltration and crypt damage. Vehicle, 2% DSS (n=3), 10 mg/kg DHEA, 2% DSS (n=4), 15 mg/kg DHEA, 2% DSS (n=4), vehicle, no DSS (n=3), 15 mg/kg DHEA, no DSS (n=4). **B)** Measured colon lengths in cm. Vehicle, 2% DSS (n=10), 10 mg/kg DHEA, 2% DSS (n=10), 15 mg/kg DHEA, 2% DSS (n=10), vehicle, no DSS (n=6), 15 mg/kg DHEA, no DSS (n=6). **C)** and **D)** Normalized MPO derived neutrophil activity (pg/μg protein) in the proximal and distal colon. Vehicle, 2% DSS (n=6), 10 mg/kg DHEA, 2% DSS (n=6), 15 mg/kg DHEA, 2% DSS (n=6), vehicle, no DSS (n=4), 15 mg/kg DHEA, no DSS (n=4). Bars represent means and error bars represent SD. Asterisks indicate significant differences from the no DSS vehicle mice (One-way ANOVA, Dunnett's multiple comparison test *post-hoc*; * P<0.05, ** P<0.01, *** P<0.001).

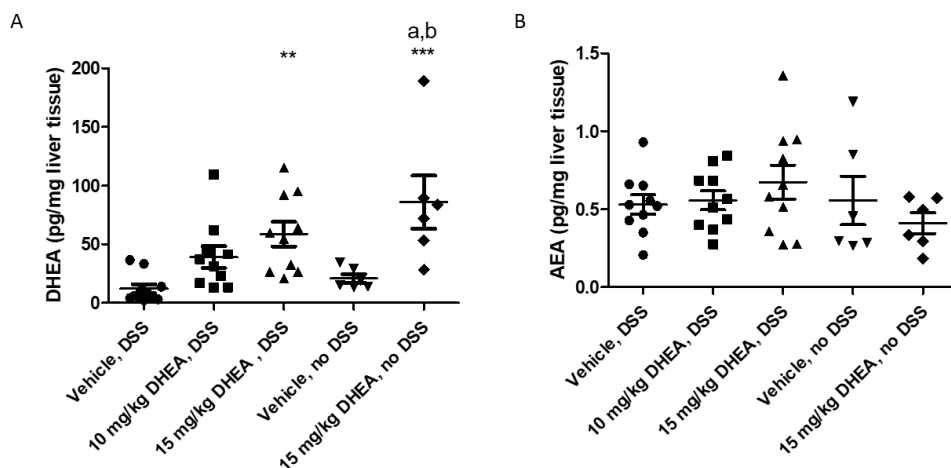


Figure 6-5 Liver tissue concentrations of DHEA (A) or AEA (B) of mice receiving i.p. injections of vehicle (arachis oil), DHEA (10 mg/kg or 15 mg/kg) in combination with or without 2% DSS in the drinking water. Vehicle, 2% DSS (n=10), 10 mg/kg DHEA, 2% DSS (n=10), 15 mg/kg DHEA, 2% DSS (n=10), vehicle, no DSS (n=6), 15 mg/kg DHEA, no DSS (n=6). Horizontal line represents the mean, and error bars show SEM. Asterisks indicate significant differences from the no DSS vehicle mice (One-way ANOVA, Dunnett's multiple comparison test *post-hoc*; * $P < 0.05$, ** $P < 0.01$, *** $P < 0.001$). a) significant to vehicle, no DSS ($p < 0.01$), b) significant to 10 mg/kg DHEA, DSS ($p < 0.05$) using One-way ANOVA, Tukey, *post-hoc*.

In order to investigate DHEA metabolism *in vivo*, the presence of hepatic DHEA derived COX-2 and CYP450 metabolites was also analyzed. COX-2 derived DHEA metabolites 13-HDHEA and 16-HDHEA were not detected (data not shown). CYP450 metabolites, 10,11-EDP-EA and 19,20-EDP-EA, were also not detected in the livers, potentially explained by the low recovery of these molecules (retrieving only 16% of 19,20-EDP-EA and 33% of 10,11-EDP-EA in quality control samples).

To further evaluate the inflammatory effect of the DSS administration and the potential resolving effect of DHEA injection on the liver, concentrations of prostaglandins PGE_2 and PGD_2 and the thromboxane B_2 (TBX_2) were measured in the mouse livers. For all three oxylipins no significant differences were observed between the groups (**Figure 6-6**).

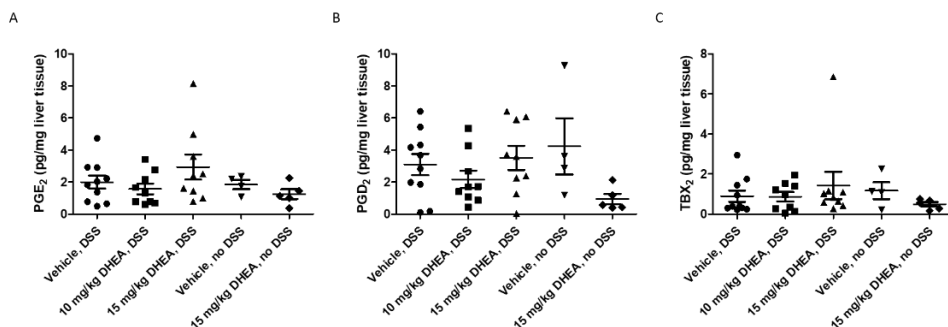


Figure 6-6 Liver tissue concentrations of PGE₂ (A), PGD₂ (B), and TBX₂ (C) in mice receiving i.p. injections of vehicle (arachis oil), DHEA (10 mg/kg or 15 mg/kg) in combination with or without 2% DSS in the drinking water. Vehicle, 2% DSS (n=10), 10 mg/kg DHEA, 2% DSS (n=9), 15 mg/kg DHEA, 2% DSS (n=9), vehicle, no DSS (n=4), 15 mg/kg DHEA, no DSS (n=5). Horizontal line represents the mean, and error bars show SEM. Statistical analysis using One-way ANOVA, Dunnett's multiple comparison test *post-hoc* was performed; no significant differences between vehicle, DSS and the other groups were obtained.

6.4.5 DHEA treatment reduces mRNA expression of pro-inflammatory genes in liver tissue

To further analyze the effect of both the DSS colitis and the DHEA treatment on the liver, mRNA gene expression levels of several liver inflammation and colitis markers were measured using RT-PCR; ICAM-1, TGF- β , LPL, CXCL-1, MCP-1, CYP4A14, IL-6, and COX-2. For ICAM-1 a significant reduction was observed in the 10 mg/kg DHEA DSS treated mice ($p < 0.001$) compared to the vehicle DSS mice (**Figure 6-7A**). ICAM-1 values were reduced to levels similar to non-DSS treated mice, indicating a full inhibition of the DSS-induced effect. Remarkably, ICAM-1 levels of the 15 mg/kg DHEA DSS treated group were not significantly reduced compared to the vehicle DSS mice. A similar result was observed for CXCL-1 expression in the DSS treated mice (**Figure 6-7B**). CXCL-1 levels were significantly reduced for the 10 mg/kg DHEA DSS group ($p < 0.001$) to levels comparable to the non-DSS treated groups. CXCL-1 levels for the 15 mg/kg DHEA DSS treated group were not significantly reduced.

For the inflammatory regulator MCP-1 a minor reducing effect of 15 mg/kg DHEA in the non-DSS group ($p < 0.05$) was obtained. MCP-1 expression in the liver of DSS-treated mice that received DHEA 15 mg/kg was significantly ($p < 0.01$) increased (**Figure 6-7C**). LPL levels were significantly induced in the 10 mg/kg DHEA DSS-treated mice ($p < 0.001$) compared to all other groups (**Figure 6-7D**). TGF- β and CYP4A14 RNA levels were not significantly affected by any of the treatments (**Figure 6-7E,F**). RNA levels of the

prototypical pro-inflammatory regulators COX-2 and IL-6 in the liver were too low to be accurately determined, indicating that both regulators were not clearly expressed in the livers of any of the treatment groups.

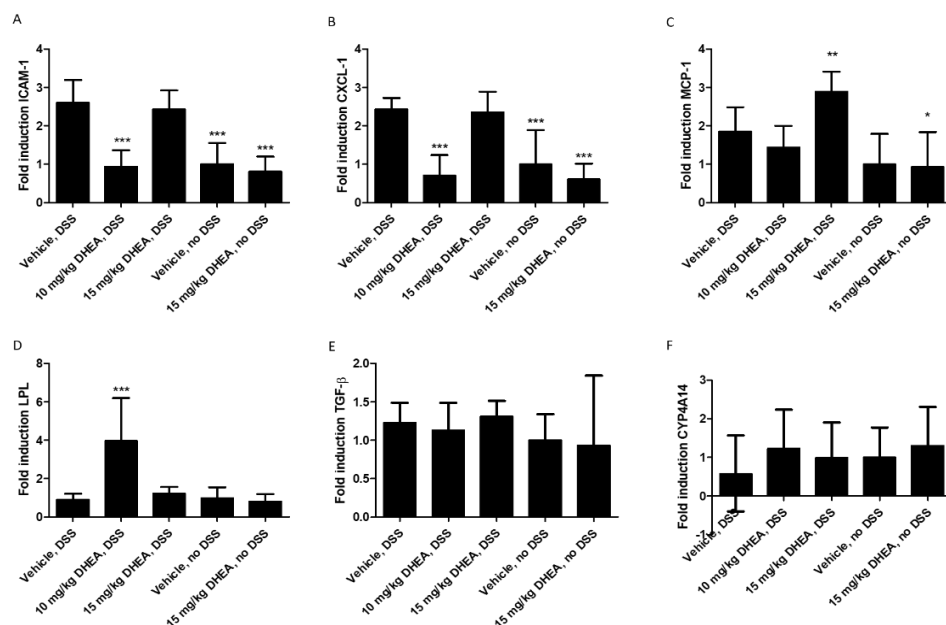


Figure 6-7 Gene expression of inflammation markers ICAM-1 (A), CXCL-1 (B), MCP-1 (C), LPL (D), TGF-β (E), and CYP4A14 (F) in livers of mice receiving vehicle treatment (arachis oil) or DHEA (10 mg/kg or 15 mg/kg) with or without 2% DSS in the drinking water. Vehicle, 2% DSS (n=10), 10 mg/kg DHEA, 2% DSS (n=10), 15 mg/kg DHEA, 2% DSS (n=10), vehicle, no DSS (n=6), 15 mg/kg DHEA, no DSS (n=6). Bars represent mean fold inductions containing standard deviations, where the vehicle, non-DSS treated group was set to 1.0. Asterisks indicate significant differences from the vehicle, DSS (One-way ANOVA, Dunnett's multiple comparison test *post-hoc*; * $P < 0.05$, ** $P < 0.01$, *** $P < 0.001$).

6.5 Discussion

In the current study we investigated the effect of i.p. injected DHEA on DSS-induced colitis in C57Bl/6 mice. Our data showed that repeated i.p. injection of DHEA leads to reduced weight loss, improved stool consistency, and reduced rectal bleeding in DSS-induced colitis. Targeted lipidomic UPLC-MS/MS analyses of the liver showed that hepatic DHEA levels were increased, indicating systemic availability and hepatic accumulation after i.p. DHEA injection. Despite the availability of the DHEA to the

liver, none of the known DHEA metabolites, 13-HDHEA, 16-HDHEA, 10,11-ED-PEA, and 19,20-EDP-EA were detected in the livers. In addition, no significant effects were found on histopathological markers of colon inflammation and production of the pro-inflammatory regulators PGE_2 , PGD_2 , and TBX_2 in the liver. Hepatic gene expression levels of ICAM-1, CXCL-1 and LPL, but not the inflammation markers TGF- β , MCP-1, IL-6, and COX-2, were modulated by 10 mg/kg DHEA injection in DSS treated mice.

Since DHEA treatment improved the manifestations of colitis such as weight loss, stool consistency, and occult blood levels in the stool, we were surprised not to observe any significant effects on colon inflammation and colon damage on day 7. Important to note is that stool consistency and rectal bleeding appeared to be more strongly reduced at day 5 when compared to day 7. Therefore, inhibition of pathological colitis markers might have occurred at time points before day 7. Body weight data and stool scores showed that the colitis worsens even after final administration of DSS (from day 5–7). Literature reports also indicate that aggravation of clinical colitis markers after DSS administration is common.^{26, 30–31} Consequently, in the present set-up, DHEA might only have attenuated the initial and still limited phenotypical colitis symptoms at day 5, while being no longer capable to reduce the augmented inflammation at day 7. In addition to this, DHEA was no longer injected at day 7 whereas this might be required for a continued effect. Studies showing positive effects of PUFA-derived compounds continued treatment until section, thus achieving longer continuation of the resolution of inflammatory processes.^{27, 32} Therefore, in future experiments DHEA treatment until anesthetization would be advisable. In addition to continuing treatment with DHEA post-DSS, starting with DHEA before initiating DSS administration can provide information about the protective effect of DHEA. Previously, i.p. injections with palmitoyl ethanolamide (PEA) at 10 mg/kg were successful in reducing DSS induced colitis,³² and i.p. DHEA injections of 10 mg/kg were successful in reducing formaldehyde-induced pain.¹⁸ In our study, a dosing of 15 mg/kg DHEA did not give better results compared to 10 mg/kg DHEA. It is thus expected that i.p. injections of 10 mg/kg DHEA result in an effective dosing. Next to the timing and dosing of the PUFA-metabolite administration, the administration route is also an important determinant for its effectiveness. Oral administration might be more attractive compared to i.p. injection, but there are no data yet about the stability of DHEA along the GI tract and within the gut epithelium. Although methodological differences in study design are apparent, the DHEA precursor DHA and several PUFA-derived metabolites were reported to reduce colitis.^{27–28} For example, orally administered DHA (30 mg/kg) increased colitis induced colon lengths, reduced colon inflammation, and reduced myeloperoxidase, but had no significant effect on the stool consistency and rectal bleeding in 5% DSS administered BALB/c mice.²⁸ For i.p. injected DHEA we did find significant effects on the stool consistency

and rectal bleeding, but not on the colon length, colon damage, and neutrophil activity. These somewhat contradicting results between DHA and DHEA could indicate that DHA and DHEA both affect colitis in a different manner. PEA given intraperitoneally at 10 mg/kg to C57BL/6 mice receiving 5% DSS via their drinking water did result in reduced colon damage and MPO activity.³² These results seem to imply that i.p. injected PEA is more potent and/or acts on different targets compared to DHEA in attenuating DSS induced colon damage. Orally administered 318 mg/kg MAG-EPA, an eicosapentaenoyl derived metabolite, was able to reduce phenotypic colitis symptoms, colon damage, and protect against DSS colitis induction in 4% DSS administered rats.²⁷ Clearly, the high oral dosing of MAG-EPA makes a direct comparison to our study invalid.

Effects on hepatic lipid mediators of inflammation, PUFA metabolites, and endocannabinoid profiles were analyzed to investigate their involvement in colitis and possible effects on DHEA injection.³³ Recent investigations have shown that changes in liver metabolites are influenced by intestinal effects of DSS-induced colitis,³⁴ further warranting our metabolic profiling study in the livers. As expected, DHEA concentrations in the liver were significantly increased with increasing DHEA dose, demonstrating systemic availability of the i.p. injected DHEA and showing that is not rapidly broken down. At present, neither kinetic nor general *in vivo* stability data on DHEA are available. DSS administration was found not to influence hepatic DHEA content. EPEA concentrations could not be quantified with adequate robustness, but were found to be low in all groups which is in correspondence with previous data on EPEA levels in mice and rat livers.³⁵⁻³⁶ AEA levels were not significantly affected in any of the groups, which seems to exclude competition between DHEA and AEA for the hydrolytic enzymes FAAH and/or NAAA under the present conditions.^{2, 10, 32, 37-38} Ambiguity exists about the effect of colitis on AEA and endocannabinoid tone in the affected tissues.^{2, 39} Most studies on this topic were performed in colon tissue, but one study in TNBS-induced colitis livers showed only a small increase in hepatic AEA levels.³² Therefore, colitis seems to have a minimal effect on hepatic *N*-acyl PUFA-derived metabolite levels. Clearly, understanding of the complex interplay between PUFAs, PUFA derivatives, endocannabinoids, and their metabolism in the gut-liver axis in colitis requires more research.

Although the livers contained substantial amounts of DHEA, DHEA-derived metabolites 13-HDHEA, 16-HDHEA, 10,11-EDP-EA, and 19,20-EDP-EA were not detected in the liver. Because 13-HDHEA and 16-HDHEA are COX-2- derived products,¹⁶ the absence of hepatic 13-HDHEA and 16-HDHEA in the current study is potentially explained by the low expression level of COX-2 in our model. CYP450-derived metabolites of DHEA, 10,11-EDP-EA and 19,20-EDP-EA were previously characterized in livers of Sprague-Dawley rats,²² but these metabolites were not detected in the current study. EDP-EAs are synthesized

under inflammatory conditions,²² but evidence of significant hepatic inflammation in our model was lacking, potentially explaining why 10,11-EDP-EA and 19,20-EDP-EA were not observed. Furthermore, literature showed that many hepatic CYP450s are actually downregulated during DSS administration.⁴⁰⁻⁴² Nonetheless, production of EDP-EAs would then still be expected in the 15 mg/kg DHEA injected no-DSS group. Therefore, it is more likely that the CYP450s responsible for the production of 10,11-EDP-EA and 19,20-EDP-EA are not expressed in the liver at all. Apart from these biological explanations, problems in the current workup (retrieving only 16% of 19,20-EDP-EA and 33% of 10,11-EDP-EA of the spiked standards) provide a likely explanation why EDP-EAs were not detected. Optimisation of the purification method for epoxidated DHEA-derived products is required for future studies on epoxide derivatives of DHEA. Additionally, the liver samples were stored for 7 years until they were extracted (stored in the bio-bank at -80°C), which could have resulted in degradation of the relatively unstable epoxides. Biological hydrolysis of epoxides by epoxide hydrolases resulting in the formation of the corresponding diol could also not be ruled out.^{22, 43} In conclusion, none of the COX-2 and CYP450- derived DHEA metabolites were detected in the liver, which is most likely due to the lack of the expression of these enzymes and/or the relative long storage period of the livers.

No significant differences were found in PGE_2 , PGD_2 , and TBX_2 concentrations in the liver. Previous *in vitro* work from our group showed that the presence of DHEA reduces the levels of PGE_2 and PGD_2 in LPS-stimulated RAW macrophages,^{16, 44} but such an inhibition was not observed in the liver despite the higher DHEA content. Again, this result is most likely explained by the poor expression of COX-2 in the livers. Detectable mRNA expression levels of the pro-inflammatory cytokine IL-6 were also not obtained, and gene expression levels of the profibrogenic regulator TGF- β were not significantly affected by DHEA. Levels of the pro-inflammatory regulator MCP-1 were only significantly reduced for 15 mg/kg DHEA and DSS-treated mice. LPL levels were significantly increased in livers of the 10 mg/kg DHEA treated mice. For LPL it is difficult to interpret the observed effects, because multiple factors influence its expression. DSS administration results in lower LPL levels in the liver,⁴⁵ whereas *n*-3 PUFA supplementation generally increases LPL expression.⁴⁶⁻⁴⁷ Additionally, CB₁ receptor activation could result in increased LPL expression.⁴⁸ Gene expression levels of ICAM-1 and CXCL-1 were decreased in the livers of 10 mg/kg DHEA injected DSS mice. ICAM-1 expression is related to recruitment of leukocytes, and previously DSS administration led to increased hepatic ICAM-1 levels.⁴⁹ CXCL-1 is a neutrophil attractant of which the expression is induced in the liver during inflammation.⁵⁰⁻⁵¹ CXCL-1 knockout mice showed increased susceptibility to DSS-induced colitis.⁵¹ Reduced hepatic CXCL-1 levels can thus be associated with attenuation of liver inflammation. Remarkably, it seems

that especially 10 mg/kg DHEA treatment resulted in a more anti-inflammatory gene profile, when compared to 15 mg/kg DHEA in the DSS treated groups. These results seem to be in correspondence with the phenotypic and pathophysiological results, which seem to indicate that there is an optimum dosing for DHEA. Nonetheless, conclusive evidence for statements about the metabolic implications or origin of the implied dosing optimum is lacking. In conclusion, 2% DSS administration can not immediately be linked to liver inflammation based on the RNA expression profiles measured, as evidenced by undetectable levels of COX-2 and IL-6. Correspondingly, others previously reported that DSS treatment alone often does not significantly induce liver inflammation, but that hepatic metabolism could be affected.^{34, 40, 45, 52}

More research is required to understand the potential effects of DHEA on colitis. Phenotypic markers of colitis were significantly reduced by DHEA, but longer treatment and other routes of administration may be required to obtain observable effects at the histological level. Future studies should also focus on the analysis of PUFA and endocannabinoid profiles in both the colon and liver of DSS-administrated mice to better understand the role of PUFA metabolism in the colon and gut-liver axis during colitis progression. Finally, more research is required to understand the biological relevance of COX-2, LOX, and CYP450 oxidation of DHEA to further substantiate the immune-regulating effect of its metabolites.

To summarize, we showed that i.p. injected DHEA leads to a small but significant reduction of the phenotypic DSS-induced colitis markers, but does not lead to reduced inflammation of the colon. Additionally, significant inflammation of the liver was not observed in our model as evidenced by the lack in expression of COX-2, IL-6, MCP-1, TGF- β , and the lack in upregulation of pro-inflammatory lipids like prostaglandins and thromboxanes. DHEA levels in the livers of the mice were significantly increased after intraperitoneal injection of DHEA, suggesting that i.p administration of DHEA leads to uptake and distribution into at least the liver. DHEA-derived metabolites of COX-2 and LOX were not detected in the liver tissues after DSS treatment.

6.6 Acknowledgements

The authors thank Hans Beijleveld, Frank Claassen, and Francel Verstappen for their assistance in the HPLC and mass spectrometry analysis; Sandra van Krimpen, Dennis J. Doorduyn, Eveline van Leeuwen, and Bram G. Soliman for their helpful assistance on this project. The authors thank the VLAG Graduate School of Wageningen University and Research for their financial support.

6.7 References

1. Alatab, S.; Sepanlou, S. G.; Ikuta, K.; Vahedi, H.; Bisignano, C.; Safiri, S.; Sadeghi, A.; Nixon, M. R.; Abdoli, A.; Abolhassani, H.; et al., The global, regional, and national burden of inflammatory bowel disease in 195 countries and territories, 1990-2017: a systematic analysis for the Global Burden of Disease Study 2017. *Lancet Gastroenterol. Hepatol.* **2020**, *5* (1), 17-30.
2. Alhouayek, M.; Ameraoui, H.; Muccioli, G. G., Bioactive lipids in inflammatory bowel diseases – From pathophysiological alterations to therapeutic opportunities. *Biochim. Biophys. Acta Mol. Cell Biol. Lipids* **2021**, *1866* (2), 158854.
3. Alhouayek, M.; Muccioli, G. G., The endocannabinoid system in inflammatory bowel diseases: from pathophysiology to therapeutic opportunity. *Trends. Mol. Med.* **2012**, *18* (10), 615-625.
4. Jairath, V.; Feagan, B. G., Global burden of inflammatory bowel disease. *Lancet Gastroenterol. Hepatol.* **2020**, *5* (1), 2-3.
5. Mak, W. Y.; Zhao, M.; Ng, S. C.; Burisch, J., The epidemiology of inflammatory bowel disease: East meets west. *J. Gastroenterol. Hepatol.* **2020**, *35* (3), 380-389.
6. Marton, L. T.; Goulart, R. d. A.; Carvalho, A. C. A. d.; Barbalho, S. M., Omega Fatty Acids and Inflammatory Bowel Diseases: An Overview. *Int. J. Mol. Sci.* **2019**, *20* (19), 4851.
7. Scaioli, E.; Liverani, E.; Belluzzi, A., The Imbalance between n-6/n-3 Polyunsaturated Fatty Acids and Inflammatory Bowel Disease: A Comprehensive Review and Future Therapeutic Perspectives. *Int. J. Mol. Sci.* **2017**, *18* (12).
8. de Bus, I.; Witkamp, R.; Zuilhof, H.; Albada, B.; Balvers, M., The role of n-3 PUFA-derived fatty acid derivatives and their oxygenated metabolites in the modulation of inflammation. *Prostaglandins Other Lipid Mediat.* **2019**, *144*, 106351.
9. Serhan, C. N.; Levy, B. D., Resolvins in inflammation: emergence of the pro-resolving superfamily of mediators. *J. Clin. Investig.* **2018**, *128* (7), 2657-2669.
10. Meijerink, J.; Balvers, M. G. J.; Witkamp, R. F., N-acyl amines of docosahexaenoic acid and other n-3 polyunsaturated fatty acids – from fishy endocannabinoids to potential leads. *Br. J. Pharmacol.* **2013**, *169* (4), 772-783.
11. Wang, Y.; Balvers, M. G. J.; Hendriks, H. F. J.; Wilpshaar, T.; van Heek, T.; Witkamp, R. F.; Meijerink, J., Docosahexaenoyl serotonin emerges as most potent inhibitor of IL-17 and CCL-20 released by blood mononuclear cells from a series of N-acyl serotonins identified in human intestinal tissue. *Biochim. Biophys. Acta Mol. Cell Biol. Lipids* **2017**, *1862* (9), 823-831.
12. Wang, Y.; Plastina, P.; Vincken, J.-P.; Jansen, R.; Balvers, M.; ten Klooster, J. P.; Gruppen, H.; Witkamp, R.; Meijerink, J., N-Docosahexaenoyl Dopamine, an Endocannabinoid-like Conjugate of Dopamine and the n-3 Fatty Acid Docosahexaenoic Acid, Attenuates Lipopolysaccharide-Induced Activation of Microglia and Macrophages via COX-2. *ACS Chem. Neurosci.* **2017**, *8* (3), 548-557.
13. Poland, M.; ten Klooster, J. P.; Wang, Z.; Pieters, R.; Boekschoten, M.; Witkamp, R.; Meijerink,

- J., Docosahexaenoyl serotonin, an endogenously formed n-3 fatty acid-serotonin conjugate has anti-inflammatory properties by attenuating IL-23–IL-17 signaling in macrophages. *Biochim. Biophys. Acta Mol. Cell Biol. Lipids* **2016**, *1861* (12, Part A), 2020-2028.
14. Balvers, M. G. J.; Verhoeckx, K. C. M.; Bijlsma, S.; Rubingh, C. M.; Meijerink, J.; Wortelboer, H. M.; Witkamp, R. F., Fish oil and inflammatory status alter the n-3 to n-6 balance of the endocannabinoid and oxylipin metabolomes in mouse plasma and tissues. *Metabolomics* **2012**, *8* (6), 1130-1147.
15. Balvers, M. G. J.; Wortelboer, H. M.; Witkamp, R. F.; Verhoeckx, K. C. M., Liquid chromatography–tandem mass spectrometry analysis of free and esterified fatty acid N-acyl ethanolamines in plasma and blood cells. *Anal. Biochem.* **2013**, *434* (2), 275-283.
16. de Bus, I.; Zuilhof, H.; Witkamp, R.; Balvers, M.; Albada, B., Novel COX-2 products of n-3 polyunsaturated fatty acid-ethanolamine-conjugates identified in RAW 264.7 macrophages. *J. Lipid Res.* **2019**, *60* (11), 1829-1840.
17. Meijerink, J.; Plastina, P.; Vincken, J.-P.; Poland, M.; Attya, M.; Balvers, M.; Gruppen, H.; Gabriele, B.; Witkamp, R. F., The ethanolamide metabolite of DHA, docosahexaenoyl ethanolamine, shows immunomodulating effects in mouse peritoneal and RAW 264.7 macrophages: evidence for a new link between fish oil and inflammation. *Br. J. Nutr.* **2011**, *105* (12), 1798-1807.
18. Paton, K. F.; Shirazi, R.; Vyssotski, M.; Kivell, B. M., N-docosahexaenoyl ethanolamine (synaptamide) has antinociceptive effects in male mice. *Eur. J. Pain* **2020**, *24* (10), 1990-1998.
19. Kim, H.-Y.; Spector, A. A., N-Docosahexaenoyl ethanolamine: A neurotrophic and neuroprotective metabolite of docosahexaenoic acid. *Mol. Aspects Med.* **2018**, *64*, 34-44.
20. Park, T.; Chen, H.; Kim, H.-Y., GPR110 (ADGRF1) mediates anti-inflammatory effects of N-docosahexaenoyl ethanolamine. *J. Neuroinflammation* **2019**, *16* (1), 225.
21. Huang, B. X.; Hu, X.; Kwon, H.-S.; Fu, C.; Lee, J.-W.; Southall, N.; Marugan, J.; Kim, H.-Y., Synaptamide activates the adhesion GPCR GPR110 (ADGRF1) through GAIN domain binding. *Commun. Biol.* **2020**, *3* (1), 109.
22. McDougale, D. R.; Watson, J. E.; Abdeen, A. A.; Adili, R.; Caputo, M. P.; Krapf, J. E.; Johnson, R. W.; Kilian, K. A.; Holinstat, M.; Das, A., Anti-inflammatory ω -3 endocannabinoid epoxides. *Proc. Natl. Acad. Sci. U.S.A.* **2017**, *114* (30), E6034-E6043.
23. Roy, J.; Watson, J. E.; Hong, I. S.; Fan, T. M.; Das, A., Antitumorigenic Properties of Omega-3 Endocannabinoid Epoxides. *J. Med. Chem.* **2018**, *61* (13), 5569–5579.
24. Watson, J. E.; Kim, J. S.; Das, A., Emerging class of omega-3 fatty acid endocannabinoids & their derivatives. *Prostaglandins Other Lipid Mediat.* **2019**, *143*, 106337.
25. Yang, R.; Fredman, G.; Krishnamoorthy, S.; Agrawal, N.; Irimia, D.; Piomelli, D.; Serhan, C. N., Decoding Functional Metabolomics with Docosahexaenoyl Ethanolamide (DHEA) Identifies Novel Bioactive Signals. *J. Biol. Chem.* **2011**, *286* (36), 31532-31541.
26. Eichele, D. D.; Kharbanda, K. K., Dextran sodium sulfate colitis murine model: An indispensable tool for advancing our understanding of inflammatory bowel diseases pathogenesis. *World J. Gastroenterol.* **2017**, *23* (33), 6016-6029.

27. Morin, C.; Blier, P. U.; Fortin, S., MAG-EPA reduces severity of DSS-induced colitis in rats. *Am. J. Physiol. Gastrointest. Liver Physiol.* **2016**, *310*(10), G808-G821.
28. Cho, J. Y.; Chi, S.-G.; Chun, H. S., Oral administration of docosahexaenoic acid attenuates colitis induced by dextran sulfate sodium in mice. *Mol. Nutr. Food Res.* **2011**, *55*(2), 239-246.
29. Koelink, P. J.; Robanus-Maandag, E. C.; Devilee, P.; Hommes, D. W.; Lamers, C. B. H. W.; Verspaget, H. W., 5-Aminosalicylic acid inhibits colitis-associated but not sporadic colorectal neoplasia in a novel conditional Apc mouse model. *Carcinogenesis* **2009**, *30*(7), 1217-1224.
30. Hall, L. J.; Faivre, E.; Quinlan, A.; Shanahan, F.; Nally, K.; Melgar, S., Induction and Activation of Adaptive Immune Populations During Acute and Chronic Phases of a Murine Model of Experimental Colitis. *Dig. Dis. Sci.* **2011**, *56*(1), 79-89.
31. Perše, M.; Cerar, A., Dextran Sodium Sulphate Colitis Mouse Model: Traps and Tricks. *J. Biomed. Biotechnol.* **2012**, *2012*, 718617.
32. Alhouayek, M.; Bottemanne, P.; Subramanian, K. V.; Lambert, D. M.; Makriyannis, A.; Cani, P. D.; Muccioli, G. G., N-Acylethanolamine-hydrolyzing acid amidase inhibition increases colon N-palmitoylethanolamine levels and counteracts murine colitis. *FASEB J.* **2015**, *29*(2), 650-661.
33. Cani, P. D.; Plovier, H.; Van Hul, M.; Geurts, L.; Delzenne, N. M.; Druart, C.; Everard, A., Endocannabinoids -- at the crossroads between the gut microbiota and host metabolism. *Nat. Rev. Endocrinol.* **2016**, *12*(3), 133-143.
34. Kim, S. H.; Lee, W.; Kwon, D.; Lee, S.; Son, S. W.; Seo, M.-S.; Kim, K. S.; Lee, Y.-H.; Kim, S.; Jung, Y.-S., Metabolomic Analysis of the Liver of a Dextran Sodium Sulfate-Induced Acute Colitis Mouse Model: Implications of the Gut-Liver Connection. *Cells* **2020**, *9*(2), 341.
35. Artmann, A.; Petersen, G.; Hellgren, L. I.; Boberg, J.; Skonberg, C.; Nellesmann, C.; Hansen, S. H.; Hansen, H. S., Influence of dietary fatty acids on endocannabinoid and N-acylethanolamine levels in rat brain, liver and small intestine. *Biochim. Biophys. Acta Mol. Cell Biol. Lipids* **2008**, *1781*(4), 200-212.
36. Balvers, M. G. J.; Verhoeckx, K. C. M.; Meijerink, J.; Bijlsma, S.; Rubingh, C. M.; Wortelboer, H. M.; Witkamp, R. F., Time-dependent effect of in vivo inflammation on eicosanoid and endocannabinoid levels in plasma, liver, ileum and adipose tissue in C57BL/6 mice fed a fish-oil diet. *Int. Immunopharmacol.* **2012**, *13*(2), 204-214.
37. Bisogno, T.; Delton-Vandenbroucke, I.; Milone, A.; Lagarde, M.; Di Marzo, V., Biosynthesis and Inactivation of N-Arachidonylethanolamine (Anandamide) and N-Docosahexaenylethanolamine in Bovine Retina. *Arch. Biochem. Biophys.* **1999**, *370*(2), 300-307.
38. Alhouayek, M.; Bottemanne, P.; Makriyannis, A.; Muccioli, G. G., N-acylethanolamine-hydrolyzing acid amidase and fatty acid amide hydrolase inhibition differentially affect N-acylethanolamine levels and macrophage activation. *Biochim. Biophys. Acta Mol. Cell Biol. Lipids* **2017**, *1862*(5), 474-484.
39. Ambrose, T.; Simmons, A., Cannabis, Cannabinoids, and the Endocannabinoid System-Is there Therapeutic Potential for Inflammatory Bowel Disease? *J Crohns Colitis* **2019**, *13*(4), 525-535.

40. Masubuchi, Y.; Horie, T., Endotoxin-mediated disturbance of hepatic cytochrome P450 function and development of endotoxin tolerance in the rat model of dextran sulfate sodium-induced experimental colitis. *Drug Metab. Dispos.* **2004**, *32* (4), 437.
41. Fan, X.; Ding, X.; Zhang, Q.-Y., Hepatic and intestinal biotransformation gene expression and drug disposition in a dextran sulfate sodium-induced colitis mouse model. *Acta Pharm. Sin. B.* **2020**, *10* (1), 123-135.
42. Hu, N.; Huang, Y.; Gao, X.; Li, S.; Yan, Z.; Wei, B.; Yan, R., Effects of dextran sulfate sodium induced experimental colitis on cytochrome P450 activities in rat liver, kidney and intestine. *Chem. Biol. Interact.* **2017**, *271*, 48-58.
43. dos Santos, L. R. B.; Fleming, I., Role of cytochrome P450-derived, polyunsaturated fatty acid mediators in diabetes and the metabolic syndrome. *Prostaglandins Other Lipid Mediat.* **2020**, *148*, 106407.
44. Meijerink, J.; Poland, M.; Balvers, M. G. J.; Plastina, P.; Lute, C.; Dwarkasing, J.; van Norren, K.; Witkamp, R. F., Inhibition of COX-2-mediated eicosanoid production plays a major role in the anti-inflammatory effects of the endocannabinoid N-docosahexaenylethanolamine (DHEA) in macrophages. *Br. J. Pharmacol.* **2015**, *172* (1), 24-37.
45. Karlsson, A.; Järgvall, Å.; Pettersson, M.; Andersson, A.-K.; Gillberg, P.-G.; Melgar, S., Dextran sulphate sodium induces acute colitis and alters hepatic function in hamsters. *Int. Immunopharmacol.* **2008**, *8* (1), 20-27.
46. Bays, H. E.; Tighe, A. P.; Sadosky, R.; Davidson, M. H., Prescription omega-3 fatty acids and their lipid effects: physiologic mechanisms of action and clinical implications. *Expert Rev. Cardiovasc. Ther.* **2008**, *6* (3), 391-409.
47. Barbosa AM, C. T., Nunes EA, Fatty liver and n-3 fatty acids ingestion: New mechanisms and perspectives from pre-clinical animal models. *Liver Pancreat Sci* **2016**, *1*.
48. Tam, J.; Liu, J.; Mukhopadhyay, B.; Cinar, R.; Godlewski, G.; Kunos, G., Endocannabinoids in liver disease. *Hepatology* **2011**, *53* (1), 346-355.
49. Soriano, A.; Salas, A.; Salas, A.; Sans, M.; Gironella, M.; Elena, M.; Anderson, D. C.; Piqué, J. M.; Panés, J., VCAM-1, but Not ICAM-1 or MAdCAM-1, Immunoblockade Ameliorates DSS-Induced Colitis in Mice. *Lab. Investig.* **2000**, *80* (10), 1541-1551.
50. Rovai, L. E.; Herschman, H. R.; Smith, J. B., The murine neutrophil-chemoattractant chemokines LIX, KC, and MIP-2 have distinct induction kinetics, tissue distributions, and tissue-specific sensitivities to glucocorticoid regulation in endotoxemia. *J. Leukoc. Biol.* **1998**, *64* (4), 494-502.
51. Shea-Donohue, T.; Thomas, K.; Cody, M. J.; Aiping, Z.; Detolla, L. J.; Kopydlowski, K. M.; Fukata, M.; Lira, S. A.; Vogel, S. N., Mice deficient in the CXCR2 ligand, CXCL1 (KC/GRO-alpha), exhibit increased susceptibility to dextran sodium sulfate (DSS)-induced colitis. *Innate Immun.* **2008**, *14* (2), 117-124.
52. Gäbele, E.; Dostert, K.; Hofmann, C.; Wiest, R.; Schölmerich, J.; Hellerbrand, C.; Obermeier, F., DSS induced colitis increases portal LPS levels and enhances hepatic inflammation and fibrogenesis in experimental NASH. *J. Hepatol.* **2011**, *55* (6), 1391-1399.

Supporting information belonging to Chapter 6

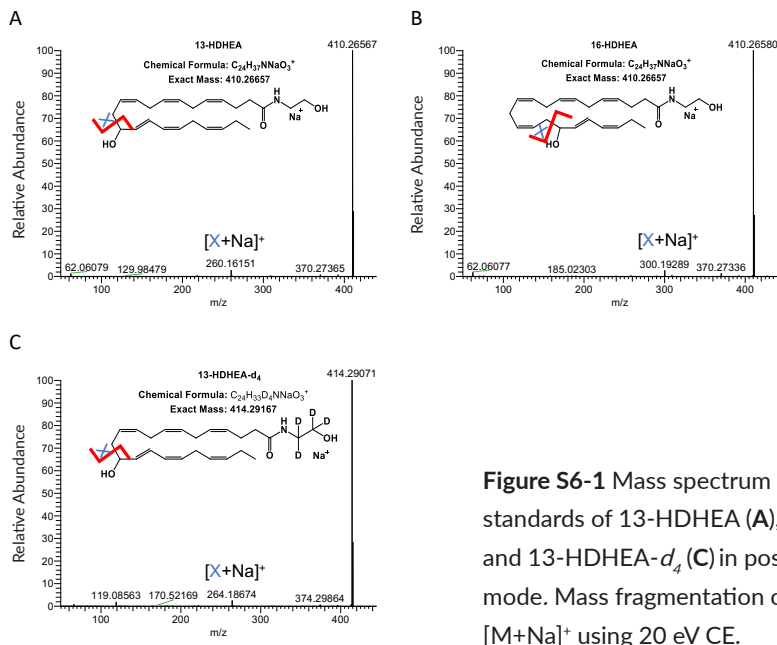


Figure S6-1 Mass spectrum of synthesized standards of 13-HDHEA (A), 16-HDHEA (B), and 13-HDHEA- d_4 (C) in positive ionisation mode. Mass fragmentation of $m/z = 410.2$ $[M+Na]^+$ using 20 eV CE.

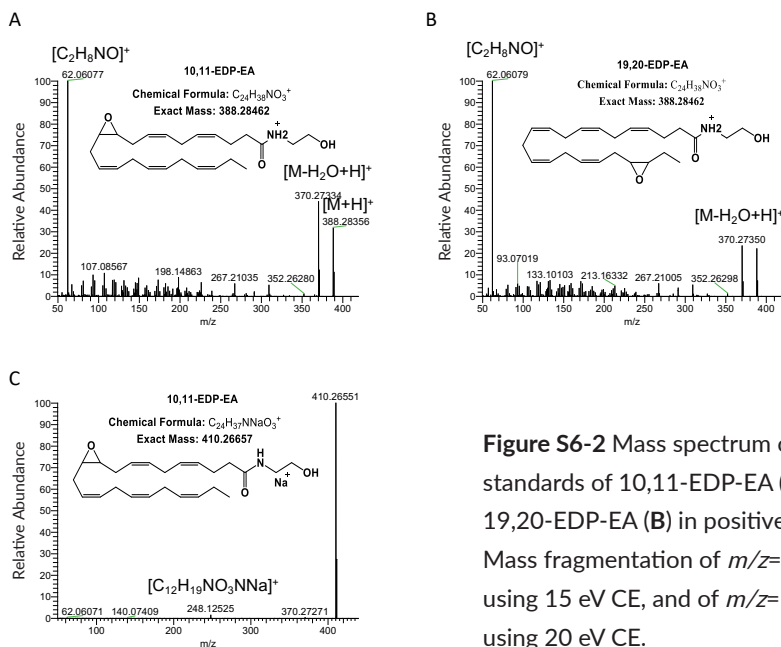


Figure S6-2 Mass spectrum of synthesized standards of 10,11-EDP-EA (A,C) and 19,20-EDP-EA (B) in positive ionisation mode. Mass fragmentation of $m/z = 388.2$ $[M+H]^+$ using 15 eV CE, and of $m/z = 410.2$ $[M+Na]^+$ using 20 eV CE.

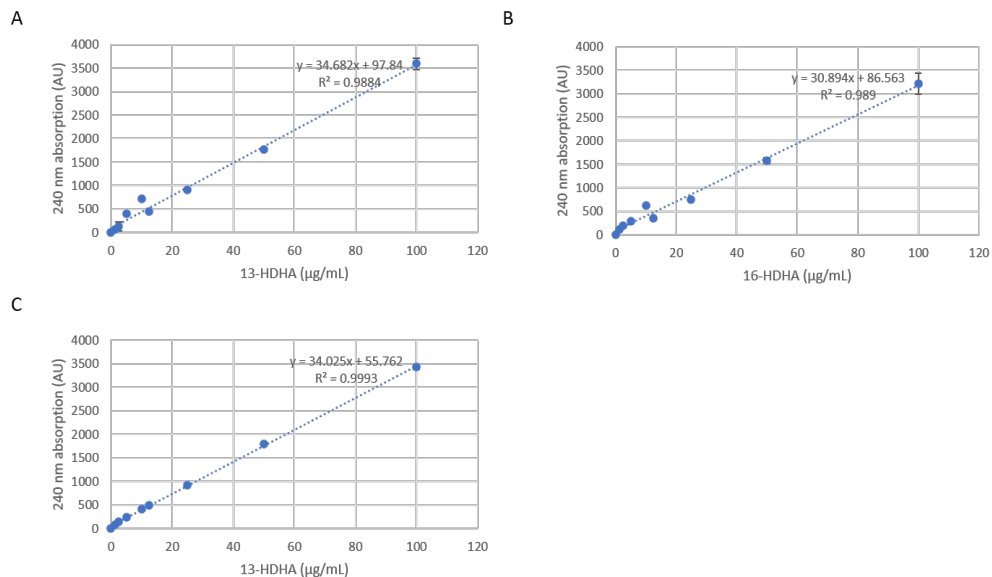


Figure S6-3 Calibration curve showing AUC at 240 nm absorption for 13-HDHA to quantify 13-HDHEA (**A**), of 16-HDHA to quantify 16-HDHEA (**B**), and of 13-HDHA to quantify 13-HDHEA- d_4 (**C**). Mean values with standard deviation of technical duplicates were plotted.

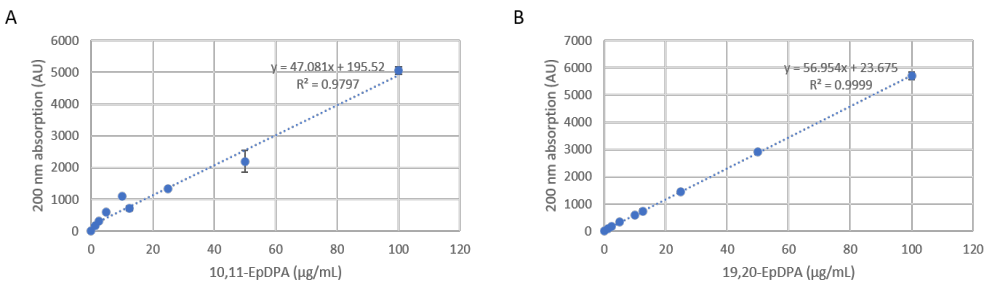


Figure S6-4 Calibration curve showing AUC at 200 nm absorption for 10,11-EpDPA to estimate 10,11-EDP-EA concentration (**A**), and of 19,20-EpDPA to estimate 19,20-EDP-EA concentration (**B**). Mean values with standard deviation of technical duplicates were plotted.

Chapter 7

Discussion

7.1 Introduction

As presented in this thesis, it is well-established that lipid metabolism plays an important role in immune regulation, and that *n*-3 PUFAs and their metabolites are linked to anti-inflammatory properties including reduction of the risk, development, and/or aggravation of (chronic) inflammatory diseases. One example of such an endogenous metabolic conversion is the production of DHEA from DHA, which has demonstrated potent anti-inflammatory properties *in vitro* (refs.¹⁻³, and this thesis). Only recently, *in vivo* antinociceptive properties of DHEA were described,⁴ which have now been complemented with phenotypic anti-colitis effects as described in Chapter 6. Earlier studies had reported on the potential anti-inflammatory and immune-regulating properties of DHEA, but several knowledge gaps about its immune targets, distribution, and metabolism remained. The aims of the work outlined in this thesis were to elucidate the molecular targets and metabolic fate of DHEA in the context of inflammation. To this end, a multi-disciplinary approach was employed, focusing on the biological roles of DHEA metabolites. By using chemical biological methods, such as probe molecules, novel protein interaction targets of DHEA were characterized. Our findings indicated potential regulatory roles for DHEA in ROS signaling, and cell migration, and generated novel insights into possible mechanisms underlying its cellular uptake. DHEA was also found to interact with COX-2, and subsequent metabolomic and lipidomic studies confirmed the interaction between COX-2 and DHEA, resulting in the identification of novel COX-2-derived products of DHEA: 13-HDHEA and 16-HDHEA, while also identifying new metabolites of EPEA: PGE₃-EA, 11-, 14-, and 18-HEPE-EA. Transcriptomics and lipidomics in LPS-stimulated macrophages revealed that 13- and 16-HDHEA have distinct anti-inflammatory properties *in vitro*. Finally, in a colitis-induced mouse model, the *in vivo* uptake and anti-inflammatory potential of DHEA was analyzed, and DHEA metabolism was characterized in the livers of these mice.

7.2 Interactions and immunological targets of DHEA

7.2.1 No interaction with GPR110, PPARs, CB receptors, and TRPV-1 in RAW264.7 cells

Although certain effects of DHEA have been attributed to its interaction with GPR110,⁵⁻⁷ PPARs,^{4, 8} CB receptors,⁹⁻¹³ and/or TRPV-1 receptors,^{4, 9} the chemical proteomics setup in Chapter 3 did not reveal interactions with any of these receptors, which is most likely due to the known low expression of these genes in LPS-stimulated RAW264.7 macrophages. Consequently, modulation of other inflammation signaling pathways

or metabolic routes, like the interaction with oxygenases, may explain the anti-inflammatory effects of DHEA in the LPS-stimulated RAW264.7 macrophage model.² A possible consequence of choosing this model could be that we might have come to (partially) different conclusions with a different cell type. At the same time, the RAW264.7 is a well-accepted model for macrophages and has also been widely used in previous studies,¹⁴⁻¹⁶ including in our lab.¹⁻²

7.2.2 ROS regulation in RAW264.7 cells by DHEA

Several literature reports described that DHEA is involved in the regulation of intracellular ROS levels. For example, DHEA reduced ROS levels in 0.1 µg/mL LPS-stimulated murine primary macrophages after 2 h incubation with 10 nM DHEA,⁷ but increased ROS levels in head and neck squamous cell carcinoma (HNSCC) cells.¹⁷ In Chapter 3 of this thesis the DHEA probes were also found to interact with regulators of ROS formation. Peroxiredoxins (Prdxs), but also proteins involved in Rho GTPase-signaling including RAS-related C3 botulinum toxin substrate 1 (Rac1) and neutrophil cytosolic factor 2 (Ncf2) (both required for the formation of the NADPH-oxidase complex)¹⁸⁻¹⁹ were identified as DHEA interactors. Interaction of these proteins with DHEA might influence complex formation, ultimately affecting intracellular ROS levels. Arachidonic acid, for example, is responsible for superoxide production in human neutrophils by interacting with the Rac1- and Ncf2-dependent NADPH oxidase complex NOX2.²⁰ Although we attempted to measure potential effects of DHEA on ROS production in RAW264.7 macrophages directly, we did not observe a significantly distinct effect yet (*data not shown*). The ROS protocol used for these experiments needs further tedious optimization before we can conclude how and if DHEA affects intracellular ROS levels in RAW264.7 macrophages. Next to DHEA, its oxidized metabolite 13-HDHEA (but not 16-HDHEA) was also proposed to induce ROS production based on the transcriptomic analysis in IPA®. Interestingly, literature previously also suggested a relation between increased ROS levels and modulation of COX-2 and/or 5-LOX by DHEA in head and neck squamous cell carcinoma (HNSCC) cells.¹⁷ These results seem to be in line with our hypothesis that 13-HDHEA, resulting from the interaction between DHEA and COX-2, potentially leads to ROS induction.

Based on the current literature, three distinct ROS-regulatory mechanisms can be distinguished for PUFAs and its derivatives. In the first mechanism, metabolic products of oxygenases (*e.g.*, COX-2 and LOX-5) are involved in the regulation of ROS. For example, COX-2-derived prostaglandin PGD₂ stimulates ROS production in Sertoli cells.²¹ This would be in line with our IPA pathway analyses in Chapter 5, which also suggested a ROS-inducing effect for 13-HDHEA. In the second mechanism, increased catalytic activity of oxygenases leads to increased lipid radical formation and thus to

increased intracellular ROS levels.²² Because DHEA conversion by COX-2 is slow, COX-2-derived lipid radicals are expected to be reduced when incubated with DHEA. It is however unknown how this process affects LOX-5 (and similar enzymes) kinetics and their related lipid-radical production. The third mechanism that has been proposed involves the increased production of enzymes like phospholipase A and COX-2 under conditions of oxidative stress. Consequently, lipid composition and lipid metabolism are changed, ultimately affecting intracellular ROS levels.²³ It is important to note that ROS mechanisms also depend on the model which is used. For example, in ferroptosis-sensitive cancer, ischemia reperfusion, and degenerative disease models ROS scavenging mechanisms are often dampened, which could lead to increased vulnerability of these cell models to ROS.^{22, 24} Although it is fair to conclude that lipid oxidation and lipid metabolism influence intracellular ROS levels, little is known about the interplay of all the different mechanisms involved. It must therefore be considered that DHEA could affect both ROS-inducing and ROS-reducing pathways resulting in a net-near zero effect. Clearly, additional research is required to confirm that the obtained interactions between DHEA and Prdxs, and small GTPase-dependent NADPH complexes are responsible for functional changes in intracellular ROS levels.

7.2.3 DHEA and cytoskeletal remodeling and cell migration

Because of their role in the innate immune response, macrophages and neutrophils are capable of chemotaxis and cell migration. Indeed, various reports showed that LPS stimulation of immune cells leads to the induction of cell migration.^{7, 25-26} According to Park and co-workers, DHEA is involved in reducing LPS-induced neutrophil migration, which was interpreted as an anti-inflammatory effect.⁷ In Chapter 3, we found evidence for the involvement of a DHEA-dependent small GTPase-signaling pathway including the regulatory proteins Rac1, Rab1 and dynamin-2 (Dnm2) in the modulation of cytoskeletal remodeling and cell migration.²⁷⁻²⁹ Moreover, DHEA-mediated reduction of prostaglandin formation could be related to reduction of cell migration, demonstrated by the fact that PGD₂ induces RAW264.7 macrophage migration.^{2, 26} Apart from the effects of DHEA itself, CYP450 and 15-LOX-derived products of DHEA have been described to reduce cell migration.^{13, 30} Effects of the DHEA-derived COX-2 products 13-HDHEA and 16-HDHEA on cell migration are difficult to interpret based on transcriptomic data alone, but functional IPA® analysis of these compounds pointed to a potential reduction in cell migration. In summary, both DHEA and its COX-2-derived metabolites 13-HDHEA and 16-HDHEA seem to affect cell migration, expectedly leading to an anti-migratory phenotype. Additional experimental studies are warranted to determine the effects and mechanism of DHEA, 13-HDHEA, and 16-HDHEA on cell migration.

7.2.4 DHEA interactions with COX-2

Previously it was hypothesized that (at least part of) the anti-inflammatory effect of DHEA was explained via an interaction with COX-2, because DHEA incubation resulted in a significant reduction of COX-2-derived prostaglandins and oxylipins while only marginally reducing the expression of the protein itself.² Other PUFA-derived metabolites like AEA and 2-AG were previously also characterized as COX-2 substrates,³¹⁻³³ fueling the hypothesis that DHEA is a competitive COX-2 substrate.^{2, 34} A direct interaction of COX-2 with the chemical probes of AEA and DHEA was indeed reported in Chapter 3, and in Chapter 4 it was demonstrated that AEA, EPEA, and DHEA can indeed act as COX-2 substrates using a cell-free hCOX-2 incubation assay. Using LC-HRMS we were the first to identify previously unknown metabolites of EPEA and DHEA, of which the structure was conformed using synthetic congeners in a targeted UPLC-MS/MS analysis. COX-2-dependent metabolism of DHEA and EPEA resulted in the production of the newly identified compounds 13-HDHEA and 16-HDHEA from DHEA, and 11-HEPE-EA, PGE₃-EA, and the unconfirmed products 14-HEPE-EA, and 18-HEPE-EA from EPEA. These experiments provided evidence for a new COX-2 metabolism 'branch' on the lipid metabolome (see also section 7.3.1).

Although DHEA was converted by COX-2, the catalytic efficiency of the conversion was limited (yielding 1.3% 13-HDHEA and 1.4% 16-HDHEA, in reference to the amount of DHEA that was added, in the cell-free enzymatic model). Kinetics of COX-2 oxidation are dependent on the length of the hydrocarbon chain (oxidation of DHA is 50% when compared to AA)³⁵ and the presence of *N*-acyl derivatives (AEA oxidation is 80% lower when compared to AA).³⁶ With respect to previous kinetic observations it is not surprising that DHEA conversion by COX-2 is slow, resulting in limited production of 13-HDHEA and 16-HDHEA. It is tempting to speculate that the immunological effect of this interaction between DHEA and COX-2 mainly consists of substrate competition with AA, explaining the significant reduction in prostaglandin and thromboxane levels.² DHEA might also induce additional allosteric effects to further regulate COX-2 activity, which is a commonly obtained phenomenon for this allosteric enzyme.³⁷ To investigate the nature of the interaction between DHEA and COX-2 in more detail, and to prove that the reduction in prostaglandin and oxylipin formation is indeed the consequence of competition between AA and DHEA in the catalytic site of COX-2, additional kinetic studies are required. Due to the limited amount of commercially available hCOX-2 these studies were not yet performed.

7.2.5 Endosomal uptake and trafficking of DHEA

Although DHEA and AEA were effectively taken up by LPS-induced macrophages, there is ongoing debate about the uptake mechanism of PUFA amides. Uptake is either

mediated via passive diffusion, mediated by the hydrolysis of DHEA and AEA by fatty acid amide hydrolase (FAAH), or via facilitated transport using a yet unidentified membrane transporter.³⁸⁻³⁹ Transcriptomic analysis in Chapter 5 revealed that besides FAAH, *N*-acylethanolamine-hydrolyzing acid amidase (NAAA) was significantly expressed in RAW264.7 macrophages that were stimulated with 1.0 µg/mL LPS for 24 h. In line with this, Alhouayek and coworkers recently demonstrated that especially during the first few hours DHEA is mainly hydrolyzed by NAAA in 0.1 µg/mL stimulated murine J774 macrophages, proving that NAAA is indeed capable of hydrolyzing DHEA.³⁴ Despite the known interaction with these enzymes, both NAAA and FAAH were remarkably not observed as binding proteins in Chapter 3. Besides FAAH and NAAA, fatty acid binding proteins (FABPs) and oxylipins are also involved in orchestration of the biological roles of PUFA amides, thereby affecting their uptake.³⁸

In Chapter 3 no membrane transporters were identified that would point towards facilitated transport of the PUFA amides. In contrast, the membrane and vesicular regulating proteins Rab1a, Dnm2, and Rab5c (the latter only for DHEA) were characterized as AEA and DHEA interactors,^{27-28, 40} suggesting endocytosis as a more likely mechanism for PUFA amide uptake. For AEA, endocytosis via lipid rafts and caveola (small invaginations of the plasma membrane) was already proposed in 2004.⁴¹ Although conclusive statements about the uptake mechanism require additional studies, current results better fit the passive diffusion model than uptake via a (novel) membrane transporter.

7.2.6 Summary of main conclusions on the interactions and immunological targets of DHEA

DHEA reduces the production of several pro-inflammatory cytokines and chemokines, reduces cell-migration, and affects ROS regulation (**Figure 7-1**).^{1-2, 7, 17, 34} Although there still are open questions regarding the mechanistic regulation of all these effects, it is concluded that part of the anti-inflammatory effects of DHEA are mediated via the interaction with COX-2, resulting in the formation of biologically active metabolites 13-HDHEA and 16-HDHEA and a reduction in pro-inflammatory prostaglandins and oxylipins. Additionally, new links between DHEA and the small GTPase pathway, peroxiredoxins, and cytoskeletal remodeling proteins were found. Involvement of previously described DHEA receptors (GPR110, PPARs, CB receptors, and TRPV-1) in LPS-stimulated RAW264.7 macrophages was not observed, which is most probably explained by the limited expression levels of these genes in this cell line. Consequently, it could be speculated that the current description of the 'endocannabinoid system' is too restrictive and requires adjustment. True endocannabinoids and endocannabinoid-like PUFA derivatives can bind to various protein and receptors that fall beyond classically recognized endocannabinoid regulators. Clearly, interaction of the endocannabinoid

and PUFA-derivative compounds with the binding targets also depend on the model which is used. Ultimately, all the interactions together regulate the binding activity and efficiency of a 'true' endocannabinoid to the classical endocannabinoid receptors like CB-receptors, TRPV-1 and PPAR's (known as the entourage effect,⁴² as introduced in chapter 1). Consequently, the scope of the endocannabinoid system should be increased. As a final observation, results from this thesis also suggested that uptake of DHEA and other PUFA amides is regulated via endocytic trafficking rather than via specialized membrane receptors.

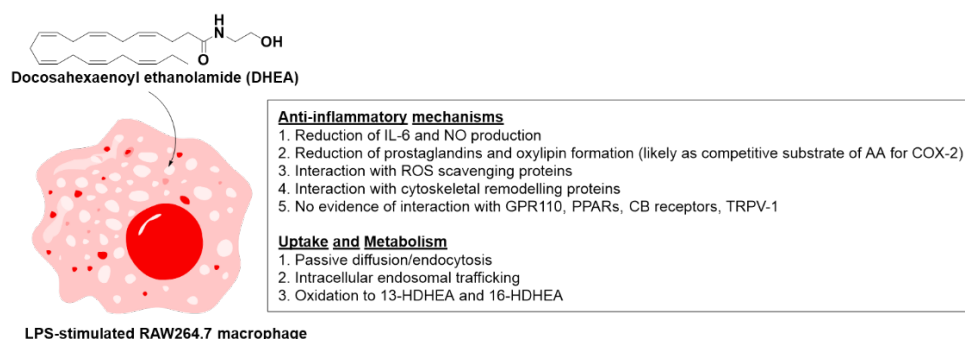


Figure 7-1 Overview of anti-inflammatory mechanisms of DHEA in 1.0 µg/mL LPS-stimulated RAW264.7 macrophages.

7.3 Implications of *n*-3 PUFA-derived *N*-acyl amines in immune regulation

Apart from unravelling the anti-inflammatory mechanism of DHEA, this thesis also focused on metabolism of PUFAs and related *N*-acyl amines. As extensively reviewed in Chapter 2, nutrition is an important factor in the metabolic regulation of PUFAs and their amides, and previous studies showed that *n*-3 PUFA amide concentrations, like those of EPEA and DHEA in plasma of humans and mice and tissues of mice, are increased after administering fish oil.⁴³⁻⁴⁵ Based on results in this thesis and work from others, it is now clear that EPEA and DHEA could be further metabolized to products that can be considered as new branches of the lipid metabolome.⁴⁶ Here we will discuss PUFA amide metabolism in a broader context, and describe its implication for immune-regulation, ending with a short discussion on the metabolic implications for humans.

7.3.1 Immune-modulating effects of DHEA and EPEA metabolism *in vitro*

N-acyl PUFA amines are prone to enzymatic oxidation by CYP450, LOXs, and COX-2. In Chapter 4 11-HEPE-EA, PGE₃-EA, and the unconfirmed products 14-HEPE-EA,

and 18-HEPE-EA were identified as novel COX-2-derived EPEA products (**Figure 7-2**). Conversion of DHEA via COX-2 was found to result in production of 13-HDHEA and 16-HDHEA, to further complement the DHEA lipid metabolome (**Figure 7-3**). Apart from reducing intracellular concentrations of DHEA and EPEA, oxidized metabolites of EPEA and DHEA usually display anti-inflammatory and/or immune-regulating properties. Indeed, 13-HDHEA and 16-HDHEA reduced transcription levels of pro-inflammatory genes, and reduced production of several pro-inflammatory cytokines. As such, the COX-2-mediated anti-inflammatory effects of DHEA might be twofold: (i) it inhibits prostaglandin formation by acting as a competitive substrate of AEA for COX-2, and (ii) its oxidation products 13-HDHEA and 16-HDHEA induce anti-inflammatory effects themselves. Although 13-HDHEA and 16-HDHEA showed distinct immune-regulating effects, their anti-inflammatory potential was limited when compared to DHEA, suggesting that COX-2 might rather be involved in catabolic clearance of DHEA. Contrary to this, others have shown that comparable CYP450 and 15-LOX-derived DHEA metabolites possessed stronger immune-regulating properties than DHEA.¹²⁻¹³ However, characterization of the biological properties of CYP450, 15-LOX, and COX-2-derived DHEA metabolites using different *in vitro* models prevents a direct comparison of their full immunological potential. It is also important to note that the 15-LOX-derived products 10,17-diHDHEA and 15-HEDPEA are the result of multiple sequential oxidations that originated from the common 15-LOX precursor 17-HDHEA. Considering this, it cannot be ruled out that 13-HDHEA and 16-HDHEA are subjected to additional oxidations, leading to more complex lipids with distinct (and possibly even increased potency) immunological effects, albeit at reduced concentrations. Finally, it is important to keep in mind that biological effects ascribed to DHEA might actually be (partly) attributed to DHEA metabolites as it is easily oxidized by a variety of enzymes to form products with distinct immune-regulating properties that can also be potent, even in small amounts.

7.3.2 Anti-tumorigenic effects of DHEA and EPEA metabolism *in vitro*

Next to anti-inflammatory properties of DHEA and EPEA derived metabolites,¹²⁻¹³ ⁴⁶ CYP450-derived DHEA epoxides displayed anti-tumorigenic properties that were mainly attributed to antiangiogenic and anti-migratory effects.³⁰ Previously, 15-LOX-derived DHEA metabolites were also identified as polymorphonuclear leukocyte (PMN) migration inhibitors,¹³ and in Chapter 5 it was described that also the COX-2-derived metabolites 13-HDHEA and 16-HDHEA alter gene expression in a way that suggests potential anti-migratory effects. In the work of Das and coworkers the inhibitory effect on cell migration translated to anti-tumorigenic properties,^{12, 30} making the nutrition-derived oxidized *n*-3 PUFA metabolites a hypothetically interesting class of newly identified antitumorigenic compounds to be investigated in more detail. Interestingly,

DHEA itself was previously also linked to anti-tumorigenic properties in breast and prostate cancer models.^{8, 10, 47} Similar to its anti-inflammatory effects it is currently unknown if and how DHEA metabolism affects the anti-tumorigenic properties ascribed to DHEA. Future studies are required to understand if it is DHEA, its metabolites, or both, that are the main contributors to the anti-tumorigenic properties, and if oxidized *n*-3 PUFA derivatives indeed provide an interesting source of nutrition-related anticarcinogens. Future work should also include metabolic screening or mapping of oxygenase expression levels in order to gain insight in the possible contribution of DHEA metabolites on the overall immune-regulating effect. In addition, it would be interesting to test DHEA and EPEA together with their known oxidized metabolites in a single study to directly compare their anti-inflammatory and antitumorigenic effects in the same biological system.

7.3.3 Potency of DHEA metabolism *in vitro*

To be able to interpret the potency of the identified anti-inflammatory and anti-tumorigenic properties, it is important to precisely determine the effective concentrations of the DHEA metabolites. Induction of significant anti-inflammatory or anti-tumorigenic effects *in vitro* requires concentrations of DHEA and its metabolites ranging from 10 nM to 10 μ M (refs.^{12-13, 30, 46} and this thesis). Quantified values of 13-HDHEA and 16-HDHEA in Chapter 4 were limited to 40 nM in 100 μ L extracts in 1.0 μ g/mL LPS-stimulated RAW264.7 macrophage extracts, which indicates that *in vitro*, the production of DHEA metabolites would yield concentrations which are below those considered to induce immune-regulating effects. Induction of immune-regulating properties in 1.0 μ g/mL LPS-induced RAW264.7 macrophages required at least 5 μ M of 13-HDHEA and 16-HDHEA, which is about 1000x higher than the measured concentrations. While interpreting these data it must be considered that local intracellular concentrations of 13-HDHEA and 16-HDHEA might be higher at accumulation sites. In conclusion, these results indicated that DHEA metabolism might not reach significance in 1.0 μ g/mL LPS-induced RAW264.7 macrophages, although immune-regulating effects in other *in vitro* models might be reached.

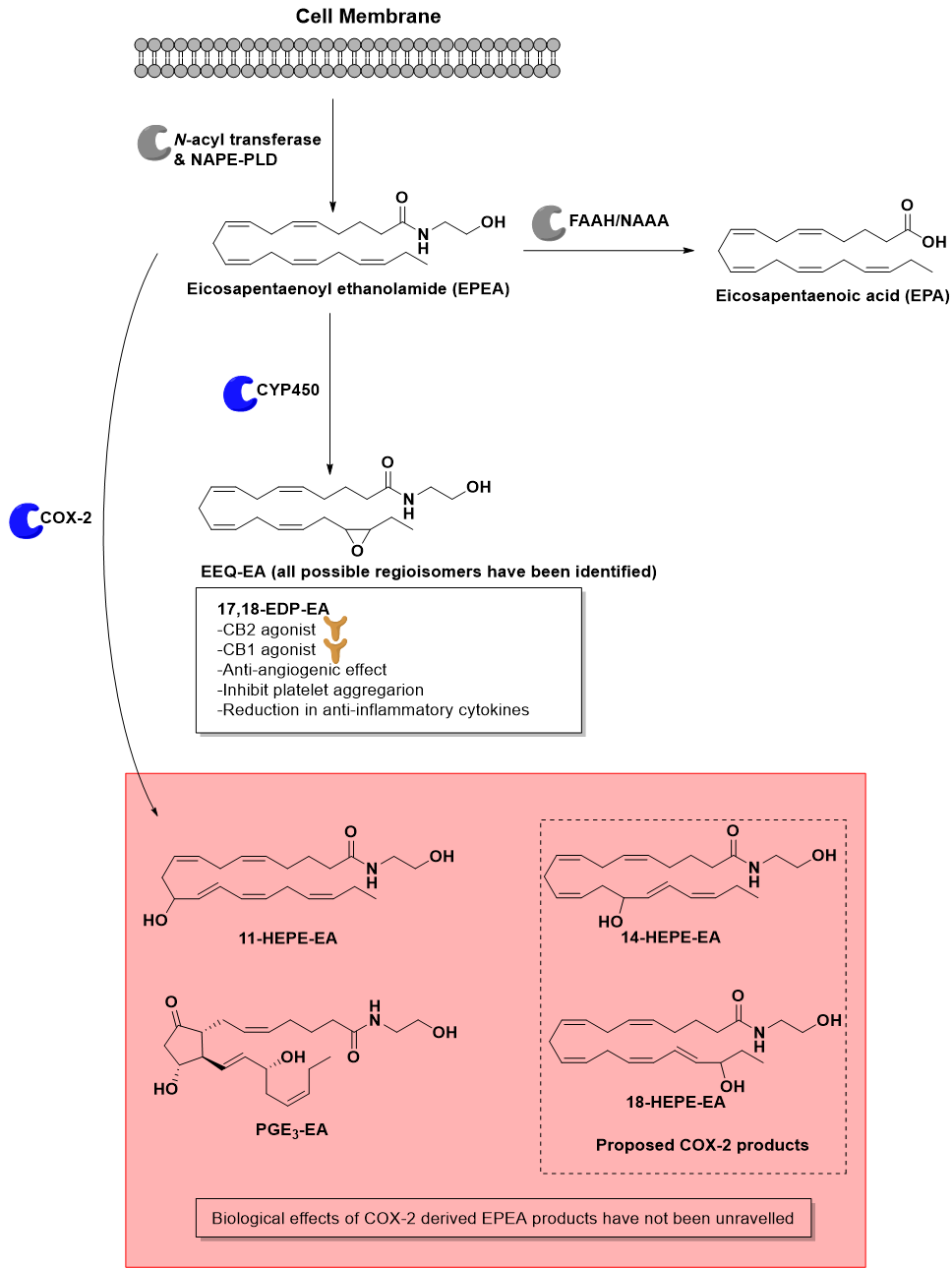


Figure 7-2 Schematic summary of EPEA metabolism. Newly characterized metabolites of EPEA described in this thesis are highlighted in red.

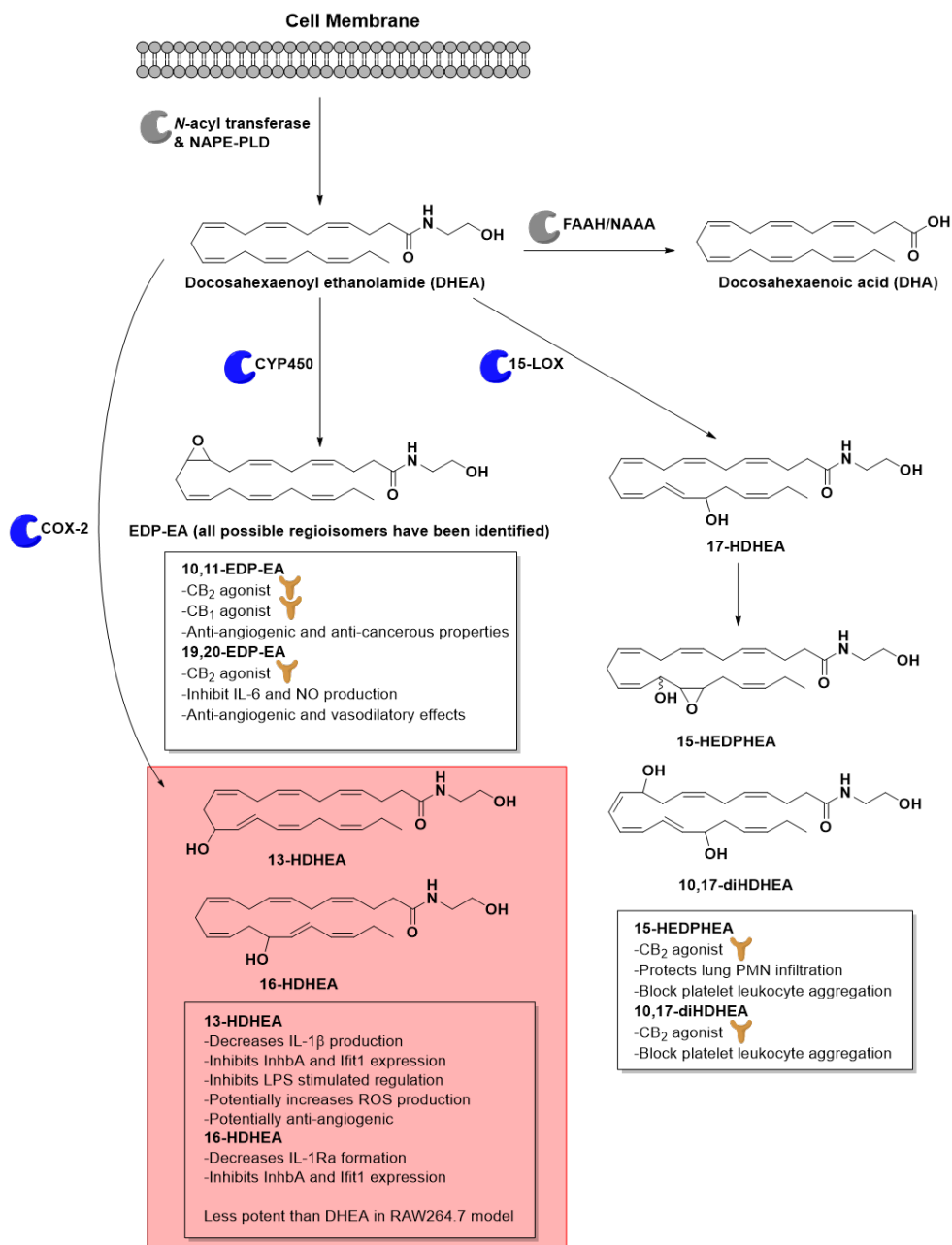


Figure 7-3 Schematic summary of DHEA metabolism. Newly characterized metabolites of DHEA and their immune-regulating properties as described in this thesis are highlighted in red.

7.3.3 DHEA metabolism *in vivo*

Although DHEA has interesting anti-inflammatory properties *in vitro*, there is still limited evidence for its *in vivo* anti-inflammatory effects (Chapter 6).⁴ Studies in this thesis showed that i.p. injection of DHEA resulted in increased DHEA levels in the liver, but did not result in measurable levels of hepatic DHEA metabolites in mice that had been administered 2% DSS through their drinking water. Furthermore, a slight decrease in colitis phenotypes was observed. Most likely, insignificant expression of the oxygenases in the liver as result of low hepatic inflammatory state resulted in the absence of detectable amounts of oxygenated DHEA metabolites. Consequently, 13-HDHEA and 16-HDHEA have not yet been characterized *in vivo*. Previous literature reports already described quantification of CYP450- derived EPEA and DHEA metabolites in rat brain and peripheral organs,¹² and 15-LOX-derived DHEA metabolites were identified in mouse brain.¹³ Accumulation of CYP450 products in peripheral tissues varied between 0-500 pmol/g tissue, and the regioisomer 19,20-EDP-EA was predominantly produced. Although this observation implies that DHEA metabolism is also active *in vivo*, 500 pmol/g tissue (equals 0.19 µg/g tissue) of CYP450-derived DHEA metabolite is at least 100x lower than the effective dosing of 2-10 mg/kg DHEA (equals 2-10 µg/g) *in vivo* (Chapter 6).⁴

Later studies in mouse lung carcinomas showed that production of the potentially anti-tumorigenic EDP-EAs was in the range of 0-55 nmol/g tissue (0-21 µg/g tissue), depending on the regioisomer.³⁰ These concentrations most likely do have potential anti-tumorigenic effects. In the same study, a 20-80% increase in EDP-EA concentration was observed in metastatic lungs compared to the lungs of control mice. DHEA levels themselves were not significantly decreased in the metastatic lungs, which seems to imply that DHEA uptake and/or production of DHEA in tumorigenic lungs is induced. Together, these results imply that DHEA metabolism and the EDP-EA metabolites may possess regulatory effects in tumor biology, where they also reach biological significance.

Although the observed DHEA metabolite concentrations *in vivo* might seem small, it should be mentioned that these are averaged concentrations from whole tissue extracts, and that local tissue concentrations of the metabolites may be higher at accumulation sites. To get more insight in the relevance of DHEA metabolism *in vivo*, additional studies are required. Main requirements for these studies are that expression levels of the oxygenases are high enough to provide significant concentrations of oxidized metabolites, which will lead to immune-regulation, and that the uptake and/or intracellular production of DHEA is also significant.

7.3.4 Translation of metabolic conversion of DHEA to 13- and 16-HDHEA to humans

Small pilot studies in our laboratory showed that DHEA levels are increased in human plasma after fish oil consumption,⁴⁸ and similar studies by Das and coworkers showed the presence of DHEA and even 19,20-EDP-EA in human plasma.¹² Consequently, it could be hypothesized that COX-2-dependent DHEA metabolism as described in this thesis is potentially also relevant for humans. To translate the DHEA *in vitro* and *in vivo* metabolism to the human situation, we sought to identify 13- and 16-HDHEA in human plasma. Unfortunately, these compounds could not be detected (*data not shown*). There are different explanations for this. (i) Experiments were performed in plasma from healthy human volunteers and, consequently, COX-2 expression might not have reached the required levels. (ii) 13-HDHEA and 16-HDHEA might be unstable metabolic products and could be prone to fast metabolic breakdown and clearance. To obtain a better perspective on the amount of 13-HDHEA and 16-HDHEA in humans, experimental observations *in vivo* and *in vitro* allow to make a hypothetical calculation. After 6 weeks of 3% fish oil diet available *ad libitum*, endogenous DHEA levels in murine plasma doubled from 0.3 ng/mL to about 0.6 ng/mL.⁴⁸ Background human DHEA plasma concentrations without dietary intervention were reported to be 0.41 ng/mL.⁴⁸ Assuming a similar increase for human DHEA plasma levels after a diet that contains 3% fish oil, DHEA concentrations would increase to ~0.8 ng/mL (or 2.15 pmol/mL). In our cell-free assay of hCOX-2 in Chapter 4 it was observed that only 1.3-1.4% of the DHEA was converted into HDHEAs. Assuming similar conversions *in vivo*, this would result in circulating concentrations of approximately 0.03 pmol/mL for the HDHEAs. Most likely, these concentrations are not physiologically relevant, but intracellular accumulation of the metabolites could ultimately lead to induction of immunological effects.

Based on previous observations, from *in vitro* and *in vivo* models, it can be assumed that oxidative DHEA metabolism is mainly active in inflamed tissues. First, DHEA synthesis and/or DHEA uptake is increased in immune-activated and tumorigenic cells to inhibit the production of pro-inflammatory regulators and processes.^{30, 43} Second, inflammatory states result in the upregulation of COX-2.⁴⁹⁻⁵⁰ Together, these events increase the possibility of detecting 13-HDHEA and 16-HDHEA in humans. Although the hypothesized concentrations of DHEA and its metabolites are relatively small in humans, dietary intervention also leads to significant increase in their production, and might ultimately lead to physiologically significant levels. As such it is believed that *n*-3 PUFA metabolism and nutrition can potentially play a role during septic state and tumorigenesis.

7.4 Chemical perspective on the synthesis and use of bi-functional PUFA-derived probes

This thesis shows that there is a need for further research on the mechanistic and metabolic regulation of *n*-3 PUFAs, their amidic metabolites such as DHEA, and their oxygenated metabolites. An important and insightful approach is the use of bio-orthogonal chemical probes, as reported in Chapter 3. Initially, the synthesis of alkyne-terminated *n*-3 PUFA probes was investigated to produce a variety of DHA and DHEA probes. This approach would allow potential modification on various parts of the hydrocarbon chain. Moreover, the diazirine moiety could have been introduced in the hydrocarbon chain of the chemical probe, similar to the AEA-DA probe that was designed by Cravatt and coworkers,⁵¹ allowing the production of an ethanolamide-derived probe that closely resembles DHEA. In the probes described in Chapter 3, the diazirine moiety was always located at the *N*-acyl-end of the probe, and resulting the biological effect of the ethanolamine in DHEA might not have been properly imitated by the probe. Even though different groups reported the successful synthesis of *n*-3 PUFA building blocks using Cu(I)-mediated cross-coupling reactions to produce methylene-skipped poly-ynes, followed by the selective reduction of the poly-ynes to *cis*-double bonds,⁵¹⁻⁵⁴ this procedure was not straightforward as skipped poly-ynes rapidly oxidize. As such, obtained yields dramatically decreased with increasing length of the poly-yne and the products could not be stored long-term in a stable manner. Nevertheless, reduction of the skipped poly-ynes by Ni(II)acetate with sodium borohydride resulted in the stereoselective production of *Z*-alkenes, even though in limited yields (<30%). Fortunately, around that time one of our targeted docosahexaenoic acid alkyne derivatives became commercially available. Therefore, it was decided to continue with the commercial DHA-alkyne in combination with 2-(3-(but-3-yn-1-yl)-3H-diazirin-3-yl)ethan-1-amine to synthesize the PUFA-derived bi-functional probes as described in Chapter 3.

Our bi-functional probes showed comparable effects on the reduction of prostaglandin and IL-6 when compared to DHEA despite the chemical alterations that could affect their biological properties and chemistry. As an ideal probe contains the smallest possible chemical modifications and displays biological behavior that is indifferent from the lead structure, we conclude that DHEA probe **3** is a proper imitation of the fatty acid tail of DHEA, but probably less suitable to study the effect of the ethanolamine moiety of the biological activity. Therefore, in an ideal case a combination of probes is used: one probe that has both probe-functionalities at the PUFA-end, one probe that has both probe-functionalities on the *N*-acyl end, and a set of two complementary probes that have one of the two functionalities on the hydrocarbon tail and the

other functionality on the *N*-acyl end of the probe (DHEA probe **3** resembles one of these two). Such a combination of probes allows proper assessment of the observed biological effects of the modifications, and informed judgements on the best probe can be made. Moreover, biological control experiments should always be performed to ensure that biological properties of the probe molecule are similar to the molecule of interest. For example, supplementing the natural compound to the experiment with the probe, should lead to diminished results for the probe, which supports identical behavior. Unfortunately, more detailed biological experiments to the role and binding interaction of DHEA with ROS regulators and small GTPase-regulating proteins could not be performed in the time-frame of the current PhD thesis, which thus only points to the need for extensive further investigations in this field.

7.5 Future perspectives

Despite the identification and characterization of new branches in the DHEA metabolome, and investigating the metabolic and phenotypical effects of i.p. injected DHEA in colitis-induced mice, several questions remain unanswered and new questions were raised. Here, I discuss some of these open questions and present my view on the future directions for research on *n*-3 PUFA amides in the field of immunology and inflammation.

First, chemical proteomic analysis in Chapter 3 and the mRNA expression data in Chapter 5 proposed a potential link between DHEA and/or its metabolites and ROS production, cellular migration, and anti-tumorigenic effects. This was not limited to DHEA and its metabolites, but also involved lipid regulators like arachidonic acid and prostaglandins. New studies are warranted to further explore direct effects of DHEA and its metabolites on ROS production and cell migration in macrophages and neutrophils. Other relevant disease models like tumorigenic, ischemia reperfusion, and degenerative disease models should be investigated as well, because in these models ROS-dependent cell death has been proposed as a potential future treatment.^{22, 24} Additional mechanistic insight in the regulation of intracellular ROS species could be gained by measuring the contribution of several particular oxygenases like COX-2, 5-LOX, 15-LOX, and CYP450 by selectively inhibiting their activity. Lipidomic analysis might reveal the regulation of other interesting lipid species like prostaglandins and oxylipins, which were previously also indicated as ROS-regulating factors.²¹

Second, mapping of the proposed endosomal uptake and trafficking is required to prove passive transport as the dominant uptake mechanisms for *N*-acyl ethanolamine

PUFA derivatives. Next to the chemical proteomic screening performed in Chapter 3, the role of PUFA-regulating enzymes like NAPE-PLD, FAAH, NAAA, and oxygenases in the uptake of the PUFA derivatives needs more investigation. Furthermore, cellular uptake and receptor binding in other cell types than RAW264.7 macrophages needs to be evaluated in order to understand the (possible) involvement of endocannabinoid-related receptors like CB₁/CB₂, GPR110, TRPV-1 *e.g.*, which were found to be expressed less in RAW264.7 cells. In these studies, the use of receptor antagonists and silencing of downstream pathways will aid in the unravelling of signaling cascades.

Third, it would be interesting to gain deeper insight in the molecular details of DHEA binding by COX-2. To this end, generating a crystal structure of the DHEA-COX-2 complex would be instrumental to analyze the binding features in the complex. Moreover, enzyme kinetics in a competition assay between DHEA and AA (and also other COX-2 substrates) could be informative to understand the interaction of DHEA in the catalytic and allosteric subunit of COX-2. Once the kinetics and interaction of DHEA with COX-2 are better understood, it should be possible to develop novel anti-inflammatory drugs that will probably not show the cardiovascular adverse effects, that are typical for so-called COX-2 selective NSAIDs. As an alternative to these NSAIDs, dietary interventions might be used to develop nutritional guidelines to attenuate chronic inflammation. To study interactions between DHEA and COX-2 in more detail, significant amounts of recombinant COX-2 need to be expressed and purified, because commercially available amounts of the enzyme are limited, and its purity is often questionable.

Fourth, to analyze and map the metabolic implications of DHEA and/or fish oils a lipidomic screening assay in several organs in a septic or tumorigenic *in vivo* model (and thus upregulation of the DHEA metabolizing oxygenases) is required. Comparing a control group receiving a 'normal' diet with a treatment group receiving fish oil and a group that receives DHEA by injection, effects of these interventions can be assessed on *n*-6 PUFA derivatives like AEA, the uptake and/or production of DHEA, the production of DHEA-derived metabolites of COX-2, LOXs, and CYP450, and levels of pro-inflammatory oxylipins like prostaglandins. Optimization of the sample extraction workup is required to properly quantify epoxide-derived metabolites that are also expected. Next to lipidomic screening, expression analysis of the enzymes in the organs would also be required, which can be performed in parallel using RT-PCR (Chapter 6). Next to COX-2, CYP450s, and LOXs, expression levels of FAAH, NAAA, and NAPE-PLD are interesting to understand the metabolic fate of DHEA *in vivo*. In follow-up experiments of these studies, specific metabolic routes could be blocked by adding enzyme inhibitors to ensure metabolic production of specific metabolites.

Fifth, to gain more insight in the biological aspects of PUFAs it is crucial to have robust, straightforward and convenient synthetic routes to produce PUFA probes. Interestingly, two synthetic strategies for the production of DHEA-derived chemical probes were recently described in the PhD thesis of dr. Gagestein from the group of prof. van der Stelt.⁵⁵ The first route described a combined synthesis route using the synthesis of two dienes that were combined using Wittig olefination. A second Wittig reaction with a minimalistic bi-functional linker resulted in the production of DHA- and DHEA-derived probes. A second 6-step synthesis route was described to produce DHA alkyne by regioselective hydrobromination to derivatize the terminal non-conjugated C=C-bond of DHA into bromohydrins, which were subsequently converted into a β,γ -unsaturated aldehyde via epoxidation, hydrolysis of the epoxide intermediate, and a final oxidative cleavage of the resulting dehydroxylated DHA structure. A Wittig reaction between the resulting aldehyde and an alkyne-terminated phosphonium salt resulted in the formation of the DHA-alkyne. Although the overall yield of this 6-step synthesis route is only 4%, the described methodology provides an interesting alternative to the complex multi-step synthesis routes involving formations of unstable poly-ynes.⁵⁵ Another approach was described by the laboratory of Janda and coworkers, who used solid supports for the synthesis of PUFA structures.⁵⁶ This methodology could simplify purification and was reported to result in excellent yields with the possibility for diversification on the tail end. Combinations of the use of bead systems with flow chemistry might provide an interesting way to develop more controllable methods compared to the conventional in solution chemistries.

Next to these specified future investigations on DHEA and its metabolites, human dietary intervention studies and clinical trials are required to understand the full potential of *n*-3 PUFA enriched diets and their implications on the occurrence and outcomes of (chronic) inflammation and carcinogenesis. Of particular relevance would be to get a better understanding of the distribution and metabolism of the *n*-3 PUFAs in the body, and to get a perspective on the biological relevance of several metabolic pathways. In the end these studies are necessary to enable the development of more tailored dietary guidelines, which could ultimately contribute to healthier individuals and improved quality of life.

7.5 References

1. Meijerink, J.; Plastina, P.; Vincken, J.-P.; Poland, M.; Attya, M.; Balvers, M.; Gruppen, H.; Gabriele, B.; Witkamp, R. F., The ethanolamide metabolite of DHA, docosahexaenoylethanolamine, shows immunomodulating effects in mouse peritoneal and RAW264.7 macrophages: evidence for a new link between fish oil and inflammation. *Br. J. Nutr.* **2011**, *105* (12), 1798-1807.
2. Meijerink, J.; Poland, M.; Balvers, M. G. J.; Plastina, P.; Lute, C.; Dwarkasing, J.; van Norren, K.; Witkamp, R. F., Inhibition of COX-2-mediated eicosanoid production plays a major role in the anti-inflammatory effects of the endocannabinoid N-docosahexaenoylethanolamine (DHEA) in macrophages. *Br. J. Pharmacol.* **2015**, *172* (1), 24-37.
3. Kim, H.-Y.; Spector, A. A., N-Docosahexaenoylethanolamine: A neurotrophic and neuroprotective metabolite of docosahexaenoic acid. *Mol. Aspects Med.* **2018**, *64*, 34-44.
4. Paton, K. F.; Shirazi, R.; Vyssotski, M.; Kivell, B. M., N-docosahexaenoyl ethanolamine (synaptamide) has antinociceptive effects in male mice. *Eur. J. Pain* **2020**, *24* (10), 1990-1998.
5. Huang, B. X.; Hu, X.; Kwon, H.-S.; Fu, C.; Lee, J.-W.; Southall, N.; Marugan, J.; Kim, H.-Y., Synaptamide activates the adhesion GPCR GPR110 (ADGRF1) through GAIN domain binding. *Commun. Biol.* **2020**, *3* (1), 109.
6. Lee, J.-W.; Huang, B. X.; Kwon, H.; Rashid, M. A.; Kharebava, G.; Desai, A.; Patnaik, S.; Marugan, J.; Kim, H.-Y., Orphan GPR110 (ADGRF1) targeted by N-docosahexaenoylethanolamine in development of neurons and cognitive function. *Nat. Commun.* **2016**, *7*, 13123.
7. Park, T.; Chen, H.; Kim, H.-Y., GPR110 (ADGRF1) mediates anti-inflammatory effects of N-docosahexaenoylethanolamine. *J. Neuroinflammation* **2019**, *16* (1), 225.
8. Rovito, D.; Giordano, C.; Vizza, D.; Plastina, P.; Barone, I.; Casaburi, I.; Lanzino, M.; De Amicis, F.; Sisci, D.; Mauro, L.; et al., Omega-3 PUFA ethanolamides DHEA and EPEA induce autophagy through PPAR γ activation in MCF-7 breast cancer cells. *J. Cell. Physiol.* **2013**, *228* (6), 1314-1322.
9. Alharthi, N.; Christensen, P.; Hourani, W.; Otori, C.; Barrett, D. A.; Bennett, A. J.; Chapman, V.; Alexander, S. P. H., n-3 polyunsaturated N-acylethanolamines are CB2 cannabinoid receptor-preferring endocannabinoids. *Biochim. Biophys. Acta Mol. Cell Biol. Lipids* **2018**, *1863* (11), 1433-1440.
10. Brown, I.; Cascio, M. G.; Wahle, K. W. J.; Smoum, R.; Mechoulam, R.; Ross, R. A.; Pertwee, R. G.; Heys, S. D., Cannabinoid receptor-dependent and -independent anti-proliferative effects of omega-3 ethanolamides in androgen receptor-positive and -negative prostate cancer cell lines. *Carcinogenesis* **2010**, *31* (9), 1584-1591.
11. Brown, I.; Lee, J.; Sneddon, A. A.; Cascio, M. G.; Pertwee, R. G.; Wahle, K. W. J.; Rotondo, D.; Heys, S. D., Anticancer effects of n-3 EPA and DHA and their endocannabinoid derivatives on breast cancer cell growth and invasion. *Prostaglandins Leukot Essent Fatty Acids* **2020**,

156, 102024.

12. McDougale, D. R.; Watson, J. E.; Abdeen, A. A.; Adili, R.; Caputo, M. P.; Krapf, J. E.; Johnson, R. W.; Kilian, K. A.; Holinstat, M.; Das, A., Anti-inflammatory ω -3 endocannabinoid epoxides. *Proc. Natl. Acad. Sci. U.S.A.* **2017**, *114* (30), E6034-E6043.
13. Yang, R.; Fredman, G.; Krishnamoorthy, S.; Agrawal, N.; Irimia, D.; Piomelli, D.; Serhan, C. N., Decoding Functional Metabolomics with Docosahexaenoyl Ethanolamide (DHEA) Identifies Novel Bioactive Signals. *J. Biol. Chem.* **2011**, *286* (36), 31532-31541.
14. Ambrozova, G.; Pekarova, M.; Lojek, A., Effect of polyunsaturated fatty acids on the reactive oxygen and nitrogen species production by raw 264.7 macrophages. *Eur. J. Nutr.* **2010**, *49* (3), 133-139.
15. Baek, S.-H.; Park, T.; Kang, M.-G.; Park, D., Anti-Inflammatory Activity and ROS Regulation Effect of Sinapaldehyde in LPS-Stimulated RAW 264.7 Macrophages. *Molecules* **2020**, *25* (18).
16. Xiang, P.; Chen, T.; Mou, Y.; Wu, H.; Xie, P.; Lu, G.; Gong, X.; Hu, Q.; Zhang, Y.; Ji, H., NZ suppresses TLR4/NF- κ B signalings and NLRP3 inflammasome activation in LPS-induced RAW264.7 macrophages. *Inflammation Research* **2015**, *64* (10), 799-808.
17. Park, S.-W.; Hah, J. H.; Oh, S.-M.; Jeong, W.-J.; Sung, M.-W., 5-lipoxygenase mediates docosahexaenoyl ethanolamide and N-arachidonoyl-L-alanine-induced reactive oxygen species production and inhibition of proliferation of head and neck squamous cell carcinoma cells. *BMC Cancer* **2016**, *16* (1), 1-14.
18. Acevedo, A.; González-Billault, C., Crosstalk between Rac1-mediated actin regulation and ROS production. *Free Radic. Biol. Med.* **2018**, *116*, 101-113.
19. Heo, S.; Kim, S.; Kang, D., The Role of Hydrogen Peroxide and Peroxiredoxins throughout the Cell Cycle. *Antioxidants* **2020**, *9* (4), 280.
20. Matono, R.; Miyano, K.; Kiyohara, T.; Sumimoto, H., Arachidonic Acid Induces Direct Interaction of the p67phox-Rac Complex with the Phagocyte Oxidase Nox2, Leading to Superoxide Production. *J. Biol. Chem.* **2014**, *289* (36), 24874-24884.
21. Rossi, S. P.; Windschüttl, S.; Matzkin, M. E.; Rey-Ares, V.; Terradas, C.; Ponzio, R.; Puigdomenech, E.; Levalle, O.; Calandra, R. S.; Mayerhofer, A.; et al., Reactive oxygen species (ROS) production triggered by prostaglandin D2 (PGD2) regulates lactate dehydrogenase (LDH) expression/activity in TM4 Sertoli cells. *Mol. Cell. Endocrinol.* **2016**, *434*, 154-165.
22. Conrad, M.; Pratt, D. A., The chemical basis of ferroptosis. *Nat. Chem. Biol.* **2019**, *15* (12), 1137-1147.
23. Korbecki, J.; Baranowska-Bosiacka, I.; Gutowska, I.; Chlubek, D., The effect of reactive oxygen species on the synthesis of prostanoids from arachidonic acid. *J Physiol Pharmacol* **2013**, *64* (4), 409-21.
24. Jiang, X.; Stockwell, B. R.; Conrad, M., Ferroptosis: mechanisms, biology and role in disease. *Nat. Rev. Mol. Cell Biol.* **2021**, *22* (4), 266-284.
25. Janeway, C. A.; Travers, P.; Walport, M.; Shlomchik, M., *Immunobiology, 5th edition*. Garland

Publishing: New York, **2001**.

26. Tajima, T.; Murata, T.; Aritake, K.; Urade, Y.; Hirai, H.; Nakamura, M.; Ozaki, H.; Hori, M., Lipopolysaccharide Induces Macrophage Migration via Prostaglandin D2 and Prostaglandin E2. *J. Pharmacol. Exp. Ther.* **2008**, *326* (2), 493.
27. Lee, M. Y.; Skoura, A.; Park, E. J.; Landskroner-Eiger, S.; Jozsef, L.; Luciano, A. K.; Murata, T.; Pasula, S.; Dong, Y.; Bouaouina, M.; et al., Dynamin 2 regulation of integrin endocytosis, but not VEGF signaling, is crucial for developmental angiogenesis. *Development* **2014**, *141* (7), 1465-1472.
28. Wang, C.; Yoo, Y.; Fan, H.; Kim, E.; Guan, K.-L.; Guan, J.-L., Regulation of Integrin β 1 Recycling to Lipid Rafts by Rab1a to Promote Cell Migration. *J. Biol. Chem.* **2010**, *285* (38), 29398-29405.
29. Marei, H.; Carpy, A.; Woroniuk, A.; Vennin, C.; White, G.; Timpson, P.; Macek, B.; Malliri, A., Differential Rac1 signalling by guanine nucleotide exchange factors implicates FLII in regulating Rac1-driven cell migration. *Nat. Commun.* **2016**, *7* (1), 10664.
30. Roy, J.; Watson, J. E.; Hong, I. S.; Fan, T. M.; Das, A., Antitumorigenic Properties of Omega-3 Endocannabinoid Epoxides. *J. Med. Chem.* **2018**, *61* (13), 5569–5579.
31. Alhouayek, M.; Muccioli, G. G., COX-2-derived endocannabinoid metabolites as novel inflammatory mediators. *Trends Pharmacol.* **2014**, *35* (6), 284-292.
32. Rouzer, C. A.; Marnett, L. J., Endocannabinoid Oxygenation by Cyclooxygenases, Lipoxygenases, and Cytochromes P450: Cross-Talk between the Eicosanoid and Endocannabinoid Signaling Pathways. *Chem. Rev.* **2011**, *111* (10), 5899-5921.
33. Urquhart, P.; Nicolaou, A.; Woodward, D. F., Endocannabinoids and their oxygenation by cyclo-oxygenases, lipoxygenases and other oxygenases. *Biochim. Biophys. Acta Mol. Cell Biol. Lipids* **2015**, *1851* (4), 366-376.
34. Alhouayek, M.; Bottemanne, P.; Makriyannis, A.; Muccioli, G. G., N-acylethanolamine-hydrolyzing acid amidase and fatty acid amide hydrolase inhibition differentially affect N-acylethanolamine levels and macrophage activation. *Biochim. Biophys. Acta Mol. Cell Biol. Lipids* **2017**, *1862* (5), 474-484.
35. Yuan, C.; Sidhu, R. S.; Kuklev, D. V.; Kado, Y.; Wada, M.; Song, I.; Smith, W. L., Cyclooxygenase Allosterism, Fatty Acid-mediated Cross-talk between Monomers of Cyclooxygenase Homodimers. *J. Biol. Chem.* **2009**, *284* (15), 10046-10055.
36. Kozak, K. R.; Rowlinson, S. W.; Marnett, L. J., Oxygenation of the Endocannabinoid, 2-Arachidonylglycerol, to Glyceryl Prostaglandins by Cyclooxygenase-2. *J. Biol. Chem.* **2000**, *275* (43), 33744-33749.
37. Smith, W. L.; Malkowski, M. G., Interactions of fatty acids, nonsteroidal anti-inflammatory drugs, and coxibs with the catalytic and allosteric subunits of cyclooxygenases-1 and -2. *J. Biol. Chem.* **2019**, *294* (5), 1697-1705.
38. Fowler, C. J., Transport of endocannabinoids across the plasma membrane and within the cell. *FASEB J.* **2013**, *280* (9), 1895-1904.

39. Maccarrone, M., Metabolism of the Endocannabinoid Anandamide: Open Questions after 25 Years. *Front. Mol. Neurosci.* **2017**, *10*(166), 1-10.
40. Barbera, S.; Nardi, F.; Elia, I.; Realini, G.; Lugano, R.; Santucci, A.; Tosi, G. M.; Dimberg, A.; Galvagni, F.; Orlandini, M., The small GTPase Rab5c is a key regulator of trafficking of the CD93/Multimerin-2/ β 1 integrin complex in endothelial cell adhesion and migration. *Cell Commun. Signal.* **2019**, *17*(1), 55.
41. McFarland, M. J.; Porter, A. C.; Rakhshan, F. R.; Rawat, D. S.; Gibbs, R. A.; Barker, E. L., A Role for Caveolae/Lipid Rafts in the Uptake and Recycling of the Endogenous Cannabinoid Anandamide. *J. Biol. Chem.* **2004**, *279*(40), 41991-41997.
42. Mechoulam, R.; Fride, E.; Di Marzo, V., Endocannabinoids. *Eur. J. Pharmacol.* **1998**, *359*(1), 1-18.
43. Balvers, M. G. J.; Verhoeckx, K. C. M.; Bijlsma, S.; Rubingh, C. M.; Meijerink, J.; Wortelboer, H. M.; Witkamp, R. F., Fish oil and inflammatory status alter the n-3 to n-6 balance of the endocannabinoid and oxylipin metabolomes in mouse plasma and tissues. *Metabolomics* **2012**, *8*(6), 1130-1147.
44. Balvers, M. G. J.; Verhoeckx, K. C. M.; Meijerink, J.; Bijlsma, S.; Rubingh, C. M.; Wortelboer, H. M.; Witkamp, R. F., Time-dependent effect of in vivo inflammation on eicosanoid and endocannabinoid levels in plasma, liver, ileum and adipose tissue in C57BL/6 mice fed a fish-oil diet. *Int. Immunopharmacol.* **2012**, *13*(2), 204-214.
45. Wood, J. T.; Williams, J. S.; Pandarinathan, L.; Janero, D. R.; Lammi-Keefe, C. J.; Makriyannis, A., Dietary docosahexaenoic acid supplementation alters select physiological endocannabinoid-system metabolites in brain and plasma. *J. Lipid Res.* **2010**, *51*(6), 1416-1423.
46. Watson, J. E.; Kim, J. S.; Das, A., Emerging class of omega-3 fatty acid endocannabinoids & their derivatives. *Prostaglandins Other Lipid Mediat.* **2019**, *143*, 106337.
47. Brown, I.; Cascio, M. G.; Rotondo, D.; Pertwee, R. G.; Heys, S. D.; Wahle, K. W. J., Cannabinoids and omega-3/6 endocannabinoids as cell death and anticancer modulators. *Prog. Lipid Res.* **2013**, *52*(1), 80-109.
48. Balvers, M. G. J.; Wortelboer, H. M.; Witkamp, R. F.; Verhoeckx, K. C. M., Liquid chromatography-tandem mass spectrometry analysis of free and esterified fatty acid N-acyl ethanolamines in plasma and blood cells. *Anal. Biochem.* **2013**, *434*(2), 275-283.
49. Hwang, D.; Jang, B. C.; Yu, G.; Boudreau, M., Expression of mitogen-inducible cyclooxygenase induced by lipopolysaccharide: Mediation through both mitogen-activated protein kinase and nf-kb signaling pathways in macrophages. *Biochem. Pharmacol.* **1997**, *54*(1), 87-96.
50. Smith, W. L.; DeWitt, D. L.; Garavito, R. M., Cyclooxygenases: Structural, Cellular, and Molecular Biology. *Annu. Rev. Biochem.* **2000**, *69*(1), 145-182.
51. Niphakis, M. J.; Lum, K. M.; Cognetta III, A. B.; Correia, B. E.; Ichu, T.-A.; Olucha, J.; Brown, S. J.; Kundu, S.; Piscitelli, F.; Rosen, H.; et al., A Global Map of Lipid-Binding Proteins and Their Ligandability in Cells. *Cell* **2015**, *161*(7), 1668-1680.

52. Eleftheriadis, N.; Thee, S. A.; Zwinderman, M. R. H.; Leus, N. G. J.; Dekker, F. J., Activity-Based Probes for 15-Lipoxygenase-1. *Angew. Chem. Int. Ed.* **2016**, *55* (40), 12300-5.
53. Hwang, S. H.; Wagner, K.; Xu, J.; Yang, J.; Li, X.; Cao, Z.; Morisseau, C.; Lee, K. S. S.; Hammock, B. D., Chemical synthesis and biological evaluation of ω -hydroxy polyunsaturated fatty acids. *Bioorganic Med. Chem. Lett.* **2017**, *27* (3), 620-625.
54. Tokunaga, T.; Watanabe, B.; Sato, S.; Kawamoto, J.; Kurihara, T., Synthesis and Functional Assessment of a Novel Fatty Acid Probe, ω -Ethynyl Eicosapentaenoic Acid Analog, to Analyze the in Vivo Behavior of Eicosapentaenoic Acid. *Bioconjugate Chem.* **2017**, *28* (8), 2077-2085.
55. Gagestein, B. Chemical tools to study lipid signalling. *PhD thesis*, Leiden Institute of Chemistry, Faculty of Sciences, Leiden University, Leiden, **2020**.
56. Qi, L.; Meijler, M. M.; Lee, S.-H.; Sun, C.; Janda, K. D., Solid-Phase Synthesis of Anandamide Analogues. *Org. Lett.* **2004**, *6* (10), 1673-1675.

Summary

Summary

Poly-unsaturated fatty acids (PUFAs) and several of their metabolites are known to be involved in the regulation of immune functions. In a general sense, *n*-6 PUFAs possess a predominantly pro-inflammatory functionality through their oxygenated metabolites, whereas *n*-3 PUFA-derived oxygenated metabolites and amine conjugates possess less pro-inflammatory or even anti-inflammatory properties. One potent anti-inflammatory mediator is the ethanolamine derivative of docosahexaenoic acid, *i.e.*, docosahexaenoyl ethanolamide (DHEA). In this thesis, the metabolic fate of DHEA and the potential immune-modulating effects of some of the resulting metabolites are further investigated. In Chapter 2, a literature review of the metabolic and immune-regulating properties of PUFAs and their acyl derivatives is presented. As described, DHEA levels in murine and human plasma and animal plasma and tissues depend on the dietary intake of *n*-3 PUFAs. Previous studies from other labs have shown that DHEA can be oxygenated by CYP450 and LOX-15 enzymes, present in different tissues, which results in compounds with increased anti-inflammatory properties compared to DHEA itself. Together with data from our own group we conclude that studying immune regulation by *n*-3 PUFAs and *n*-3 PUFA derivatives is complex and for example depends on the relative contribution of different metabolic pathways. Recent studies have shown that the use of chemical probes, in particular synthetic PUFA-related compounds containing bio-orthogonal handles that aid in the unraveling of said compounds, can provide an interesting alternative to conventional immunological tools to investigate the immune-regulating effects of the PUFAs.

In Chapter 3 bi-functional synthetic chemical probes were synthesized and used to map the biological interactions of the anti-inflammatory mediator DHEA and the *n*-6 PUFA-derived ethanolamine conjugate arachidonoyl ethanolamide (AEA) in LPS-stimulated murine RAW264.7 macrophages. Diazirine and alkyne moieties were installed into DHEA and AEA-related structures to allow covalent coupling to interacting proteins using 366 nm UV-light. Subsequent CuAAC click coupling to a fluorescent probe or biotin enabled visualization and enrichment of bound proteins. Despite the small chemical alterations present in the probe when compared to native DHEA, the bi-functional chemical derived DHEA probes displayed similar anti-inflammatory properties compared to DHEA itself, as shown by similar reductions in IL-6 and prostaglandin E₂ (PGE₂) release. We found that uptake of the PUFA-derived probes successfully resulted in cytosolic localization in the suggested regions of the ER, Golgi-system, and showed vesicular compartmentalization. Chemical proteomic interactome mapping using affinity purification with biotin and subsequent LC-MS/MS analysis of the proteome, showed that both AEA and DHEA interacted with the oxygenation enzyme cyclooxygenase 2

(COX-2), but also with peroxiredoxin I, peroxiredoxin IV, different proteins involved in the Rho GTPase signaling pathway, and with Rac1 and its related interactome proteins. Immunolabelling studies further supported the possible molecular interaction between the PUFA-derived amides and COX-2 and Rac1. Bio-informatic analysis of the proteome interactors suggested regulatory roles for DHEA in cytoskeletal remodeling, cell migration, and ROS scavenging. The protein interactions obtained in the chemical proteomic screening provided new insights in protein interactions that are involved in the immunological effects of DHEA. Future studies can now be designed to specifically exploit these mechanisms.

Because COX-2 is involved in prostaglandin synthesis, which is reduced by DHEA, and was later found to be a target in the chemical proteomic study of Chapter 3, it was hypothesized that DHEA is a competitive substrate inhibitor of arachidonic acid (AA) conversion by COX-2. To test this hypothesis, Chapter 4 describes the development of a cell free enzymatic assay to measure conversion of the known COX-2 PUFA substrates AA, eicosapentaenoic acid (EPA), and docosahexaenoic acid (DHA). Formation of predicted metabolites was verified by LC-HRMS, after which *N*-acyl ethanolamine-derived PUFAs arachidoyl ethanolamide (AEA), eicosapentaenoyl ethanolamide (EPEA), and DHEA were added to the enzymatic assay. For AEA, production of prostaglandin ethanolamide E2 (PGE₂-EA and PGD₂-EA), 11-hydroxyeicosatetraenoyl ethanolamide (11-HETE-EA), and 15-HETE-EA were verified. For EPEA the novel products prostaglandin E3 ethanolamide (PGE₃-EA), and 11-hydroxypentaenoyl ethanolamide 11-HEPE-EA (and the postulated products 14- and 18-HEPE-EA) were obtained, and for DHEA oxidation by COX-2 resulted in 13- and 16-hydroxydocosahexaenoyl ethanolamide (13- and 16-HDHEA). Metabolic conversion of EPEA and DHEA was limited resulting in product yields that were smaller than 2%, indicating that oxidation of *n*-3 PUFA-derived amides occurred at slow rates. Conversion of DHEA by COX-2 was also obtained in 1.0 µg/mL LPS-stimulated RAW264.7 macrophages, and corresponding slow oxidation rates of DHEA provided an explanation for the decreased prostaglandin and oxylipin concentrations.

In Chapter 5 the immune regulating potential of 13-HDHEA and 16-HDHEA was explored. It was shown that 13-HDHEA or 16-HDHEA incubations reduced the production of inflammatory cytokines TNFα and IL-1β in LPS-stimulated RAW264.7 macrophages, but had no significant effects on levels of nitric oxide (NO), IL-6, and the prostaglandins PGE₂ and PGD₂. Transcriptomic analysis revealed upregulation of more anti-inflammatory related genes and reduction of pro-inflammatory related genes, especially with respect to toll-like receptor 4 (TLR4) and its downstream regulators. 13-HDHEA and 16-HDHEA showed distinct anti-inflammatory regulation compared to DHEA, but the anti-inflammatory properties of DHEA itself were more potent in our LPS-stimulated

RAW264.7 macrophages. Therefore, it was proposed that COX-2 metabolism of DHEA could act as a regulatory mechanism to limit the anti-inflammatory properties of DHEA.

In Chapter 6 the effects of 10 mg/kg and 15 mg/kg intraperitoneally injected (i.p.) DHEA were tested in a C57Bl/6 mice model of DSS-induced colitis. It was shown that the classical phenotypic markers of colitis, such as reduced body weight and rectal bleeding, were reduced, and stool consistency was improved. However, pathophysiological markers in the colon such as colon length, cellular infiltration, and neutrophil activity were not significantly affected by DHEA treatment. DHEA metabolism in the liver of these mice was investigated showing that increased doses of the injected DHEA lead to increased DHEA levels in the liver, but not to the production of DHEA metabolites. Hepatic AEA levels and oxylipin levels were not affected, which was attributed to the fact that COX-2 was not expressed in the livers of 2% DSS induced mice. Expression of other inflammatory cytokines in the liver was only limitedly affected, and it was concluded that the used DSS dosing does not induce a significant inflammatory response in the liver.

The thesis is concluded by a general discussion regarding the findings, in which it is further elaborated on that the anti-inflammatory mechanism of DHEA depends on interaction with COX-2, ROS formation, cytoskeletal remodeling, but also on metabolism catalyzed by oxygenases. In relation to this, it is crucial to acknowledge that different models used in the different studies have provided different results with regard to the effects of PUFA-derivatives and their underlying mechanisms, which makes biological interpretation more complex. Furthermore, *in vivo* PUFA metabolism will also be affected by the nutritional intake of *n*-3 PUFAs, leading to tissue-specific distribution and metabolism of *n*-3 PUFAs and their derivatives. Although the work of this thesis describes several novel interactions in the anti-inflammatory regulation of *n*-3 PUFAs and PUFA derivatives, future research is required to understand the full metabolomic overview and consequences of DHEA and its derived metabolites, and to develop dietary approaches that might lead to a reduction of (chronic) inflammation.

Acknowledgements

Acknowledgements

“Pressure makes Diamonds,
And hard work pays off.”

Danny Vera

I truly believe that if you really aspire something in life, you are able to achieve that goal as long as you keep working for it. Nothing comes at once, so you always have to keep fighting for your goals. Without perseverance and determination life would have been different, and this thesis would not have been delivered. Thanks to Danny Vera for a beautiful and inspiring song on this.

After four years (ok actually four years and several months) this thesis is the result of an extraordinary and multidisciplinary collaboration between the Laboratory of Organic Chemistry and the Division of Human Nutrition and Health. This thesis would not have existed without the help (both physically and mentally) of many people who I would like to thank; starting with my promoters Han Zuilhof and Renger Witkamp and co-promoters Bauke Albada and Michiel Balvers. I would like to thank all of you for the confidence in me, the help in the project, and mentoring in my personal development. I would like to add a few personal words to all of you.

Han, thank you for recommending me to Bauke and Michiel. Without your recommendation I would not have had the Skype interview in Denmark that started this adventure. I would also like to thank you for keeping the labs open during the COVID-19 pandemic, which allowed me to finish my practical work. We all know: “Standing still is the fastest way of moving backwards.” Finally, during one of your AOC lectures on transition states and reaction kinetics I learned that optimums could be local, and that changes of the parameters can lead to even higher optima. Thank you for this insight, and I hope to put this into practice in my following career steps.

Renger, I would like to thank you for your enthusiasm in this project, but also science in general. If I was ever out of ideas, or even fed up with science, you were always able to inspire me again. I can fairly say that it is because of your enthusiasm that I started to enjoy the sometimes small but valuable successes in the life of a scientist. Nothing should ever be taken for granted. Thank you for this.

Bauke, I would like to thank you for the nice adventures that we shared in the past four years. You showed me the wonderful and delicious country of Israel during the both educational and fun PhD trip. I will never forget your remarkable, but often true expressions like: “dat is zoiets als een caravan aan je fiets hangen” or “dat is zoals het schieten met een bazooka op een kuikentje”. Finally, not to let it be forgotten (Han I hope you kept on reading...), we even experienced together that Feyenoord became the champion of season 2016-2017.

Michiel, I would like to thank you for sharing the world of PUFAs and endocannabinoid biology with me and teaching me the beauty of UPLC-MS/MS. I would also like to thank you for the small talks we had about the daily life as a scientist, but also the more personal talks about life in general. I will remember the nice moments we shared at the ICRS in Leiden, and the ‘bitterballen’ and dinner together with Bauke to celebrate the successes in science.

I would also like to thank the thesis committee, Prof. dr. Kersten, dr. Alhouayek, Prof. dr. Garssen, and Prof. dr. Van der Stelt for their time and critical evaluation of my thesis.

Then a big thank you to my paranymphs Tessa de Bie and Jordi Keijzer. Thank you for the mental and physical support during my thesis defence. It feels comfortable to defend my thesis with the two of you having my back. In addition, I would like to thank you for the small talks about science but also life in general. You are both wonderful colleagues and great persons!

I would also like to thank Mieke Poland for teaching me the ‘real’ biology, and her assistance in several biological analyses. I thank Frank Claassen, Elbert van der Klift, Hans Beijleveld, and Francel Verstappen for their endless patience in helping me to learn all the errors of mass spectrometers and HPLC’s. You taught me that machines only execute programmed jobs and that it is always us (or malfunctioning software) to blame for the errors. I would also like to thank Barend van Lagen, Niels de Roo, and Tatiana Nikolaeva for their NMR assistance. I would like to thank Norbert de Ruijter for sharing his knowledge and interest in confocal and fluorescence microscopy with me, Twan America for assisting and helping with the proteomic analysis, and Guido Hooiveld and Mark Boekschoten for supporting me with the transcriptomic analysis. Your help and knowledge was very much appreciated, and I definitely learned a lot from you all.

Special word to Milou Santbergen and Jordi Keijzer for their emotional support (read complaining about failed experiments and general struggles in life). It was nice to have shared lunch during spring and summer to clear our minds. Together with Sevil Sahin we organised the PhD trip to Israel, which was a great learning experience. I would not have wished for a different team than ours to organise this trip.

I thank my office mates from 8038; Jordi Keijzer, Yuri Damen, and former office mates Jorick Bruins, Sjoerd Slagman, Dieuwertje Streefkerk, Danielle Chinello, Fridolin Treindl, Tunan Gao, and Tjerk Sminia for the fun in the office. The appearance of COVID-19 made me realise that working from home is not as much fun as sharing a laugh and a tear in the office. Apart from all the fun our combined thinking also more than once led to novel insights for the project. Thanks for all of this!

Thanks to Mara van Trijp for accepting me as temporary office mate at HNH during the COVID-19 pandemic. Although, it was short I would like to thank you for the fun and social talks we had in the office (*e.g.* the life our cats).

I would also like to thank the people from the Nutritional Biology group, and in particular the people from the former Pharmacology group; Miranda van der Ende, Xiaolin Li, Tessa de Bie, Paulina Vinke, Wout van Orten-Luiten, and Francisca Noya Leal, Rogier Plas, Klaske van Norren, Jocelijn Meijerink, Mieke Poland.

All the staff members and AIO's from the Laboratory of Organic Chemistry and the department of Human Nutrition and Health are thanked for their input during discussions, but also for their involvement in the many social activities. It was great talking to all of you.

In addition, I would like to thank my students for their enthusiasm and work. Stijn Kral, Floor Leurs, Carolina Tabares Mafla, Arthur Samurkas, Fay Schrouf, Milena Lam, Sandra van Krimpen, and Daan Bogers thank you for your assistance in the project. I hope you enjoyed our collaboration as much as I did.

A great thank you to Pol Grootswagers, Frans Kampers, and later also Benthe van der Lugt for joining me in spreading the Tour de France 'yellow fever' through Helix. I am sure it was well-received and it is good to see that the tradition is continued.

Acknowledgements

A special thanks to all my teammates from Sliedrecht Sport. You have become my second family and at the volleyball I was always able to keep my mind from work. Together we achieved great things like promotion to the Eredivisie, semi-finals in the Dutch cup, and several listings in the top of the Eredivisie.

A special thanks to my parents and family who always support(ed) me in my adventures. Without your inspiration I would not have become the person that I am today. My final and most special acknowledgement goes to Yara, my wife (finally, after extending our wedding due to COVID-19). Thank you so much for your mental support and willingness to listen to all the PhD struggles. I also admire your flexibility when it comes to me chasing my dreams. Doing a PhD in Wageningen, no problem! Playing Eredivisie volleyball when not working, no problem! Potentially moving to a different country, no problem! Not doing so, no problem! Without your everlasting support over the last 4/5 years I could not have pulled this off. I know that our life can be a bumpy ride every now and then, but I also know that we can always fall back onto each other. I loved you, love you, and always will love you!

About the author

10.1 Curriculum Vitae

Ian-Arris de Bus was born on 15 December 1992 in Zwijndrecht, the Netherlands. After graduating from secondary school CSW Van de Perre in Middelburg in 2011, he started the study Molecular Life Sciences at Wageningen University. During his study he specialised in the field of Chemical Biology, and performed his MSc. thesis on a multidisciplinary collaborative study between the Laboratory of Organic Chemistry and the Laboratory of Cell Biology and Immunology, followed by a 6 month internship at the Jensen group in the Laboratory of Organic Chemistry at Copenhagen University. In September 2016 Ian started his PhD on a multidisciplinary research project at Wageningen University and Research shared between the Laboratory of Organic Chemistry (group of prof. dr. Han Zuilhof) and the department of Human Nutrition and Health (group of prof. dr. Renger Witkamp). In this research project he investigated the anti-inflammatory role of *n*-3 PUFA metabolites, especially that of docosahexaenoyl ethanolamide, as described in this thesis. In his young academic career Ian has always been interested in unravelling complex biological problems by using chemical tools and analyses. In this light, Ian provides the link between experts in the biological, immunological, pharmacological, chemical fields, motivated by the idea that teamwork and collaborative power leads to improved solutions for complex problems.



10.2 List of Publications

2021 **de Bus I.**, America A.H.P., de Ruijter N., Lam M., Witkamp R.F., Zuilhof H., Balvers M.G.J., Albada B. "Bi-functional probes of PUFA-derived N-acylethanolamides identify peroxiredoxins and small GTPase-signalling proteins as their molecular targets in LPS-stimulated RAW264.7 macrophages". Manuscript submitted at ACS Chemical Biology.

2021 **de Bus I.**, Van Krimpen S., Hooiveld G.J., Boekschoten M.V., Poland M., Witkamp R.F., Albada B., Balvers M.G.J. "Immunomodulating effects of 13- and 16-hydroxylated docosahexaenoyl ethanolamide in LPS stimulated RAW264.7 macrophages". *Biochimica et Biophysica Acta (BBA) - Molecular and Cell Biology of Lipids*, *1866*, 158908.

2019 **de Bus I.**, Zuilhof H., Witkamp R.F., Balvers M.G.J., and Albada B. "Novel COX-2 products of n-3 polyunsaturated fatty acid-ethanolamine-conjugates identified in RAW264.7 macrophages". *Journal of Lipid Research*, *60*, 1829-1840.

2019 **de Bus I.**, Witkamp R.F., Zuilhof H., Albada B., and Balvers M.G.J. "The role of n-3 PUFA-derived fatty acid derivatives and their oxygenated metabolites in the modulation of inflammation". *Prostaglandins and Other Lipid Mediators*, *144*, 106351.

2017 van Andel E., **de Bus I.**, Tijhaar E. J., Smulders M. M. J., Savelkoul H. F. J., and Zuilhof H. "Highly Specific Binding on Antifouling Zwitterionic Polymer-Coated Microbeads as Measured by Flow Cytometry". *ACS Applied Materials & Interfaces*, *9*, 38211-38221.

10.3 Overview of completed training activities

Discipline-specific courses	Organizing insitute	Year
BioNEC Symposium	BioNEC	2016
WUR Molecular Life Sciences series	WUR	2017-2020
Wageningen SOC symposium ^a	KNCV	2017, 2018
Chains ^a	NWO	2017, 2019
Advanced Organic Chemistry	VLAG	2017-2019
Annual Symposium on the Cannabinoids ^a	ICRS	2018
7th European Workshop on Lipid Mediators ^a	UCL	2018
Metal Organic Chemistry	HRSMC	2018
Figon Dutch Medicine Days ^b	Figon	2019
General courses		
VLAG PhD week	VLAG	2016
Project and Time Management	WGS	2017
Presenting with Impact	WGS	2018
Scientific Writing	WGS	2018
Course Leadership	PhotoBioCat	2019
Career Perspectives	WGS	2019
Other activities		
Preparation of Research Proposal	ORC/HNH	2016
Weekly Group Meetings	ORC/HNH	2016-2020
Colloquia	ORC/HNH	2016-2020
PhD Study Tour to Denmark and Sweden	ORC	2017
PhD Study Tour Israel	ORC	2019
Organising Committee PhD Study Tour Israel	ORC	2019

^a Poster presentation; ^b Oral presentation

The research presented in this thesis was financially supported by the VLAG graduate school of Wageningen University.

Financial support from Wageningen University for printing this thesis is gratefully acknowledged.

Printed by GVO Drukkers & Vormgevers B.V., Ede, The Netherlands

Cover by auhtor

Layout by Loes van de Kraats – Kema

